Mobile Multi-Parameter Measurements for the dynamic Analysis of Gradients in Brewing Vessels

vorgelegt von
Dipl.-Ing.
Anika Bockisch
geb. in Potsdam

von der Fakultät III-Prozesswissenschaften
der Technischen Universität Berlin
zur Erlangung des akademischen Grades

Doktorin der Ingenieurwissenschaften
-Dr.-Ing.-
genehmigte Dissertation

Promotionsausschuss:

Vorsitzender:	Prof. Dr. Lorenz Adrian, Fachgebiet Geobiotechnologie, Institut für Biotechnologie, Technische Universität Berlin
Gutachter:	Prof. Dr. Peter Neubauer, Fachgebiet Bioverfahrenstechnik, Institut für Biotechnologie, Technische Universität Berlin
Gutachter:	Prof. Dr. Thomas Becker, Lehrstuhl für Brau- und Getränketechnologie Wissenschaftszentrum Weihenstephan für Ernährung, Landnutzung und Umwelt, Technische Universität München
Gutachter:	Dr.-Ing. Frithjof Thiele, Head of Corporate Technology at Radeberger Gruppe KG

Tag der wissenschaftlichen Aussprache: 13.07.2018 in Berlin

Abstract

Industrial processes have to be competitive and thus efficient. Products have to be produced with a high reproducibility and quality. At the same time, the scale of these processes reaches up to several 100 m³ and was even increasing in recent years. This is challenging since the power input is limited in large-scale processes. Therefore, mixing times are increasing in parallel to the volume, whereas heat and mass transfer rates are decreasing. This leads to spatial gradient formation, e.g. for the pH-value, dissolved oxygen (DO), dissolved carbon dioxide (DCO_2), temperature or cell concentration. Hence, substrate consumption and metabolite synthesis rates are often altered during scale-up.

Since the available sensor technology, which is usually located at an arbitrarily chosen spot in large-scale reactors, is not designed for the consideration of heterogeneities, the knowledge about gradients and their magnitude is rather low. *Off-line* or *on-line* data obtained with devices installed at one single position of the tank are not representative for the major part of the liquid phase. Computational fluid dynamics do not necessarily contribute to a better process understanding, if uncoupled from kinetic models, which consider consumption and synthesis rates. In addition, cellular synthesis rates can be affected by the gradient formation, which would also lead to false assumptions in the models. In this thesis, mobile, multi-parameter sensor tools have been developed for *in-situ* and *on-line* measurements of various process parameters in order to improve process monitoring in industrial bioreactors. Sensors for the pH-, DO-, DCO_2-value, redox potential, conductivity, temperature, and pressure were integrated into sensor units. These monitoring tools were applied in various brewing tanks of different geometries and scales and frequently moved along the height of the liquid phase in the 3 m^3, 24 m^3, and 170/199 m^3 scale. The time-dependent and spatial parameter distribution was correlated to data from *off-line* metabolite analysis (carbohydrates, main carbon metabolites, sterols).

The long-term application of miniaturized sensors with a small membrane diameter and electrolyte volume is challenging in complex brewing media due to the risk of clogging or toxification of the electrolyte by chemical compounds, e.g. DCO_2. This negatively affects the measurement stability and sensor drift. With larger sensors, however, the pH-value, redox potential, temperature, and DO-value were measured in brewing fermentations of up to 220 h with a pressure of up to 1.9 bar without significant losses in the measurement stability and with a negligible increase in the sensor drift. In the brewing processes, only a few spatial gradients were detected along the tank height, e.g. for the redox potential with a maximum of 66 mV during the onset of the fermentation and for the pH-value with a maximum of 0.17 pH-units during the main fermentation in the 170/199 m^3 scale. During the filling process, even larger gradients of up to 110 mV for the redox potential and 0.2 pH-units were determined. In the 3 m^3 scale, the gradients were maximum 23 mV and 0.04 pH-units during the onset of the fermentation. Monitoring of gradients during this operation step allows for *real-time* adaption of the filling process, reducing time and energy losses. Correlation analyses of *on-line* sensor data with *off-line* data from metabolite analysis showed that the carbohydrate concentrations, especially for glucose and fructose, correlated best with the *on-line* data (pH-, DO-value, redox potential, temperature) ($R^2 > 0.9$), followed by the total sterol content.

The mobile multi-parameter measurement devices developed and applied in this thesis allow for a fast detection of gradients in large-scale processes. By the correlation of the sensor data from multi-position measurements with the data from metabolite analysis, the impact of gradients on the bioprocess performance can be described. Hence, critical reactor zones and process phases can be identified rapidly and the filling process as well as tank geometries in combination with filling levels can be optimized for anaerobic fermentation processes.

Zusammenfassung

Industrielle, großskalige Prozesse müssen wettbewerbsfähig und daher effizient sein. Produkte müssen mit hoher Reproduzierbarkeit und Qualität hergestellt werden. Gleichzeitig werden in diesen Prozessen Maßstäbe von mehreren 100 m³ erreicht, die in den letzten Jahren sogar weiter gestiegen sind. Das bringt Herausforderungen mit sich, da der Energieeintrag in diesen großskaligen Prozessen limitiert ist. Dadurch verlängern sich mit steigendem Volumen Mischzeiten, wogegen Wärme- und Stoffübertragungsraten sinken. Das führt zu räumlichen Gradienten, z.B. beim pH-Wert, Gelöstsauerstoff (DO), gelöstem Kohlenstoffdioxid (DCO_2), bei der Temperatur oder Zellkonzentration. Somit verändern sich Substratverbrauch und metabolische Syntheseraten während der Maßstabsvergrößerung häufig.

Da die verfügbare Sensortechnik, die oft an einem zufällig gewählten Ort in großskaligen Reaktoren installiert ist, nicht für die Betrachtung von Heterogenitäten ausgelegt ist, ist das Wissen über Gradienten und ihr Ausmaß sehr gering. *Offline* oder *online* gewonnene Daten, die mittels Mess- oder Probenahmetechniken gewonnen werden, die nur an einem einzigen Punkt im Tank installiert sind, sind nicht repräsentativ für den Großteil der Flüssigphase. Computer-basierte Fluiddynamik (CFD) trägt nicht notwendigerweise zu einem verbesserten Prozessverständnis bei, wenn sie losgelöst von kinetischen Modellen angewandt wird, die Verbrauchs- und Syntheseraten mit einbeziehen. Zusätzlich können zelluläre Syntheseraten von Gradienten beeinflusst sein, was wiederum zu verfälschten Annahmen in den Modellen führen würde. In dieser Dissertation wurden mobile Multiparameter Sensor-Tools für eine *in-situ* und *online* Messung verschiedenster Prozessparameter entwickelt, um die Prozessüberwachung in industriellen Bioreaktoren zu verbessern. Sensoren für die Messung des pH-, DO-, und DCO_2-Wertes, dem Redoxpotential, der Leitfähigkeit, der Temperatur und dem Druck wurden in Sensoreinheiten integriert. Diese Sensoreinheiten wurden in unterschiedlichen Brautanks mit verschiedenen Geometrien und Maßstäben eingesetzt und im 3 m^3, 24 m^3 und 170/199 m^3 Maßstab regelmäßig entlang der Flüssigkeitshöhe bewegt. Die zeit- und ortsabhängige Parameterverteilung wurde mit den Daten aus den *offline*-Analysen der Metabolite (Kohlenhydrate, Haupt-Kohlenstoff-Metabolite, Sterole) korreliert.

Die Langzeitnutzung von miniaturisierten Sensoren mit kleinem Membrandurchmesser und geringem Elektrolytvolumen in komplexen Braumedien ist herausfordernd, da das Risiko besteht, dass sich die Membranen zusetzen oder der Elektrolyt durch chemische Substanzen, wie z.B. DCO_2, „vergiftet“ wird. Dies beeinflusst die Messstabilität und das Driftverhalten der Sensoren negativ. Mit den größeren Sensoren wurden dagegen der pH-Wert, das Redoxpotential, die Temperatur und der DO-Wert ohne signifikante Verluste in der Messstabilität und mit einer vernachlässigbar geringen Sensordrift in Braufermentationen von bis zu 220 h und mit einem Druck von bis zu 1,9 bar gemessen. In den Brauprozessen wurden nur wenige ortsabhängige Gradienten entlang der Tankhöhe ermittelt, z.B. für das Redoxpotential mit maximal 66 mV während der Angärphase und für den pH-Wert mit einem Maximum von 0,17 pH-Einheiten während der Hauptgärphase im 170/199 m^3 Maßstab. Während des Befüllvorgangs wurden sogar größere Gradienten von bis zu 110 mV und 0,2 pH-Einheiten gemessen. Die Gradienten im 3 m^3 Maßstab waren maximal 23 mV und 0,04 pH-Einheiten groß (während der Angärphase). Eine Gradientenüberwachung während dieses Prozessschrittes erlaubt eine Echtzeitanpassung des Befüllvorgangs, was Zeit und Energie einspart. Die Korrelationsanalysen der *online* Sensordaten mit den Daten der *offline* Metaboliten-Analyse zeigten, dass die Kohlenhydrate, darunter vor allem Glukose und Fruktose, am besten mit den Sensordaten (pH-, DO-Wert, Redoxpotential, Temperatur) korrelieren ($R^2 > 0,9$), gefolgt vom totalen Sterolgehalt.

Die mobile Multiparameter-Messtechnik, die in dieser Arbeit entwickelt und angewandt wurde, ermöglicht eine schnelle Bestimmung von Gradienten in großskaligen Prozessen. Mit Hilfe der Korrelation der Sensordaten aus den Multipositionsmessungen mit den Daten der Metabolitenanalyse kann der Einfluss von Gradienten auf die Bioprozessleistung beschrieben werden. Somit können kritische Reaktorzonen und Prozessphasen schnell identifiziert und der Befüllvorgang sowie Tankgeometrien in Verbindung mit dem Füllstand für anaerobe Prozesse optimiert werden.

List of Contents

Declaration of Originality

The presented work was conducted at the chair of Bioprocess Technology, Department of Biotechnology under the scientific supervision and support of Dr. - Ing. Stefan Junne and Prof. Dr. Peter Neubauer.

I hereby declare on oath that this submitted dissertation is entirely my own original work and that I did not make use of any other than the cited literature or other means. Working packages, supported by others, such as by subcontractors, are clearly indicated.
I am aware of the University's regulations concerning plagiarism, including disciplinary actions that may result from plagiarism. Any use of the published or unpublished works, in any form, of any other author is properly acknowledged and clearly referenced or cited.

This work has not yet been submitted to another examination institution – neither in Germany nor outside Germany and neither in the same nor in a similar way. Further, this work has not yet been published.

Eidesstattliche Erklärung

Die vorliegende Arbeit wurde am Institut für Biotechnologie, Fachgebiet Bioprozesstechnik unter der Betreuung und Unterstützung von Dr. - Ing. Stefan Junne und Prof. Dr. Peter Neubauer angefertigt.

Ich erkläre hiermit eidesstattlich, dass diese eingereichte Dissertation komplett meine eigene Arbeit darstellt und mich keiner anderen als der angegebenen Literatur oder sonstiger Hilfsmittel bedient habe. Arbeitspakete, die von anderen, wie z.B. Unterauftragnehmern, unterstützt wurden, sind klar gekennzeichnet.
Die Regularien der Universität bezüglich Plagiaten einschließlich der Disziplinarverfahren, die aus Plagiatsvorwürfen resultieren, sind mir bekannt. Jegliche Verwendung von veröffentlichten oder unveröffentlichten Arbeiten/Ergebnissen von jeglichen Autoren in jeglicher Form ist entsprechend gekennzeichnet und klar referenziert oder zitiert.

Diese Arbeit wurde bisher an keine andere Prüfungsbehörde geschickt – weder in Deutschland, noch außerhalb von Deutschland und weder in derselben noch in einer ähnlichen Form. Sie wurde weiterhin bisher nicht publiziert.

Berlin, 28. 02. 2018

Anika Bockisch

Acknowledgements

During a long period, many people contributed to this thesis project. I am very grateful for the opportunity, given by Peter Neubauer, to perform my PhD thesis at the Chair of Bioprocess Engineering. I definitely learned a lot during the time in this group in science, organization, and social aspects. Peter, I appreciated your constant enthusiasm, your willingness to pursue ideas and visions, and your openness for innovation.

I express my special gratitude to Stefan Junne for supervising and surveying my thesis and his constant support. Stefan, thank you for your valuable suggestions, your realistic view in certain situations, your constructive feedback, and fruitful discussions during my work. I also appreciated your support during some external experiments, especially under harsh climatic conditions on the top of outdoor tanks and during night or weekend times.

Many thanks to Jan Biering from the VLB Berlin. Jan, thank you so much for introducing me into the world of brewing, for all the important suggestions from a brewer's point of view and constructive feedback as well as constant support. Although it was not your thesis, you helped me with my experimental work even on weekends and during night shifts. I enjoyed our trips to several breweries for experimental purposes, although this was always associated with long working hours.
I also want to thank the people who have been working in the pilot brewery plant at the VLB Berlin: Kurt Marshall, Victor Kunz, and Kolja Gigla. You provided me with materials for my experiments in the laboratoy scale, teached me in brewing science, and were always open for interesting discussions. Thanks also to Thomas Tyrell, Roland Folz, and Roland Pahl for your constructive feedback and important suggestions during the first two years of this project.

Without the openess of three breweries and the disposition to take risks, the experiments conducted in the industrial scale during this thesis would not have been performed. Thanks to Wilko Bereit, Nils Hein, Florian Johannes, Bernhard Wagemann, Stefan Meyer, Sandra Nicklich, and Georg Rammelmeier for all your support and interesting conversations and thanks to all the other colleagues in the breweries who helped me with installations of the technique or laboratory equipment.

An important partner during the project was the „Kurt-Schwabe-Institut für Mess- und Sensortechnik e.V." in Meinsberg. I want to thank Sandra Sachse, Ute Enseleit, and Winfried Vonau for the good collaboration and the constant willingness to improve the monitoring technique.

Many thanks go to Prof. Dr. Thomas Becker and Dr.-Ing. Frithjof Thiele for reviewing my thesis. Frithjof, thank you so much for your support, especially for organizing the opportunity to conduct experiments in really large-scale fermentation vessels. Without this scale, the thesis would not have the same format. I also appreciated your constant interest in the project progress and the fruitful discussions with you, whenever this was possible.

For the financial support of the first 2.5 years of the thesis in the frame of the project DynaBrau (project number: 10033235), I want to thank the Investitionsbank Berlin (IBB) and the European Fond for regional Development (EFRE) of the European Union.

I also express my gratitude to my bachelor student Ammar Al Shameri and master student Konstantin Böttger for their work. A special thanks goes to you, Konstantin, for your immense support with the design of programmes for the visualization and correlation of my data. I appreciate the amount of time you put into this work.

I want to thank my former and present colleagues at the Chair of Bioprocess Engineering at TU Berlin for the great atmosphere in the lab and office and during BVT-team events.
Brigitte and Irmgard, thanks for all the effort you put into making everything work in the laboratories and for supporting my practical work in the lab. Thomas, thank you for your support during the construction of devices for the installation of the sensor technique.
Erich, it was a pleasure having you as a colleague, roommate and dialog partner. With you, it was even fun to conduct experiments in a biogas plant. I already miss your special humor. Martin, Juan, and Andres, I enjoyed sharing a room, the coffee breaks, and the entertaining moments with you.
Anna Maria, Anja, and Klaus, I appreciate(ed) very much having you as colleagues and PhD fellows. Thanks for your support in the lab, the exchange of ideas, and the nice meetings in the kitchen for coffee preparation or in free time.
Olga, I am very thankful for the short time you were with us, for the nice discussions, and for all the programming and data handling you elaborated for this project. Without your contribution, the project would not have progressed in the same way.

Finally, I thank my family for their continuous support and motivating conversations. Ruth and Manfred, you always encouraged me to be curious and interested in science and teached me to stay the course. Ich bin euch sehr dankbar!

And last but not least, Massimo. You have been with me already during my diploma thesis. Thank you for your patience and being on my side during all these years. Grazie per ascoltate quando ne avevo e ho bisogno e semplicemente per eserci sempre.

List of Abbreviations

General

ANN	Artificial Neural Networks
Bi-dest. water	Bi-distilled water
Bf	Bottom fermenting
CCT	Cylindroconical Tank
CFD	Computational Fluid Dynamics
CIP	Cleaning in Place
DCO_2	Dissolved Carbon Dioxide
DO	Dissolved Oxygen
EBC	European Brewing Convention (regulations for analysis, SOPs)
EMP	Emden-Meyerhof-Parnas Pathway
EN	Electronic Nose
ET	Electronic Tongue
FAN	Free Amino Nitrogen
FDA	Food and Drug Admission (United States)
FID	Flame Ionization Detector
GC	Gas Chromatography
H/D	Height to Diameter (ratio)
HM	Hamilton Germany GmbH (Process Analytics)
HPLC	High Performance Liquid Chromatography
KSI	„Kurt-Schwabe-Institut für Mess- und Sensortechnik e.V.“, Meinsberg
MATLAB	MATrix LABoratoy
MIMS	Membrane Inlet Mass Spectroscopy
MLR	Multi-Linear Regression
NTC	Negative Temperature Coefficient Thermistors
OE	Original Extract
ORP	Oxidation-Reduction Potential
PAT	Process Analytical Technology
P. chrysogenum	*Penicillium chrysogenum*
PC	Principal Component
PCA	Principal Component Analysis
PLS	Partial Least Square (Regression)
PPP	Pentose Phosphate Pathway
RE	Real Extract
S.	*Saccharomyces* spp.
Tf	Top fermenting
UV/VIS	Ultra-Violet / Visible Spectroscopy

Chemical Substances

ADP	Adenosine di-phosphate
ATP	Adenosine tri-phosphate
CO_2	Carbon dioxide
°C	Degree Celsius
$\overline{\varepsilon_T}$	Mean specific energy dissipation rate
°P	Degree Plato, measure for the extract (= dissolved components of the unfermented wort: mainly carbohydrates, vitamins, proteins, aroma compounds)
$C_6H_{12}O_6$	Glucose
C_2H_5OH	Ethanol
H_2O	Water
m_{alc}	Alcohol in g per 100 g of beer
O_2	Oxygen
P_i	Inorganic phosphate

Symbols in PCA / PLS

A / *X*	Matrix of *on-line* sensor data
B / *Y*	Matrix of *off-line* analysis data
a	Number of model components / PLS dimension
m	Response variables
n	Number of observations
ncomp	Number of principal components
p	Number of predictor variables
R^2	Regression coefficient
x	Measured values (for regression coefficient calculation)
y	Predicted values (for regression coefficient calculation)
μ	expected value / mean value of the probability distribution
σ^2	Variance
w	Weightings

List of Figures

Appendix B

List of Tables

1. Introduction

The volume of industrial production processes reaches up to several 100 m³ and is even increasing. Since the power input is limited in large-scale processes, mixing times are increasing at higher volumes and heat and mass transfer rates are decreasing. Instead, metabolic activity remains as fast as in the small scale. This leads to spatial gradient formation, e.g. for the pH-value, dissolved oxygen (DO), dissolved carbon dioxide (DCO_2), temperature or cell concentration.

Process analyzers, such as sensor technologies, however, are usually not designed for the detection of gradients. Often, a limited number of sensors is installed at an arbitrarily chosen spot in the liquid phase of large-scale reactors. Most brewing fermentation vessels, for example, are equipped only with one temperature sensor. *On-line* data recorded at a single position of a reactor are not representative for the major part of the liquid phase. Model-based methods, e.g. computational fluid dynamics (CFD), are also used for the simulation of the fluid flow and heterogeneities, as discussed in the scientific background section of this thesis. CFD, however, does not necessarily improve process understanding, if this technique is applied uncoupled from data concerning mass transfer rates and kinetic models, which consider consumption and synthesis rates.
Therefore, there is a need for submergible sensor devices that can be applied directly in the liquid phase of large-scale reactors and directed to various positions. With such a technique, the knowledge about the appearance of gradients and their magnitude can be increased. The devices should further allow for multi-parameter measurements since the impact of gradients on the cell physiology and metabolic activity is parameter dependend. In contrast to the application in biofuel or bulk chemical production, these techniques have to meet certain requirements when used in the food and beverage industry, e.g. high stability and sterilizability of the wetted parts.
In this thesis, such mobile multi-parameter tools were constructed and applied in various brewing fermentations. The brewing process is of special interest for the investigation of gradients because it is an unstirred process, operated in various types of brewing fermenters with different geometries, and reaching volumes of several 100 m^3. Further, accessibility is given in contrast to pharmaceutical production processes with many restrictions.

The first part of this thesis comprises a literature review of the different fields of this thesis, namely the brewing process including yeast metabolism and available tank geometries, natural and mechanical mixing as well as gradient formation in large-scale processes, and an overview about available process analytical tools for (*on-line*) bioprocess monitoring, which includes methods for multivariate data analysis and model-based process monitoring.
Based on the knowledge obtained from the literature research and the scientific gap, research questions were expressed and targets for this work were set.
In the next part, the methods section, the development of mobile multi-parameter sensor tools for improved *in-situ* and *on-line* monitoring is elucidated. In the beginning, the evaluation process of two sensor sets is presented. Miniaturized sensors for the pH-, DO-, DCO_2-value, redox potential, temperature, and pressure and commercially available sensors for the pH-, DO-value, and redox potential with integrated temperature sensor were applied in various brewing fermentations in the laboratory scale (3.6 to 170 L). The sensor stability, accuracy, and drift during long-term applications in complex brewing media was tested in several fermentations. Afterwards, the first constructions for sensor positioning as well as flow cells for the application in the laboratory scale are illustrated. The

integration of the sensors into housing units was a further improvement, which is described. These were constructed particularly for the measurement of spatial gradients in the liquid phase of industrial, closed brewing fermenters. Along with this development, constructions for the installation of the mobile sensor units in various tanks, the cable connections, and the technique for the movements of the units were designed. Further, systems for the visualization of time and space resolved data were constantly improved. Finally, the application of the flow cells and sensor units in various brewing fermentation tanks of different geometries and sizes from 0.15 to nearly 200 m^3 is described. Additionally, methods for the parallel *off-line* analysis of several parameters (carbohydrates, main carbon metabolites and sterols) are listed. The section closes with the description of the method for multivariate data analysis.
In the results section of this thesis, data obtained with the optimized monitoring tool for the investigation of the liquid phase in large-scale, closed brewing vessels are presented. This was finally consisting of three commercially available sensors, which were integrated into a housing unit of stainless steel, and a silicon hose for sealing the data transfer cables. The mobile multi-parameter measurements in brewing processes of different scales revealed that these are mostly well mixed along the tank height. Only a few significant gradients in the pH-value and redox potential were determined during long-term fermentations of up to 220 h. Finally, the results of the correlation analysis between the time-dependent and spatial distribution of *on-line* sensor data and data from *off-line* studies are displayed.
In the next part, the results are discussed in relation to the literature and state of the art. Concerning brewing processes and the application of advanced *in-situ* sensor technique, however, the available literature is limited. Challenges and limits of the developed tools during both, design and application, are discussed as well.

This thesis presents the development of mobile multi-parameter sensor tools and their applicability in unstirred large-scale brewing tanks with a volume of up to 200 m^3. The technique provides an insight into the core of the liquid phase of large-scale reactors, improving process monitoring and the knowledge about heterogeneities. Critical reactor zones and process phases can be identified. This was shown for the filling phase in the 170/199 m^3 scale, as the brewery eliminated a process step related to the filling based on the results obtained by the mobile multi-parameter sensor technique. The correlation of data from metabolite analysis with sensor data allows to investigate the impact of gradients on the cell.

2. Scientific Background

In the following first two sections, an overview of the brewing process, the yeast and typical geometries of brewing tanks is provided, followed by a description of mixing and fluid dynamic studies of the liquid phase inside these tanks during fermentation. The third section presents process analytical tools for the monitoring of anaerobic fermentations processes, especially of the liquid phase in large-scale reactors.

2.1. The Brewing Process

The brewing process is one of the oldest and important fermentation processes. Research and development in this field for process optimization has been performed for decades. Nevertheless, there is still a great demand for improved process monitoring control, especially regarding *on-line* and *real-time* monitoring techniques of the different process steps in order to constantly increase cost efficiency, process stability, and product quality. This demand is even enhanced by the constant development of new brands and beer types for the dynamic beer market as well as the increasing fermentation volumes of up to 400 m^3 (Becker et al., 2001).

2.1.1. Steps of Beer Production

According to the German purity law of 1516, only water, hops and malt are allowed to be used in the beer brewing process. A beer produced according to this law is regarded as a protected “traditional nutrient” and no other ingredients or additions are allowed except of yeast, as this necessary ingredient was not known when the law was established (Becker and Tippmann, 2016; Narziss and Back, 2016). The yeast was even regarded once as contaminant (Hough et al., 1982). In other countries, other starch sources than malted barley or wheat are used such as rice, maize, and sorghum or carbohydrate sources such as cane sugar, beet sugar or syrups, namely adjuncts (Lloyd, 1986).

The brewing process consists of several steps (Fig. 1) (Boulton, 1991). After the initial step, the **roasting of the grain** (wheat, barley, sorghum etc.), the resulting malt is delivered to the brewery.

The first step in the brewery is the **milling** of the grain. Afterwards, the **mashing** process of the malt starts, where the sugar content and its composition are modified by temperature and pH variation. Enzymes are inactivated (e.g. proteases or β-glucanases in order to maintain the foam stability) or activated (e.g. α- and β-amylases or limit dextrinases). The latter degrade the polysaccharides (mainly starch) to mono-, di-, or trisaccharides, which can be used as primary substrate by yeast (Stenholm and Home, 1999; Willaert, 2006). These are mainly glucose, fructose, saccharose, maltose and maltotriose (Stewart, 2016). The detailed conversion to ethanol is described in the section yeast metabolism (2.1.2).
The final apparent attenuation (measured with a hydrometer) in the mashed medium shall be higher than 75 % (without the addition of saccharose) in order to achieve an optimal ratio between maltose and maltotriose for the start of the fermentation and a lower α-glucan content for the later filtration (Annemüller and Manger, 2009e; Annemüller and Manger, 2009g). The final apparent attenuation represents the total amount of soluble saccharides in the wort, which can be converted by the yeast

cells (under laboratory conditions) and is therefore important for the final beer quality (Castritius et al., 2012). A normal bottom fermenting beer has an attenuation of 75 – 85 % (Annemüller and Manger, 2009e).
Additionally, fatty acids, carbohydrates and amino acids are converted during the mashing step into different molecules by enzymatic or thermal activity, which influence the aroma of the wort. Monitoring and control of this step is generally of high importance.

The next step is conducted in the **lauter tun**, in which spent grains are separated from the wort. The solid particles are collected as brewers' grains and used for other purposes, e.g. as animal feed or feedstock for biogas generation. The lautering process is followed by the **wort boiling**. Here, all enzymes are deactivated and the hops is added (either as extract, pellets, granulate or hop umbels). Afterwards, the trub is separated in a **whirlpool** or separator, the wort is **cooled** down, and the final wort is transferred into a fermentation tank. These tanks can be of different size, geometry and setup in vertical or horizontal direction. The most common form is the vertical cylindroconical tank (CCT) (Annemüller and Manger, 2009i; Speers and Stokes, 2009).

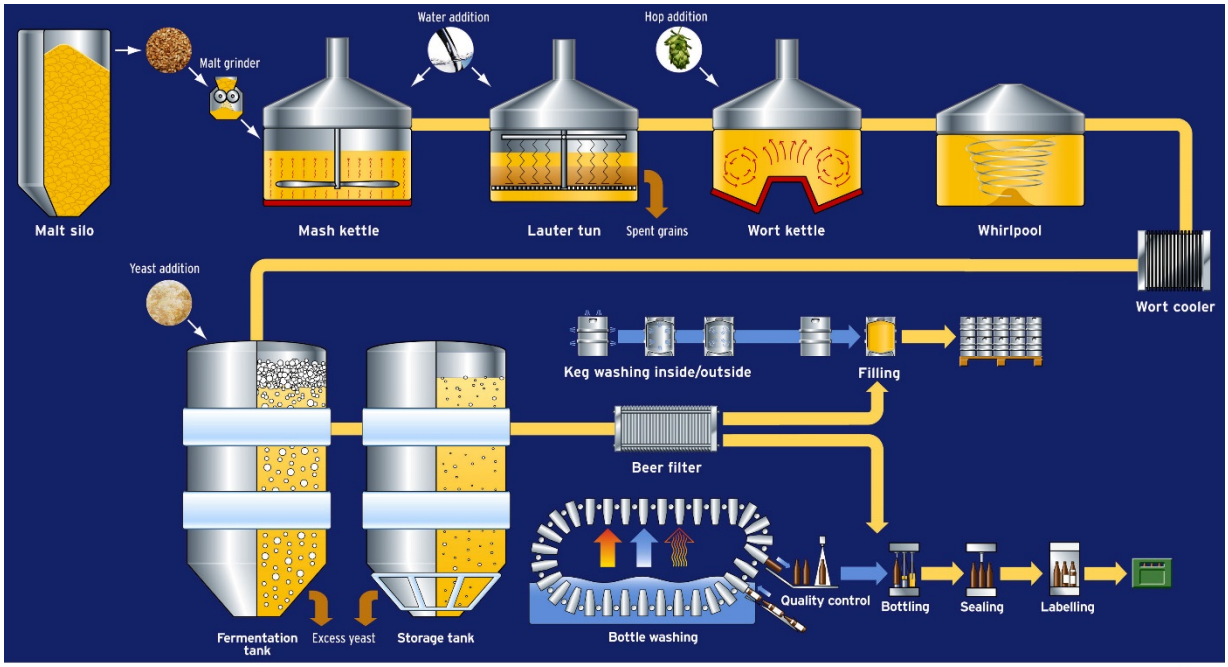

Fig. 1: The brewing process from brewing to bottling with permission of (Deutscher-Brauer-Bund-e.V., 2018).

At this time point, yeast cells are added and the **primary fermentation** starts. Yeast converts the sugars glucose, fructose, maltose and maltotriose in the given order into biomass, different alcohols, carbon dioxide and different flavor compounds (see 2.1.2 for more details). Various strains and species of yeast are used for beer brewing worldwide (Boulton and Quain, 2001a). The yeast type is of high importance since it has an impact on the amount of produced alcohols, carbon dioxide (CO_2), and flavor compounds as well as the growth and flocculation behavior. All these parameters can influence the medium density or the liquid flow and hence, the convection. Usually, the yeast is discarded after 5 - approx. 15 times of re-pitching (the reuse of yeast after a short regeneration in wort for the inoculation of a new brewing batch) in order to avoid mutations and contaminations (Boulton, 1991; Kobayashi et al., 2007; Powell and Diacetis, 2007). The reuse of the yeast cells, however, avoids the time-consuming propagation step for every single fermentation. The continuous propagation/curation

of pure yeast strains in parallel to the process is required in order to maintain viability and activity (Kobayashi et al., 2007; Raines, 2009). The extensive reuse of the same yeast cells might lead to stress (Jenkins et al., 2003), alterations in the protein expression level (Kobi et al., 2004) or of the cell physiology and cell surface (Smart, 2007) as well as to increased by-product formation (Kobayashi et al., 2007). Nevertheless, some authors claim that the same yeast cells can be reused up to 13 (Speers and Stokes, 2009) or even more than 100 times without relevant changes at the genetic level or in fermentation performance (Powell and Diacetis, 2007).

The growth temperature during propagation and fermentation differs naturally for each yeast strain (Abdel-Banat et al., 2010; Walsh and Martin, 1977), which has to be considered, if various strains are applied. Brewers' yeasts are divided into two main classes: top and bottom fermenting yeasts (see 2.1.2). Top fermenting yeast floats on the top of the liquid and has its optimal fermentation performance between 15 and 25 °C (Annemüller and Manger, 2009j). Bottom fermenting yeast settles down and optimally performs at lower temperatures during fermentation, i.e. 8 - 18 °C for industrial scale (Annemüller and Manger, 2009b).

With increasing temperature, the fermentation process becomes faster and less cost intensive due to decreased tank occupation. The amount of un-/wanted side products and flavor compounds, however, is increased by higher temperatures as well, e.g. diacetyl or esters (Boulton and Quain, 2001c; Saerens et al., 2008b; Suomalainen, 1981) as well as fusel alcohols (Institute-of-Brewing, 1976). Hence, a compromise between these aspects has to be found. The identification of a production process optimum might be supported by adequate process monitoring tools.

Beside the temperature and fluid flow in a vessel or the yeast strain, the fermentation time is influenced by the yeast vitality and concentration, the wort composition and gravity, the dissolved oxygen (DO) concentration at pitching, and pressure (Hoggan, 1977). Furthermore, the targeted quality of the beer and the market price as well as the storage capacity in a brewery influence the main fermentation time, which takes 3 - 6 days (for top fermenting yeast) or 6 - 12 days (for bottom fermenting yeast) (Annemüller and Manger, 2009c; Annemüller and Manger, 2009j). The fermentation itself consists of three main phases: filling of the tank with wort and yeast, start (acceleration) phase, and main fermentation phase. Different parameters, such as the amount of yeast and yeast aeration before pitching, original extract (OE) and the pH-value of the wort, the temperature regime, and the pressure have to be set for the fermentation process and differ for each type of beer and among different fermentation tanks and breweries. There are also tanks, which are open to the top. Hence, processes in these tanks can be performed only at hydrostatic pressure and might take longer.

After the primary fermentation the **secondary fermentation** starts, which is mainly a maturation and aroma stabilizing process (Willaert, 2007). The first step is the *diacetyl rest*, in which the temperature is increased by several degrees (e.g. to 12 - 18 °C for bottom fermentation) in order to accelerate the degradation of diacetyl by the yeast cells (Annemüller and Manger, 2009g). Diacetyl is causing an undesired butter-like aroma in the beer. Reaching the target temperature at larger volumes of several 100 m^3 already might last 1-2 days, followed by at least a day for the degradation. When the threshold value of total diacetyl (< 0,1 mg L^{-1} (Annemüller and Manger, 2009f)) is reached, the tank is *cooled* down stepwise to about 5 °C for first yeast sedimentation and harvest (Briggs et al., 2004).

At this point the *maturation* process of the "green" beer starts. This step can be conducted either directly in the fermentation tank or by transferring the beer into maturation tanks. During maturation (5 - 21 days depending on the method and volume) further undesired aroma compounds, which were produced during the fermentation, are degraded or converted (Annemüller and Manger, 2009f; Haukeli and Lie, 1978). Compounds responsible for the level of bitterness (trans-iso-alpha-acids) can

be converted into tri- and tetra-cyclic degradation products, especially at higher temperatures (Caballero et al., 2012; Intelmann et al., 2009; Pangborn et al., 1977). There are many more reactions, which form, convert or degrade certain substances with different intensity, depending on the maturation temperature (Vanderhaegen et al., 2006). Hence, this process is of high importance for the beer quality. It requires proper monitoring in order to avoid unnecessary maturation time and storage capacity on one side, and ensure the time needed for optimal maturation on the other side.
Then, the beer will be transferred into storage tanks, also called "lagering" tanks, for **final maturation** with even lower temperatures than 0 °C (e.g. -1 °C) in order to stop yeast activity (Böttcher and Meironke, 2012) and support sedimentation of protein and polyphenol compounds (Briggs et al., 2004). It remains there for several days or weeks for the following last steps: extract degradation to end level, binding of DCO_2, further degradation of off-flavor compounds, and excretion of desirable flavor-active compounds from the yeast (Annemüller and Manger, 2009h; Willaert, 2007).

The fermentation and maturation represent up to 91 – 94 % of the time required for conventional beer production and 85 – 90 % of the time for large-scale production. It consumes a lot of resources and energy, besides the mashing and wort boiling processes (Annemüller and Manger, 2009c). Nevertheless, only a limited number of process analytical tools is available for the process monitoring of this important stage of the brewing process (Daoud and Searle, 1990; Peris and Escuder-Gilabert, 2013). Mostly, only one temperature sensor is installed at one point of a large-scale reactor. Data obtained by a single sensor at one spot, however, are not representative for the major part of the liquid phase (see also section 2.2.2.).
There are *on-line* and *in-line* sensors available that measure the pH-value, dissolved oxygen (DO), DCO_2, redox potential, conductivity, temperature, pressure or biomass also in the brewing process and allow multi-parameter measurements directly in the liquid phase (Bockisch et al., 2014; Sachse et al., 2015). Nevertheless, the number of measurable parameters is still limited and there is a demand for sensors that are characterized by long-term stability, provide accurate measurements also at high cell or gas concentrations, and are equipped with wireless data transfer or at least can send data via cables across long distances (see also section 2.3.)

2.1.2. The Yeast Metabolism in Brewing Fermentation

2.1.2.1. Yeast Strains

The choice of strain is decisive for the beer flavor, beside the wort composition and fermentation temperature (Dack et al., 2017). The formation of aroma compounds such as fusel alcohols, fatty acids, esters, and phenols differs among various yeast strains and is further influenced by the maturation process (Annemüller et al., 2011; Suomalainen and Lehtonen, 1979). Even low-alcohol or alcohol-free beer can be produced with nearly the same flavor just by choosing the right strain, e.g. *Pichia kluyveri* species (Saerens and Swiegers, 2017).

As previously mentioned, top and bottom fermenting brewing yeasts are distinguished: Top fermenting yeast, e.g. *Saccharomyces cerevisiae* (*S. cerevisiae*), has an optimal fermentation performance at 15 - 25 °C (Annemueller and Manger, 2009i; Saerens et al., 2010) or 18 - 24 °C (Lodolo et al., 2008), depending on the strain. Bottom fermenting yeast, e.g. *Saccharomyces carlsbergensis* (*S. carlsbergensis*), optimally ferments between 8 and 18 °C (Annemueller and Manger, 2009a) or

8 and 15 °C (Saerens et al., 2010). *S. carlsbergensis*, mostly used in bottom fermenting brewing processes, is a hybrid strain of *S. cerevisiae* and *S. bayanus*, also known as *S. pastorianus* (Le Jeune et al., 2007; Lodolo et al., 2008; Saerens et al., 2010).
Propagation temperatures are higher, e.g. 20 - 25 °C for bottom fermenting yeast (Schmidt, 1993). Top fermenting strains can have a maximum growth temperature range of 35 - 43°C, whereas bottom fermenting strains do not grow above 35 °C (Marais, 2010).
Bottom fermenting yeast sediments and is kept in flow only by the convection movement caused by formation of dissolved carbon dioxide (DCO_2) bubbles and temperature gradients. Top fermenting yeast forms conglomerates, rises up and floats on the top of the liquid.

In the first two to four days of fermentation yeast cells are still growing and dividing. Since division occurs asymmetrically and growth asynchronously, the cell population is heterogeneous in this stage. This is true for both, top and bottom fermenting strains. The cells are in different morphologic phases within the cell division cycle, differ in cell size, and are characterized by different numbers of accomplished reproductions (Ginovart et al., 2011; Porro et al., 2009). The distribution of these parameters has an influence on the fermentation performance and changes during the fermentation.

The today's yeast propagation process for the production of alcoholic beverages and foodstuffs is based on methods developed between 1881 and 1883 to obtain pure cultures. The pure yeast strain *S. carlsbergensis* has been propagated firstly by Emil Christian Hansen from the Carlsberg using the pure culture method he developed between 1881 and 1883 (Bamforth, 2006; Dequin, 2001; Hansen, 1896). For the final method, a drop of gelatin containing nutrient medium and a diluted cell suspension was placed on a cover slide, which was separated into 16 squares of the same size. After the gelatin was cooled, the slide was placed (upside down) on a sterile moisture chamber (Böttcher's chamber). Incubation of the chamber at 25 °C allowed the cultivation and observation of cell multiplication from one single cell up to 8 days by means of a microscope (Guilliermond, 1920). In order to ensure that only one single cell will enter each of the squares on the slide, flasks containing sterile media were inoculated with diluted cells and vigorously shaken. After sedimentation of the cell(s), the number of cells on the bottom could be counted. Only flasks containing one cell were further used for the preparation of the cover slides (Hansen, 1896).
Methods for the isolation of pure yeast cultures that were easier to handle were developed by Paul Linder in 1893 (Lindner, 1893). The "drop culture" method served for pure yeast and bacteria cultivation and the droplet culture procedure for the observations of pure cultures under the microscope. The cells were diluted until each drop contained only one cell and then placed by a writing nib in a sterile petri dish with sterile medium for cultivation or a sterile object slide for microscopy. Hence, isolated pure cultures could be further cultivated in larger devices containing sterile medium (Guilliermond, 1920; Marschall, 2000; Umbreit, 1960). Lindner also developed other methods for systematization and taxonomy of microorganisms such as adhesion, stroke of a pen or brush stroke culture (Lindner, 1895; Marschall, 2000).
In the same years around 1895, Max Delbrück was developing "natural" pure yeast cultivation methods. During the 1st world war, lipid and protein sources were limited as well as the waste yeast from alcohol production. Hence, a cultivation method to increase the protein and lipid content in yeast for feeding and nutrition was developed. Mineral salts, such as ammonium, and molasses (waste from the sugar industry with 50 % sugar content) were used as a medium and the suspension was aerated at the fermentation start. Due to this, he also called the yeast noble fungus ("Edelpilz"). Additionally, the pH-value, alcohol content, temperature, yeast and carbohydrate concentration, nitrogen addition,

and aeration were optimized for enhanced yeast fermentation performance (Delbrück, 1898; Hayduck, 1920; Marschall, 2000). This method supported the yeast selection in a natural way by suppressing the growth of spoiling bacteria or unwanted yeast species (Hayduck, 1920; Marschall, 2000). The drying process of yeast, applied already before 1914, was another important invention for the constant supply with yeast for feeding and nutrition (Marschall, 2000). At this time the yeast strains were also distinguished according to their enzyme content and activity (Delbrück, 1898).
Later, his colleague Friedrich Hayduck improved the cultivation method in order to reach a higher biomass by the stepwise addition of a carbohydrate source to an aerated yeast suspension. This concept was patented in 1915 and the basis of today's fed-batch technology (Hayduck, 1915; Marschall, 2000; Subramanian, 2017). The basis was actually already invented by Rainer in 1887, but the added solution was diluted, not concentrated (Gélinas, 2014). The exact addition rates were determined in 1919 by Søren Sak (Gélinas, 2010).
Delbrück was also significantly involved in the foundation of the Gärungsgewerbe Berlin, the today's Versuchs- und Lehranstalt für Brauerei Berlin (VLB), including the department for pure yeast cultivation in 1892, which later supplied breweries with pure yeast cultures. Beside many publications in brewing magazines, journals, and books he established teaching and study courses for brewers and created the basis for the today so called brewing congress of the VLB in October ("Oktobertagung"), which connected people from the brewing industry with those from research and science (Hayduck, 1920).

2.1.2.2. Anaerobic, alcoholic Fermentation

The main task of yeast cells during the brewing process is the conversion of carbohydrates to alcohols, mainly ethanol, and carbon dioxide according to the following simplified equation (2.1):

$$C_6H_{12}O_6 + 2\,ADP + 2\,P_i \rightarrow 2\,C_2H_5OH + 2\,CO_2 + 2\,ATP + 2\,H_2O \qquad (2.1)$$

With $C_6H_{12}O_6$ = glucose, ADP = adenosine di-phosphate, P_i = inorganic phosphate, C_2H_5OH = ethanol, CO_2 = carbon dioxide, ATP = adenosine tri-phosphate, and H_2O = water.

In contrast to respiration under aerobic conditions only 2 molecules of ATP are produced (Lewis and Powell, 2017; Semkiv et al., 2016). Additionally, different metabolites are produced during this reaction, which influence the beer flavor.

Some yeast strains are capable to convert dextrin materials, such as *S. diastaticus* (a sub-species of *S. cerevisiae*) (Stewart et al., 2013). Most brewing yeast strains, however, cannot convert long-chain polysaccharides. These have to be degraded enzymatically during the milling process into chains of maximal three saccharides. The wort, i.e. the medium for yeast cells, contains the trisaccharide maltotriose, the disaccharides saccharose, maltose, and the monosaccharides galactose, fructose and glucose (Faria-Oliveira et al., 2013; Stewart, 2006; Stewart et al., 2013). These carbohydrates are then further degraded inside or hydrolyzed outside the cell (Fig. 2). Saccharose is degraded extracellularly to glucose and fructose by the enzyme invertase, maltose and maltotriose intracellularly by α-glucosidase (maltase) (Stewart et al., 2013). The monosaccharides glucose and fructose are utilized at first by the yeast, not only due their simpler molecule structure but also because they can pass the cell membrane via diffusion, mediated by specific hexose permeases without energy losses (Fig. 2). Larger saccharides, such as maltose and maltotriose, require energy (ATP conversion to ADP) for the active transport into the cell (Bisson et al., 1993). Further, the gene expression for the transporter and maltase is repressed by glucose (Stewart, 2016).

The first step of glucose conversion is the glycolysis, also called Embden-Meyerhof-Parnas pathway, in which 1 molecule of glucose is converted to 2 molecules of pyruvate, generating 2 molecules of ATP, NADH, and water, respectively (Fig. 2) (Semkiv et al., 2014). This step is followed by the conversion of pyruvate to 2 molecules of acetaldehyde and the release of 2 molecules of CO_2, catalyzed by the enzyme pyruvate decarboxylase. The last step is the conversion of acetaldehyde to ethanol by alcohol dehydrogenase using the NADH as a reducing agent that was generated in the first step (Stewart, 2016).

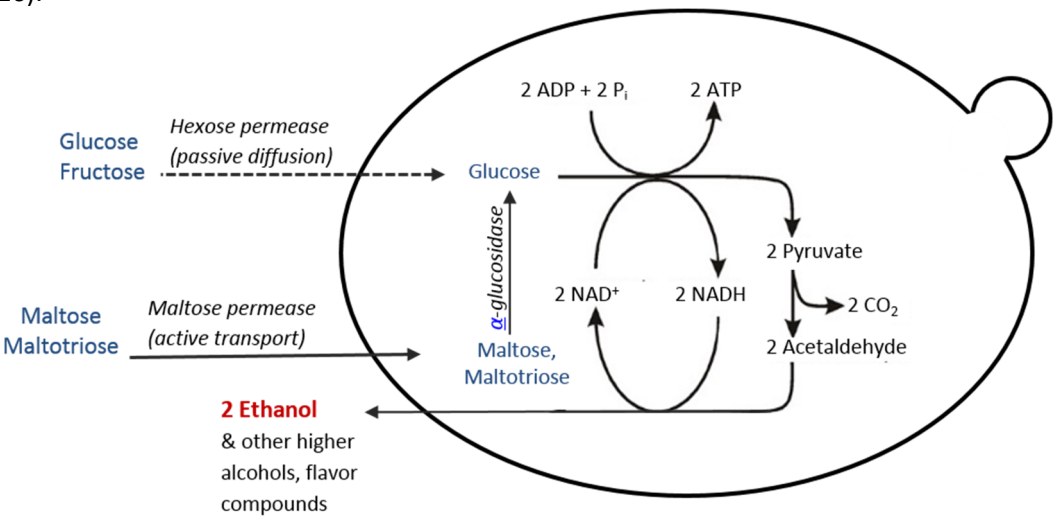

Fig. 2: Carbohydrate uptake and conversion to ethanol by a yeast cell.

This reaction shows that yeast can couple anabolism and catabolism. Organic molecules are used for both energy (ATP) generation by oxidation and as carbon sources for biosynthesis. There exist multiple carbon and energy sources for yeast, carbohydrates are preferred though. Alternatively, polyols, alcohols, organic acids, and amino acids can be metabolized by yeast as well, leading to changes in the aroma and flavor profile of a beer.

2.1.2.3. Aerobic Respiration and Sterol Biosynthesis

During aerobic fermentation or respiration in yeast 18 molecules of ATP are produced from one molecule of glucose, including 2 molecules of ATP from glycolysis (Pfeiffer and Morley, 2014). The amount depends on the specific phosphate/oxygen ratio of the organism, which is about 1.2 in *S. cerevisiae* (de Kok et al., 2012; Hinkle, 2005). In eukaryotes, however, up to 38 ATP can be produced during the overall respiration process (equation (2.2)), e.g. if ethanol is re-metabolized (Pfeiffer and Morley, 2014; Ring et al., 2012). In contrast as stated above, only 2 ATP are generated during alcoholic fermentation (Lewis and Powell, 2017; Semkiv et al., 2016).

$$C_6H_{12}O_6 + 6\,O_2 + 38\,ADP + 38\,P_i \rightarrow 6\,CO_2 + 6\,H_2O + 38\,ATP \qquad (2.2)$$

with $C_6H_{12}O_6$ = glucose, O_2 = oxygen, ADP = adenosine di-phosphate, P_i = inorganic phosphate, CO_2 = carbon dioxide, H_2O = water, and ATP = adenosine tri-phosphate.

It was shown that wort oxygenation significantly decreases the formation of esters, which is caused by a decreased expression of the alcohol acetyl transferase gene ATF1. Additionally, lower glycogen and trehalose levels (both stress indicating substances) were observed at the end of fermentation in case of the high cell density fermentations with oxygenated wort (Verbelen et al., 2009b). Further, oxygen

limitation negatively affects yeast vitality as well as fermentation rates and performance including the production of aroma compounds (Kucharczyk and Tuszyński, 2017; Rees and Stewart, 1999).

During yeast pitching and at the onset of the fermentation the supply of oxygen is further essential since the synthesis of unsaturated fatty acids, membrane lipids, and sterols requires oxygen (Annemüller et al., 2011). Sterols are essential for the stability of yeast cell membranes and their functionality, such as the membrane permeability or fluidity beside their importance for cell growth and budding (Sara Teixeira de et al., 2015; Stewart et al., 2013; Willaert, 2012). The membrane sterols directly influence the ion channel activity and therefore transport mechanisms (Al Khamici et al., 2016). Oxygen levels of 7 mg L^{-1} or lower during pitching and aeration can lead to impaired cell wall structure and stability during fermentation (Verbelen et al., 2009b).
In scale-down experiments with induced oxygen oscillations it was found that the sterol synthesis was even positively influenced by oscillating conditions. Especially the esterified content of some sterols was increased under these conditions, e.g. for ergosterol. If the cells were exposed to longer time frames of oxygen limitation (1 h), however, this accumulation was delayed and a higher accumulation of the precursor squalene was detected (Marbà-Ardebol et al., 2017). A high squalene content was also determined in the lipid fraction of a brewing yeast strain *S. uvarum* after usage in an industrial beer fermentation with 56 % of the neutral lipids and 33 % of total lipids (Blagovic et al., 2001). This high level might be a response and adaption to several stress factors during the brewing process, such as oxygen depletion. The lipid fraction was analyzed in *S. cerevisiae* after one, two, and three times re-usage in an industrial brewing process. The highest levels for squalene in the mitochondria and the plasma membrane were determined after re-pitching the yeast one and two times (Juresic et al., 2017).
Due to their function for membrane functionality, sterols also play a role in stress adaptation (Hu et al., 2017). In a study with *S. cerevisiae*, where the genes involved in ergosterol biosynthesis (ERG 2 – 6) were deleted, a higher sensitivity to salt stress or cationic drugs (hyperosmotic stress) and a lower resistance to antifungal drugs was observed (Kodedová and Sychrová, 2015).

The biosynthesis of ergosterol starts with acetyl-coenzyme A and consists of two main parts: the pre-squalene pathway with the synthesis of mevalonate and farnesyl pyrophosphate and the post-squalene pathway starting with the precursor squalene over free (unbound) lanosterol, dimethylzymosterol, zymosterol, fecosterol, and episterol with the final product ergosterol in yeast (Fig. 3) (Klug and Daum, 2014; Maczek, 2009). Squalene can be synthesized under aerobic an anaerobic conditions, whereas the post-squalene pathway requires oxygen (Hu et al., 2017; Maczek, 2009). The involved enzymes belong to the group of haem proteins, which obviously need oxygen (Boulton and Quain, 2001b). The required amount differs depending on the biosynthesis step: 1 O_2 molecule for the conversion of squalene to lanosterol, 9 O_2 molecules for the conversion of lanosterol to zymosterol, and 2 O_2 molecules for the synthesis of ergosterol (Maczek, 2009; Rosenfeld et al., 2003).

The “de novo” sterol synthesis is important for cell growth and polarization (Makushok et al.). High ergosterol and unsaturated fatty acid content (oleic acid) during the stationary phase lead to increased specific fermentation rates in yeast fermentation, when oxygen is added (Rosenfeld et al., 2003). This can be explained by the importance of free ergosterol for the membrane viscosity including the transmembrane transport system as stated above. The free intermediates zymosterol, fecosterol, and episterol are also integrated in smaller amounts into the lipid double layer of the membrane (Maczek, 2009). Without ergosterol, however, the cells are not viable and many stress responses depend on its presence, e.g. the synthesis of UV-absorbing or antioxidant compounds (Villarreal et al., 2016).

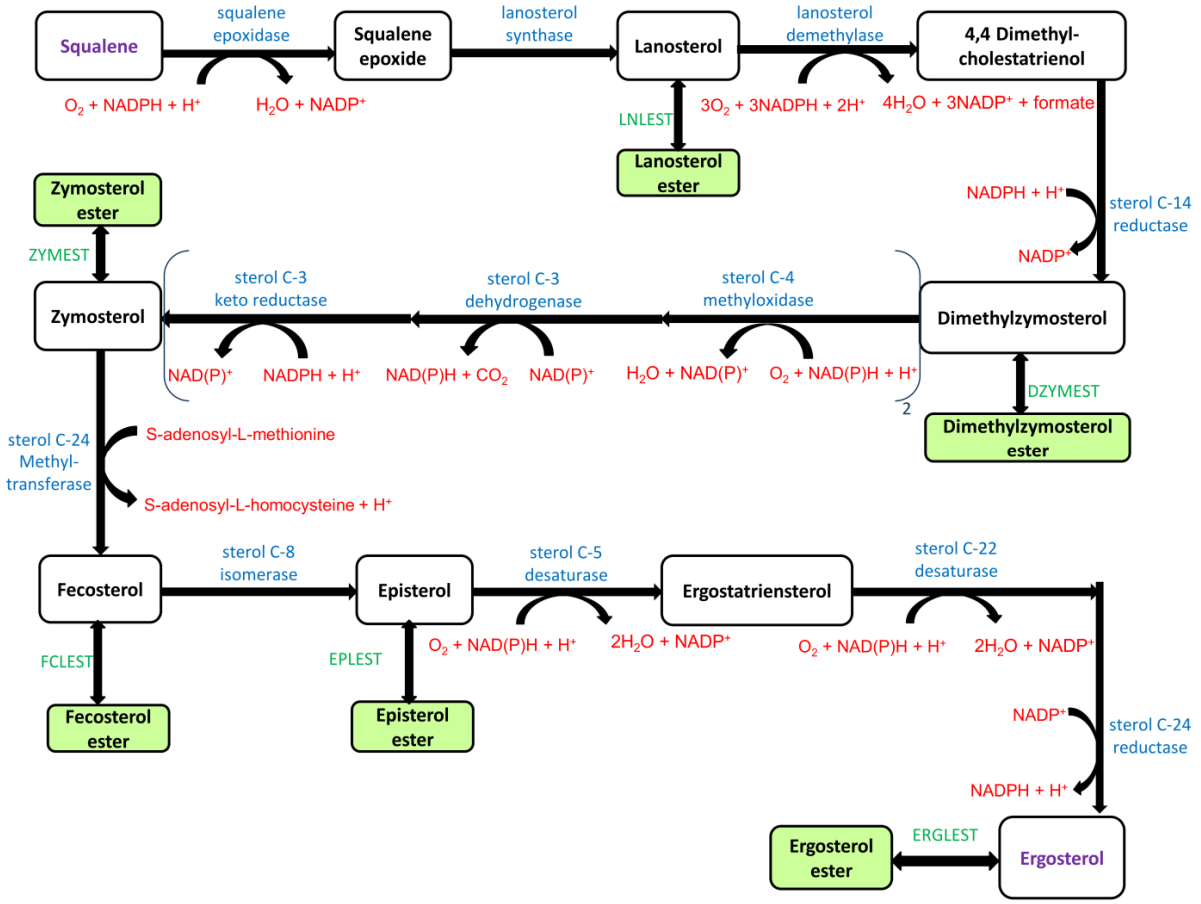

Fig. 3: Post-squalene biosynthesis of ergosterol in *S. cerevisiae*.
Enzymes involved in the biosynthesis of the intermediates towards ergosterol are indicated in blue, reaction and cofactors in red. The synthesis of the sterol esters (green boxes) is catalyzed by sterol-ester synthases (EC. 2.3.1.26), written in green. The oxygen plays an essential role in several steps of the sterol biosynthesis. Graphic based on (Caspeta et al., 2014; Fraser et al., 2010; Mo and Bard, 2005).

The content of esterified sterols is determined by the difference in the content of total and free (non-esterified) sterols. Esterified sterols can be stored as a reserve in lipid particles with a higher amount than the free sterols (Maczek et al., 2006). Since the esterification of the intermediates is located at the free hydroxyl group, squalene cannot be esterified. Sterol esterification does not require oxygen. Usually, the sterol esterification rate and ester content increase with the start of the stationary phase (Bailey and Parks, 1975; Boulton and Quain, 2001b). If the sterol esterification is inhibited, the sterol biosynthesis is down-regulated, leading to a decrease of the total intracellular sterol content (Arthington-Skaggs et al., 1996). In order to use the stored esterified sterols for the metabolism in case of low availability of free sterols, they can be hydrolyzed by membrane bound enzymes (Maczek, 2009).

If sterols are lacking due to inhibited zymosterol synthesis and further interruption of the ergosterol synthesis pathway, cells are not viable, unless sterols are added to the medium. Exogenous sterol uptake, however, only occurs at oxygen depletion (Boulton and Quain, 2001b). Growth and polarizability decrease whenever lanosterol is lacking. Nevertheless, zymosterol covers most of the functionalities, even if the long synthesis way to ergosterol is not completed (Klug and Daum, 2014).
In case of too high levels of free sterols, cells can esterify free sterols as mentioned above. This protects the cells against damage of the lipid membranes by exceeded levels of free sterols and maintains the required sterol level for membrane stability (Maczek, 2009). Further, the sterol biosynthesis can be

down-regulated or sterols can be acetylated in case of sterol excess and further secreted into the medium in order to avoid toxification (Ploier et al., 2014). Since sterols are insoluble, their transport or secretion needs active transporters. Sterols can further be stored in lipid droplets (Hu et al., 2017).

The oxygen solubility is reduced in higher-gravity worts, which are often applied in industry due to their economical benefit. These media are characterized by higher levels of dissolved carbohydrates, leading to higher oxygen demand during catabolism and oxygen limitation. In order to avoid these limitations, the addition of unsaturated fatty acids to wort was suggested as an alternative to oxygenation. Studies testing the effect of the supplementation of unsaturated fatty acids to cropped yeast under anaerobic conditions on the following fermentation performance were performed (He et al., 2014; Moonjai et al., 2002). It was found that the ratio of unsaturated fatty acids to total fatty acids increased from 0.53 to 0.66 and the ratio of trehalose to glycogen increased from 0.17 to 0.49. Cell growth and attenuation was similar to the values obtained by pre-aeration of cropped yeast. The ester content instead, was reduced by 22 % in the fermentation with the supplemented culture.

Although during aerobic respiration more molecules of ATP are produced, Crabtree-positive yeasts can use the fermentation mode for energy generation, i.e. produce ethanol, even if oxygen is present (Pfeiffer and Morley, 2014). In this case the respiratory activity is repressed by higher levels of glucose. This can be the case at the onset of a brewing fermentation (Lodolo et al., 2008). Oxygen at later stages should be avoided though since it might lead to the formation of off-flavors, e.g. increased concentrations of acetaldehyde, which is formed by the oxidation of ethanol.

2.1.2.4. Wort Composition and Metabolic Conversion

Beside carbohydrates yeast also requires the following substances for growth and high fermentation performance: nitrogen sources, fatty acids, vitamins, ions, and minerals. Apart from the yeast strain and (bio-)chemical reactions during maturation, the wort composition strongly influences the beer aroma and flavor, mainly due to the formation of esters and alcohols (He et al., 2014). Unbalanced levels of these volatile compounds lead to an unpleasant beer flavor without further process regulation (Dragone et al., 2007; He et al., 2014).

The carbohydrate source influences the amount of most volatile compounds. The level of volatile compounds was proven to be lower with maltose than with glucose and fructose (Engan, 1972; Younis and Stewart, 1998). At higher overall levels of carbohydrates, i.e. high gravity worts with 16 - 18 % of dissolved solids, alcohol and acetate ester levels are generally increased (Anderson and Kirsop, 1974; Dragone et al., 2007). At higher gravities of 18 - 24 % the influence of the carbohydrate source (e.g. maltose, glucose, saccharose) can even be different than at lower gravities (Lei et al., 2016). Hence, the optimal fermentable sugars have to be selected according to the wort gravity beside the consideration of the strain specificity.

The free amino nitrogen (FAN) content is essential for yeast growth and the synthesis of by-products, influencing beer flavor and stability. With increasing FAN levels, higher production rates and concentrations of isoamyl acetate (Hashimoto et al., 2012) or acetate esters in general were detected (Saerens et al., 2008a). Since the FAN content affects the transcription of genes that are related to ester and higher alcohol formation (Lei et al., 2012; Saerens et al., 2008b), it has an impact on the beer flavor. Different branched-chain amino acids were proven to increase ester and alcohol formation, e.g. histidine (Lei et al., 2013) and leucine (Hashimoto et al., 2012), or decrease the levels such as valine (Hashimoto et al., 2012). A low FAN content in combination to high gravity, however, leads to increased

ester and alcohol levels as well. Further, cell growth, viability, flocculation, gene expression, and sugar and amino acid uptake are increased at these conditions (Lei et al., 2012).
An increasing amount of unsaturated fatty acids (UFAs) in the fermentation medium results in a decrease in ethyl and acetate ester synthesis, while increasing fermentation temperatures lead to the opposite (Saerens et al., 2008a). The expression of genes responsible for the ester formation are repressed in the presence of UFAs (Saerens et al., 2010).
Vitamins and ions are necessary for the functionality of enzymes and coenzymes. Therefore, their presence indirectly influences beer quality and flavor as well due to the impact on yeast growth, metabolic activity, and fermentation performance (Walker, 2004).

2.1.2.5. Yeast Viability, Vitality, and Stress Factors

The yeast quality in the brewing industry is defined by its activity and production rate during fermentation and maturation, the resulting beer quality including flavor and aroma compounds as well as the number of re-pitchings without quality losses (Annemüller and Manger, 2009a; Stewart, 2016). In contrast to the viability, which is a measure for the ratio of living and dead cells, the vitality describes the physiological cell state, the metabolic activity, and the capability of reproduction. Several factors during a brewing process can cause cell stress and impact cell viability and vitality. Hence, vitality also includes the ability of yeast to handle different stress situations while still reproducing and performing at the aimed level (Thiele, 2006).

The fermentation performance of a yeast strain can be influenced by the medium composition / uptake of nutrients (carbohydrates, amino acids, peptides), osmotic pressure, oxygen availability, alcohol tolerance, and flocculation behavior (Stewart, 2016). Osmotic pressure is caused by high carbohydrate concentrations or high ethanol content, which can also provoke a toxic effect. Yeast flocculation is an asexual aggregation, which is based on the Ca^{2+}-dependent interaction between lectins, i.e. flocculins, and cell wall polysaccharides such as mannans and glucans. Lectins bind specifically to carbohydrates located on the cell surface. Hence, the flocculation behavior and intensity depends on the type of carbohydrates (Nayyar et al., 2017). It was found that the stress tolerance against ethanol, high temperatures, and acetic acid in yeast can be increased by the addition of zinc. Additionally, a gene (*FLO1*) responsible for flocculation in certain yeast strains was related to increased tolerance to acetic acid and ethanol (Cheng et al., 2017).
Further, very low or high temperatures, changes in the pH-value, oxidative stress or hydrostatic pressure due to the large liquid volume in large-scale fermentations can cause stress in yeast cells leading to a decrease in cell vitality and viability, fermentation performance as well as productivity.
Insufficient mixing decreases the mass transfer and leads to heterogeneities in nutrients, temperature, pH-value, oxygen, DCO_2 and yeast cells. This increases the stress level further (Annemüller et al., 2011; Annemüller and Manger, 2009a). The influences of gradients, with focus on the process parameters measured in this work, on the cell and their stress responses are discussed in detail in the discussion section.

2.1.3. Geometry of Brewing Vessels

The choice of the vessel geometry is of importance for the brewing process since it has an impact on the yeast performance and fluid flow (Caballero et al., 2016). During the long tradition of beer brewing various vessel forms of different volumes were developed, made of different materials such as wood, welded aluminum, enamel-lined steel, coated steel or chromium-nickel coated steel (Maule, 1986). Until the beginning of the 20th century open fermentation vessels, often constructed as horizontal tanks, were used (Annemüller and Manger, 2009i). The fermentation of Gueuze beer in Belgium is even nowadays conducted in open tanks. At Heineken, still horizontal but closed fermentation tanks are used. Due to the low height to diameter (H/D) ratio, the surface is much larger allowing an intensive exchange between liquid and gas phase. Hence, oxygen transfer is enhanced at the onset of the fermentation, whereas the hydrostatic pressure on the yeast cells is low during fermentation. These two aspects and the type of yeast, the Heineken “A-yeast”, lead to a higher production of esters, resulting in a fruity banana note (Difford's-Guide).

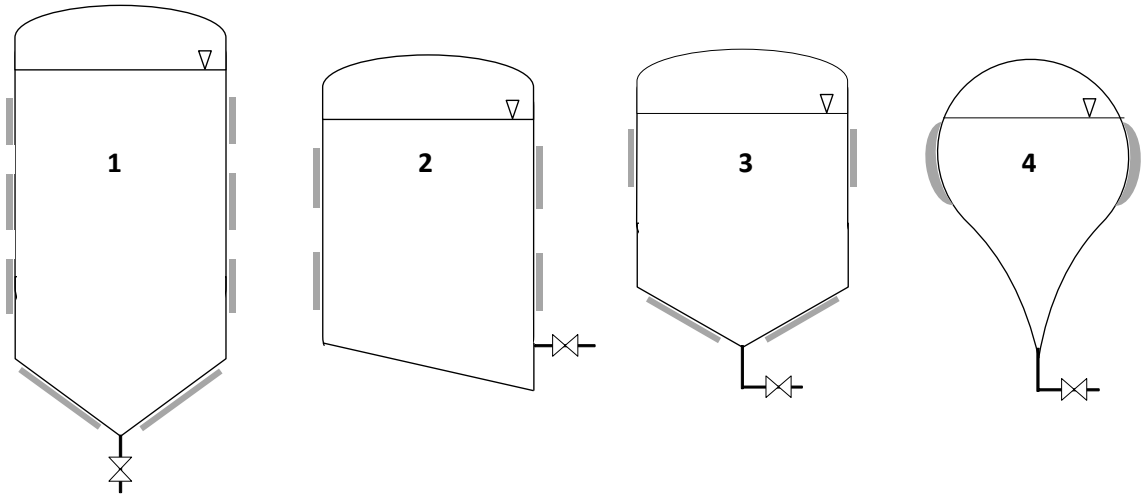

Fig. 4: Comparison of different closed, vertical tanks.
Each grey field indicates one cooling zone. 1: CCT, 2: Asahi tank, 3: Unitank, 4: Spheroconical tank. Based on (Annemüller and Manger, 2009i).

The first closed vertical fermentation tank in a CCT form was developed by Dr. Leopold Nathan (Wackerbauer, 1995). He held two patents in 1908 and 1927. In 1930, it was possible to well aluminum. In the following years, tanks with a volume of up to 10 m^3 were made of aluminium (Maule, 1986; Nathan, 1930). Already in the 1960s, this vessel form was established with a volume of up to 320 m^3 at the Whitbread's Luton Brewery in the United Kingdom (Maule, 1976).
Along with the invention of the vertically installed CCT, other closed tank forms were entering the market worldwide (Fig. 4), which have many advantages in comparison to open brewing vessels, e.g. the lower risk of contamination and contact with oxygen, which influences the beer stability (Annemüller and Manger, 2009i). In Japan, the first “Asahi tank” was installed in 1965 in the Asahi brewery, in America the "Unitank” was used in 1968 for the first time in the Rainier brewery, and in Spain the “spheroconical tank” was established in 1972 (Annemüller and Manger, 2009i; Maule, 1986). All these forms are characterized by different H/D ratios, cooling zones, and conus angles for yeast recovery (Fig. 4). The Asahi tank, however, does not allow a one-tank procedure for fermentation and maturation and yeast recovery is difficult due to the lacking cone. Further, overpressure for CO_2 capture cannot be applied. Nevertheless, the investment for this and the Unitank are lower in comparison to the other two designs due to the thinner wall construction (Wackerbauer, 1995). The

Unitank allows the operation of fermentation, maturation, and cold conditioning in a single vessel. The spheroconical tank also allows for the conduction of several process steps in one tank. In contrast to other tank designs however, it provides the best ratio of surface area to volume, minimizing cleaning and operation costs. Further, the spherical form leads to reduced foam formation and allows for the application of high pressure for CO_2 saturation, e.g. during lagering (Martin et al., 1975). The construction, however, is more complex causing higher investment costs (Hoggan, 1977; Maule, 1986). This might be the reason why this form was used in the commercial scale in Spain only.

Nevertheless, the CCT prevailed and is used in most of the breweries nowadays. There are many arguments for the use of the CCT form as stated already by Nathan (Maule, 1986; Nathan, 1930), despite the fact the investment costs for such a tank are not low in comparison to some other geometries (Wackerbauer, 1969). The CCT geometry and material has the following technical and economical advantages in comparison to other tank designs according to literature (Boulton, 1991; Hoggan, 1977; Maule, 1986; Shardlow, 1972; Stewart et al., 2013; Wackerbauer, 1969):

1) Lower operating costs;
2) Minimized space requirements due to the vertical installation (also outdoor) and one-tank-procedure (fermentation, first maturation and cold conditioning in one tank);
3) Better mixing due to improved fluid flow by rising gas bubbles (convection) → faster fermentation and reduced process time;
4) Improved temperature control due to the slender shape / lower diameter of the vessel and separated cooling zones;
5) Increased foam stability and decreased losses of hop flavor compounds (isohumulones);
6) Easier filling, emptying and cleaning in place (CIP), also with hot detergents → tank can be used flexibly for different beer types;
7) Facilitated yeast separation and recovery from the cone, which allows to use the same tank for fermentation and maturation; and
8) Higher CO_2 release due to the different fluid flow in this tank form and the possibility of CO_2 collection well as the application of top pressure due to the stable material (stainless steel).

Concerning the investigation of gradients, especially points 3) and 4) and the increased CO_2 release (i.e. the formation of bubbles) are of interest. Wackerbauer and co-authors (1969) confirmed these aspects (1-8) comparing important fermentation parameters during fermentation in a cylindroconical and an open barrel-formed vessel with a volume of 25 m^3 under the same process conditions, respectively.

In order to make use of these advantages and support mixing, the ratio of fluid height to diameter shall be optimized. The optimal ratio is described differently in literature and seems to increase during the decades due to technical developments: 1.5:1 (Unterstein, 1986), 3:1 (Boulton, 1991) or ≤ 5:1 (Annemüller and Manger, 2009i). Depending on this ratio, the cone shall have an angle of 60°-70° (max. 90°) in order to support convection (see 2.2.2), allow fast yeast sedimentation and recovery and facilitate cleaning (Annemüller and Manger, 2009d; Boulton, 1991; Maule, 1986).

Beside the vessel dimensions, the fermentation and head space volume also have an influence on certain fermentation parameters, e.g. the temperature distribution, pH-value or the apparent extract (Speers and Stokes, 2009). In tanks with large volumes, the number of cooling jackets and the spots for their installation increases. There should be at least two side jackets to ensure proper cooling

during the chilling process and temperature control during fermentation and maturation for both, bottom and top fermenting yeast. One should be located at the lower and one at the upper part (Maule, 1976). Unterstein proposes even three to four cooling zones, which are well distributed along the tank height and equipped with a temperature sensor and controller, respectively (Unterstein, 1986). It is also advantageous to install a cone cooling jacket for mixing the volume at the end of the fermentation and during storage since the formation of CO_2 bubbles by yeast and therefore the convection in a tank is reduced (Wackerbauer, 1995). Nevertheless, still some heat energy is released in the cone, which requires proper cooling at this zone anyway (Maule, 1976).

2.1.4. The Beer Market in Europe and the World

The beer production represents one of the most important biological processes in terms of turnover and size. Nevertheless, during the past 7 years, a slight decrease in the beer and shandies consumption and a slight increase in the consumption of low calorie drinks with nutritional benefit is observed in some countries within Europe, which were considered as traditional beer drinking nations, e.g. Germany, United Kingdom, and Belgium, respectively. In contrast, the beer consumption increased in countries, in which other alcoholic drinks such as wine or vodka were consumed to a greater extend in former times, e.g. Russia, China, Italy or Spain (Colen and Swinnen, 2016). This might be also related to the economic situation of costumers (Poelmans and Swinnen, 2012). The highest number of breweries, including microbreweries, is found in Germany and the United Kingdom (Van de Walle, 2014). Despite the slight decrease in total consumption, there is an increasing demand for hand-crafted beer, produced in micro-breweries. In the past 10 years, the number of breweries in Germany with a production of up to 100,000 m^3 per year increased to about 740 in 2016. Instead, the numbers for breweries with larger production volumes per year remained nearly constant (Statista, 2018a; Statista, 2018b).

Beer production in these craft breweries is often characterized by low production volumes, high variations and flexible production. Hence, beers from these breweries often have a taste that differs quite a lot from established brands, making them individually recognizable by the consumer. They often emphasize their high quality and regional roots in marketing strategies, supporting an increasing requested by consumers (Witham, 2015). This change of the beer market situation is especially obvious in case of Germany (Adams, 2006).

The majority part of consumed beer, however, is still produced in large-scale fermentation plants due to a fully developed distribution grid, marketing efforts, a lower price level compared to craft beers and a comparably good reputation at the customers. Nevertheless, the market has been under consolidation for a further increase of cost efficiency in the past decades, which has yielded to mergers and acquisitions forming large, world-wide operating enterprises, e.g. Anheuser-Busch, Radeberger Gruppe KG, Bitburger Braugruppe, and others (Swinnen, 2012). Some of them also entered the market of craft-brewing in order to increase their market shares (Tremblay and Tremblay, 2005).

Since the customer is expecting high quality standards for every type of beer, breweries are forced to improve their processes for stable operation and increased product quality, while reducing production time and costs. This is conducted for example with:

- an improved raw material yield,
- more efficient interconnection of process steps,

- integration of monitoring methods and automation or
- higher substrate conversion rates and temperatures.

The two latter ones affect the yeast performance, and therefore the whole process including the product quality. In order to monitor process states and disturbances rapidly, adequate sensor technology, which can be applied *in-line*, *on-line* or at least *at-line* to gain data in *real-time* is required.

2.2. Mixing in the Brewing Process

2.2.1. Large-scale Processes

Fermentation processes can be divided into batch, fed-batch or continuous processes (Johnson, 1987). In the **batch** operation mode, there is no substrate added and no product recovered until the end of the process, i.e. there is no external flow in or out. The advantage is the risk reduction of contamination is low. Nevertheless, there is no possibility of process regulation apart from aeration, agitation, and temperature.

The brewing process, as subject of this thesis, is in most cases a batch process. The tank is filled once with wort and yeast and the product and yeast cells are harvested only at the end of the process for reuse (Buhligen et al., 2014).

In a **fed-batch** mode, substrate is added (flow in). This feed rate can be adopted. Thereby, the process can be regulated and operated with substrate limitation in order to avoid oxygen depletion, side product formation, osmotic stress, or even catabolic repression. The fed-batch process is the standard operation mode used for aerobic cultivations of yeast (Badotti et al., 2008; Unrean and Nguyen, 2013) or bacteria (Åkesson et al., 2001; Wang et al., 2015b). The product is generally not removed until the end of the process (Yamanè and Shimizu, 1984). High cell densities, providing higher product yields, can be reached in a fed-batch without oxygen limitation in bacterial (Restaino et al., 2013; Sohoni et al., 2015) or yeast cultivations (Min-hua et al., 2013; Vu and Kim, 2009).

The fed-batch mode is also applied for anaerobic processes. In anaerobic fed-batch processes with *Clostridium butyricum* the production process of 1,3-propanediol from the waste compound glycerin (from biodiesel production) was improved, reaching 71 g L^{-1} in a reactor with 6.6 L volume. The glycerin concentration in the feed was 50 g L^{-1}. The product can be used as a chemical agent in organic synthesis, e.g. in the production of biodegradable polymers (Lin et al., 2017). Fed-batch cultivations with the bacterium *Ralstonia eutropha* were used for polyhydroxyalkanoate (PHA) production, reaching concentrations of about 0.60 g_{PHAs} g_{VFAs}^{-1} (VFAs: volatile fatty acids). A stream containing 63 g L^{-1} carboxylic acids served as a feeding solution during the production phase (2nd phase) under NH_4^+ - limitation. The feed was added after the growth phase (1st phase), which was run under aerobic conditions, as soon as the glucose was nearly consumed (0.1 g L^{-1}) (Domingos et al., 2018).

For the brewing process, some fed-batch approaches can be found in literature for high gravity fermentations in the laboratory scale (Lin et al., 2014; Vu and Viet Man Le, 2010). There are, however, some challenges such as the increased fermentation times in the range of days (Vu and Viet Man Le, 2010), during which the main products CO_2 and ethanol might accumulate and inhibit the maturation of yeast. On the other side, enhanced yeast growth was detected in a study of Lin and co-authors (2014). This led to the production of unwanted off-flavors (e.g. diacetyl), higher alcohols and esters,

which negatively influenced the flavor profile of the product. The feeding solution was a glucose syrup, added in the end of the primary fermentation as soon as the original glucose concentration decreased to 10 g L^{-1} in the 7.5 L working volume. The maximum final ethanol concentration in the green beer was determined with 67.9 g L^{-1}. By increasing the OE to 15 °P and the yeast concentration for pitching to 2 × 10^7 cells mL^{-1} and lowering the fermentation temperature to 10 °C, the production of unwanted side products could be reduced. Nevertheless, long maturation times of up to 12 days were needed to decompose compounds such as acetaldehyde until a concentration below the quality threshold was reached (Lin et al., 2014).
In order to reduce the stress for the yeast cells caused by high carbohydrate concentrations in high gravity fermentations, 1.5 L of a feed solution was added after 108 h of fermentation time to 1.5 L wort with an OE of 15.5 °P. The feed did not only contain glucose syrup but consisted of wort (23.3°P), 30 % maltose syrup adjunct, yeast extract (optimum at 0.25 % (w/v) and Tween 80 (optimum at 0.8 % (v/v). Under these conditions the yeast fermentation performance was increased, the fermentation time was decreased, and higher ethanol concentrations were yielded (8.73 % (v/v) (Vu and Viet Man Le, 2010).
Scale-up investigations of these experiments, however, have not been performed. In the industrial scale (up to several 100 m^3), the occurrence of spatial gradients at the feed site is very likely, as the brewing process is a non-stirred process and often operated at very large scales.

There is a time frame in batch and fed-batch processes, in which no production is conducted due to cleaning, sterilization and refilling of the reactor. This can be overcome with a **continuous** operation mode, in which a continuous nutrient supply (flow in) and product recovery (flow out) takes places and steady state conditions can be achieved (Chicoye et al., 1978). This allows for higher volumetric productivity, e.g. in baker's yeast fermentation (Kariminiaae-Hamedaani et al., 2005). Furthermore, the costs for the substrate utilized only for biomass production are reduced since the growth phase is not separated from the production phase as in the other operation modes. Challenging are mutations of the microorganisms during long-term cultivation, contamination, cell aging or the control of the optimal dilution rate for cell growth and maximum production rate.

Some attempts of continuous beer fermentation have been made using immobilized yeast cells, which show a lower accumulation of toxic metabolites, lower operating costs, and a high volumetric productivity (Stewart et al., 2013). As fermentation system an air-lift reactor can be applied (Brányik et al., 2002). Maule reviewed other possibilities such as the installation of a series of fermenters in a cascade or the use of membrane or tower fermenters (Maule, 1986).
The continuous process mode might shorten the fermentation and maturation time from weeks to days as it was shown by Kronlöf and co-authors (1992). This group used a modified yeast strain and immobilized it on packed bed reactors of 1.6, 5, and 25 L volume for continuous fermentation. The strain is expressing the enzyme α-acetolactate decarboxylase, which directly converts α-acetolactate to acetoin without the synthesis of diacetyl. Diacetyl is provoking an off-flavor in the green beer, which has to be decomposed again in the maturation phase. Hence, this time-consuming phase can be omitted with the presented method (Kronlöf et al., 1998; Kronlöf and Linko, 1992).
Despite the higher production rate and reduced fermentation time, however, many challenges occur during a continuous process, e.g. the removal of CO_2 in the headspace, clogging of the tank, contamination, excess of biomass or wash out, and the formation of off-flavors due to cell changes and aging over time as a result of immobilization (Brányik et al., 2005; Verbelen et al., 2006). The flavor can be controlled partially by the wort aeration before pitching. A finnish group investigated how different

aeration strategies affect immobilized yeast during the primary fermentation in a continuous process and the resulting flavor profile (Virkajärvi et al., 1999). Two packed bed reactors and a buffer tank were used. Porous glass beads (Siran) served as carrier material. Mixed air with changing rates of synthetic air and CO_2 was used for wort aeration right at the precolumn (before the 1st reactor), while the feeding rate with wort remained constant. An air feed with low carbon dioxide content stimulated the 3-methyl butyl acetate production in the precolumn, whereas the air feed rates did not affect the aroma profile in the main column (Virkajärvi et al., 1999). The stability of this continuous fermentation cultivation method was tested before and approved to be stable for more than 14 month regarding contamination and flavor stability except of two compounds (ethyl acetate and propanol) (Virkajärvi and Kronlöf, 1998). Beside porous glass beads, other carrier materials, namely diethyl-aminoethyl-cellulose and diatomaceous earth, were tested regarding their influence on the beer flavor in tubular reactors with a volume of 1.6 L (Virkajärvi and Pohjala, 2000). The results indicated that the optimal carrier material depends on the yeast strain and the desired beer flavor and properties.

2.2.2. Natural Convection and Mixing in the Brewing Process

For this study, the brewing process was selected as a model process for large-scale processes since it is usually an unstirred process. Consequently, it is of special interest for the investigation of spatial gradients and inhomogeneities. The liquid phase in a brewing vessel is only mixed by natural convection, due to CO_2 (i.e. bubble) formation by yeast and due to temperature and density gradients (McLeod et al., 2009; Schuch, 1996d). Already Delbrück realized in the 19th century that the yeast activity is decisive for the convection flow inside a vessel, beside factors like the viscosity of the medium, the temperature, the aeration mode and intensity, the vessel geometry as well as the application of pressure during fermentation (Hayduck, 1920).

Temperature gradients are induced with the cooling system (downwards movement of the liquid at the reactor wall) and the heat produced by yeast (upwards movement in the center of the reactor) (Nienow et al., 2010). Since the beer has a maximum density at about 3 °C, the volume will fall down from the cooling layer when reaching this temperature and rise below and above this temperature, provoking a constant movement of the liquid phase (Maule, 1976) and leading to the formation of local streams. This was proven in a model tank of 20 L by light section technology using flour as a tracer in water. In this method, a light section is generated in the fluid by a laser (e.g. Argon, 100 mW) and the light reflected from the particles that pass the section is detected (Schuch and Denk, 1996).

Since the CO_2 (bubble) formation, the main driver for fluid motion, and the amount of produced heat strongly depends on the metabolic activity at the different cell growth phases, the local power input and fluid flow is uneven during fermentation (Boswell et al., 2003b). This might lead to an uneven distribution of nutrients, DCO_2, ethanol, pH-value or yeast cell concentration and consequently to the formation of gradients (García et al., 1994). It is even more likely in zones, where wort and yeast are added during the fermentation onset, e.g. at the bottom part of the fermenter. In turn, the amount of yeast cells in motion is influencing the degradation velocity of carbohydrates during fermentation and off-flavor compounds during the maturation (Schuch, 1996a). This might lead to additional local concentration gradients. It also has an impact on the amount of evolved CO_2 and ethanol since the degradation of carbohydrates is directly correlated to these parameters (Daoud and Searle, 1990; Garcia et al., 1993) (see also chapter 2.1.2).

The CO_2 formation in a brewing tank is not only depended on the yeast activity, including the production rate of CO_2, and the H/D ratio of a tank but also from the bottom form of a fermenter. This

was investigated already by Delente and co-authors who optically measured the fluid flow velocity in relation to the filling height in a brewing fermentation. They used a glass cuvette of 10 X 10 X 10 mm as a minireactor and optical methods for the examination of the bubble movement and volumes. By relating the bubble agitation power to the fermentation parameters, the group determined a velocity of 0.15 m s^{-1} at a fluid height of 9 m and a velocity of 0.23 m s^{-1} at a fluid height of 27 m (Delente et al., 1969). According to this study, CO_2 is released always at the lowest position of a tank (Fig. 5).
Nowadays, it is known that this release occurs unsteady and at random positions of a tank. Important to consider during tank construction is the hydrostatic pressure that limits the velocity of the rising gas bubbles. Hence, tanks of a certain diameter (e.g. 4.2 m) and conus angle (e.g. ≥ 60°) are limited in height (e.g. 25 – 30 m) in order to support this natural convection movement (Borkmann et al., 1978).

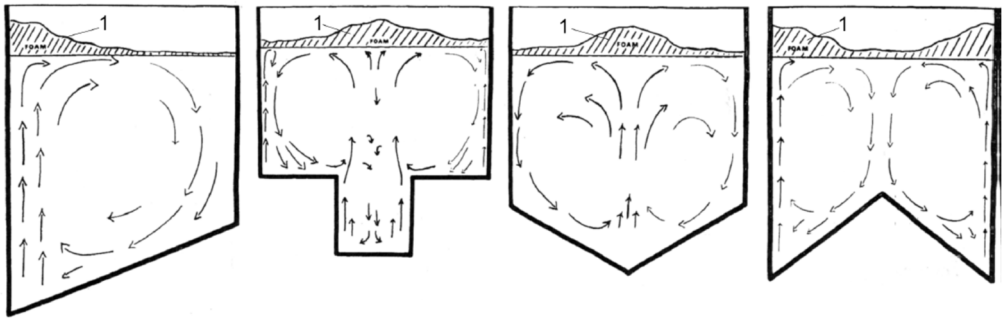

Fig. 5: Influence of the bottom form of a tank on the CO_2 release and fluid flow
according to (Delente et al., 1969), modified by (Annemüller and Manger, 2009g). 1 indicates the foam layer.

In large-scale brewing processes, the tank is filled with several brews over several hours. Only the first brew contains yeast cells. Hence, it is likely that the first batch has already started to ferment when the next brew is filled in. Consequently, two separated fermentations can be present simultaneously, which are characterized by different densities, temperatures, amounts of nutrients or cell count. This phenomenon is called stratification (Kapral, 2008). Both layers mix or “turn over” when a certain cell density is reached in the region with lower fermentation rate, i.e. the brew without yeast addition. The higher metabolic activity evokes higher CO_2 and heat generation, and thus a lower density as colder zones with lower gas formation. Cold zones are also evolved by the constant cooling power of the cooling jackets. This phenomenon was proven in studies, in which sampling was conducted at different heights of the reactor after the layers were mixed, detecting a sudden temperature and CO_2 shift in certain zones (Kapral, 2008). This can change during fermentation as there are different stages, in which critical conditions appear in certain zones (e.g. too low/high cell concentration, low metabolic activity and carbohydrate conversion rate, etc.), influencing process efficiency.

Several discussions about the sufficiency of the power input by CO_2 bubble formation for mixing the volume of a brewing vessel can be found in literature (Nienow et al., 2010; Okabe et al., 1992). The mean specific energy dissipation rate $\overline{\varepsilon_T}$ (i.e. the power input per mass of medium in a bioreactor), which is originated by the maximum rate of natural CO_2 release, was determined to be about 0.035 W Kg^{-1} in a beer fermentation of 300 m^3 (Luyben, 1997). Similar maximum values of $\overline{\varepsilon_T}$ = 0.045 W Kg^{-1} were also found earlier for brewing tanks of 400 - 500 m^3 with an H/D ratio of about 4:5. The maximum evolution rate for CO_2 was calculated with 1.2 x 10^{-4} (m^3 s^{-1}) m^{-3} (García et al., 1994). These $\overline{\varepsilon_T}$ - values are far lower than in stirred industrial processes with 6 W Kg^{-1} and higher, e.g. in aerobic industrial bioprocesses (Amanullah et al., 2004). Studies revealed that not only an increasing size but also the H/D ratio of a fermenter has an impact on the mean energy dissipation rate (Nienow et al., 2010).

Attempts have been made to improve mixing in large-scale brewing processes. These include mechanical agitation using impellers, gas-injection, e.g. by a bubble column, or the recirculation of the fermentation volume by a loop (Boswell et al., 2003b). The loop construction can be used also for the recycling of the headspace gas of a fermenter. The gas can be recirculated via the loop to the bottom part of the tank at a controlled flow rate in order to improve mixing. It was shown that the liquid circulation can be improved by this technique at the small scale. Nevertheless, compared to mechanical agitation, the level of higher alcohols is enhanced, foam formation is increased at very high power input, and the settling of yeast cells can be observed at later fermentation stages (Boswell et al., 2003b).

Before the application of these agitation systems, however, the effect of mechanical stress on the cells has to be investigated. This was done in various studies. Brewing fermentations of 500 mL reactors, equipped with two standard Rushton-type impellers, were investigated using a *S. cerevisiae* strain and lager wort. The A specific power input of ≈ 0.03 kW m^{-3} was set as a threshold, at which the difference between stirred and unstirred fermentations is negligible. Above this threshold (until $\overline{\varepsilon_T}$ = 0.25 W Kg^{-1}) the fermentation rate increased, leading to lower fermentation times (reduction from 168 h to 100 h) without significant losses in viability (only 6 - 9 % dead cells at the attenuation limit, respectively). On the other hand, the levels for higher alcohols as well as the cell dry weight increased, whereas the amount of esters decreased and the content of produced ethanol remained unchanged (Boswell et al., 2002). In further studies, the impact of fluid mechanical stress on *S. cerevisiae* during continuous cultivation for 15 days in an agitated, aerated bioreactor of 1 and 2.5 L volume was investigated by the same group (2003a). The two agitation setups of these processes resulted in a mean specific energy dissipation rate of $\overline{\varepsilon_T}$ = 0.045 and 4.5 W Kg^{-1}. Only little changes in the cell physiology and morphology were detected by flow cytometry. Mainly budding cells were affected by agitation as they tend to be larger before cell division (Boswell et al., 2003a). These results were found also in other studies, where a temporary decrease in cell division at $\overline{\varepsilon_T}$ = 6 W Kg^{-1} during a chemostat cultivation with animal cells was determined by multi-parameter flow cytometry. The cells, however, regenerated completely, when $\overline{\varepsilon_T}$ was reduced to 0.045 W Kg^{-1} again (Nienow et al., 2010).

An example of using mechanical agitation in combination with a loop construction in industrial scale is the Rotary Jet Mixing Technology, which was developed in 2003 by the Danish company ISO-MIX (today Alpha Laval). It can be applied in the food industry for mixing liquids, the dispersion of gases and powders or even for tank cleaning. Existing fermenters can be retrofitted easily (Alpha-Laval, 2003; Alpha-Laval, 2010). It does not contain large baffles, which enables proper cleaning and can reduce the sheer stress on the cells (Nordkvist et al., 2011). The principle is based on the rotation of the main unit in horizontal and vertical direction, which constantly is filled with fermentation liquid due to hydrostatic pressure (Fig. 6 A). The four jets are attached to the unit re-inject the liquid into the tank via nozzles. This causes a circulation of the liquid phase (Nordkvist et al., 2011). The Rotary Mixing Technology is combined to a pumped loop (Fig. 6 A), which can be used for pitching and aeration, the addition of stabilizing agents, the *in-line* installation of sensors for process monitoring, or even the integration of a cooling system using a plate-type heat exchanger (Boulton and Nordkvist, 2014). Alpha Laval claims to reduce the brewing process time by up to 30 % including the diacetyl rest time since the yeast remains longer in suspension (Alpha-Laval, 2010). Furthermore, the utilization of extract is improved (resulting in a higher ethanol yield), the process shows higher consistency, and yeast vitality can be improved, which was shown for several breweries (Boulton and Nordkvist, 2011).

The reduction in time by using the rotary jet during fermentation and cooling was proven in different lager brewing fermentations with a volume of about 500 m^3. The size and the recirculation rate of the

jet were chosen in such way that the mean specific energy dissipation rate was 0.0034 W kg^{-1}. The highest reduction in time was 27 % and also the process reproducibility was increased. The beer quality and taste instead, were not negatively influenced (Nienow et al., 2011). Along with these outcomes, the yeast sedimentation behavior was investigated in brewing tanks of about 160 m^3 without agitation. Nine Aber sensors for the measurement of biomass and temperature were integrated in axial direction in the tank center, using a boom arm and a winch. The results showed that about 50 % of the cells sediment to the tank cone when 50 % of fermentable sugars are still available. At a level of 25 % of fermentable sugars, the number of sedimenting cells was increasing to even 90 % (Nienow et al., 2011). This shows the potential for the application of mechanical mixing mechanisms in brewing processes in order to increase the production yield.

A similar system is the ECO-FERM™ from GEA (Fig. 6 B), which can be inserted via VARIVENT® connections. This mixing system has no movable parts. It simply consists of a hydraulic jet, which is installed at the tank bottom and enhances the natural convection by supporting the rising movement of CO_2 bubbles at very low energy consumption (GEA, 2017). By this, more active yeast cells remain in suspension. Hence, the process time is reduced due to improved mixing and homogeneity concerning yeast cell concentration, temperature, nutrients, etc. Nevertheless, since the brewing industry is quite traditional, these techniques have been only implemented in a few breweries.

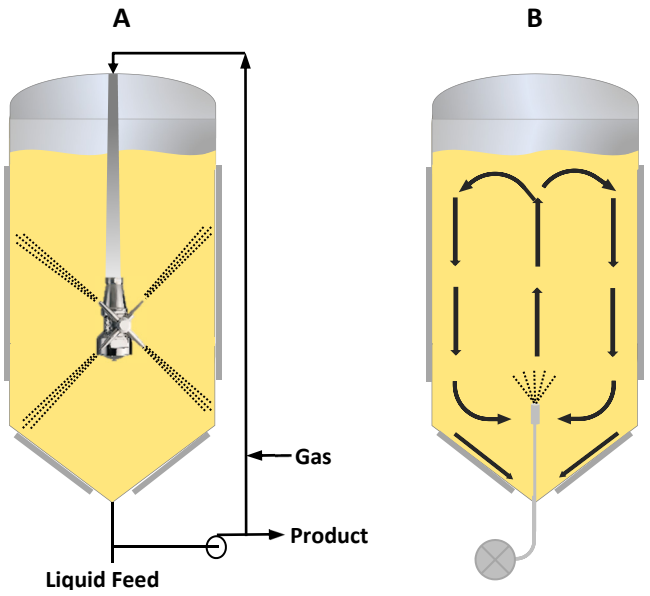

Fig. 6: Mechanical mixing strategies in the brewing process.
A: Rotary Jet Mixer (Alpha Laval) integrated at the top into a fermentation tank and connected to an external loop. B: Hydraulic jet technology (GEA) integrated at the bottom of a fermentation tank.

Another approach can be an accelerated fermentation applying large low-speed stirrers and higher temperatures. High temperatures, however, can favor the presence of undesired volatile / flavor compounds and decrease yeast vitality (Stewart et al., 2013).

2.2.3. Gradient Formation in Large-scale Processes due to insufficient Mixing and Limitations of Power Input

In large-scale processes, circulation and mixing times are increased up to a minute range since the power input is limited (Hewitt and Nienow, 2007; Junker, 2004; Lara et al., 2006). Consequently, heat

and mass transport are decreased, while metabolic synthesis and substrate consumption rates remain as fast as at the laboratory scale. This results in an uneven distribution of nutrients, the DO-, DCO_2-, pH-value, temperature or cell concentration (Haringa, 2017; Lara et al., 2006; Wang et al., 2015a). Hence, temporal and spatial gradients are formed in large-scale processes (Delafosse et al., 2015; Hewitt and Nienow, 2007). This is especially the case in unstirred processes like the brewing process and might influence the by-product formation and decrease biomass formation and product yield (Bylund et al., 1998; Hewitt and Nienow, 2007; Larsson et al., 1996). Furthermore, the hydrostatic pressure in large-scale processes might lead to gradients of dissolved gasses (Hewitt and Nienow, 2007). The investigation of the multiple and individual cell response to these alternating conditions in a reaction tank is essential for a proper process understanding and control since it is influencing the process efficiency and product quality (Bylund et al., 1998; Wang et al., 2015a).

Since experimental tests at large-scale are economically and technically not feasible, several methods for mimicking large-scale conditions and the investigation of inhomogeneities and gradients are available at laboratory scale. The range of simulators is broad: from single stirred tank reactors (STR), in which pulses are used for the simulation of different reactor zones in combination with rapid sampling units, to two- and three-compartment reactor systems for the application of permanent changes, e.g. oscillatory feeding (Neubauer and Junne, 2010). The latter can consist of a cascade of different STRs or a combination of STR and plug flow reactors (PFRs), in which regulation systems like feed or aeration can be installed in the STR or plug-flow reactor, depending on the research aim (Lara et al., 2006).
The STR-PFR system, consisting of a stirred tank reactor (simulating homogenous zones) and one or two plug flow reactors (simulating inhomogeneous zones) has been well established (Lemoine et al., 2015; Neubauer and Junne, 2010). Two or three different compartments can be combined in one reactor system, in which the cells are circulating (George et al., 1993). By this, the influences of the oscillating conditions on the cells' metabolism, physiology and product yield can be investigated (Junne et al., 2011). It was developed by the group of S. O. Enfors (KTH, Sweden) in the 1990ies and applied for the investigation of the cultivation or fermentation of different microorganisms, e.g. yeast (George et al., 1993; Larsson et al., 1996), *Corynebacterium glutamicum* (Käß et al., 2014; Lemoine et al., 2016), *Escherichia coli* (Enfors et al., 2001; Marbà-Ardebol et al., 2016) or *Bacillus subtilis* (Junne et al., 2011).

2.2.4. Computational Fluid Dynamics of Large-scale Phenomena

Computational Fluid Dynamics (CFD) can solve questions about fluid dynamics and fluid flows by approximation, which cannot be solved by measurements due to physical or mechanical restrictions. This is a challenge especially in large-scale processes and in turbid media or non-transparent bioreactors where optical methods fail. Anderson describes CFD as a "collection of numbers", which requires high performance and high-speed computers due to the large data volume (Anderson, 2009). The behavior of several other parameters has to be considered for CFD modelling like heat flow, mass transfer, phase changes, chemical reactions, mechanical movements or the displacement of solids (Pragati and Sharma, 2012). Due to its complexity, however, CFD allows for the simultaneous investigation of various physical and (bio-) chemical parameters at the same time. It can be used for process design, process understanding, and optimization (Sun and Norton, 2007). Its application for various fermenter designs can reduce process development time, while process conditions can be tested, which cannot be validated experimentally w/o much effort (Vial and Stiriba, 2013).

Numerous methods for 2D and 3D simulations for turbulent and laminar flow pattern are existing (Marshall and Bakker, 2004). CFD simulations for the brewing process were conducted by Batchuluun and co-authors (2014; 2011) in a fermentation cylinder with a volume of 60 L. At first, different initial and cooling zone temperatures were applied for the investigation of different density / velocity and temperature distributions in a tank, leading to the natural convection movement. The one-phase model was extended with the consideration of the accelerated fluid flow due to rising CO_2 bubbles ("induced convection"). This approach considers variations in the bubble diameter, which additionally influence the flow pattern.
For the cooling process in large-scale brewing tanks a CFD model was set up, which were cooled from 10 to -1 °C in 16 h, assuming a reduction of biochemical reactions at low temperatures. The fermenter was 22 m high and 7.2 m in diameter with a filling volume of 600 m^3. Temperature gradients of up to 2.45 °C after 22 h of cooling along the tank axis were determined, whereas the temperature gradient along the radial direction was low (Yuan et al., 2009).
CFD was further used for studies of the mixing time and quality or mass transfer in bioreactors as well as for the control and optimization of cleaning, sterilization or pasteurization processes, e.g. in the food industry (Pragati and Sharma, 2012).

Ultrasonic Doppler Velocimetry can also be applied for the investigation of the flow pattern in turbid media. With this technique a two-dimensional fluid velocity field was determined during beer fermentation in CCTs (270 L and 30 m^3) and validated in model fluids such as glycerin (Böttcher and Meironke, 2012; Meironke, 2014a). Since it is not invasive, it does not affect the fermentation. This technique, however, requires retrofitting of a tank or special laboratory tanks. In this study, several acrylic glass windows and cooling zones were integrated into the investigated reactors for optical and temperature measurements.

2.2.4.1. Application of CFD in Hybrid models

CFD is a fast and cost-efficient method to mimic industrial-scale conditions in comparison to experiments. Without experimental data, however, the theoretical models cannot be validated and adapted (Gnoth et al., 2007; Hänel, 2004). CFD models for brewing processes often do not take into account the bubble formation and its impact on the fluid flow and gradient formation. Hence, *on-line* measurement techniques, which can be applied *in-situ* are still necessary. In addition, CFD usually does not consider kinetic conversions and mass transfer to and from the inside of a cell. The impact of gradients on cellular synthesis rates and cell physiology is unknown, which would also lead to false assumptions of the models. However, if biochemical conversions inside the cell, changes in the cell physiology, and the mass flow of the liquid phase are combined, hybrid models are created and interactions between environment and cells (e.g. stress responses to oscillating conditions) are considered (Haringa, 2017; Herwig, 2010; Wang et al., 2015a).
A hybrid model that combines CFD simulation and biochemical reaction kinetics was developed for the xanthan gum production. The fluid flow was simulated in a 70 m^3 industrial reactor with a 25 w-% aqueous xanthan solution. Beside the reaction kinetics, the gas-liquid mass transfer, and the propagation of gaseous NH_3 were also integrated in the model (Moilanen et al., 2005). Data from an ethanol fermentation process of 2 L with *S. cerevisiae* were used for a parameter fit of a former kinetic model (Herbert's microbial kinetics model). The adapted model considers the power input by the stirrer speed and the aeration rate (gas bubble formation). Data from glucose, ethanol and biomass

concentration were used for prediction. Their special variations in a reactor were estimated by coupling the kinetic model to the CFD simulation. Sensitivities of the kinetic parameters were depending on the concentrations of glucose, ethanol and biomass during time (Teng and Chiat, 2016).

An important method in the field of hybrid models is the Euler-Lagrange approach in combination to CFD. In the Euler approach, the (multi-phase) fluid phase is treated and simulated as a continuum. The Lagrange approach instead, allows to investigate the intracellular states of individual cells and therefore the detection of population heterogeneities (Lapin et al., 2004; Wang et al., 2015a). The cells are individually tracked in the fluid flow across time and space and recorded as lifelines (Delvigne et al., 2017; Haringa et al., 2016). This could be also used for tracking cell-cycle oscillations or cell-cycle-specific product formation in yeast (Lapin et al., 2004).
In order to investigate the metabolic responses of cells (changes in substrate consumption and metabolic synthesis) to substrate inheterogeneities in large-scale reactors, substrate limited *Penicillium chrysogenum* cultivations in a stirred vessel of 54 m^3 with two Rushton turbines were conducted by Haringa and co-authors (2017; 2016). Single-phase hydrodynamics cultivation conditions without oxygen limitation were assumed. CFD combined to the Euler-Lagrange approach was used for the evaluation of the fluid flow, particularly the fluctuations in substrate consumption, and cell tracking concerning their metabolic status. The time frame, in which the specific substrate uptake rate changed due to variations in the extracellular substrate (lifelines), was divided into metabolic regimes, each characterized by a consistent cell response. Further, the residence time distribution, the magnitude of uptake variations and their duration within each regime as well as the transition of cells between the regimes was recorded. A 9-pool metabolic model was applied for *P. chrysogenum*, consisting of 5 intra-cellular metabolite and 4 enzymatic data bases, which were connected to the extracellular substrate concentration (Tang et al., 2017). By using this coupled hydrodynamic-kinetic simulation, magnitudes and frequencies of oscillating conditions in a reactor and their impact on the cell metabolism during a fermentation were determined. Further, this approach allows to identify critical reactor zones as it was shown for the localization of the feed. A change from the reactor top to a spot below the top impeller reduced the loss in penicillin yield from 18 % (in comparison to the ideal mixed case) to only 9 % (Haringa, 2017; Haringa et al., 2016). The results are used for the design of scale-down reactors that mimic industrial conditions.
Due to the high biomass concentration of *P. chrysogenum* (55 g kg^{-1} dry weight) and fast substrate conversion, however, this is challenging. Similar experiments were performed in a 22 m^3 stirred reactor with 4 Rushton impellers and *S. cerevisiae* and evaluated by the Euler-Lagrange CFD approach. Three regimes were defined for: 1. ethanol production / glucose consumption, 2. glucose consumption, and 3. low glucose uptake. The results showed a higher suitability for the design of scale-down simulators as the biomass was only 10 g kg^{-1} (dry weight) and therefore the substrate consumption was slower. Multi-compartment reactor setups are feasible for this cultivation without complications with mass transfer due to the higher circulation times and different rheology (Haringa, 2017; Haringa et al., 2017).

All these approaches clarify that CFD techniques are a useful complementary tool for the simulation of different kind of processes and scales, if coupled to data from kinetic and mass transfer studies and if bubble formation is considered in case of brewing processes. Measurement techniques with process analyzers that are applicable *in-situ*, and monitoring tools for the determination of metabolite concentrations or cell physiological parameters, however, are still irreplaceable for model setup and validation.

2.3. Process Analytical Technology for Process Monitoring

Process Analytical Technologies (PAT) comprises methods for the design, analysis, control, and optimization of productions processes in different industries by the measurement of Critical Process Parameters, which affect critical quality attributes (Food-and-Drug-Administration, 2004a). Since 2002, the United States Food and the Drug Administration (FDA) and European Medicines Agency have included the application of PAT in the pharmaceutical industry in their definition of Good Manufacturing Practices (Gnoth et al., 2007; Rathore et al., 2010), which was expanded to biochemical, biotechnological and food production processes.
In the latter two, the requirements for PAT regarding purity and cleanliness are higher than in chemical processes (Kessler and Becker, 2010). Furthermore, the measurement of classical process parameters like pressure, temperature, pH- or DO-value is usually not sufficient, even if time and space resolved data are obtained. This is caused by the multivariate, dynamic and non-linear character of bioprocesses, in which even small or short disturbances can have a great impact (Alford, 2006; Geier et al., 2016). Hence, already during the development of PAT methods complex intracellular interactions and interdependencies on the cellular level as well as processes on the molecular level and metabolic activities have to be considered (Herwig, 2010; Schocker and Kleinert, 2010).

In former times, many processes were characterized by an exact pre-definition of every process step and a quality analysis of the final product only. PAT instead is defined by process-oriented validation and implements quality analyses, monitoring and control during the whole production chain: from the raw material throughout production and downstream-processing until the final product is achieved (Geier et al., 2016). Hence, PAT is essential for complex process understanding, the stable process operation, and process optimization (Herwig, 2010; Maiwald, 2010). Ideally, all actions of the different process phases are interlinked via information management systems (Maiwald, 2010).
In case of process disturbances it is important to detect these rapidly in order to assure a fast or even *real-time* intervention and continuous quality (Read et al., 2010), already during process and product development (Reid et al., 2012). It can be realized only with a certain automation and digitalization level and *real-time* monitoring tools such as *in-situ*, *in-line* or *on-line* techniques or model based approaches, which replace step by step time and resource consuming *off-line* or *at-line* analysis (Alford, 2006; Geier et al., 2016).

According to the FDA definition, PAT methods can be classified in the following four categories (Food-and-Drug-Administration, 2004a):

a) Process analyzers;
b) Multivariate tools for the determination of variable dependencies in process design, data acquisition and analysis;
c) Process control tools;
d) Continuous improvement and knowledge management tools.

Process analyzers (a) can be classified according to their localization and distance to the process into *off-line*, *at-line*, *in-line*, *on-line* or even *in-situ* techniques (Kessler, 2012). The measurement of biological, physical, and chemical parameters can be invasive, such as *in-situ* sensors, or non-invasive, such as *off-line* or *at-line* techniques, e.g. chromatographic methods. Depending on the target substance (nutrient composition, product concentration, other metabolites) and process conditions different techniques are available:

- Multiple sensor technologies, based on chemical, physical, optical or mechanical measurement principles (see 2.3.2);
- Biosensors (e.g. antibody-antigen interaction, affinity assays, enzymatic reactions, nucleic acid interaction);
- Optical techniques (e.g. ultra-violet / visible spectroscopy (UV/VIS), fluorescence spectroscopy, infrared spectroscopy (near infrared, mid infrared), Raman spectroscopy, photo-optics, optical fibers, *at-line* and *in-situ* microscopy, flow cytometry);
- Mass spectrometry, e.g. for gas analysis; and
- Chromatographic methods (e.g. gas chromatography (GC), high performance (high pressure) liquid chromatography (HPLC), ion exchange chromatography, hydrophobic interaction chromatography, affinity chromatography, adsorption chromatography).

An efficient monitoring and quality assurance for a production process can only be obtained by the combination of process analyzers with the methods mentioned in b) to d). They are important for a proper data evaluation and correlation, statistical analysis, and interpretation. (Alford, 2006; Maiwald, 2010). Beside this, alternative methods are necessary in very complex processes or when process analyzers cannot be installed in a sufficient amount due to accessibility in the production plant, cost issues or lacking sensor technology. At this point, soft sensors can be employed (Becker and Krause, 2010; Clementschitsch and Bayer, 2006; Gnoth et al., 2007; Herwig, 2010). They determine the missing values or variables of target based on the available limited data set (e.g. from *off-line* analysis or *on-line* sensor data) by mathematical modeling and can be applied in all steps of the process chain (Becker and Krause, 2010; Chen et al., 2004). There are two main approaches (Becker and Krause, 2010; Herwig, 2010):

1. Data driven methods. They are used when the knowledge about the process and dependencies (mathematical relations) of process parameters, data sets or signals are unknown ("Black-Box-Model"). In this case, the independent parameters are indirectly represented in the data set.
2. Model- and knowledge-based methods. They can be implemented at a greater knowledge about the process and parameter dependencies or correlations ("White-Box-Models").

Data driven methods are based on chemometric methods (statistical and multivariate data analysis, see 2.3.4 for details), "learning systems" such as neural networks or linguistic approaches such as fuzzy logic, for example. An adequate data basis for the design of the data driven models can only be provided by the application of the right sensor technology, which is preferably applicable *in-situ* or *on-line*. Further, it must be considered during the model setup that pure data driven approaches provide just an approximation and overfitting is a risk (Becker and Krause, 2010). Pure data driven methods cannot fully describe complex phenomena in bioprocesses, e.g. product inhibition or cell death (Alford, 2006).
Artificial neural networks (ANN) can recognize data pattern and dependencies between input and output variables in complex, non-linear processes (Becker et al., 2002). These in- and output data are connected by vectors, which possess different weight or importance in the network (Zak, 2003). The network is continuously adapted and "learning" by creating, cancelling or strengthening connections just as in the brain (Chen et al., 2004; Zak, 2003). Hence, data from different methods can be correlated and the acquired process knowledge can continuously be integrated for process optimization (Jenzsch et al., 2006).

In fuzzy logic systems some knowledge about the process is already included, which defines them as "Grey-Box-Models". They can be useful especially at high process complexity (Becker and Krause, 2010). This method is based on if-when-rules, determines the relevance of rules and takes decisions based on these rules for process regulation. This can be used for example for temperature control using the temperature as output data and state variables like the growth rate as input data (Geier et al., 2016; Honda and Kobayashi, 2004). It is essential for the evaluation of the process status and the fast detection of deviations from the target values and control limits concerning both, product quality and process performance (Becker and Krause, 2010; Geier et al., 2016). By this, non-linear process behavior can be controlled and corrective actions can be taken in time, e.g. during the brewing process (Geier et al., 2016).

Fuzzy logic was used for the identification of disturbances in anaerobic wastewater treatment plants. A strategy of this approach was the division of the detected faults into different classes, namely: sensor, sub-process, and process faults and their subsequent isolation (Steyer et al., 2001). Fuzzy control was applied for the *on-line* state estimation of a fed-batch cultivation with *S. cerevisiae*, controlling substrate and air flow rate. By this, set points of the specific growth rate, elapsed time, dissolved oxygen and ethanol concentration were kept at optimal levels for maximum biomass formation (Karakuzu et al., 2006).

In *model-based methods*, experimental data are combined with (un-)structured mechanistic models in order to prove the lacking information about variables. They are based on differential algebraic equations describing for example reaction kinetics, mass and heat balances, stoichiometric reaction equations or cell regulation mechanisms (e.g. metabolic flux analysis) (Becker and Krause, 2010; Herwig, 2010). An application example is the use of the oxygen uptake rate or carbon dioxide evolution rate, which are calculated on the basis of experimental data, and their correlation to substrate consumption (e.g. glucose) or cell growth (Alford, 2006). For the development of mechanistic models, uncertainty and sensitivity analysis are essential in order to obtain reliable models (Sin et al., 2009). A further model-based method is the simulation of the fluid flow, i.e. CFD as explained in chapter 2.2.4. Since pure model-based methods do not sufficiently describe heterogeneities or changes in cell physiology, hybrid models can be an alternative (2.2.4.1) (Herwig, 2010).

In order to comprise the maximum number of parameter dependencies, the combination of knowledge-based models, data-driven methods, and analytical methods is recommended (Alford, 2006; Herwig, 2010). The above mentioned techniques are implemented in "Quality-by-design" methods in order to meet the quality requirements (Becker and Krause, 2010; Herwig, 2010). Quality-by-design is a tool for planning process operational procedures for a stable running process including the consideration of disturbances that can occur. This approach requires process experience and knowledge about the relations and dependencies between variables and optimal process parameters (Gnoth et al., 2007; Read et al., 2010). Therefore, multivariate statistical process monitoring and control are often applied, especially in complex and dynamic biological processes (Clementschitsch and Bayer, 2006). Multivariate statistical process control can be further combined to constant feedforward and feedback control systems to improve process efficiency (Food-and-Drug-Administration, 2004b; Gnoth et al., 2007).
Additionally, appropriate data management systems, including the interlink of various data sets, information technology structures, tools for *real-time* visualization of process data, and smart alarm systems are essential for stable process operation (Alford, 2006; Geier et al., 2016; Maiwald, 2010).

2.3.1. Requirements for Sensor Technology and Challenges for Sensor Development

There is still a demand for the further development towards more stable and intelligent sensors, which show low drift during long-term application (Maiwald, 2010). *Off-line* and *at-line* analysis methods are time-consuming, bind human resources and deliver results with time delay to the process. Hence, sensor systems should allow at least *on-line* or even *in-situ* monitoring of physical, chemical, and biological parameters for the continuous provision with data in *real-time* (Chen et al., 2004; Geier et al., 2016; Peris and Escuder-Gilabert, 2013).

Hauptman and co-authors (2002) summarized the requirements for process sensors as follows:

- High accuracy and reproducibility;
- High reliability;
- Low cross-sensitivity; and
- Non-invasive measurement.

Further demands exist regarding their application in certain processes:

- Robustness (against pressure, temperature, vibration) and chemical corrosion resistance;
- No damaging effect on the process (e.g. contamination);
- Low response time;
- Low level of maintenance;
- Easy system integration by standard mountings and output signals; and
- Good compliance with sterility and hygienic standards (steam sterilization, CIP cleaning), e.g. for the food and pharmaceutical industry (Hauptmann et al., 2002).

In bioprocess monitoring, sensors for the *on-line* or *in-situ* measurement of cell mass in complex media, substrate, metabolites or product concentration are still not available with all the requirements mentioned above, although they represent basic parameters of a process and many bioprocess models (Alford, 2006). This might be caused by the water matrix, other components of complex media, or gas bubbles in anaerobic fermentation processes (e.g. in beer production or due to stirring), which influence the signal and sterility requirements (Clementschitsch and Bayer, 2006; Kessler et al., 2012; Zosel et al., 2011). Further, clogging of the sensor membranes in complex media is a challenge. Some of the issues (sterility, drift, membrane clogging) can be overcome by the application of non-invasive optical spectroscopic methods, which are additionally suited for the investigation of cell physiological properties (Herwig, 2010).
In beer production plants, for example, the number of available *on-line* or *in-line* sensors is even lower and often only a restricted number of parameters is measured during fermentation (temperature, pressure, filling level). Sensors for *in-situ* measurements are lacking completely, hindering the investigation of the liquid phase of large-scale reactors. Most of the control actions are performed manually and samples are often analyzed *off-line*, which results in a time delay and needs many human and plant resources (Geier et al., 2016). Guiding parameters, such as extract and diacetyl content, are important for the determination of the process status and decisive for the start of the next process step. An *on-line* measurement technology for these parameters would be of great benefit but is still not available or economically not feasible.

Beside the development of the sensor functionality itself, there is a constant development of sensors towards miniaturization, self-maintenance, and self-diagnostic mechanisms (“smart sensors”) in order

to fulfill the requirements of increasing automation. This is coupled to the improvement of tools for the information transfer to computer control systems via bus systems or wireless data transfer (Alford, 2006). Finally, if there is no "hard" sensor technology available at all for monitoring a target parameter with the required accuracy and distance to the process (*on-line*, *in-line*, *in-situ*), additional techniques for the indirect determination of parameters based on experimental data might be an alternative, such as the previously mentioned multivariate models and soft sensors.

2.3.2. Available Sensor and Analysis Technologies for Bioprocesses and Application Examples

Sensors can be applied in the liquid phase *in-line*, *on-line* or even *in-situ* in contrast to other process analyzers like spectroscopic or chromatographic methods. Sensors are classified according to their measurement principle:

1. Physico-chemical sensors: potentiometric (including electronic noses and tongues), capacitance, acoustic, calorimetric;
2. Optical sensors: UV/VIS, optical fibers, fluorescence, infrared and Raman spectroscopy.

In the following, a selection of these techniques and their application in brewing or other anaerobic processes - preferably *in-situ* or *in-/on-line* - is presented.

2.3.2.1. Physico-chemical Sensors

i. Potentiometric Sensors

Potentiometric sensors measure the difference in the potential between a measuring and a reference electrode, which is caused by altering analyte concentrations in the electrolyte/electrode system. This method is usually applied for pH measurements. Often, a single-rod glass electrode containing a thin glass membrane as sensitive layer is used. They are applied in both aerobic and anaerobic processes. In contrast to solid-state electrodes, e.g. of antimony or bismuth, the measurement range is larger and the sensitivity to certain redox components is much lower (Vonau and Guth, 2006).

One example is the pH-monitoring during anaerobic sludge digestion in wastewater treatment plants in order to avoid overload while utilizing maximum reactor capacity (Steyer et al., 2002). A miniaturized pH sensor developed by the "Kurt-Schwabe-Institut für Mess- und Sensortechnik e.V. Meinsberg" (KSI, Germany) was applied in different biogas plants (Kielhorn et al., 2015) and brewing reactors (Bockisch et al., 2014; Sachse et al., 2015). In the brewing process, monitoring of the pH-value by *on-line* sensors serves for the monitoring of the process status and process performance. Beside this aspect, however, it is useful for the detection of beer spoiling organisms that can grow below the aimed final pH-value of around 4.0 (e.g. *Lactobacillus* spp.) or above the starting value of around 5.0 (Ault, 1965).

Indirect pH measurement can be conducted using a light-addressable potentiometric sensor (LAPS). It consists of a doped silicon, which functions as a semi-conductor and is covered by a thin insulator layer (e.g. silicon nitride or a pH sensitive layer) that gets in contact with the aqueous solution. For the electrical contact between the different layers, a metal pad is placed on the non-isolated back of the sensor unit and a reference electrode in the analyte solution (Owicki et al., 1994; Wagner et al., 2012). When the semiconductor surface is illuminated by a modulated light beam (e.g. LED) the light is absorbed by the semiconductor material and electron-hole pairs are formed. These pairs separate in

the electric field of the space-charge region into electrons (moving to the silicon layer) and holes (accumulating at the insulator area = depletion area) (Owicki et al., 1994). This light-induced charge separation can be detected as photocurrent and its amplitude depends (at a fixed bias voltage) on the sensor surface charge, i.e. the local analyte concentration. Combined information about the light beam position and the photocurrent amplitude provide a spatially resolved map of the ion concentration distribution at the sensor surface (Wagner et al., 2012; Werner, 2014). Werner and co-authors (2011) monitored the extracellular acidification with a LAPS based on a pH change during an *Escherichia coli* cultivation.

The measurement of DCO_2 is of interest in many anaerobic bioprocesses. In principal, DCO_2 can be measured with potentiometric, indirect determination using the Severinghaus principle. This technique is based on the relation between the amount of carbon dioxide and the pH-value. The sensor consists of a membrane, which is permeable to CO_2, but not to ions or water. This membrane separates the gaseous or liquid analyte medium from the electrolyte, a bicarbonate solution. The pH-value in the electrolyte decreases in parallel with increasing DCO_2 concentrations. Hence, the CO_2 partial pressure is indirectly determined by measuring the pH-value of the electrolyte. Further, for *in-situ* gas analysis of CO_2 or air, solid electrolytes can be used, which possess a short response time and can be applied at high temperatures (Zosel et al., 2011).

Another example for a measurement of a potential difference is the redox or oxidation-reduction potential (ORP) sensor. Redox potential sensors are often applied for measurements in anaerobic fermentation processes since they are more sensitive than many DO sensors to low levels (<1 ppm) of dissolved oxygen. The monitoring of the redox potential is of great interest because the metabolism of many substances such as carbon, hydrogen, oxygen, nitrogen or sulfur as well as gene expression or protein biosynthesisis are based on redox reactions (Liu et al., 2013; NewBrunswickScientific, 2008). Redox monitoring using a Mettler Toledo probe was applied during anaerobic yeast fermentation in a 5 L laboratory scale reactor for increased ethanol production (NewBrunswickScientific, 2008). Liu, Xue, Lin, and Bai summarize methods for monitoring the redox potential in the liquid phase during the process of acetate-butanol-ethanol production with *Clostridium spp.* The authors discuss how the redox potential measurement can assist during the enhancement of the process efficiency (Liu et al., 2013).
The use of glass is an advantageous method for redox measurements due to its inertness. Noble metal electrodes instead, show poor reproducibility and might be inoperative after contact with catalytic poisons, such as SO_2 or other sulfur compounds or after exposure to proteins. Gaseous oxygen or hydrogen in the samples can influence the half-cell potential as well. The applicability of electron conducting glasses was shown by Vonau and co-authors (2010).

Conductivity measurements can be performed *at-line* or even *in-situ* in anaerobic processes. In complex medium it can be used for both the analysis of the medium composition and ion strength as well as the microbial growth and extracellular metabolite concentration.
A device for the monitoring in electrically conductive liquid of anaerobic digestion processes was invented and patented in 2009. Voltage pulses are applied between its electrochemical electrodes. The electric current, which is the generated response, represents electrochemical changes in the broth. The signals serve as a measure for the process status in general. They have, however, not been linked to any specific parameters yet (Louthander et al., 2009).

Hamilton Bonaduz AG (Switzerland) developed a probe, which can be applied *in-situ* in anaerobic fermentations and sterilized (Hamilton_Company, 2014a). The sensing part consists of four electrodes, which measure changes in resistivity. By adequate housing, this sensor can become submergible and data can be transferred across long distances (> 30 m) due to the integrated preamplifier (see 4.1). A housing unit, containing the conductivity sensor among others, is applied in brewing and biogas plants.

Ion sensitive field effect transistor technology (ISFET)

The ion concentrations in a solution, e.g. for measurements of the pH-value, can also be measured using solid-state sensor materials like antimony or bismuth electrodes Ion sensitive field effect transistor technology (ISFET). With changing ion concentration in the sample, the current at the transistor changes correspondingly. Various methods for the ISFET production of ISFETs are available (Jimenez-Jorquera et al., 2010).
The small size, robustness, solid-state nature, the low power consumption, the possibility of the fabrication of a large number, a short response time, and low output impedance are advantageous. Further, mechanisms for compensation and data processing circuits can be integrated on the same chip. These sensors can be integrated in (semi)automated flow systems or in miniaturized analytical systems, and were applied for wastewater characterization (Jimenez-Jorquera et al., 2010). A challenge during the development of ISFET technology for volatile compounds, passing between liquid and gas phase, is therefore the construction of the gas permeable membrane, the packing technology and the design of a potential stable reference, e.g. for CO_2-sensors (Vonau and Guth, 2006; Zosel et al., 2011). Alternatively, it was shown that volatile components can be measured coulometrically after gas stripping and separation with solid phase sensors (Schelter et al., 2014).
ISFETs can be easily integrated into multi-parameter chips, e.g. for the measurement of extracellular acidification rates (Brischwein et al., 2003; Ceriotti et al., 2007). The simultaneous determination of the pH-value, penicillin and temperature was realized by means of a hybrid sensor array including (bio-)chemical and physical sensors based on the same transducer principle (Poghossian et al., 2001).
In the brewing industry, ISFET sensors are applied mainly due to their robustness against damage (no glass) and solid-state nature (Esslinger, 2009). A commercially available encapsulated sensor for the *in-line* pH measurement during beer production was developed by Mettler Toledo Inc. (United States), named InPro®3300/ISFET (Mettler-Toledo-GmbH-Process-Analytics, 2004). The accuracy was reported to deviate about 0.15 pH-units from that of a conventional glass electrode. This, however, is sufficient for many *in-line* applications during centrifugation and filtration after the fermentation process. For the application in various processes in food and pharmaceutical industry, the “ISFET pH combination electrode” was developed by Jumo GmbH & Co. KG (Germany), providing various process connections and sensor lengths (Jumo, 2011).

Electronic tongues (ET) and noses (EN)

Electronic tongues and noses can be applied *at-line* or *in-line, e.g. by* using a bypass. They are progressively applied in the food and beverage industry for process monitoring and product control (Peris and Escuder-Gilabert, 2013), e.g. for the estimation of volatile compounds and CO_2 concentration in the brewing or wine industry. Since they consist of several sensors (multi-sensory approach), ETs can be used to analyze complex liquids and EN to investigate complex gas samples very cost effectively. Each sensor of the sensors array is sensible to multiple substances and a substance can be detected by several sensors with different response intensity (Ghasemi-Varnamkhasti et al.,

2011). The majority of ET systems uses electrochemical sensors (potentiometric, voltammetric, amperometric), and optical sensors (Witkowska et al., 2010).
A big advantage is that often no sample preparation is necessary, the devices can be very small and therefore suitable for mobile use. The systematic similarity to the human olfactory and tasting system allows for the correlation of the sensor data to results from sensory panels (Ghasemi-Varnamkhasti et al., 2011). Nevertheless, these arrays often show a drift due to changing temperature or humidity, are therefore instable during long-time usage and the sensible detecting elements of the sensor tend to be contaminated in complex material (Ghasemi-Varnamkhasti et al., 2011). Further, a high number of pre-measurements with a large amount of samples is necessary for the calibration or model setup (Peris and Escuder-Gilabert, 2013; Witkowska et al., 2010).
Especially challenging is the application in alcoholic beverages since the samples show high foam levels, must be degassed before analysis, and the sensor responses can be masked by water and ethanol, decreasing the sensor sensitivity for low concentrated volatile compounds (Ghasemi-Varnamkhasti et al., 2011). This issue can be solved by the combination to other analytical instruments, such as solid phase micro-extraction where adsorbent resins with insensitivity to ethanol and water are used. By this, detection limits of up to parts per trillion are achieved (McKellar et al., 2002). An alternative can be the pre-treatment of the headspace in order to remove components like ethanol and water (Ghasemi-Varnamkhasti et al., 2011; Villanueva et al., 2006). This method was applied for off-flavor analysis in beer and wine with an EN (consisting of 18 metal oxide semiconductor gas sensors) (Ragazzo-Sanchez et al., 2009).
ET/EN technique can be used also in the brewing industry for raw materials analysis. By the latter step, process times for maturation and procedures during a very early step in the process chain, the milling, can be optimized (McKellar et al., 2002). Portable solutions for the indirect determination of the alcohol content and the color with a screen-printed ET array were applied by Blanco and co-authors. The prediction models worked accurately for examples of four different types of beer (Blanco et al., 2015). A paper-based ET, sensitive to sodium, calcium, ammonia and a cross-sensitive, anion-selective electrode was used to analyze 34 beer samples. The system was able to discriminate between the pH-value, alcohol content, presence of stabilizers and antioxidants, and dyes or carbohydrates added to the wort (Nery and Kubota, 2016).
The combination of different electronic systems, i.e. EN with ET, coupled to multivariate data analysis can provide even more information (Apetrei et al., 2010). During *at-line* monitoring of a fermentation processes of cheese starter cultures (*Lactobacillus* and *Lactococcus* spp.) an ET, containing 30 non-specific potentiometric sensors, was used for the determination of organic acid concentrations. Process control charts were subsequently set up by the processing of the sensor signals with PLS regression (Esbensen et al., 2004). A sensor array, consisting of 10 potentiometric electrodes and 3 voltammetric transducers, i.e. a hybrid ET (h-ET), was applied during a brewing process (Kutyla-Olesiuk et al., 2014; Kutyla-Olesiuk et al., 2012). Physico-chemical parameters were analyzed *off-line* by h-ET during fermentation and maturation stage and processed by PLS and further statistical tools. The results showed that this techniques allows for the determination of the fermentation process stage and the detection of process disturbances and statistical analysis showed even an improvement compared to the application of the ET-techniques separately (Kutyla-Olesiuk et al., 2012).
All these ET/EN approaches, however, do not allow an *in-situ* monitoring. They deliver, however, *real-time* data by *at-line* or *in-line* measurements, which can be processed by adequate statistical and multivariate methods.

ii. Capacitance Sensors

Capacitance measurements allow for the determination of the amount or cell density of viable cells in a suspension. Since viable cells are polarized, they function as little capacitors (Fig. 7) and assemble electric charges at the membrane interface (Kell et al., 1987). An alternating electrical field is set up at the sensor tip for the measurement of the polarization level of the cells. The received signal is displayed as permittivity in pF cm^{-1} and can be correlated to the viable cell density. Fully depolarized particles, i.e. with a non-functional membrane, are not detected at all. This is an important advantage of this technology since cell debris, micro-carriers, gas bubbles or other particles in suspension, e.g. from the media, are not taken into consideration.

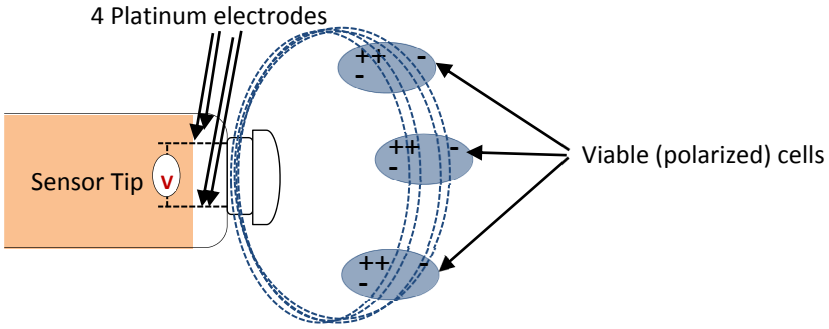

Fig. 7: Principle of a capacity sensor.

Electrochemical impedance spectroscopy at frequencies below 1 kHz was used for biomass monitoring in aerobic and anaerobic batch cultivations with yeast in media containing mineral salt and malt extract. In anaerobic cultivations a good correlation to the cell dry weight was found beyond a threshold of 1 g L^{-1} beyond a threshold of 1 g L^{-1} (Slouka et al., 2017).

A commercially available sensor is the *in-situ* "Incyte" probe from the Hamilton Bonaduz AG (Switzerland, (Hamilton_Company, 2015)). During the biomass monitoring of an anaerobic lactic acid bacteria fermentation an optimal frequency of 5.7 MHz (in the range of 0.3 - 10 MHz) was determined for the "Incyte" technology and a biomass detection sensitivity of 0.2 g L^{-1} (0.01 pF cm^{-1}) could be proven (Arnoux et al., 2004; Arnoux et al., 2005). This sensor was also applied for the monitoring of *Lactobacillus* sp. and *S. cerevisiae* fermentation (Kiss and Németh, 2015). The prototype of the "Incyte" probe, developed by Fogale Nanotech (France), was applied for the concentration measurement of flocculating *S. cerevisiae* during a continuous alcoholic fermentation (Mas et al., 2001). The permittivity with the "Incyte" probe can be measured at 17 different frequencies (frequency scan). This is of importance since the permittivity, i.e. the polarization properties, of the cells vary at different signal frequencies (higher polarization/Capacitance at lower frequencies). By this, additional information about the cell physiology, e.g. about the homogeneity of a cell population, can be gained (Yardley et al., 2000).

Other capacitance sensors are the four-pin and the annular electrode, developed by Aber Instruments Ltd. (United Kingdom (Aber-Instruments, 2015)). The four-pin probe with 4 platinum electrodes at the top of the probe was developed for *in-situ* measurements in a single use bioreactor (disposable flush probe "BioPAT® ViaMass" in cooperation with Sartorius Stedim, Germany (Carvell et al., 2016)) or normal stirred tank reactors (reusable probe). They are as well equipped with a multi-frequency mode for the measurement at different frequencies. The multi-use four-pin probe was applied in a 15 L yeast (*Arxula adeninivorans*) cultivation at 0.5 MHz and 15.649 MHz (Knabben et al., 2010) and was proven to function also for high cell density *Escherichia coli* fermentations (Knabben et al., 2011). A different

frequency range for this probe (0.1-10 MHZ) was applied in *real-time* determination the viable cell mass of *S. cerevisiae* in a 20 L cultivation (Xiong et al., 2008). A further development by Aber instruments Ltd. (United Kingdom) is the annular probe, in which the four pins are mounted annularly on a shaft. This probe showed even higher signal intensity and sensitivity than the four-pin probe with higher signal-to-noise ratio during biomass monitoring in a Streptomyces cultivation (Ferreira et al., 2005).
A submersible dielectric sensor was applied in a *S. cerevisiae* cultivation in a 10 L reactor. It consisted of an outer and an inner electrode, which were coated with platinum (Mishima et al., 1991). The authors also proved that the influence of the agitation and aeration rate is negligible.

iii. Acoustic Sensors

Ultrasound-based methods utilize acoustic effects. An ultrasonic field is build up and the transmitted acoustic waves are influenced by the investigated liquid and interact with it (Hauptmann et al., 2002). This results in sound reflections by interface layers, sound diffraction at edges, varying frequency velocities due to dispersion and distortion, and attenuation [acoustic Doppler Effect, (Gomez-Tejedor et al., 2014)]. Information about physical parameters like the filling level or distances, the surface structure of a liquid phase, the flow velocity (e.g. in pipes), pressure and temperature changes as well as process parameters, e.g. component concentrations or particle sizes and distributions are obtained (Hauptmann et al., 2002; Ihunegbo et al., 2012).
Acoustic sensors are non-destructive to process and microorganisms, and can be fast adapted to different process systems (Becker et al., 2001). They are further very stable during long-term usage, show high resolution and accuracy, and are applicable for *in-line* measurement due to their fast response time. Nevertheless, they are still not established as a standard analysis tool in industry as they are not applicable *in-situ*, the acoustic properties of the analyzed medium must be known, gas bubbles disturb the ultrasonic signal, complex signal processing is necessary, and the frequency cannot be increased infinitely since the attenuation of sound increases with frequency (Hauptmann et al., 2002).

With the application of the simple vibration acoustic sensor for the control of liquid levels some of the challenges can be overcome. A possible construction form is a tuning fork and is excited at its resonance frequency resulting in a vibration. This vibration is stimulated by a piezoelectric drive, which also compensates the energy loss (Endress&Hauser, 2015). At the transition of the sensor between different phases or masses with different density and viscosity, e.g. from a gaseous to a liquid phase, the oscillation frequency and amplitude of the tines is changing. This change can be detected. This method can be applied in different liquids, independently of the electrical or conductivity properties and even in liquids with surface contamination, currents, turbulences, solid content, gas bubbles or aggressive medium components (Endress&Hauser, 2015). One instrument, developed for this purpose is called “Liquiphant” and can be applied at high viscosities (> 0.5g cm^{-3}), temperatures between -40 and 150 °C, and a pressure of up to 40 bar.

During a brewing process, continuous monitoring of the original gravity can be conducted with acoustic ultrasound measurements. Since beer consists mainly of three components, namely water, alcohol, and extract these three can be distinguished by ultrasound measurements concerning their sound velocity, density and refractive index, respectively. During the fermentation progress these parameters change with time. The sound velocity was determined to be of lower significance since one molecule

of alcohol is formed out of two sugar molecules and the influence of alcohol is half of that of carbohydrates (Hauptmann et al., 2002).
In a study of Becker and co-authors (2001), the *on-line* investigation of the changes in extract / density during a beer fermentation was also realized by ultrasonic velocity measurements. A piezo crystal sensor was attached at the outer surface of a CCT with a diameter of 4.5 m and a fermentation volume of 300 m^3. The sensor was functioning alternating as emitter and receiver. The time of flight was recorded only after the ultrasonic signal had passed the fermenter twice. Interferences during the fermentation were identified, such as a strong sensitivity to changing temperature and the DCO_2 concentration. Hence, improvement concerning measuring accuracy, calibration model (temperature influence), and reproducibility are necessary. Further, the measurement of pressure has to be integrated because this parameter influences the amount of DCO_2, which itself influences the ultrasonic velocity (Becker et al., 2001).
The determination of the bubble size distribution in a reactor is of great interest since it influences the fluid flow. Further, bubbles of certain sizes might hinder the propagation of emitted sound signals through the liquid phase as it is shown for the localization system in this thesis. An ultrasound-based method for the determination of the bubble size distribution in gas–liquid two-phase systems was developed by Chen and co-authors (2017). Artificial bubbles with a radius range of 5 – 87 µm and a mean radius of 30 - 35 µm were used. The system was applied in a yeast propagation tank using a bypass pipeline for bubble recirculation. Microscopic photographies were used as a reference. The bubble size distribution was estimated using a model based on the resonant attenuation approximation (developed by Medwin). Although a good accuracy (Root Mean Square Error of Validation of 0.1243 %v/v) was achieved and the data matched well the reference method, many optimization steps are still required for this measurement technique (Chen et al., 2017).

Two-dimensional Ultrasonic Doppler Velocimetry (UDV) was used for the measurement of the convection flow and flow velocity field during real beer fermentation in a model tank (270 L) and a CCT (30 m^3), which have been designed for these investigations (Meironke, 2007; Meironke, 2014b). The determined flow field was validated using the model fluid glycerin as well as artificial heat and CO_2 formation (heating coils and aeration) at the 270 L scale (Meironke and Böttcher, 2014). Challenging for this process is the multi-phase flow character due to the wort turbidity (this excludes techniques like Laser Doppler Anemometry or Particle Image Velocimetry), the CO_2 bubbles, and the concentration changes of nutrients and metabolites influencing the sound velocity (Meironke, 2014a; Meironke and Böttcher, 2014).

Nowadays, several systems for *in-line* sound velocity measurements are available, e.g. for the determination of sugar concentration (original gravity), extract, and alcohol the “Beer-Monitor Basic” of Anton Paar (Anton Paar GmbH, Austria) or the “LiquiSonic system® Plato & Brix” (Sensotech GmbH, Germany) with an accuracy of 0.1 m s^{-1} for the sound velocity (Sensotech-GmbH, 2017). Another sensor, the “LiquidSens”-Sensor, was developed by SensAction AG (Germany). It measures the velocity of the sound waves, the density, and the temperature of a liquid at the same time. This is realized by using surface acoustic waves (waves with a high amplitude and a long propagation on the liquid surface) and the simultaneous measurement of their amplitude and transmission time both through the liquid and along the surface (sound velocity). There are many fields for application, e.g. the analysis of the composition of oils, liquids or milk as well as other nutrients (SensAction, 2017).

An overview of the further use of ultrasonic sensor systems as acoustic chemical sensors, i.e. for the analysis of substance concentrations, the monitoring of polymerization, crystallization or fermentation

processes, and the analysis of liquid multi-phase systems such as suspensions, emulsions, and dispersions is given by Henning and Rautenberg (Henning and Rautenberg, 2006).

2.3.2.2. Optical Sensors and Process Analyzers

Optical sensors possess some advantages over many other methods: they are non-invasive, do not interfere with the cultivation medium or cell metabolism and do not require any analyte to be consumed. Since they can be used for *real-time* and *in-situ* measurements without complicate sampling, the risk of contamination is minimized. On the other side, this requires robustness against steam sterilization or chemical disinfectants and temperature stability, which is not provided by all optical techniques (Petrova et al., 2006). During development and optimization of optical measurement systems, several challenging aspects have to be considered: Dye leaching for fluorescence sensors, photobleaching (e.g. in UV/VIS) leading to a baseline drift (Vojinović et al., 2006), and interferences due to autofluorescence or cross-sensitivities to other parameters and thus low specificity (Petrova et al., 2006).

Despite the challenges, several methods were proved for the *on-line* investigation of the liquid phase of a reactor. The potential of optical techniques for *at-line* or *on-line* monitoring of the liquid phase in bioprocesses is described in some reviews, e.g. by Claßen or Becker and co-authors (2007; 2017). There is a broad range of general optical methods: ultraviolet / visible light (UV/VIS) -, infrared - (IR -), Raman, fluorescence -, pulsed tetrahertz spectroscopy (PTS), optical biosensors, *in-situ* microscopy, surface plasmon resonance (SPR), and reflectometric interference spectroscopy (RIF). In the following, a selection of UV/VIS- and fluorescence-based methods with the focus on anaerobic processes and at least *at-line* access is presented.

i. Ultraviolet / Visible Light Spectroscopy (UV/VIS)

UV/VIS spectroscopy uses light absorption at a certain wavelength range (UV: 1 - 400 nm and VIS: 400 - 700 nm) and provides qualitative and quantitative information of the analyzed sample. Cells interact with the light, absorb or scatter the light (Alupoaei and García-Rubio, 2004). The absorbance is depending on the size and refractive index of cells (Brown and Jaffé, 2001). It has to be considered that substances, which alter the surface of particles or cell membranes, influence the absorption or reflection spectra. The effects of nonionic surfactants on the UV/VIS absorption of bacterial cell membranes were investigated by Brown and Jaffé (2001).

By the application of the multi-wavelength method for the generation of for UV/VIS spectra, the limitation to a fixed wavelength can be overcome. This method provides information about the number, size, shape, chemical composition, and internal structure of the suspended particles (Alupoaei and García-Rubio, 2004). By data processing and the integration into a model, spectral patterns for a wide range of bacteria and vegetative cells could be interpreted as well (Alupoaei and Garcia-Rubio, 2005; Alupoaei et al., 2004). The model is based on the knowledge about light scattering, techniques in spectral deconvolution, and the approximation of optical characteristics of the main constituents of microorganisms. Due to this broad knowledge base, it could be adapted also for yeast cultivations, mixed cell suspensions or the control of contaminations, e.g. in the food industry (Kiefer et al., 2010).

Garn and co-authors (1989) developed a technique for the *in-line* monitoring of fermentations by UV/VIS spectroscopy. A sampling loop (bypass) and sterilizable crossflow microfilters were constructed

for the *on-line* monitoring of glucose and ethanol content during a *S. cerevisiae* fermentation. The method was proven to reach the same accuracy as *off-line* analyses and a higher reproducibility. The signal, however, can be influenced by interferences with medium particles. Hence, for the determination of the optimal detection limit both the sample dilution and the suppression of matrix effects have to be considered. Detection limits of 5 mg L^{-1} for glucose and ethanol, 1 mg L^{-1} for phosphate, and 50 mg L^{-1} for ammonia were determined for standard solutions.

Absorption in this wavelength range is used as well for the measurement of the optical density, e.g. in a probe of the Hamilton Bonaduz AG (Switzerland). Light is emitted by an LED and absorbed by an integrated luminophor, which subsequently changes to an excited state and releases a part of the energy as fluorescence. Some energy is transferred to the oxygen molecules in the presence of oxygen, resulting in a lower fluorescence signal (luminescence quenching). In contrast to other DO sensors, the medium is separated from the detector by a membrane that is only permeable for oxygen. Hence, the interference of medium components or gases with the detector is avoided. Further, this sensor works without an electrolyte, which might cause problems due to leakage. Due to its sensitivity, also at low concentrations (e.g. at 1 %-vol: ± 0.05 %-vol) and a low detection limit (0.01 %-vol), the sensor can be applied also in anaerobic fermentations like the brewing process (Bockisch et al., 2014).

ii. Fluorescence Spectroscopy and Optical Fibers

Most of the methods for UV/Vis spectroscopy mentioned above cannot be applied *in-situ*. This can be overcome by using light conducting fibers, which can be inserted into a tank. Via fibers the light of an analysis instrument, sensitive to sterilization, is introduced into and the signal is conducted out of the reactor. These signals can be further processed externally by the corresponding instrument (Vojinović et al., 2006).

Fiber-optics can be applied for the monitoring of oxygen. In several anaerobic processes, e.g. the brewing process, it is of high importance to monitor traces of oxygen since the presence or absence of oxygen may influence the process or lead to unwanted oxidation processes, e.g. during bottling.
The phosphorescence (RTP) measurement principle was utilized in a sensor for the multi-position monitoring of DO in water (Díaz-García et al., 2001). The amount of oxygen directly influences the RTP of light, which is trapped in a sol gel solid matrix and emitted by a metal chelate. Four RTP oxygen sensor flow cells, each containing one bifurcated optical fiber, were assembled in order to measure the oxygen content in four water streams. A xenon flash-lamp emitted light to different sites of the four sensing active regions, respectively. Hence, the RTP signals from each of the four sensing materials could be differentiated. Multi-channel phosphorescence detection was realized by a cooled intensified charge-coupled device (ICCD). By the change of the RTP sensing material, monitoring systems for other parameters could be easily developed (Díaz-García et al., 2001).

For the measurement of DO and gaseous oxygen as well as the pH-value directly in the liquid phase of a reactor, dipping probes from PreSens GmbH (Germany) can be used. These chemical sensors utilize the polymer optical-fiber (POF) technology. In case of the oxygen probe, the partial pressure of both dissolved oxygen and gaseous oxygen is measured. The polymer optical fiber has a polished distal tip that is coated with an oxygen-sensitive foil. The LED light excites the sample molecules evoking a fluorescent signal. If an oxygen molecule hits the sensor spot, excess energy is transferred to the oxygen molecule, leading to a decreased fluorescent signal intensity.

A similar type of dipping probe from PreSens is applied for DCO_2 detection. For this approach, the luminescence lifetime is measured based on the overlaying signals of an analyte-sensitive indicator and an inert reference sensor. The luminescence of the indicator can be suppressed by CO_2, leading to a reduced signal intensity. These probes can be applied in many bioprocesses, e.g. in yeast fermentations (Klein et al., 2013). The analyte, however, has to be fluorescence-active and requires a specific combination of emission and excitation wavelengths. This is not easy to realize in fluorescence sensors that are designed for *in-situ* application (Wolfbeis, 2005).
For shake flasks, sensor spots from PreSens for the optical biomass determination in the liquid phase are available. The measurement is based on the detection of light scattered by particles inside the liquid. The data can be easily correlated to data from OD_{600} measurements or the DCW (Schmidt-Hager et al., 2017; Tietgens et al., 2017).

Another fluorimetric pH sensor was developed by the PreSens GmbH (Germany) for *in-situ* application in single-use bioreactors using an ion permeable polymer matrix. This is immobilized on the inner wall of the reactor, containing the reference and the indicator dye. For this sensor, however, fluorescent background due to the accumulation of peptides, cell debris as well or viable cells is a challenge and leads to decreased resolution and dynamic range (Janzen et al., 2015). Two fluorescence sensors were evaluated during anaerobic *Clostridium acetobutylicum* cultivations. Further improvements could be achieved by retrofitting the sensors with a black colored hydrogel layer on the fluorescence material. The background fluorescence signal of the medium (transparent reactor wall) was decreased by the integration of an adhesive photoresistant foil at the bioreactor bottom, shielding the fluorescence readers (Janzen et al., 2015).

Optical fibers without fluorescence can be used for the pH monitoring by the measurement of the specific absorption spectra of a pH sensitive dye or pH indicators (Jeevarajan et al., 2002; Vojinović et al., 2006). A set of 16 pH indicators for *in-situ* measurements was used during high pressure treatment of food products. The spectral data were analyzed using a multivariate data model and pH-values, which were calculated based on the measurement in five standard solutions and the consideration of thermodynamics under high pressure. By this tool, a pH-value with an accuracy of 0.02 pH-units is measurable at pressures up to 450 MPa (Stippl et al., 2004). Although this is far higher than in brewing fermentation processes, it might be a useful tool in fermentations with overpressure.
DCO_2 can be measured as well using pH indicators. Uttamlal and Walt applied a modified Severinghaus principle by separating the carbonate buffer, containing the entrapped pH indicator dye, from the broth by a CO_2 permeable membrane (Uttamlal and Walt, 1995). DCO_2 molecules permeating from the broth, e.g. beer, lead to a change in the pH-value in the buffer. The change in the pH-value is correlated to the external DCO_2 concentration by the Henderson-Hasselbach equation. The sensor device is even steam sterilizable. The dynamic range of DCO_2 was determined to be 0 - 0.2 atm with a sensitivity of $\pm 2.5 \times 10^{-3}$ atm (at 0 - 0.25 atm) and $\pm 2.5 \times 10^{-2}$ (> 0.25 atm). A linear correlation between temperature and DCO_2 concentration (0.2 % per 1°C) could be determined at 5 - 35 °C for temperature compensation. Photobleaching, changes in dye concentration, a drift in the photodetection system, or lamp intensity fluctuations are challenges for this measurement principle. Applying the “ratiometric method” during sensor calibration these problems can be minimized. This method uses the ratio of the relative intensity of the luminophor at one emission maximum, when exciting the dye at two different excitation maxima (Uttamlal and Walt, 1995).

In anaerobic yeast-based processes, ethanol is either the main or a side product. The increasing market for bio-based fuels requires the development suitable sensors (Thungon et al., 2017). A miniaturized

optical radiometric sensor, applicable for *in-situ* measurements, was developed by Petrova and co-authors (2006) for the monitoring of short-chain alcohols, such as methanol, ethanol or propanol. It is equipped with the fluorescent dye Nile Blue Chloride. This dye is immobilized in a hydrogel during cross-linking of poly-(ethylene glycol) dimethacrylate. The dye emits a single fluorescence peak in solution and a dual emission peak in the gel, which allows the detection of alcohols. The sensor is sensitive for short-chain alcohol concentrations in a range between 5 % and 90 % v/v. Due to the embedding in the hydrogel, it also provides stable measurements after thermal sterilization. The highest sensitivity is achieved in acidic and neutral media like they are present in many anaerobic processes, for example in the brewing processes (Petrova et al., 2006). This system is regarded as a contribution towards the achievement of small-scale, portable alcohol measurement systems, which can also be linked to an upstream process with (single-use) *in-line* connectors (Thungon et al., 2017).

Osmotic pressure also might have an influence on an optical sensor. This problem and others such as dye leaching and cross-sensitivities to ions can be solved by using solid-state sensors. A possible construction, which is steam-sterilizable, is the integration of a fluorescent dye into a hydrophobic silicone membrane, containing quaternary ammonium hydroxide for silicone etching. The measurement is based on CO_2 quenching, leading to a transfer of fluorescence resonance energy between a donor and an acceptor. Finally, the fluorescence lifetime is measured (Chang et al., 1998). On the other side, the emission spectra have to be detected with conventional spectrometers. This was done during a continuous *Escherichia coli* fermentation (Ge et al., 2003). In this study, it was proven that with increasing base concentration the sensor stability increased but the sensitivity decreased.

2.3.2.3. Application of data driven and Model-based Analytical Tools in the Brewing Process

The installation of complex technique in the liquid phase or at the wall of a reactor is not always feasible or the technique is not available. Hence, the number of progressive process control strategies in the food, fermentation, and beverage production is increasing, by which the product quality is maximized and production costs are reduced (Kondakci and Zhou, 2017). Various applications of data driven and model-based methods for process control in food processing, e.g. in baking, fermentation, and brewing processes or dairy production were reviewed by Kondakci and Zhou (2017). Some more examples for the application of data driven and model-based methods in the brewing industry are given in the following.

The changes in specific gravity during beer production can be determined *on-line* by the correlation to the *on-line* measured CO_2 formation. Since the CO_2 formation is stoichiometrically related to the carbohydrate consumption rate, yeast growth, and ethanol formation it can be used representatively for *on-line* fermentation monitoring (Daoud and Searle, 1990). The amount of CO_2 was measured in a non-invasive way during a pilot-scale beer fermentation (10 – 13 m^3) using a dry gas meter integrated in a by-pass pipe (Daoud and Searle, 1990).
A virtual plant operator was designed by Birle and co-authors (2015) for the *on-line* control of yeast propagation by using ANN and fuzzy logic control systems. The optical density, temperature, pressure, density DO, and pH-value were monitored using a sensor array. These data were integrated into a ANN for *on-line* biomass determination. In combination to a temperature dependent metabolic growth model, the temperature and aeration were set by the system as follows. The deviation of the predicted biomass values from the reference, obtained by the metabolic model, was fed into the fuzzy

temperature control system, whereas the deviation of the measured extract from of the reference, the predicted cell count, and the DO concentration was used as input for the fuzzy aeration control system. Hence, this technique allows for the dynamic optimization of yeast propagation processes in *real-time* (Birle et al., 2015).

Another data driven model approach is the multivariate statistical process control. It was applied for the monitoring and control of a beer fermentation process and created based on PCA and PLS methods (see 2.3.4). The experimental data set for the model was obtained by sensor measurements of temperature, pressure, conductivity, and turbidity as well as ultrasonic technique. By the implementation of a fuzzy logic system combined to an online control chart the process course could be monitored and deviations from the target values and control limits were detected in *real-time.* This enables the estimation of the process status and fast intervention (Geier et al., 2016).

For the prediction of the process course of a beer fermentation in a pilot plant (0.15 m^3), ANN combined to feedforward control were used. The input values were obtained by monitoring the gravity, pH-value, and diacetyl. The process temperature and time were selected as control values. The model output showed that the process time was reduced by 20 % with the optimization of the temperature profile during the process (Becker et al., 2002).

The beer quality can be evaluated by the investigation of the foamability and chemical composition. To overcome elaborate analyses in the laboratory, a method combining robotics, near infrared spectroscopy, and machine learning algorithms, such as ANN, was developed. Samples from eight top, seven bottom, and six spontaneous fermented beers were analyzed with six replicates. 15 foam-related parameters were determined using the foam analyzer RoboBEER (a robotic pourer). The chemical constitution was analyzed by near infrared spectroscopy. The data were used for the prediction of parameters related to the foamability (pH-value, alcohols, extract / density, maximum foam volume) by PLS and ANN. The near infrared spectroscopy analysis also revealed protein content specific overtones that were correlated to certain beer foaming characteristics. The ANN method resulted to be more accurate with a regression coefficient of $R^2 = 0.95$ (Gonzalez Viejo et al., 2018).

2.3.3. Mobile Multi-Parameter Sensor Technology

For process monitoring and control, it is necessary to measure several cultivation parameters simultaneously and directly in the liquid phase of the process in order to detect small and rapid changes. For the multi-parameter *in-situ* monitoring during an *S. cerevisiae* cultivation, a sensor chip containing enzyme sensors (amperometric) and impedance spectroscopy was developed. By this, nutrients, metabolites (lactate), and cell mass were measured simultaneously. Substance detection was possible in a linear range of up to 600 mM for glucose and 900 mM for lactate (Mross et al., 2015). This sensor system, however, was applied only in lab-scale reactors and no statement is given concerning long-time stability or the use in medium with high gas concentration such as green beer.

A submergible and autoclavable chip of only 6 mm diameter was designed for the measurement of pH-value (ISFET), temperature (resistance), DO (amperometric), and viable biomass concentration (impedance) during yeast cultivation in micro-well plates (Krommenhoek et al., 2008). Although this device can be applied directly in the liquid phase, no evidence has been reported for the application in industrial scale or for long-term stability in anaerobic fermentation with higher gas content. Especially the latter aspect is a challenge beside the increased clogging of micro-membranes or enhanced toxification of small electrolyte volumes as the author of this these has experienced even for larger sensors with higher mechanic stability.

Beside the multi-parameter aspect, there is a need for space-resolved measurements. As explained in 2.2.3, gradients in nutrient and metabolite concentration, DO, DCO_2 and temperature exist, especially in large-scale processes due to limited power input. This is the case for both aerobic (Enfors et al., 2001) and anaerobic processes (Kielhorn et al., 2015). Nevertheless, in most cases in industry the sensors are installed at only one position of the reactor. Especially in large-scale, data from one sensor cannot represent the whole reactor volume (Bockisch et al., 2014).

For this purpose, Schuch investigated the distribution of temperature, yeast cells, pH-value, ethanol and diketone content as well as other important fermentation parameters in model tanks (Schuch, 1996b; Schuch, 1996c). These were of different H/D ratio and size (maximum volume: 4.5 m^3), constructed or retrofitted for these experiments. For the determination of the space resolved parameters, he inserted ports for temperature sensors or sampling units at different heights of the reactor wall (Schuch, 1996a; Schuch, 1996d).
A further development of a submergible device is the mobile multi-parameter-sensor with miniaturized electrodes, which can be also applied in industrial-scale anaerobic fermentations (Sachse et al., 2015). Up to six sensors can be integrated due to the miniaturization of the sensors (length: around 30 mm, tip diameter: 3-4 mm). With this sensor unit, the pH-value, redox potential (both using a common silver chloride reference electrode), DO, DCO_2, temperature and pressure can be measured directly in the liquid phase. Due to the integrated temperature electrode, all temperature-dependent parameters can be easily compensated. The modular construction allows the exchange of electrodes according to the aim of application. By now, this mobile multi-parameter sensor unit has been installed in brewing reactors (Bockisch et al., 2014) and biogas digesters (Kielhorn et al., 2015). It provides information about the distribution of system parameters and allows the investigation of the fluid flow.

The low number of studies available in literature – especially in industrial scale - indicates the demand for new mobile multi-parameter sensor techniques, which can be:

- inserted directly in the liquid phase of large-scale bioreactors,
- moved locally flexible inside the reactor,
- applied during long fermentation times including robust data transfer, and
- withstand harsh, complex media.

This thesis shows an alternative to the existing techniques by using both miniaturized and commercially available sensor systems (Bockisch et al., 2014) (see also Materials and Methods).

2.3.4. Multivariate Data Analysis

For correlation analysis and data evaluation of multivariate data sets, the number of variables shall be reduced without the loss of important information (Kessler, 2006). Dependencies of different variables might be of linear, co-linear or non-linear nature. Hence, they require different, i.e. multivariate, analysis methods. The analysis output can be used for process understanding and optimization (Geier et al., 2016).

In the field of biology, pharmacy, and (bio-)process engineering, especially PCA and PLS methods are established since a large number of different data sets can be analyzed and data of importance as well as their dependencies can be identified. For a comprehensive summary, see (Aït-Sahalia and Xiu, 2017; Cernuda et al., 2017).

Principal component analysis (PCA) and partial least square (PLS) regression

The PCA reduces the data dimensionality with a minimum loss of information. The major part of data variation is summarized and common properties, i.e. principal components (PC), are identified (Aït-Sahalia and Xiu, 2017; Jolliffe and Cadima, 2016). Since they are uncorrelated, the PCs represent different properties. In many cases, one PC represents more or less one measurement method (Ghasemi-Varnamkhasti et al., 2011).
An axis is placed through a multidimensional data set that includes most of the variance. Each sample is projected vertically to this axis forming point clouds and clusters. By linear combination of the original *X*-variables, the variables obtained from experiments are converted into latent variables and scores. The PC scores are defined by the location of each sample along this one-dimensional axis. Hence, by this method the data is reduced to one dimension on one axis, i.e. PC. A 2nd axis is located orthogonally to the 1st one, which represents the maximum remaining variance. Then, a 3rd, 4th or even more axes can be located orthogonally to the previous one (Ghasemi-Varnamkhasti et al., 2011). The aim is, however, that only the first few PCs consider the majority of the variance of the original data, containing the most important information, in order to delete the last ones and obtain a simplified model (Palermo et al., 2009).
In this study, PCs are generated from the relation of the independent data *X* (*on-line* sensor data) and dependent data *Y* (data from *off-line* analysis). For a PC regression, a PCA of the matrix *X* is performed, followed by a multilinear regression between the scores obtained in the 1st step and the response matrix *Y* (Palermo et al., 2009).

The PLS regression is a suitable method for modeling data of multiple dimensions or response variables and high levels of co-linearity while considering each single response (Palermo et al., 2009). The PLS regression coefficients serve for the identification and selection of relevant predictors where the relevance is indicated by the magnitude of their absolute values.
The matrix *X* is decomposed to Matrix *T*, representing the *X*- scores, the matrix *P'*, representing the *Y*-loadings, and an error matrix *E* (equation (2.3)). In the same way, the matrix *Y* is constructed (Equation (2.4)).

$$X = TP' + E \tag{2.3}$$

$$Y = UQ' + F \tag{2.4}$$

The matrices *X* and *Y* are called "outer" relation and modeled by the score vectors *T* and *U*. It is aimed to minimize the norm of F while keeping the relation between *X* and *Y* by the equation (2.5), i.e. the "inner" relation, with *D* being a diagonal matrix.

$$U = TD \tag{2.5}$$

The *X* - scores are orthogonal and generated by linear combinations of the original variables x_k with the *weightings* w^*_{kl} ($k = 1, 2, \ldots, p$; $l = 1, 2, \ldots, a$), leading to the equation:

$$T = XW^* \tag{2.6}$$

Hence, the PLS serves for the construction of a matrix of latent variables that are generated by the linear transformation of *X* with the matrix of weights: $W^*(p \times a)$.

Using the „inner" relation (equation (1.3)), the following equation is generated (Palermo et al., 2009):

$$Y = UQ' + F = TDQ' + (HQ' + F) = TC' + F^* = XW^*C' + F^* = XB + F^* \tag{2.7}$$

with the matrix *B* ($p \times m$), i.e. the PLS regression coefficients, defined by the equation:

$$B = W * C' \tag{2.8}$$

3. Research Questions and Aim of the Project

The overall aim of this study was the investigation of large-scale bioprocesses with the special focus on spatial gradients that might appear in the liquid phase and their magnitude. The development of analytical tools for the multi-parameter *in-situ* and *on-line* determination of spatial gradients of process parameters was a major part of this project. During the realization of the project, several research questions arised:

1. *What is a suitable sensor tool for the long-term measurement and investigation of gradients in the liquid phase of large-scale fermentation tanks? Which sensor response, measurement accuracy, and stability are required to determine the magnitude of gradients?*

Answering these questions was the aim during the first and most challenging step of this thesis: the development of a submergible sensor technique, which can be applied in large brewing tanks, independently from the tank geometry or size, and is minimally invasive. Housing units with sensors were required that withstand harsh conditions, measure accurately without recalibration during a time of ten days or more - i.e. show a drift of max. 2 % during this time - and possess a response time below 30 sec. The sensor tools also shall meet the requirements for disinfection or even sterilization of a beverage or food production process.

Two systems were already available: a) miniaturized sensors developed by the “Kurt-Schwabe-Institut für Mess- und Sensortechnik e.V.” Meinsberg (KSI) for the pH-value, the redox potential, the DO- and DCO_2-value, the conductivity, the pressure, and the temperature and b) commercial sensors developed by the Hamilton Germany GmbH (HM) for the pH-value, the redox potential, the DO-value, the conductivity, and the temperature (integrated in each sensors).

A minimum of four parameters was aimed to be measurable simultaneously. In case of proven sensor stability, more sensors integrated in one unit would be beneficial.

2. *How is the data transfer between the sensors and the acquisition computer realized in closed fermentation tanks without losses in signal stability? What is the maximum distance that can be overcome with the sensors selected in step 1?*

A stable data transfer across long distances of at least 5 m for the small-scale and 30 m for the large-scale was aimed as well as the development of adequate data visualization systems for *real-time* monitoring, such as LabVIEW- or Python-based programs. A stable data transfer across more than 5 m required amplifiers that are integrated directly in the sensors head before signal transport, which limited the choice of sensor suppliers.

3. *How can we localize the sensor units inside a tank in order to relate the on-line data to positions (x, y, z) and obtain both, time and space-resolved data?*

It was attempted to localize the sensor units by ultrasound. The sensor signal, however, was interrupted as soon as the amount of small gas bubbles increased due to CO_2 formation. This was the case at the onset of the fermentation and during the main fermentation phase, covering the most important fermentation phases for the investigation of gradients.

Therefore, it was aimed in the following to determine the sensor position with the pressure sensor of the miniaturized sensor unit up to the scale of 24 m^3. It measures the hydrostatic pressure, representing the sensor location in vertical direction. Additionally, pre-defined positions were marked on the rope that was used for the positioning of the sensor units.

4. *Are there gradients formed in unstirred large-scale brewing fermentations and what is their magnitude?*

After the proof of concept concerning the sensor functionality in the laboratory scale (up to 0.17 m^3), the sensor technique should be applied at multiple positions in large-scale brewing fermentation processes with a fermentation volume of 3 m^3, 24 m^3, and 170 m^3.

By this, it should be investigated whether gradients exist in certain phases, of which magnitude they are, and at which positions they appear. Critical reactor zones should be identified in order to define optimal positions for the installation of sensors, which monitor representative zones of a reactor. The identification of critical process phases by the sensor technique was a further aim in order to provide suggestions for process optimization.

5. *How do yeast cells react to stress caused by heterogeneities in large-scale reactors? Which changes in the concentration of carbohydrates, main carbon metabolites, and sterols can be determined?*

In order to investigate the physiological and metabolic state of cells and define sensitive parameters of the different fermentation stages for deeper process understanding, *off-line* analysis of carbohydrates, main carbon metabolites, and sterols were performed using GC and HPLC methods.

6. *Which parameter dependencies can be identified between the on-line data, obtained with the mobile multi-parameter sensor tool, and the data from off-line analysis?*

The last aim was the correlation of *on-line* and *off-line* data in order to identify dependencies between these parameters by multivariate data analysis (PCA, PLS). This idea supports the identification of possible soft sensors, with which unmeasurable parameters can be predicted based on *in-situ, on-line* measurements.

4. Materials & Methods

4.1. Mobile Multi-Parameter Sensor Technology for *on-line* Monitoring

4.1.1. Applied Sensors and Measurement Principles

Two different multi-position sensors were applied:

a) Miniaturized sensors from the KSI (Germany) for redox potential, pH-value, reference (for redox potential, pH-value), dissolved oxygen, temperature (Fig. 8 A, B), dissolved carbon dioxide (Fig. 8B), and pressure (Fig. 8 C).

b) Commercial sensors from HM (Planegg-Martinsried, Germany) for the redox potential (EASYFERM PLUS ORP Arc), pH-value (EASYFERM Plus ARC), DO (VISIFERM DO ARC), and conductivity (CONDUCELL 4USF ARC) (Fig. 9).

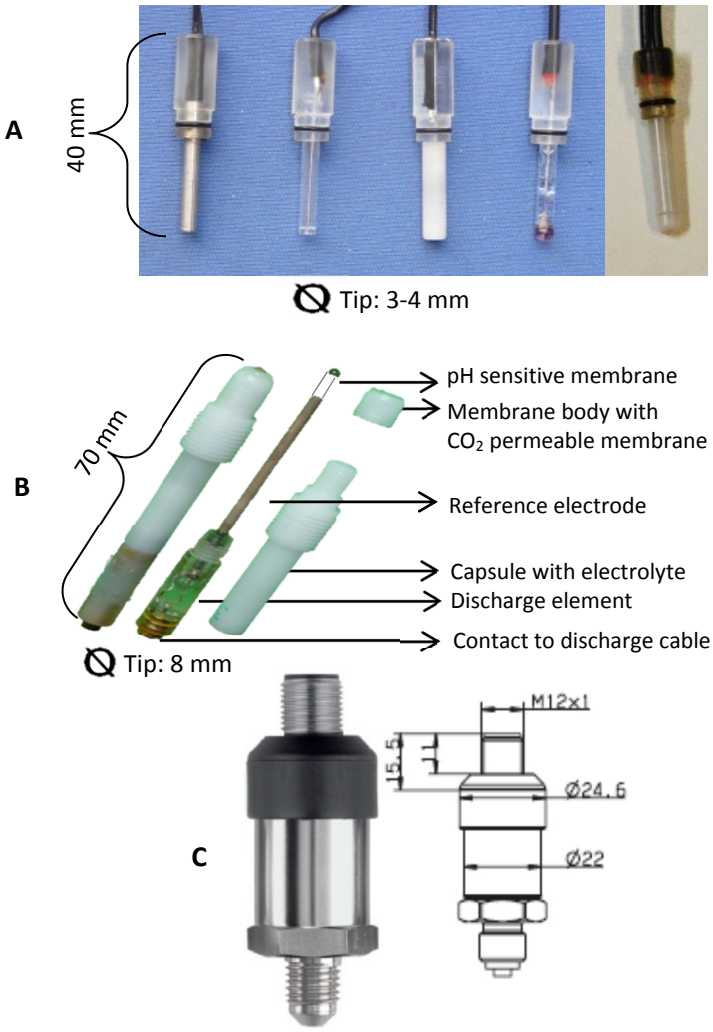

Fig. 8: Miniaturized sensors (KSI, Germany).
A: Sensors from left to right: temperature, redox potential, reference, pH-value, DO; B: DCO_2 sensor;
C: pressure sensor JUMO MIDAS 08, type 401002 (JUMO GmbH & Co. KG).

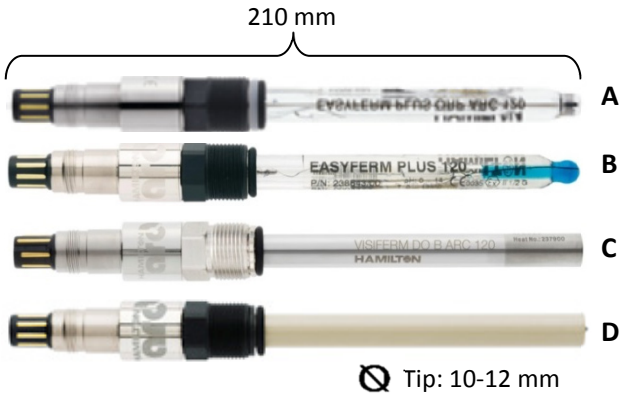

Fig. 9: Arc-sensors (HM).
A: Redox potential; B: pH-value; C: DO; D: Conductivity. Temperature sensors are included in each sensor as well as reference electrodes for A and B.

Measurement principles:

The various measurement principles and main sensor components as well as the construction materials are displayed in Table 1. Most of the sensor measurement principles are based on potentiometry and resistivity. In addition, optical and amperometric measurement principles were used for the measurement of dissolved oxygen.

Due to the optical measurement principle of the DO-sensor from HM, no interferences with the medium components, e.g. CO_2, SO_2 occur, which extends the long-term stability. The sensor is resistant against ethanol, methanol, H_2O_2, ethylene oxide, and beta-gamma irradiation (Hamilton_Company, 2011). Furthermore with the optical measurement system, very small oxygen concentrations can be measured during long-term usage (Georgy, 2015). This is important for both the measurement of gradients and the determination of oxygen traces in the food industry with products sensitive to oxidation processes, e.g. beer or lipids.

For the application in the food industry also the commercially available sensors for the pH-value and redox potential with electrolyte are suitable due to the composition of the applied electrolyte “Foodlyte”, which is biocompatible, food-safe, not cytotoxic, and can withstand autoclavation at high temperatures of up to 140 °C (Hamilton_Company, 2012c).

4.1.2. Measurement Stability / Drift

Several measurement devices were applied in different fermentation processes and constantly developed based on their performance, drift properties, and suitability for their long-term application in the brewing process (Table 2). The first measurement system consisted in separated miniaturized sensors, followed by their integration into silicon flow cells (section 4.1.3). A further improvement was the use of stainless steel flow cells, which avoided oxygen permeation and allowed the fixation of the sensors due to their modular construction. For *in-situ* and multi-position measurements, the miniaturized sensors were integrated in a submergible sensor unit (Fig. 13). These devices were developed by or in cooperation with the KSI. Due to long-term instability (5.1.1), the commercially available sensors from HM were added as a second system and integrated in a housing unit as well (Fig. 14).

For testing the sensor performance and long-term stability as well as the handling of the sensor flow cells and units, canisters, fermentation columns, and small-scale tanks with a volume of up to 0.17 m^3 were used in the laboratory scale (Table 2). During these tests up to a fermentation volume of 40 L the sensors were not moved along the tank height because the investigation of gradients was not the focus here. The sensor technique might have influenced the fluid dynamics in the small volumes and therefore not been representative for larger scales concerning gradient formation.
The fermentations columns are available for a fermentation volume of 3.6 and 40 L (Fig. 10) and allow for the simulation of different media composition or fermentation conditions, e.g. overpressure of up to 3 bar, in a small volume (Folz and Tyrell, 2011).
Further, they allow for sampling at a more centered position than in CCTs, the installation of equipment via VARIVENT® connections, and the usage of by-pass constructions for flow cells with integrated sensor technology. Hence, there were very useful for the first testing of the sensors in complete fermentation processes under conditions similar to the industrial scale. The latter were used for testing the sensor drift (see below).
The pre-tests were then followed by the application of the sensor units in the semi- and industrial scale (3, 24, 170/199 m^3) for the investigation of gradients (not included in Table 2). With increasing scale, continuous improvements were made regarding the sensor unit construction, the data transfer and the installation on the tank dome.

Fig. 10: Fermentation columns at laboratory scale.
A: 3.6 L; B: 40 L fermentation volume; C: Bypass solution for the application of the sensor flow cell in 3.6 L fermentation columns using a pump.

Table 1: Measurement principles and components of the applied sensors.

Sensor	Principle Micro-Sensors (KSI)	Main Components / Materials	Principle Commercially available Sensors (HM)	Main Components / Materials
DO	**Amperometric** - Defined working potential = 800 mV - 3-electrode system: cathode, anode, reference electrode - Cathode and anode: separated from the sample by gas permeable membrane - O_2 is reduced by an electrolyte at the platinum cathode, silver is oxidized at the anode → electrical current proportional to pO_2	- Capsule: Polyoxymethylene (POM) with screwable cup - Microcathode diameter: 30 µm - Gas-permeable membrane: polypropylene - Aqueous electrolyte	**Optical** Oxygen-dependent luminescence quenching via 2 LEDs (phase fluorimetry)	- Wetted parts: stainless steel, EPDM and silicone (both FDA approved) - Blue LED for excitation of luminophor & red reference LED - Screwable, exchangeable cap containing an O_2 - sensitive luminophore and an O_2-permeable membrane
pH-value	**Potentiometric** - Dependency of electrochemical potential on the ion concentration - Measurement of potential difference between reference system and medium	- Shaft and spherical membrane: glass - Reference electrode: Platinum wire with sintered AgCl body - Electrolyte: pH = 7, AgCl & KCl saturated buffer	**Potentiometric** (like micro-sensors, difference: integrated reference electrode)	- Wetted parts: stainless steel, EPDM for O-rings (FDA approved), Pt for redox potential (ORP) - Electrolyte: pressurized PhermLyte (clog-free diaphragm) - Reference System: silver ion barrier → silver chloride reservoir is separated from the reference electrolyte by a diffusion distance - Diaphragm: HP-COATRAMIC - ORP Element: Platinum Ring
Redox Potential	**Potentiometric** - Dependency of electrochemical potential on the ion concentration - Measurement of potential difference between reference system & medium	Thick-film technique: - Ceramic sensor chip (Al_2O_3) with Pt discharge - Planar redox glass layer (electrochemical effective area) - Final covering polymeric sealing layer	**Potentiometric** (like micro-sensors, difference: integrated reference electrode)	
Reference electrode	**Constant potential** As reference for pH-value, redox potential measurements	- Capsule for electrolyte: Polyoxymethylene (POM) with screwable cup - Ag/AgCl electrode, Electrolyte: KCl gel - Diaphragm: porous aluminium oxide ceramics	**Integrated in each sensor**	

Temperature	**PT 1000** Dependency of the electrical resistivity on the temperature of platinum	- Nickel-Platinum-jacketed wire - Shaft: stainless steel	**22 kΩ NTC** (Negative Temperature Coefficient Thermistor) Temperature dependent resistor, integrated in each sensor
DCO_2	**Potentiometric** 2 electrode system: reference electrode and integrated pH electrode (Severinghaus principle)	- Sensor shaft: Polyoxymethylene (POM) - Membrane: gas-permeable, polymethylpentene - Inner pH electrode: glass body, filled with buffer solution - Electrolyte cup: contains glycol solution	/ /
Pressure	**Piezo-resistive** Change of the electrical resistance of a material due to pressure → measurement of distension	- Sensor shaft: stainless steel - Plug connection: stainless steel, nickel-plated brass - Sensor: thick-film on ceramic basis with Al_2O_3 (96 %)	/ /
Conductivity	/	/	**Resistivity** (4-electrode contact measurement) - Wetted parts: PEEK, EPDM for O-Rings (all FDA approved), stainless steel - Electrode Material: USF: stainless steel
Corresponding literature or websites	(Päßler et al., 2010; Sachse et al., 2015)		**Arc Series:** (Hamilton_Company, 2012b) **DO**: (Hamilton_Company, 2014b; Hamilton_Company, 2016d) **pH-value**: (Hamilton_Company, 2012a; Hamilton_Company, 2016b) **Redox potential**: (Hamilton_Company, 2012a; Hamilton_Company, 2016c) **Conductivity**: (Hamilton_Company, 2014a; Hamilton_Company, 2016a)

Table 2: Overview of experiments and equipment for testing sensor functionality, stability and drift. (Chronological order.)

No.	Scale / Volume	Fermenter / Vessel	Sensor Equipment	Miniaturized Sensors (KSI)					Larger Sensors (HM)			
				pH	Redox	DO	Temp. & DCO_2	Pres-sure	pH	Redox	DO	Conduc-tivity
1	0.17 m^3 (170 L)	Pilot tank	Flow cell KSI, silicone	✔	✔	✔						
2	0.0036 m^3 (3.6 L)	Fermentation columns	Flow cell KSI, silicone	✔	✔	✔						
3	0.01 m^3 (10 L)	Canister	Single sensors KSI	✔	✔	✔						
4	0.15 m^3 (150 L)	Pilot tank	Sensor unit KSI	✔	✔	✔	✔	✔				
5	12 L (0.012 m^3)	Canister	Sensor unit KSI	✔	✔	✔	✔	✔				
6	0.17 m^3 (170 L)	Pilot tank	Sensor unit KSI	✔	✔	✔	✔	✔				
7	0.0036 m^3 (3.6 L)	Fermentation columns	Flow cell KSI, stainless steel with fixed sensors	✔	✔	✔	✔					
8	0.0036 m^3 (3.6 L)	Fermentation columns	Flow cell, stainless steel with fixed sensors and bypass	✔	✔	✔	✔					
9	0.16 m^3 (160 L)	Pilot tank	Sensor unit and single sensors KSI	✔	✔	✔	✔	✔				
10	3 m^3 (3000 L)	Brewery Tank		✔	✔	✔	✔	✔				
11	0.04 m^3 (40 L)	Fermentation columns: Test of drift during time		✔	✔	✔	✔	✔				
12									✔	✔	✔	✔
13			Sensor unit KSI & HM sensors (no integration into unit)	✔	✔	✔	✔	✔	✔	✔	✔	✔
14				✔	✔	✔	✔	✔	✔	✔	✔	✔
15	0.15 m^3 (150 L)	Pilot tank: Test of drift during time		✔	✔	✔	✔	✔	✔	✔	✔	✔

The 24 and 170/199 m^3 scale as well as later experiments in the 3 m^3 scale are not represented here as they were not part of the testing phase of the sensor systems.

An important step for the application of the various devices for multi-parameter monitoring in the liquid phase of industrial scale reactors besides testing sensor functionality and handling is the determination of the long-term stability and drift in different processes. For the estimation of the sensor drift during time and the maximum stability without recalibration in a real long-term fermentation process, several experiments have been performed. In the following, two selected experiments in the laboratory, one in the semi-industrial and one in the industrial scale are described:

(1) Application of the miniaturized sensor unit (KSI) in a beer fermentation for about 92 h in 3 m^3 wort (pH = 5.3, original gravity = 11.2 %) with the bottom fermenting yeast *S. cerevisiae,* Saflager W-34/70 at 11 - 12 °C. This corresponds to number 10 in Table 2.
The reference measurements were conducted in standard sterile wort with a pH-value of 5.2 and 11.5 % original gravity (VLB Berlin e.V., Germany) before and after the fermentation. Both reference measurements were conducted in the same batch of sterile wort as at the fermentation start. The sensors were calibrated once before the experiment.

(2) The miniaturized sensor unit (KSI) and commercially available sensors (HM) without integration into a unit were applied in two long-term beer fermentations (170 h and 190 h) at the laboratory scale in fermentation columns with 40 L of wort, i.e. complex media. For the preculture 1 L wort containing 60 g of the bottom fermenting yeast *S. cerevisiae,* Saflager W-34/70 (Fermentis) was stirred and aerated for about 45 min. It was then pitched in 40 L of wort (Export-wort: pH = 5.2, original gravity = 13.0 %) and fermented between 10.5 and 11.5°C. This corresponds to number 13 and 14 in Table 2.
In order to measure the sensor accuracy and drift in standard solutions with a daily frequency, the sensors were taken out of the fermentation broth once per day and inserted in the corresponding standard solutions for 10 minutes, respectively: pH = 4.01 and 7.0, solutions with a redox potential of 124 mV and 250 mV (Fluka Chemie GmbH / Sigma-Aldrich Chemie GmbH, Munich, Germany), solutions with conductivity of 100 mS (Fluka Chemie GmbH / Sigma-Aldrich Chemie GmbH, Munich, Germany), and standard sterile wort with a pH-value of 5.2 and 11.5 % original gravity (VLB Berlin e.V., Germany) for the DCO_2 reference.

(3) Application of both sensors systems in a fermentation for 69 h in 0.15 m^3 wort (pH = 5.2, original gravity: 14.2 % [2/3 export with 13 %, 1/3 high gravity with 16.5 %]) with top fermenting yeast *S. cerevisiae,* Safale S-04 (Fermentis) at temperatures of 21.7 - 23.4 °C. This corresponds to number 15 in Table 2.
A start reference measurement in standard solutions directly after the calibration and a reference measurement at the end of the fermentation (before deconstruction of the experimental setup) were recorded. The sensors were inserted in the corresponding standard solutions for 10 minutes, respectively: pH = 4.01, 7.0, and 10.0, and a solution with a redox potential of 250 mV (same as in (2)). The reference point for the DO sensor was set to 102 % saturation for the miniaturized system and 100 % saturation for the HM system in deionized water, which was aerated.

(4) Application of the HM sensors system in two long-term beer fermentations for about 222 h in 170 m^3 wort (pH = 4.9, original gravity: 14 %) with a bottom fermenting yeast strain at 10.5 - 11.5 °C for the main fermentation, 12.5 °C for the diacetyl rest and 9 - 12 °C during the cooling phase (depending on the position). This is not represented in Table 2 since it was an industrial scale fermentation and not a pre-test as in the laboratory scale.
The values recorded after calibration in standard solutions were considered as the reference values before the application of the sensors in the brewing media and a reference measurement at the end of the fermentation (before deconstruction of the experimental setup) was performed as for the other experiments. For this, the sensors were inserted in the corresponding standard solutions for 10 minutes, respectively: pH = 4.01 and 7.0, and a solution with a redox potential of 250 mV (same as in (2)). The reference point for the DO sensor was set to 100 % by the O_2 saturation [%] in air.

The results for all reference measurements are displayed in this order in section 5.1.1. Even after long-term application in harsh media, the larger, commercially available sensors resulted to be suitable concerning drift and accuracy for the anaerobic brewing process.

4.1.3. From Flow Cells to Mobile Multi-Parameter Sensor Units

In order to apply the miniaturized sensors in industrial fermentations, they have to be integrated into devices, which are compatible to tank access points. The first development made in this project was a flow cell made of polydimethylsiloxane (Fig. 11).

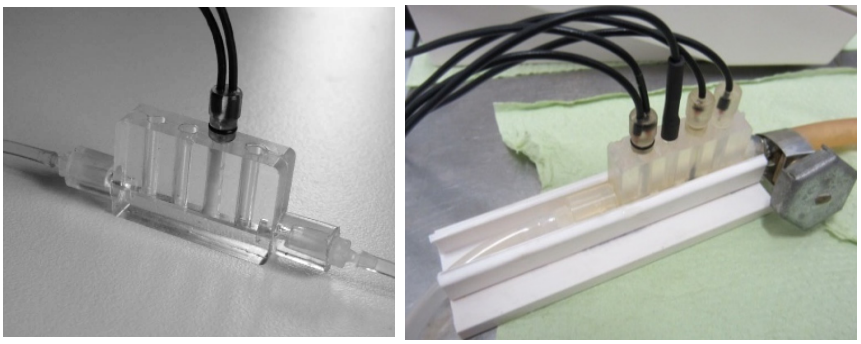

Fig. 11: Flow cell: Polydimethylsiloxane with miniaturized sensors (KSI, Germany).

This system was followed by a construction made of stainless steel, in which the sensors could be fixed avoiding a shift caused by hydrostatic pressure and reducing the amount of oxygen transfer into the flow cell (Fig. 12) (both KSI). The devices can be installed fast and flexibly at different fermenter systems. However, these devices also have some challenges:

- A bypass has to be constructed, which has to be disinfectable in case of the brewing process or even sterilizable for pharmaceutical applications.
- The sensors measure in a very small volume compared to the tank volume while they are exposed to a continuous flow stream.
- The flow and pressure have to be regulated in order to allow stable measurements, e.g. by a ball valve (Fig. 12 A, B).

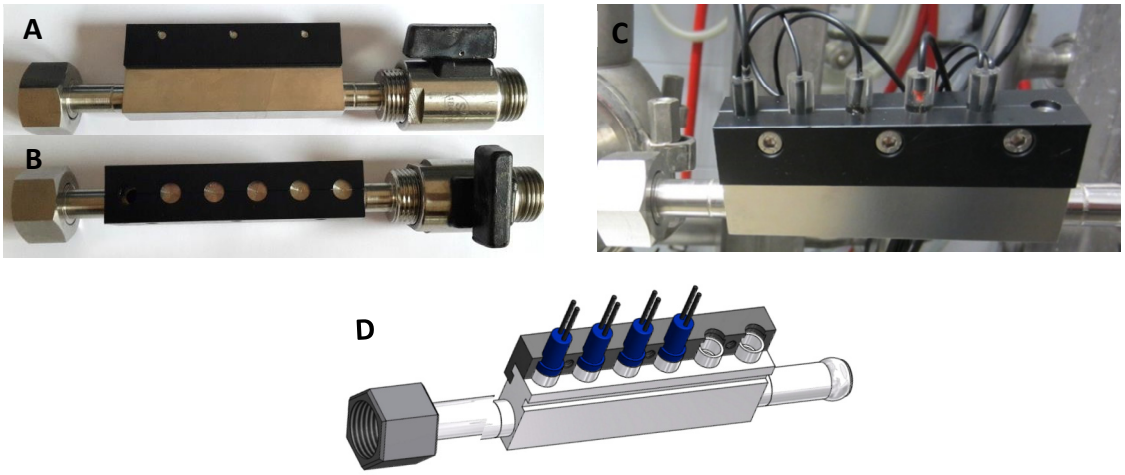

Fig. 12: Flow cell with sensor fixation: stainless steel, PEEK (KSI, Germany).
A&B: sensor flow cell with blind plugs (stainless steel) and flow stream regulation valve (A: open, B: closed),
C: Sensors integrated into the flow cell and connected to fermentation columns by a bypass construction.
D: Cross section of the flow cell and fixing mechanism.

A further development was the *in-situ* measurement with the sensors. For this, mobile housing units were developed in cooperation with the KSI. for the miniaturized sensors (Fig. 13) and the Exner Process Equipment GmbH for the sensors from HM (Fig. 14). Both housings are made of stainless steel. The cable connections and inner components of the small sensory unit are made of polyetheretherketone (PEEK). Its unscrewable hood protects the electrodes against mechanical influences and offers the possibility to change the electrodes. At the larger unit (Exner Process Equipment GmbH, Germany) there are metal rods integrated into the core component in which the electrodes are screwed in.

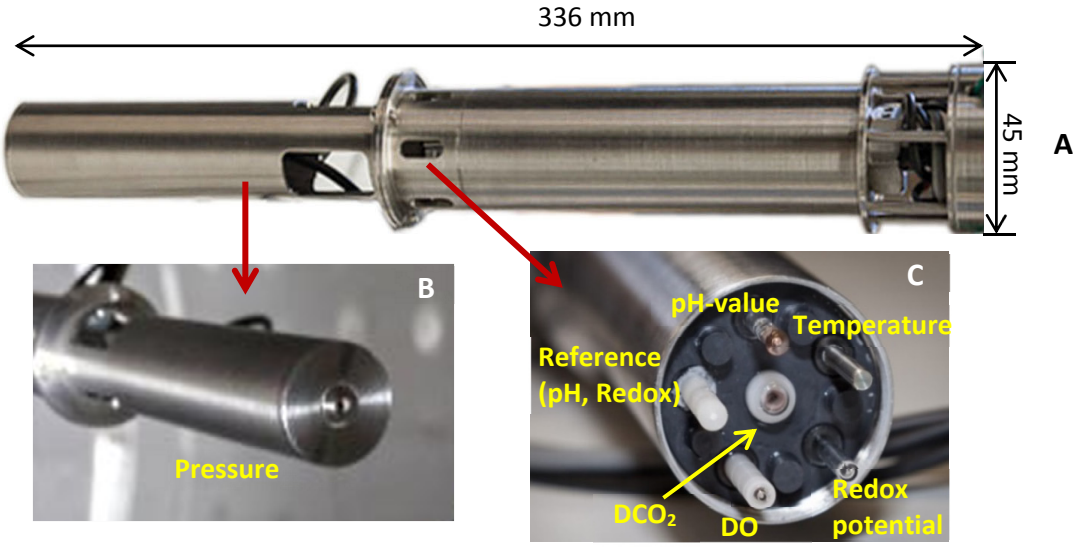

Fig. 13: Sensor unit for seven miniaturized sensors (KSI, Germany).
A: complete sensor unit, B: view on the integrated miniaturized sensors with unscrewed protection hood, C: pressure sensor unit.

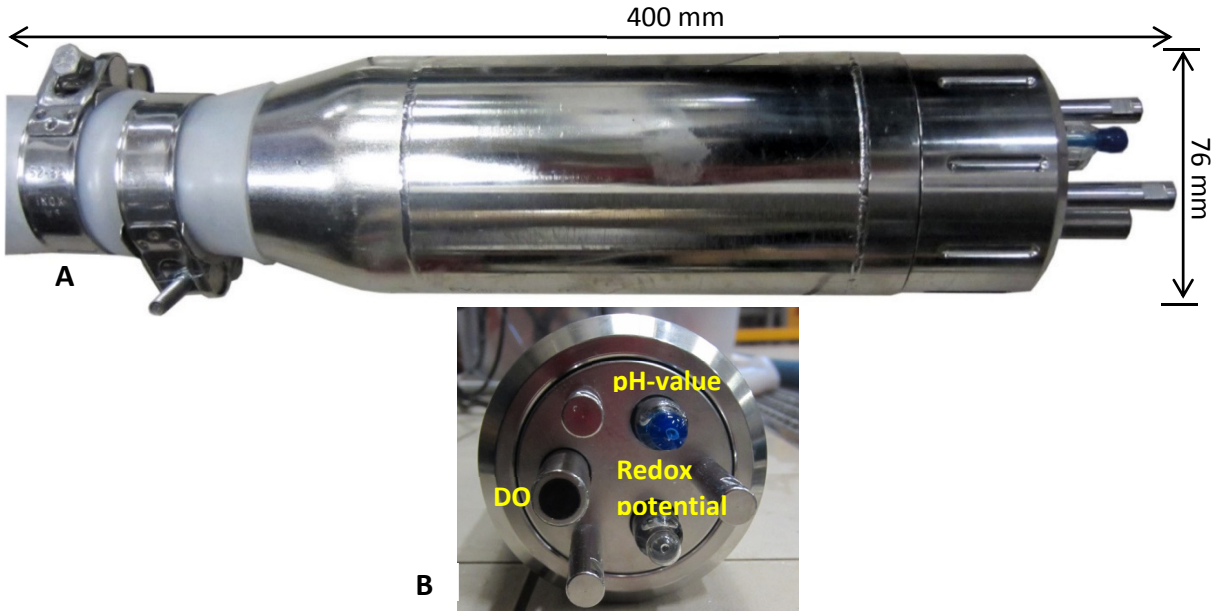

Fig. 14: Sensor unit for three commercially available sensors made of stainless steel.
(Sensors: HM; housing unit: Exner Process Equipment GmbH, both Germany). A: complete sensor unit, B: bottom part of the sensor unit with integrated sensors and protection hood and rods.

Beside specific features of some sensors, there are basic differences between both sensor unit systems. Their dis-/ advantages are listed in Table 3. The decision for one unit depends on the application, especially concerning media, time and accessible fermenter entrances or openings.

Table 3: Advantages and disadvantages of the two sensor systems (incl. sensors, units, and pre-amplifier).

	Miniaturized Sensors (KSI)	**Commercially available Sensors (HM)**
Long-term stability /Accuracy	**-**	**+**
Sterilizability (steam, CIP)	**-**	**+**
Number of parameters	**+** (6)	**-** (3+1)
Easy to handle sensor exchange	**-**	**+**
Maximum distance for data transfer / integrated pre-amplifiers	**-** (5 m)	**+** (> 30 m)
Easy to handle sensor unit including cables in industrial tanks	**+**	**-**

Due to the higher amount of electrolyte in the larger sensors and the larger tip diameter the sensors from HM are less sensitive to membrane clogging and electrolyte toxification than the miniaturized sensors. Hence, they provide more accurate and stable measurements during long-time application in complex and harsh media, e.g. in the brewing process (see 4.1.2).

All sensors from HM are steam sterilizable, autoclavable and CIP compatible, allowing an easy use in fermentation processes. The miniaturized sensors instead cannot be steam sterilized or cleaned with acids or base. However, they can be disinfected with alcohol, which is sufficient for certain applications such as in the brewing or biogas process.

Concerning the multi-parameter approach the miniaturized sensors are of advantage since three more sensors can be integrated allowing the measurement of a broad range of different parameters. However, the exchange of the miniaturized sensors can be realized only in cooperation with the supplier since the sensors are fixed and sealed by bonding. The commercially available sensors instead can be screwed in separately and are sealed by O-rings as well as the cap, which is screwed over the core component (Fig. 15).

For multi-position measurements in large-scale processes taller or wider than 5 m the miniaturized sensor unit cannot be applied. The data are transferred without amplification and can therefore not be transmitted across more than approx. 5 m of cable length. The sensors of the ARC-series from HM are equipped with a pre-amplifier at the sensor head (Hamilton_Company, 2012b). Hence, the data transfer can be realized across long distances (30 m approved). Furthermore, the sensors can easily be calibrated at any place and prior to usage due to the Arc technology, which makes it suitable for outdoor applications (Steinweg, 2016).

Fig. 15: Modular construction of the HM sensor unit.
A: Sensors are inserted into a cylinder by screw thread and sealed by O-rings. B: The cylinder containing the sensors is inserted into the housing, sealed again by O-rings. C: The cylinder is finally sealed with a cap containing O-rings.

A challenge for certain fermentation tanks can be the handling of the large sensor unit. An opening of 80 mm in diameter is necessary to enter the tank. Furthermore, for the application in large fermentations tanks the sealing, fixation, movement, and disinfection of the cable construction as well as the power supply must be realized. The construction of 25 m cable length sealed in a silicon hose is weighing about 10 kg, the sensor unit itself is weighing about 2.5 kg.

4.1.4. Data Acquisition

For the miniaturized system separate pre-amplifiers were used, which have to be installed outside a tank: LM 2000 or KM 3000 (both Sensortechnik Meinsberg GmbH, Germany). The data were transferred via an RS-485 interface and acquired on a personal computer with the software LMremote (Sensortechnik Meinsberg GmbH) for the LM 2000 instrument. For the KM 3000 system the interface RS-232 and the software Python (Python Software Foundation, USA) was used (program on Python written by Dipl.-Ing. Olga Sheshukova). The latter can be also connected to a *real-time* data monitoring via a browser-based Front End, which is available from any location. The distance the signal can be transferred via cables without data losses is 5 m.

The data of the HM sensors were preamplified by the preamplifiers integrated into each sensor head. They were transferred via a USB-ModBus RS-485 Converter (Hamilton Germany GmbH) to a personal computer, where there were recorded with the software LabVIEW (National Instruments, USA), (program written by Dipl.-Ing. Dirk Itzeck, modified by Dipl.-Ing. Anika Bockisch). It was proven for up to 30 m that the signal can be transferred via cables across long distances without data losses. If applied outdoor and close to other electronic devices the cables have to be well isolated, shielded and equipped with a drain wire.

4.2. Application of the mobile Multi-Parameter Sensor Units

4.2.1. Fermentation Scales and Tank Geometries

After the test of the sensor functionality and stability, the multi-parameter sensor units were applied in the various fermenter volumes and fermentation repositories as displayed in **Fehler! Verweisquelle konnte nicht gefunden werden.**. The different geometries of the tanks are presented in Fig. 16. The measurement results are mainly presented from measurements in the 3 m^3 and 170/199 m^3 scale.

Table 4: Scales and geometries of fermentation. CCT: cylindroconical tank.

Scale	Fermentation repository	Research Institute (VLB) / Brewery	KSI	HM
0.04 m^3	Fermentation Columns*	VLB	Sensor unit	Sensor unit
0.15 - 0.17 m^3	CCT	VLB	Sensor unit	Sensor unit
3 m^3	CCT	Brewery	Sensor unit	Sensor unit
24 m^3	CCT	Brewery	Sensor unit	Sensor unit
170/199 m^3	CCT	Brewery	/	Sensor unit

* Only for drift and stability tests.

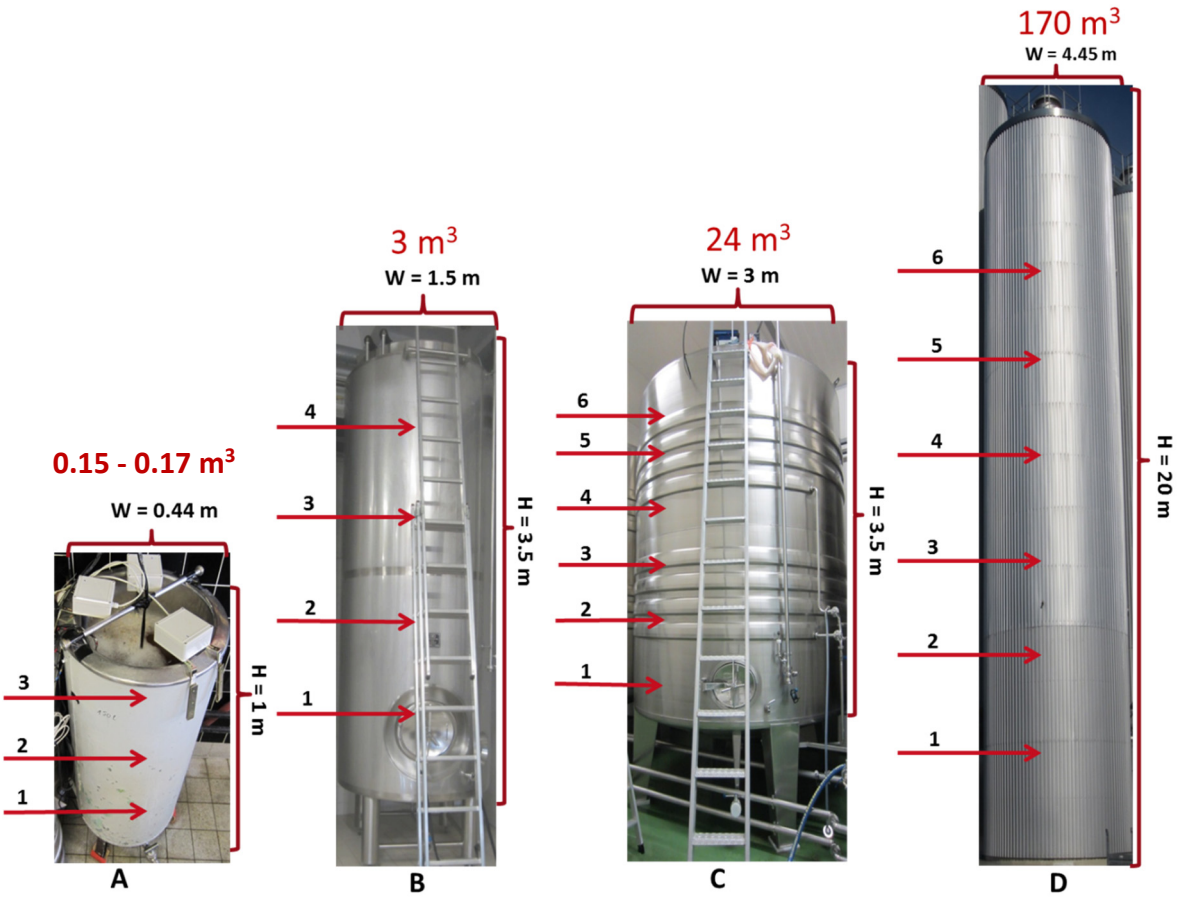

Fig. 16: Tank geometries and fermentation volumes, in which the sensor technique was applied. A: 0.15 - 0.17 m^3, 3 positions; B: 3 m^3, 4 positions; C: 24 m^3, 6 positions; D: 170 m^3, 6 positions.

4.2.2. **Process Conditions** (only for the application of the sensor units)

All investigated processes in fermentation tanks were performed without mechanical agitation and aeration (after pitching). The fermentations were performed at different original gravity, different yeast strains and therefore different target temperatures as explained in Table 5. The experiments were mostly performed twice or even three times. Only the 24 m^3 scale was available just once. The numbers in the table represent the first (1) and second (2) experiment, respectively.

The number of batches of boiled wort that was added stepwise during the filling process was one batch in the 0.15 – 0.17 m^3 scale, 2 batches in the 3 m^3 and 24 m^3 scale, and 6 - 7 batches in the 170 m^3 scale, respectively. The temperature was regulated with one cooling jacket in the 3 m^3 scale and three cooling jackets in the 170 m^3 scale, whereas 0.15 - 017 m^3 scale fermentations were conducted without any controlled temperature regulation. In the 24 m^3 scale two zones with cooling coils were installed and the fermentation cellar was cooled to 8 - 10 °C. The extract was degraded from original 11.7 to 3.7 °P in average in the 0.15 – 0.17 m^3 scale, 11.3 to 3.1 °P in the 3 m^3 scale, 11.3 to 3.0 °P in the 24 m^3 scale, and 13.6 °P to 2.9 °P in the 170 m^3 scale, respectively. The adjusted pH-value at the fermentation onset was in the range between 5.3 and 4.85 for all processes that are displayed in Table 5.

Table 5: Process conditions of fermentations conducted in CCTs.
Top Fermenting: tf; bottom fermenting: bf.

	0.15 m^3	**0.17 m^3**	**3 m^3**		**24 m^3**	**199 m^3**	**170 m^3**
	E 1	**E 2**	**E 1**	**E 2**	**E 1**	**E 1**	**E 2**
Temperature range (without diacetyl rest & cooling phase)	17 - 21 °C	9 - 24 °C	12 - 12.2 °C	12 - 13 °C	8.5 - 9.5 °C	10.25 - 11 °C	10.25 - 10.75 °C
Yeast strain	tf (Safale S-04)		bf (Saflager W34/70)		bf (Saflager W34/70)	bf	
Original gravity in wort [%]	11.6	11.8	11.2	11.3	11.3	13.65	13.62
No. of batches and volume	1 x 0.15 m^3	1 x 0.17 m^3	2 x 1.5 m^3		2 x 12 m^3	7 x 28.5 m^3 (6.5 after transfer)*	6 x 28.3 m^3

* 185.7 m^3 after releasing 13.5 m^3

In the 2nd experiment of the 170 m^3 scale, the tank was flushed with CO_2 (“bubbling”) for 5 min twice after the filling procedure was finished. This should improve mixing of the batches and was the standard procedure in this brewery but was not conducted in the 1st experiment for comparison. In the 1st experiment in the same scale instead, the entrances for the rope and cable hose of the measurement technique at the tank dome were not sealed. This led to a high foam formation and spilling over of a part of the tank content at the tank dome, probably due to changes in the overpressure. Since it was a risk of contamination and decreased fermentation performance, a volume of 13.5 m^3 was transferred between 53.6 h and 53.7 h, leading to a final volume of 186 m^3 for the remaining fermentation time (Table 6). Around the time of 50 - 55 h, only a reduced number of measurements could be performed. In the 2nd experiment, the entrances were sealed well reaching an overpressure in the tank of 0.4 bar at the end of the fermentation.

4.2.3. Process phases

The fermentation process is one of the most time-consuming steps of the whole brewing process. It can be separated in different process phases itself, which can be performed in one tank or the tank can be changed for certain phases such as the diacetyl rest phase (slightly increased temperature), the cooling phase for the sedimentation of the yeast cells (cooling down of the tank to about 4 °C or even lower), and the storage phase for the maturation (constant temperature of about 4 °C).
In the different breweries the process phases displayed in Table 6 differed in their length or were realized only partially. All were conducted in one tank, except from the 24 m^3 scale, in which the complete fermentation volume was transferred 18 h after the filling of the pre-fermentation tank was finished into the fermentation tank (26 h of total time). In all experiments, the filling, main fermentation, (diacetyl rest), and partially the cooling process were monitored.

Table 6: Process phases and corresponding time frames of the investigated brewing processes.
E = experiment.

	0.15 m^3 E1	**0.17 m^3 E2**	**3 m^3, E1**	**3 m^3, E2**	**24 m^3**	**199 m^3, E1***	**170 m^3, E2**
Filling process	Not monitored (max. 10 min)		0 - 24.5 h	0 - 25.2 h	0 - 9 h	0 - 15.3 h	0 – 13 h
Bubbling	Not conducted		Not conducted		Not conducted	Not conducted	2 x 5 min (13.0 - 13.1 h, 13.47 - 13.45 h)
Fermentation phase	0 - 100 h	0 - 85 h	24.5 - 141.7 h	25.2 - 122.5 h	0 - 27 h (tank 1) 27 - 145 h (tank 3)	15.3 - 122 h	13 - 97 h
Rising the temperature for diacetyl rest (by 2 °C)	Not conducted		Not conducted		Not conducted	122 h - 204.5 h	97 h - 204.8 h
Start of cooling	After transfer of green beer in storage tanks		141.7 h	122.5 h	86 h	204.5 h	204.8 h

* 185.7 m^3 after releasing 13.5 m^3.

4.2.4. Measurement with the mobile Multi-Parameter Sensor Units

4.2.4.1. Movement of the Sensor Units in Brewery Tanks

Both sensor units were inserted from the top of the investigated brewing tanks via existing openings such as a sight glass or the opening for the Clean-In-Place (CIP) pipe (Fig. 17). Since the reactors could not be retrofitted, the sensor units were moved in both scales only in vertical direction using the existing openings. This was realized for the 200L scale by a simple rope, in the 3 m^3 scale via a fishing rope and in the 170 m^3 scale with a rope winch containing a stainless steel rope. The 0.15 – 0.17 m^3 scale was investigated only considering the changes during time and the sensor performance.

In all cases, the positions (Fig. 16) were marked prior to the experiment at the different ropes. The number of positions depended on the fermentation volume and tank height and was defined as displayed in Table 7. It was considered that strong foam formation at the gas-liquid interface could have an impact on the sensor signal during the main fermentation phase. Hence, the positions marked in Table 7 (no. 5 in the 3 m^3 scale and no. 7 in the 170/199 m^3 scale) were not considered for data evaluation since they were located close to the gas-liquid interface.

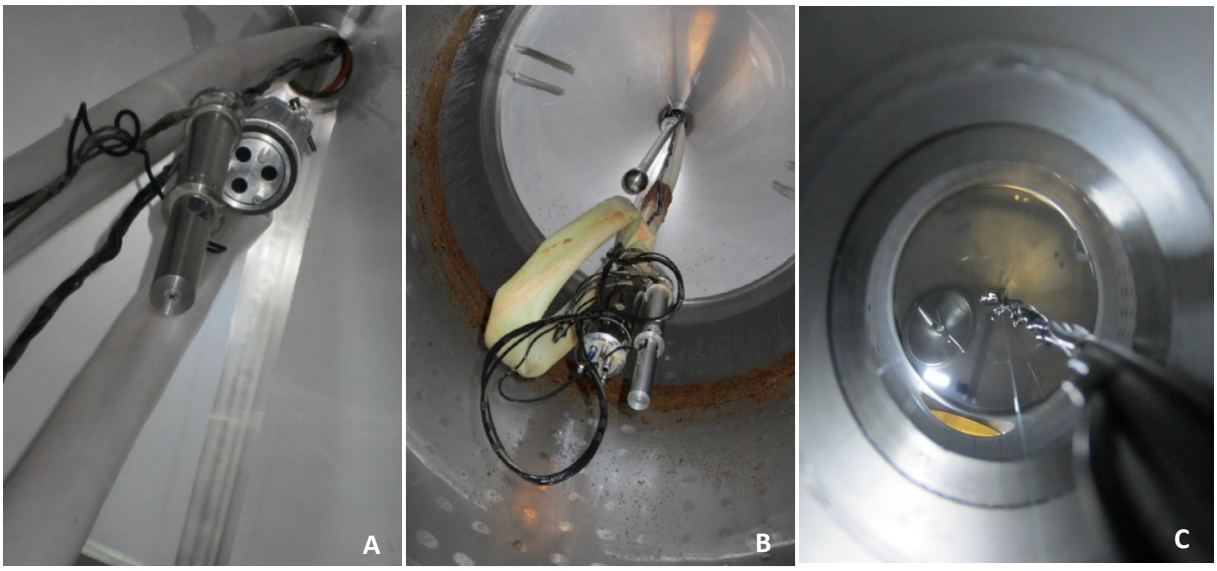

Fig. 17: Integration of the sensor unit into a brewing tank of 3 m^3 fermentation volume via the cleaning port (CIP) at the tank dome. A: before the fermentation; B: after the fermentation. C: View from the top to the bottom. Photographs with permission of Jan Biering.

Table 7: Positions of the sensor units in the different tanks investigated in breweries.
Displayed is the height [m] of the sensor diaphragms for each system from the tank bottom. For the miniaturized probe, the pressure sensor was located 16 cm lower.

Position	**3 m^3**		**24 m^3**		**170/199 m^3**
no.	**KSI [m]**	**HM [m]**	**KSI [m]**	**HM [m]**	**HM [m]**
1	0.45	0.65	0.21	0.4	2.9
2	0.95	1.15	0.71	0.9	6.1
3	1.45	1.65	1.21	1.4	8.4
4	1.95	2.15	1.71	1.9	10.6
5	2.45†	2.65†	2.21	2.4	12.9
6			2.46	2.65	15.2
7					17.41*

* Only before the transfer of 13.5 m^3 in the 1st experiment. †Sensors at these positions were partially located in the foam layer and not included in data evaluation.

In the 2nd experiment in laboratory scale at 0.17 m^3 of fermentation volume, the sensor position was changed the 1st time during the experiment series to the positions displayed in Fig. 18:

- 10 cm beneath the liquid surface in the center (1),
- at the fermenter bottom in the center (2),
- 10 cm beneath the surface at the vessel wall (3), and
- at the fermenter bottom at the vessel wall (4).

In this scale, the positions were changed quite fast (all within max. 4 min). The time frames were improved, i.e. elongated for the following experiments.

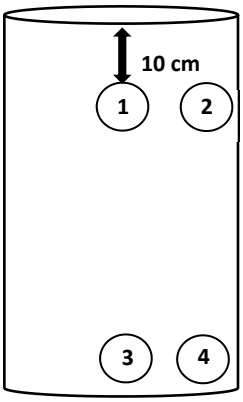

Fig. 18: Positions of the sensors in the laboratory scale (0.17 m^3).

The challenge in large tanks with a high production of CO_2 and foam formation is to seal the entrances for rope and cable hose, while allowing a movement of the rope for sensor positioning. This was realized for the larger sensor unit by the application of O-rings and silicone sealing gel between two discs as well as the fixation of the sealing construction by screws and hex flange bolts on the tank dome after the installation of the technique (Fig. 19).

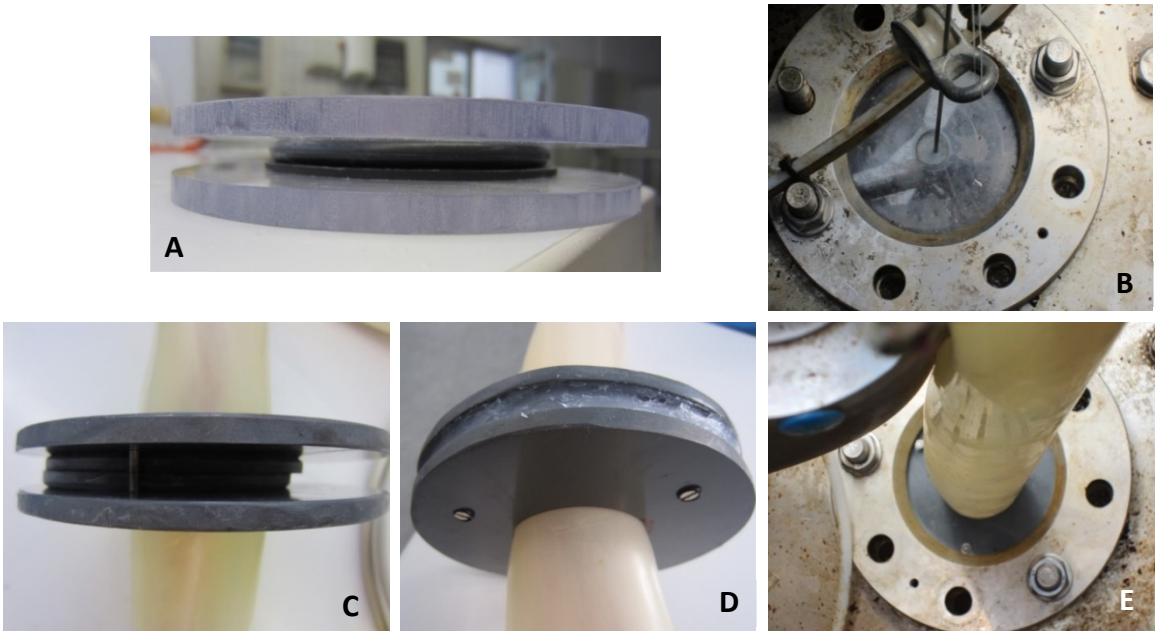

Fig. 19: Sealing mechanism at the tank opening for the rope and cable hose in a large-scale tank (170 m^3).
A: O-rings between acrylic glass discs (A), squeezed between the tank and flange at the rope entrance (B). O-rings between two plastic discs surrounding the cable hose (C), sealed by a silicone gel and fixed by screws (D). The construction is squeezed between the tank and flange at the entrance for the cable hose (E).

4.2.4.2. Frequency of Position Changes and Sampling (for off-line Analysis)

Beside the fermentation phase and stage, the measurement and sampling frequency in this study was also depending on the accessibility of the brewery (Table 8). In the laboratory scale (0.15 and 0.17 m^3),

access to the reactors was always given in contrast to the breweries with restrictions at certain days or hours due to operational reasons. In the laboratory scale, the sensor units were not moved to different distances due to the small volume and the main aim of testing the sensor performance. The breaks between the sampling points over night were between 9 and 12 h.

In the 3 m^3 scale, the filling process with two batches lasted already 24 h. Hence, on the 1st day the sensor movement to all positions and sampling was performed only once. The over-night breaks in this scale lasted 18 - 25 h. In the 2nd experiment, sampling was conducted only for the fermentation performance control, not for *off-line* metabolite analysis in order to allow a higher frequency for sensor positioning (Table 8).

In the 24 m^3 scale, the frequencies for movements and sampling were quite low due to electrical problems with the acquisition of the HM sensor unit until about 70 h of fermentation time. Due to this and due to operational reasons of the brewery, the time frame without any action over night was between 9 h and 19 h.

Table 8: Frequency of movements of the sensor devices (bold numbers) and sampling time points in the investigated processes.
If one number is written, this is valid for both moving and sampling time points (including the fermentation performance control = fpc). In the 2nd experiment in the 3 m^3 scale, sampling was conducted only for the fpc.

	0.15 m^3, E1	**0.17 m^3, E2**	**3 m^3, E1**	**3 m^3, E2**	**24 m^3**	**199 m^3, E1***	**170 m^3, E2**
Day 1	**3**	**5**	**1**	**1**	**2** (3 x sampling)	**8** (1 x sampling, 7 x fpc*)	**7** (1 x sampling, 8 x fpc*)
Day 2	**3**	**4**	**2**	**4** (3 x fpc*)	**3**	**7** (3 x sampling & fpc*)	**6** (3 x sampling & fpc*)
Day 3	**3**	**3**	**2**	**3** (2 x fpc*)	**2**	**3**	**6** (3 x sampling & fpc*)
Day 4	**3**	**2**	**1**	**1**	**2**	**3**	**5** (3 x sampling & fpc*)
Day 5	**2**	**2**	**1**	**1**	**1**	**2**	**4** (3 x sampling & fpc*)
Day 6	**1**	**/**	**1**	**1**	**1**	**1**	**1**
Day 7			**1**	**1**	**1**	**0** (Only 1 x fpc*)	**0** (Only 1 x fpc*)
Day 8			**1**	only 1 fpc*		**0** (Only 1 x fpc*)	**0** (Only 1 x fpc*)
Day 9						**3** (1 x sampling & fpc*)	**3** (2 x sampling, 1x fpc*)
Day 10						**2** (2 x sampling, 1 x fpc)	**2** (2 x sampling, 1x fpc*)

*fpc: fermentation performance control

The highest frequency could be achieved in the 170/199 m^3 scale with up to eight times of moving the sensors to all six or seven positions (Table 8). The time frame without any moving or sampling was about 6 -7 h until the 6th day and on the last day of records, apart from the time of the strong foam formation in the 1st experiment (13 - 15 h distance). On the 7th and 8th, the reactor was not accessible in both experiments due to operational reasons of the factory. On the 9th day, actions started around 3 p.m. and 4 p.m.

4.2.4.3. Sensor Responses, Acquisition Time Frames and Frequencies

The miniaturized sensors show a higher response time of ca. 1 min than the commercially available sensors. Stable values are reached between 1 -2 min for the miniaturized system (longer times especially for the pH sensor), whereas the commercially available sensors reach them below 30 sec.

In order to consider the sensor response and stabilization time, certain time frames must be considered between position changes and during data evaluation (the sensors measure continuously). Hence, in the 3 m^3 scale with the application of both, the miniaturized and the commercially available sensor unit, these were left at one position for 20 min, respectively. The acquisition frequency was 2 min. The recorded data of the 1st min on each position were excluded from further evaluation in order to neglect values of the sensor stabilization time. All data recorded during sensor movement were excluded from the data evaluation as well. The exact time frames of the sensor movements and the corresponding time windows for acquisition can be seen in Table 20 in the appendix A, i (page 165).

In the 24 m^3 scale, when both sensor systems were applied, the sensor units rested at each position for 10 min. The time was reduced since six positions were investigated in one measurement frame (i.e. the movement to all target positions within a short time frame). A quasi-stationary state was assumed for the slow brewing process at one measurement frame. By this, the measurement frequency was set to 30 sec. Data during movements of the sensor units and of the 1st min on each position were excluded as in the 3 m^3 scale.

In the 170/199 m^3 scale, the HM sensor systems with the commercially available sensors was applied only. The unit was left at each position for 6 min since six positions were investigated across a large tank height (meaning longer times of movements). A quasi-stationary state was assumed for one complete measurement window in this case as well. The measurement frequency was 30 sec. The exclusion of data during movements or other disturbances was performed as in the other scales. Due to the fast response time, only the 1st data set (after 30 sec) on each position had to be excluded. The exact time frames of the sensor movements and the corresponding time windows for acquisition are summarized in Table 20.

4.3. *Off-line* and *at-line* Analysis

At-line or *off-line* analysis samples were taken at the sampling ports, which were located at the height of the different tanks and scales as presented in Table 9. The frequency of the sampling differed between the processes since the fermentation time differed and the breweries were not accessible all time (e.g. weekends). In the 170/199 m^3 scale, sampling was conducted three times per day until the fermentation time of 122 h, then one to two times per day. No samples were taken between 125 h

and 200 h - after the main fermentation phase. In the 30 m^3 scale, the samples were taken twice a day until 51 h, afterwards one to two times.

Table 9: Positioning of the sampling ports for the different tanks and scales.

Fermentation volume [m^3]	Height of liquid column [m] (estimated)	Height of sampling (port) [m] (from the tank bottom)
0.4 (only reference measurements)	0.13	0.5
1.5	0.88	0.22 & 0.65
1.7	1	0.5
3	2.5	0.3
24	2.8	0.2
170/199	16	5

In order to take a representative sample, the beaker or container for sampling was pre-rinsed with the sample. In case of long distances between the sampling port at the tank and accessible sampling location in the cellar (at 170/199 m^3) also the pipes were pre-rinsed. Finally, a volume of 0.5 - 1 L was taken for the following analysis (except f), which was taken at last and g), which was measured directly at the tank):

a) Fermentation performance control (pH-value, extract, cell count)
b) Dry cell weight*[2, 3]
c) Metabolite concentration (extra-, intracellular) by HPLC-RID
d) Carbohydrate concentration (extra-, intracellular) by HPLC-RID
e) Sterol content by GC-FID
f) *At-line:* DCO_2, DO_2, temperature with DCO_2 analyzer "Haffmanns"[1, 2]
([1] only at 3 m^3/ [2] only at 24 m^3 / [3] only at 170/199 m^3)

The sample pretreatment and final analyses are described in the following.

a) Fermentation performance control: pH-value, remaining extract, cell count

For the extract measurement, which is based on the density, the sample was filtered with a folded filter (Sartorius AG, Göttingen, Germany) with a retention of particles of 12 - 15 µmm (grade 1288). The solution was then analyzed by a flexural resonator (Anton Paar, Graz, Austria) at laboratory scale until 0.15 m^3, a floating glass hydrometer at the 3 m^3 and 24 m^3 scale, or an Alcolyzer Beer Analyzing System (Anton Paar, Graz, Austria) at the 170/199 m^3 scale (Fig. 21).

Since the extract is usually measured by hydrometers, which do not consider the lower density of alcohol in comparison to water, only the apparent extract can be determined directly during the fermentation. Hence, this is lower than the real extract (RE) and usually expressed in degrees plato [°P]. The RE can then be calculated based on the Balling formula, which describes the formation of 1 g ethanol, 0.11 g yeast, and 0.9565 g CO_2 from 2.0665 g unfermented extract (RE in mass %):

$$\mathrm{OE} = \frac{(2.0665 * m_{alc} + RE) * 100}{100\ \mathrm{g} + (0.11\mathrm{g} + 0.9565\ \mathrm{g}) * m_{alc}} \quad (4.1)$$

With m_{alc} = alcohol in g per 100 g of beer (Bamforth, 2016; Cutaia et al., 2009).

For the determination of the cell count in the 0.15 - 0.17 m^3 and 3 m^3 scale, the cells were diluted with 0.9 % (≥ 99.9 %, Cellpure®, Carl Roth GmbH, Germany) to about $2*10^6$ - $1*10^7$ cells mL^{-1} and then counted on a Neubauer chamber with a depth of 0.1 mm and an area of 0.0025 mm^2, which equals to a volume of 0.25 nL. For each sample 4 quadrats were counted. In the 170/199 m^3 scale the cells were diluted, counted automatically by a cell counter (Fig. 21).

b) Dry Cell Weight

For the dry cell weight determination in the 24 m^3 scale, small petri dishes, each containing one cellulose nitrate round filter with a pore size of 0.2 µm (Sartorius, Germany), were pre-weighed and labelled before the experiment. For each sample, a double estimation was prepared. The filter was placed with a pipette in a metallic filter mount (Fig. 20 A) and closed (Fig. 20 B). Then, the sample was filtered, the mount opened, and the filter placed in small petri dishes in order to avoid contamination (Fig. 20 C). The filters were dried for 7 days in the half-open dishes and weighted for the dry cell weight determination.

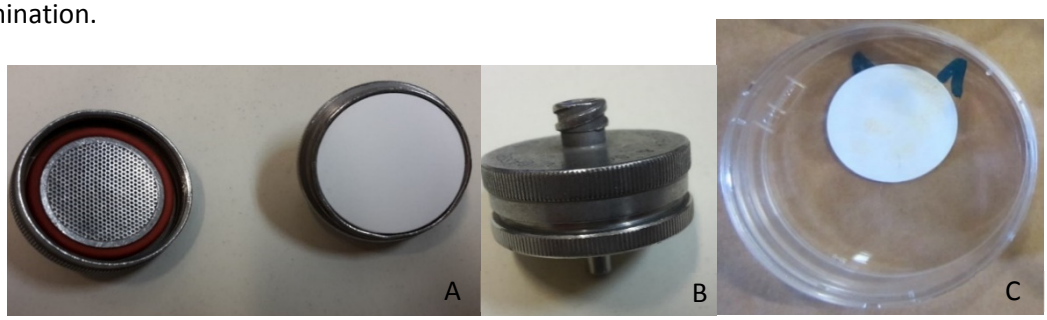

Fig. 20: Dry cell weight estimation.
Mounting of the filter (A, B) and "chamber" (C) for filter drying.

In the 170/199 m^3 scale, 2 x 1 mL of the sample were transferred into 2 dried and pre-weighed 1.5mL Eppendorf tubes for double estimation. Then they were centrifuged in a table centrifuge (Rotilabo®-Mini-Centrifuge, Carl Roth GmbH, Germany) at 2000 x g (6000 rpm) for 10 min, washed once with 1 mL of 0.9 % NaCl (≥ 99.9 %, Cellpure®, Carl Roth GmbH, Germany) and centrifuged again. The supernatant was discarded. The Eppendorf tubes were left open for drying in the oven at 70 °C and finally in the desiccator until the mass constant. The difference between the weight of the empty and the filled tubes was calculated and the dry cell weight was determined.

c) Carbohydrate Concentration (extracellular) by HPLC-RID

The HPLC instrument was of the Agilent Technologies 1200 Series (Agilent Technologies, Waldbronn, Germany), consisting of the degasser G1322A, the isocratic pump G1310A, the autosampler G1329A, the column oven G1316A, and the refractive index detector (RID) G1362A. The Hyplex Ca^{2+} column (Varian, Agilent Technologies, Waldbronn, Germany) was used with a size of 300 x 7.7 mm and a particle diameter of 8 µm.
The carbohydrate composition was determined on the basis of the retention times of the following carbohydrate standards: Fructose, galactose, D-(+)-glucose, D-(+)-maltose, maltotriose. The carbohydrates were quantified by the integration of the peak areas and comparison to the calibration curves with the software package ChemStation, Revision B.04.01 (Agilent Technologies, Waldbronn, Germany).

Sample preparation:

For the determination of the extracellular content, 2 x 1.5 mL of the sample were filtered by a syringe filter of 0.8 µm pore size (Rotilabo®-syringe filters, CME, unsterile, Carl Roth GmbH, Germany) and stored immediately at -20 °C until analysis by HPLC-RID (an overview about the used materials and chemicals is given in Table 21 - Table 23, the analysis program and instrument settings are explained in detail in appendix A, ii.b). The samples were diluted with bi-distilled (bi-dest.) water (generated by the instrument EASYpure II (Wilhelm Werner GmbH, Germany) before analysis, especially for those from the onset of the fermentation, in order to keep the range of the calibration curves.

d) Main Carbon Metabolite Concentration (extra-, intracellular) by HPLC-RID

The HPLC instrument was of the Agilent Technologies 1200 Series (Agilent Technologies, Waldbronn, Germany) with the same composition as for the carbohydrates. The HyperREZ column carbohydrate H^+ (Thermo Fisher Scientific, USA) with a size of 300 x 7.7 mm and a particle diameter of 8 µm was used for main carbon metabolite analysis.
The concentrations were determined using the following standards: Acetaldehyde, acetic acid, ethanol absolute, glycerin, malate, D(+)-maltose, pyruvate. The main carbon metabolites were quantified by the integration of the peak areas and comparison to the calibration curves with the software package ChemStation, Revision B.04.01 (Agilent Technologies, Waldbronn, Germany).

Sample preparation:

The determination of the extracellular concentration of the main carbon metabolites the samples were prepared as described in c) for the carbohydrates and diluted with bi-dest. water (generated by the instrument EASYpure II (Wilhelm Werner GmbH, Germany) before analysis, especially for those from the end of the fermentation, in order to keep the range of the calibration curves. The main carbon metabolite concentrations were analyzed by HPLC-RID (an overview about the used materials and chemicals is given in Table 24 - Table 26, the analysis program and instrument settings are explained in detail in appendix A, iii.b).

For the determination of the intracellular concentration of main carbon metabolites, a solution of 1 g L^{-1} butanol (internal standard, > 99.8 % ROTISOLV ® HPLC, Carl Roth GmbH, Germany) in 70 % H_2CO_4 (perchloric acid) (ROTIPURAN® Supra, 70 %, Carl Roth GmbH, Germany) was prepared. The necessary amount of 5 mL single use “SOFT-JECT” syringes (Henke-Sass Wolf GmbH, Germany) was labelled, 1 mL of perchloric acid solution was sucked up in each, and closed with a membrane adapter (SARSTEDT, Germany). The syringes were stored at -20 °C until usage.
After each sampling, 4 mL of the sample were sucked into the pre-filled syringe, thereby mixed with perchloric acid. The filled syringes were shaken for 15 min on ice on a horizontal shaker. The content was transferred into a 50 mL conical tube (VWR, Northern America) and neutralized with 845 µL of 5 mol L^{-1} K_2CO_3 (≥ 99 % p.a., Carl Roth GmbH, Germany) on ice. 2 mL of cell-free supernatant of this solution was obtained by filtration through a membrane filter with a pore size of 0.8 µm (Rotilabo®-syringe filters, CME, unsterile, Carl Roth GmbH, Germany). Samples were stored at -20 °C until analysis by HPLC-RID as described previously (see also appendix A, iii.b). The samples were diluted with bi-dest. water in order to keep the concentration in the range of the calibration curves.
The intracellular fraction was calculated by subtracting the extracellular part from the concentration in the suspension.

e) Sterol Content by GC-FID

The used gas chromatograph GC -2010 plus (Shimadzu, Germany) was equipped with a flame ionization detector (FID). The capillary column (wall coated open tubular fused silica, Varian, Germany) was covered with dimethylpolysiloxane (d_f = 0.12 µm coating CP-Sil5CB; d_f = film thickness) and had a length of 25 m and an inner diameter of 250 µm. The autosampler AOC-20i was used for automated sample handling. More details about the instrument and program can be found in the appendix A, iv.c.

The sterol composition was determined on the basis of the retention times of the following sterol standards: cholesterol, ergosterol, lanosterol, squalene, and zymosterol. The sterols were quantified by integration of the peak areas and comparison to the calibration curves with the software package GC solution, version 2.2 (Shimadzu, Germany). Details about the other chemicals used for sterol analysis can be found in the appendix A, iv.a in Table 28.

Sample preparation:

At each sampling time point four conical 50 mL centrifuge tubes (VWR, North America) with screw cup were filled with 45 mL sample and stored immediately at -20 °C. Of each two tubes were later used for the analysis of total and free sterol content, respectively. 1. The content of esterified sterols was determined by the difference of the content of free and total sterols. Due to the low cell density compared to other processes a large volume is necessary for one analysis and hence, only single estimation was possible. The procedure for sample preparation for the analysis of the total and free sterol content (non-esterified) was as described in Appendix A, iv.b (based on a protocol described previously by Maczek and co-authors (2006).

f) CO_2 Haffmanns Analyzer

The application of the DCO_2 analyzer (Pentair-Haffmanns / Netherlands) (Fig. 21 A) allows the *at-line* determination of DCO_2, DO_2, and temperature of the analyzed sample. This was applied for the 3 m^3 and 24 m^3 scale as an additional fermentation performance control tool.

g) Additional Analyses at 170/199 m^3

Fig. 21: Analysis instruments for fermentation performance control.
A: DCO_2 Analyzer (Haffmanns), B: Alcohol Analyzer (Anton Paar), C: Cell Counter.

In the largest scale of 170/199 m^3, the following analyses were performed in the laboratory of the brewery once per day: Extract (original wort content ("Stw.GG") GG [%], ES [%]) by the Alcolyzer Beer Analyzing System (Anton Paar, Graz, Austria) (Fig. 21 B), pH-value by a pH meter, and the cell count by a cell counter (Fig. 21 C). Additional at the end of the fermentation the following parameter were determined: Alcohol content [Vol %], Vs [%], EW [%] (all Alcolyzer Beer Analyzing System), color [EBC] by light absorption at 430 nm, vicinal diketones diacetyl & pentanedione [mg L^{-1}] by GC, and the density SL20 / 20 °C (weight ratio between water and sample at 20 °C) by a pycnometer.

4.4. Multivariate Data Analysis

For correlation analysis of *on-line* measurements (pH-value, redox potential, DO-value, and temperature (called A in the following)) and *off-line* analyses (concentrations of carbohydrates, main carbon metabolites and sterols (called B in the following) in the 3 m^3 and 170/199 m^3 scale, PCA and PLS regression were applied to these data (explained in detail in 2.3.4). All calculations for PCA and PLS regression were performed using MATLAB 2013b (version 8.2.0.701) by MathWorks®.

Since *on-line* data were measured every 0.5 - 2 min during the complete fermentation time and *off-line* samples were taken only several times per day (see 4.2.4.2), only the measurement frame around sampling was considered for correlation analysis. Within this measurement frame (see also page 82 for definition), the arithmetic mean value for the recorded *on-line* parameters at a position close to the sampling port was calculated. This allowed for the comparison of the *on-line* data, obtained by the measurement at different positions, with the *off-line* data, obtained by sampling at only one fixed position and at a certain time point. These mean values for every *on-line* parameter were then used for correlation analysis. Since these data showed that the tanks are quasi-homogenous, it can be assumed that also at positions with a higher distance to the sampling port the correlation was similar. Important to notice is that the data of different experiments were not correlated due to different process conditions in the different scales and even some differences in the conduction of experiments in the same scale. Hence, every data set for correlation consisted in *on-line* and *off-line* data from the same experiment.

In order to obtain normally distributed data for PCA and PLS regression for the experiment comparison, a standardization or z-transformation was performed using the function "zscore". This process is defined as the transformation of a random variable "*X*" (in this work *A* and *B*) so that the resulting random variable "*Z*" shows a normal distribution and has an expected value of zero and a variance of one. The square root of the variance is equal to the standard deviation "σ", i.e. one. The expected value "μ" or mean value of the probability distribution and the variance "σ^2" are defined according to equation (4.2) and (4.3):

$$E(X) = \mu \tag{4.2}$$

$$Var(X) = \sigma^2 \tag{4.3}.$$

The standardized variable "Z" is the normal random variable of a standard normal distribution and is obtained by equation (4.4):

$$Z = \frac{X - \mu}{\sigma} \tag{4.4}$$

with the following equations concerning the expected/mean value and the variance:

$$E(Z) = E\left(\frac{X - \mu}{\sigma}\right) = \frac{1}{\sigma}(E(X) - \mu) = 0 \quad (4.5)$$

$$Var(Z) = Var\left(\frac{X - \mu}{\sigma}\right) = Var\left(\frac{X}{\sigma}\right) = \frac{1}{\sigma^2}Var(X) = 1 \quad (4.6).$$

The calculations for PCA and PLS regression were based on the function "plsregress" with *n* PCs (*ncomp*):

$$[\mathrm{AL}, \mathrm{BL}, \mathrm{AS}, \mathrm{BS}, \mathrm{BETA}, \mathrm{PCTVAR}, \mathrm{MSE}] = \mathrm{PLSREGRESS}(\mathrm{A}, \mathrm{B}, \mathrm{ncomp}, \dots) \quad (4.7).$$

A is a matrix of predictor variables of the dimensions *n* x *p*, consisting of rows that represent the observations and columns that correspond to variables. *B* is a matrix of response variables of the dimensions *n* x *m*. Both serve as input for the PLS.
AL is a matrix of predictor loadings of the dimensions *p* x *ncomp* and *BL* is a matrix of response loadings of the dimensions *m* x *ncomp*. In both, each row consists of coefficients that define a linear combination of PLS components approaching the original predictor or response variables, respectively. The predictor scores *AS* are the PLS components that are linear combinations of the variables in *A*. *AS* is an orthonormal matrix of the dimensions *n* x *ncomp*, consisting of rows that represent the observations and columns that correspond to components. The response scores *BS* instead, represent combinations of the responses that have maximum covariance with the PLS components *AS. BS* is a non-orthogonal and not normalized matrix of the dimensions *n* x *ncomp* with rows corresponding to observations and columns representing the PCs.
BETA provides a matrix of the dimensions (*p+1*) x *m*, containing the PLS regression coefficients, which provide a summary of the relation between *A* and *B*. Hence, it is an important factor for the model setup and validation. It is further used for the following term in the MATLAB program:

$$BfitPLS = [ones(n, 1)\ AT1] * betaPLS \quad (4.8).$$

PCTVAR results in a matrix with two rows and *ncomp* columns, which contains the percentage of variance explained by each PLS component in *A* in the 1st row and *B* in the 2nd row, respectively.
The function part MSE results in a matrix with two rows and (*ncomp*+1) columns, containing estimated mean-squared errors for the predictor variables in *A* in the 1st row and the response variables in *B* in the 2nd row, respectively.

The correlation coefficients were determined by the following calculations in MATLAB for the analyzed *off-line* components with *x*: the measured values, and *y*: the predicted values:

$$\mathrm{rsquaredPLS} = 1 - \left(\frac{RSS_{PLS}}{TSS}\right) \quad (4.9)$$

where RSS is the residual sum of squares: $RSS_{PLS} = \sum_{i=1}^{n}(y - f(x))^2$ (4.10)

and TSS the total sum of squares: $TSS_{PLS} = \sum_{i=1}^{n}(y_i - \bar{y})^2$ (4.11).

The final graphs were generated by the "scatter" function for the loading plots (PCA) (see 5.3.1) and "plot" function for the cross-validation (see 5.3.2).
The multivariate data analysis was conducted using the functions "fitlm" and "Curve Fitting" in the MATLAB toolbox. Predictions using the model were generated by the function "predict".
All mentioned functions were available in the MATLAB download space.

5. Results

5.1. *On-line* Monitoring of Brewing Processes in different Scales

5.1.1. Sensor Accuracy, Stability and Drift during long-term Fermentation

For the accurate interpretation of the obtained sensor data and correct measurements, it is of high importance to estimate the sensor drift during time in a real fermentation process and finally the maximum stability that can be achieved without recalibration. A high accuracy as well as stability and low drift is a condition for the determination of small gradients as it was aimed in this project. For stability and drift measurements in brewing media, several reference measurements were performed as explained in detail in 4.1.1.

The 1st reference measurements were performed for the miniaturized sensor unit in standard sterile wort according (see 4.1.1 (1)). Between these measurements the sensors were applied in a yeast fermentation for 92 h. The mean values and the corresponding standard deviation are displayed in Table 10. Each of these values was determined by the arithmetic mean of a certain amount of values in a certain time frame as shown in the following, for which the sensor response time was already considered: time frame: 5 min for the pH-value and 3.5 min for the redox potential, DCO_2, and DO, considering 22 - 31 values (measurement frequency: 10 sec) before the fermentation and 42 - 60 values (measurement frequency: 5 sec) after the fermentation.

In the following, both the miniaturized and the HM sensor systems were applied together in two long-term yeast fermentations for 170 and 190 h in the laboratory scale in order to measure daily the sensor accuracy and drift of both sensor systems in standard solutions. The procedure of the fermentation and reference measurements is described in 4.1.1 (2). The results are displayed in Fig. 22 for the 170 h fermentation (data displayed only until 150 h due to an acquisition error for the miniaturized sensor system after 120 h).

Table 10: Reference measurements in wort before and after the application of the sensors in a yeast fermentation (92 h, 3 m^3) with the miniaturized sensor system (KSI).

Reference solutions	pH-value	DO_2 [%]	DCO_2 [g L^{-1}]	Redox potential [mV]	Wort temperature [°C]
Start: Absolute value (KSI) / Standard deviation	**4.84** 0.007	**28.43** 2.82	**0.037** 0.001	**206.80** 4.47	**20.23** 0.05
End: Absolute value (KSI) / Standard deviation	**5.65** 0.003	**0.31** 0.01	**10.46** 5.31E-15	**24.03** 0.24	**23.17** 0.05

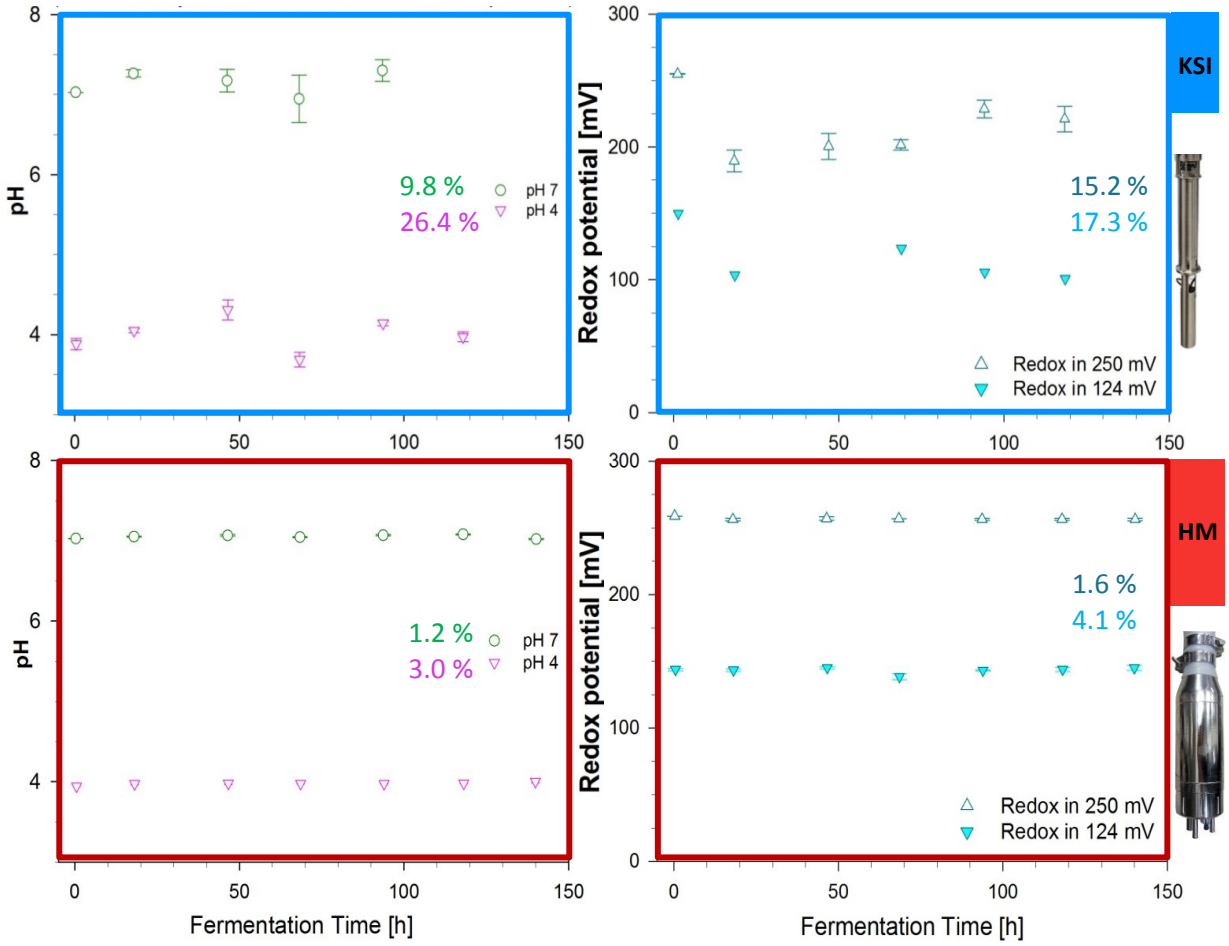

Fig. 22: Sensor drift during long-term application of both sensor systems in a brewing process of 170 h in 40 L.

The deviation during time was calculated by the difference between the reference value right after the calibration / before fermentation start in the corresponding standard solutions and the value with the highest measured difference compared to the start value during the complete fermentation time. Each of these values was determined by the arithmetic mean of at least 9 values recorded in a time frame of 10 min (measurement frequency: 1 min), considering the sensor response time. The maximum determined deviation during the complete fermentation time, regarding both reference experiments, is displayed in Table 11 for each parameter, respectively.

Table 11: Deviation of the sensors during time after the application in a yeast fermentation (170 h, 40 L). Red: HM system, blue: miniaturized system from KSI.

Reference solutions	pH = 7	pH = 4	DO [%-sat]	Redox potential 250 [mV]	Redox potential 124 [mV]	Conductivity 100 [mS]	DCO_2 [g L^{-1}]
Absolute Deviation	0.09	0.12	3.05	4.23	5.87	8.62	-----
Deviation [%]	**1.24**	**2.96**	**3.05**	**1.63**	**4.09**	**12.12**	-----
Absolute Deviation	0.69	1.06	17.24	37.79	26.59	-----	26.59
Deviation [%]	**9.82**	**26.38**	**17.24**	**15.20**	**17.32**	-----	**17.32**

It can be seen that the commercially available sensors from HM exhibit a higher stability during long-term application (up to 170 h). Additionally, they provide more accurate measurements. This can be explained by the fact that the miniaturized sensors are equipped with sensor membranes of a very small diameter (reference electrode for the pH-value and redox potential, DO), sensible to clogging, as well as a very low electrolyte volume (DCO_2, pH-value, redox potential) with the risk of toxification. This makes them more sensible to harsh environment in long-term applications, for example in brewing media with high CO_2 formation. Since the temperature and pressure measurements of the miniaturized sensors are based on resistivity, they measure stable also for a long time in a brewing process. This was proven for up to 190 h in brewing fermentations in the laboratory scale.

The latter results concerning the sensor stability were performed either with only one sensor system and one reference solution or with the application of the sensors in a scale < 0.15 m^3, focusing on daily reference measurements. In the following, the data from measurements in standard solutions parallel to experiments in industrial scale are shown, where only a start reference in standard solutions directly after the calibration and a reference measurement at the end of the fermentation were recorded.

Table 12 shows the average values for the reference measurements before and after the fermentation in 0.15 m^3 fermentation volume during 69 h and the corresponding standard deviations (procedure described in 4.1.1 (3). Each of these values was determined by the arithmetic mean of a certain amount of values in a certain time frame as shown in the following, for which the sensor response time was already considered: HM system: before sensor application: 65 values, considered time frame: 8 min (measurement frequency: 8 sec); after sensor application: 10 values, considered time frame: 10 min (measurement frequency: 60 sec); KSI System: 60 values, considered time frame: 10 min (measurement frequency: 10 sec.).

Table 12: Reference measurements before and after the application of the sensors in a yeast fermentation (69 h, 0.15 m^3) with both systems.
Red: HM system, blue: miniaturized system from KSI.

Reference solutions	pH = 10	pH = 7	pH = 4	O_2 [%-sat]	Redox potential, 250 [mV]
Start: Absolute value / Standard deviation	**10.38** 0.01	**7.2** 0.01	**3.97** 0.08	**100.14** 0.05	**246.86** 0.01
End: Absolute value / Standard deviation	**10.57** 0.63	**7.21** 0.01	**4.07** 0.01	**99.77** 0.13	**244.28** 0.58
Start: Absolute value / Standard deviation Frequency: 10 sec	**9.74** 0.52	**7.1** 0.3	**4.28** 0.57	**101.1** 0.59	**238.65** 30.25
End: Absolute value / Standard deviation	**9.32** 0.29	**7.09** 0.85	**3.93** 0.39	**14.14** 5.81	/

Reference measurements with HM system were performed in two large-scale fermentations of 170/199 m^3 (each more than 222 h) after the application according to the description in 4.1.1 (4). The average values and the corresponding standard deviations are shown in Table 13. Each of these values was determined by the arithmetic mean of 40 (1st experiment) and 35 (2nd experiment) values in a time frame of 574 and 500 seconds, respectively (measurement frequency: 15 sec).

Table 13: Reference measurements before and after the application of the sensors in a yeast fermentation (222 h, 170/199 m^3) with the HM system.

Reference solutions	pH = 7	pH = 4	O_2 (at air) [%-sat.]	Redox potential, 250 [mV]
Value at calibration	**7.02**	**4.01**	**99.95**	**256.97**
End Exp. I **Average value /** **Standard deviation**	**7.12** 0.03	**4.07** 0.02	**94.11** 0.24	**254.75** 0.31
End Exp. II **Average value /** **Standard deviation**	**7.16** 0.01	**4.10** 0.03	**94.93** 0.49	**261.39** 0.71

It can be seen independently from the time point, duration or fermentation geometry that the HM sensors provide stable measurements during long-term applications in complex, harsh brewing media with a very small drift during time. Even a data transfer across long distances (cable length of up to 30 m) does not affect these measurements.
Using a standard solution of pH = 4.01, the drift after long-term application was between 0.06 and maximum 0.17 pH-units and for pH = 7.0 between 0.01 and maximum 0.14 pH-units. In a standard solution of 250 mV for the redox potential, the drift was determined to be between 1.88 and 4.4 mV. The DO sensor showed a drift of 0.8 % up to maximum 1.8 % saturation after the long-term application in brewing media, based on a calibration at 100 % oxygen saturation. For the temperature, the spatial gradients along the height of up to 0.4 °C were located in the range of the temperature changes, which were caused by the cooling system (0.3 - 0.6 °C). The temperature (on / off) regulation is represented by the oscillating temperature course in the corresponding graphs in 5.1.2.3.

The maximum sensor accuracy is determined by the technical specifications of the sensors and the corresponding calibration standard solutions. The accuracy of the commercially available sensors for the respective parameters was: pH-value: ± 0.02 – 0.05; redox potential: ± 5 mV; DO: ± 0.05 %vol. at 1 %vol., ± 0.2 %vol. at 21 %vol., ± 0.5 % vol. at 50 %vol., and temperature: ± 0.2 °C. In case of the miniaturized sensors, the drift was higher than the accuracy of the sensors as stated above and therefore the limiting parameter concerning the suitability of the sensors for long-term applications.

5.1.2. Multi-Parameter Measurements at different Heights with mobile Sensor Units

Several attempts have been made to use miniaturized sensors, integrated into flow cells or finally into the sensor unit. At later stage, also commercially available, larger sensors were applied and an adequate housing was constructed (see 4.1.1 - 4.1.2). During the constant development, technical improvements concerning both sensor technology and housing for *in-situ* monitoring or integration into bypasses for *in-line* measurements were achieved. Finally, the best handling as well as

measurement accuracy, stability in harsh and gas saturated media, and drift after long-term application were achieved using the sensor housing units.

In the following sections of the results part, especially concerning the fermentation performance control and the complex *off-line* analyses (section 5.2), the focus was set on the investigation of the appearance of gradients and their size in each scale as well as on the correlation analysis of data within one scale, not on the comparison of the results obtained in different scales.
In the brewing process, many factors vary between the different production places and might even differ from batch to batch. These are for example the quality of the raw material (malt, water, hops), the yeast strain, the vessel geometry and size as well as the temperature regime. Further, pH- and extract-values at the fermentation onset might be different as it can be seen comparing the 3 m^3 and 170/199 m^3 scale (Fig. 29 and Fig. 37). In the 170/199 m^3 scale, a seasonal beer was brewed containing a higher original gravity. Hence, it is not feasible to compare detailed analysis results from different processes with each other.

5.1.2.1. Localization of the Sensor Units by the Measurement of (hydrostatic) Pressure

The 1st approach for the localization of the sensor unit was based on ultrasound. It consisted of one emitter, which was mounted on the sensor unit, and three detectors (time resolution of 0.5 µs), which were mounted on the tank wall and connected via cables to the recorder (Fig. 23). The frequency of the emission signal was 30 kHz with an emission power of 10 – 12 W. The acquisition frequency was 1 sec. Due to the low signal strength and short cable length the system was limited to the laboratory scale of 0.15 - 0.17 m^3.

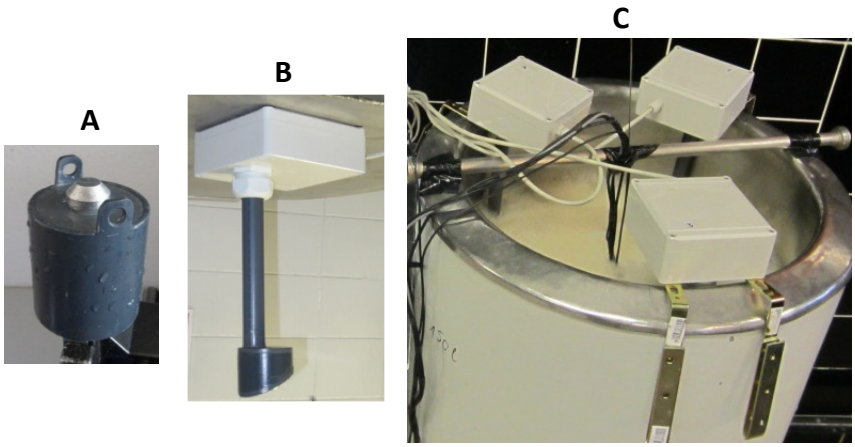

Fig. 23: Sensor localization system based on ultrasound (teleBITcom GmbH, Germany).
A: Emitter; B: One of the three receivers; C: Application of the localization systems in the scale of 0.15 - 0.17 m^3 in a brewing fermentation.

The most challenging, however, was the propagation of the ultrasonic waves through the brewing medium. The sensor signal was interrupted as soon as the amount of (especially small) gas bubbles increased due to CO_2 formation. This was the case at the onset of the fermentation and during the main fermentation phase, covering the most important fermentation phases for the investigation of gradients. Tests of the ultrasonic system in fermentations with high yeast cell concentrations (up to 80 Mio cells mL^{-1}) proved the assumption that not the turbidity but gas bubbles are the disturbing factor (data not shown).

In Fig. 24, the signals of the three receivers (blue, red, violet) of the localization system during a top fermenting process of about 50 h are displayed. The black signal is the overall signal of all receivers, i.e. when all three receive a signal. This was required for a localization in x-y-z-direction. The fermentation accelerated at about 3 - 4 h with a decreasing activity after about 10 h of fermentation, which was proven by the fermentation performance control. It can be seen in the magnification (Fig. 24 B) that during this time frame the receivers were not constantly recording signals. Due to the offset of records, the overall (black) signal was interrupted for even 25 min, hindering the calculation of the sensor position. At later fermentation stages, the signals were mostly recorded again by all receivers since the yeast activity and thus, the CO_2 bubble formation decreased.

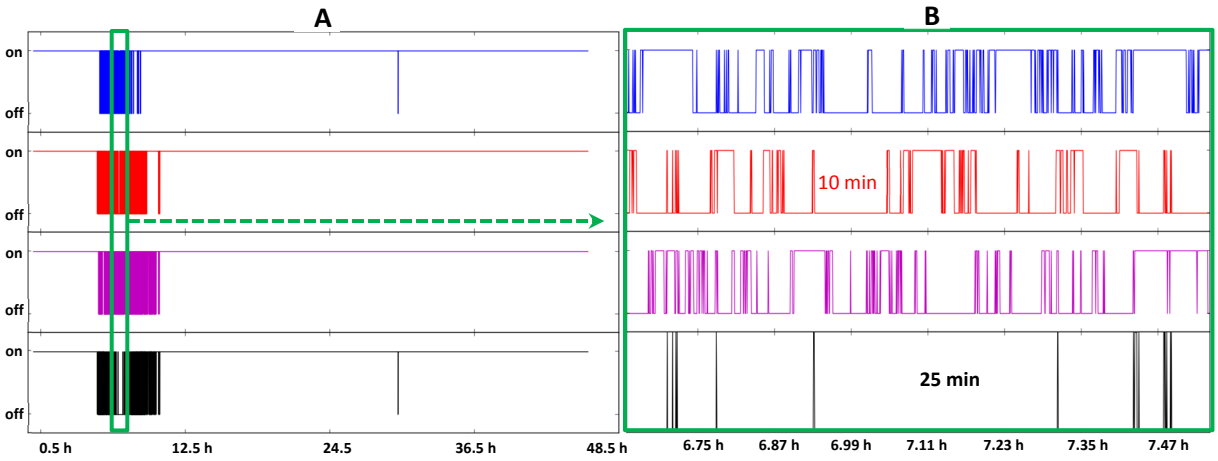

Fig. 24: Ultrasonic signals of the sensor localization system in a fermentation of 50 h with top fermenting yeast. On = signal received, off = signal not received. A: Signal during the complete fermentation time; B: Magnification of the onset of the fermentation (black frame in fig. A) with a time distance of 7:12 min.

An approach for optimization was the collection of the data of each single receiver during a time frame of 10 min, match them, and ascribe them to one time point for localization. This would have worked for the fermentation displayed in Fig. 24. For other fermentations, however, this approach was not suitable as presented in Fig. 25. Data from a fermentation with top fermenting yeast during about 90 h are shown. The shortest time frame of signal loss for one receiver was 1.5 h (red) during the transition of the fermentation onset to the main fermentation phase (Fig. 25 B). For the overall (black) signal the signal was lost even for 3 h. Hence, the time frame needed for the collection of data from all three receivers would be too long for the detection of gradients in a fermentation process.

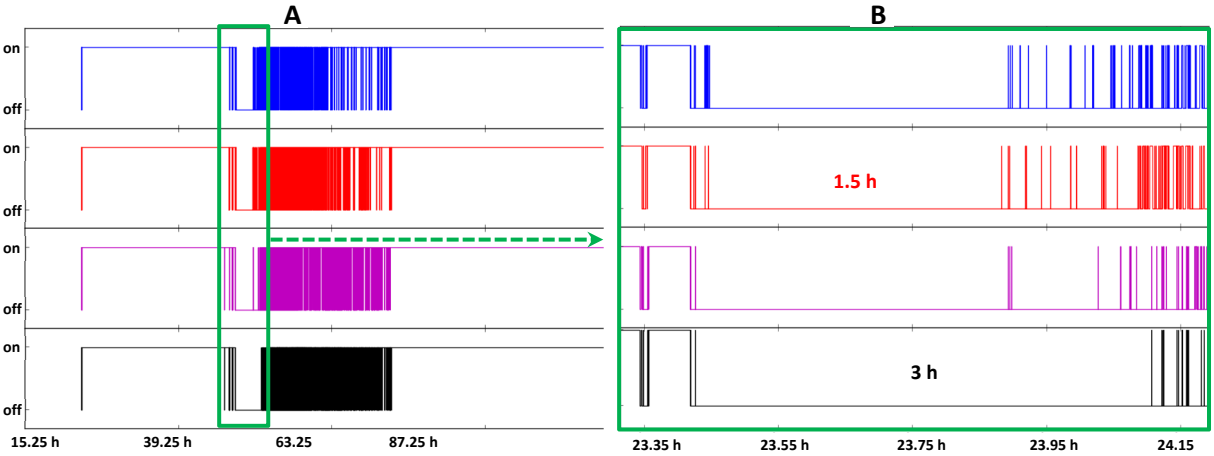

Fig. 25: Ultrasonic signals of the sensor localization system in a fermentation of 90 h with top fermenting yeast. On = signal received, off = signal not received. A: Signal during the complete fermentation time; B: Magnification of the onset of the fermentation (black frame in fig. A) with a time distance of 12 min.

The data show that the system would be suitable for the investigation of later fermentation stages, when yeast activity is decreasing. Beside the challenge of gas bubble formation in the brewing process, however, the aimed accuracy of ± 3 - 5 cm was not achieved in brewing media. This was proven by manual control in the 0.15 - 0.17 m^3 scale. Furthermore, the system was not constructed for applications in industrial, closed fermentation tanks. Hence, the ultrasound-based localization system was not applied any longer in the following experiments in larger scales.

The miniaturized sensor unit, instead, was localized by the integrated pressure sensor in vertical direction. The measurement was based on the hydrostatic pressure, depending on the height of the liquid column above the sensor. Due to the maximum cable length of the sensor unit of 5 m, it could only be applied up to a scale of 24 m^3 or a tank height of about 4 m.
During different beer fermentations, changes in the position of the sensor unit along the height could be tracked by this sensor Fig. 26. A zoom of two time frames (85 - 86 h and 94 - 95 , in which the sensor unit was moved to six different positions in a tank of 24 m^3 volume is shown in Fig. 26 B. By this, also the filling level during a filling process with several batches can be monitored Fig. 26 C).

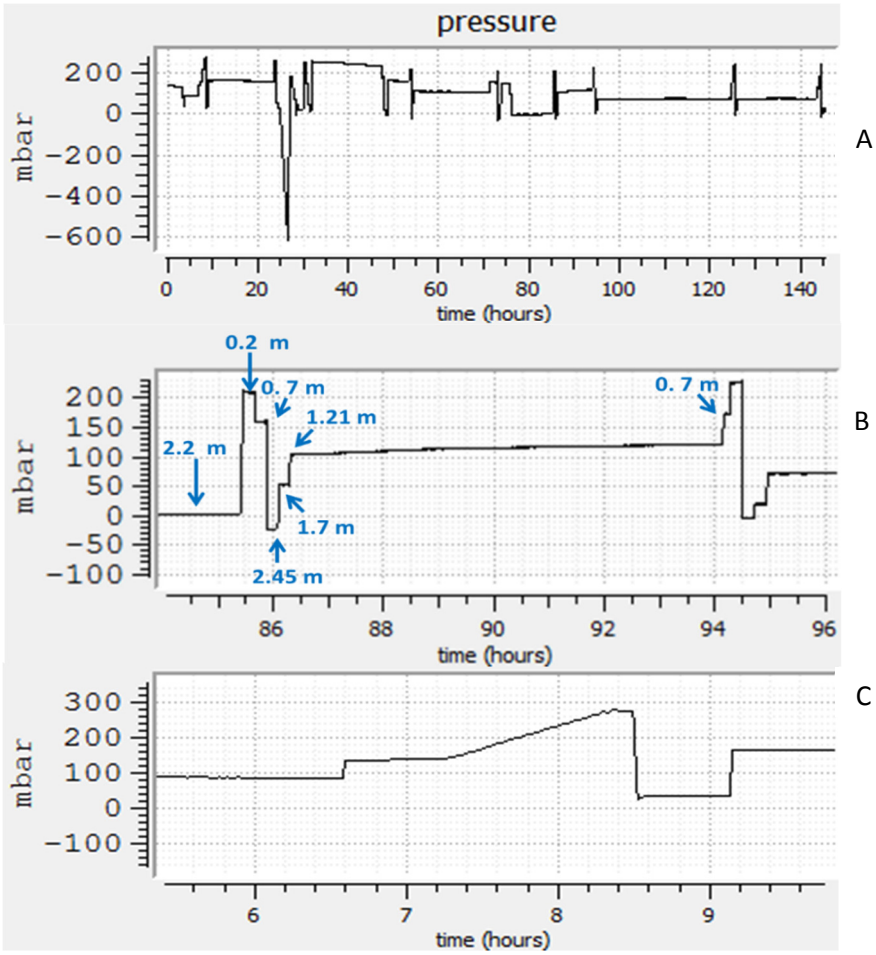

Fig. 26: Pressure measurement with the pressure sensor in a fermentation of 24 m^3 during 145 h. The sensor was integrated in the miniaturized sensor unit (KSI, Jumo GmbH & Co. KG, both Germany). Data were acquired with the KM 3000 (KSI) and displayed with a program based on the software Python (Python Software Foundation, USA). A: Complete fermentation with sensor position changes; B: Zoom of time frames with sensor movements; C: Zoom of the filling process (7 - 8.5 h).

5.1.2.2. Mobile Multi-Parameter Measurements in the Pilot Scale (0.15 and 0.17 m^3)

After experiments regarding the functionality, applicability, and stability in laboratory scale (see Table 2), the 1st multi-position experiments were performed in the pilot scale with a volume of 0.15 m^3 and 0.17 m^3 (maximum vessel volume: 0.2 m^3) and top fermenting yeast. The following parameters were measured by the KSI sensor unit: redox potential, pH-value, DCO_2, temperature, and DO (see 4.1.1).

For the correct interpretation of the monitored and analyzed data and to prove the functionality of the *on-line* monitoring system, a fermentation performance control was performed during all experiments once a day, analyzing the *off-line* pH-value (by a common pH probe), the cell concentration (by a Thoma chamber or automatic cell counter), and the extract. The extract is defined as the content of non-volatile dissolved compounds (carbohydrates and other solids). The apparent extract, measured by a hydrometer, is typically expressed in degrees Plato [°P] in brewing science. The extract can be also expressed as mass density and calculated according to the following formula:

$$p = \frac{d-b}{a} \tag{5.1}$$

with p = °P, d = density in kg $(m^3)^{-1}$ (measured by hydrometer), b = constant of 997 kg $(m^3)^{-1}$, and a = constant of 4.13 kg $(m^3\,°P)^{-1}$.

In Fig. 28, the data of the *on-line* measurements and the fermentation performance control of two fermentations (0.15 and 0.17 m^3 fermentation volume), performed as described in 4.3, are presented. The main fermentation phase with the highest activity concerning growth, carbohydrate degradation, and CO_2 release was between 25 and 73 h in the 0.15 m^3 scale and between 25 and 70 h in the 0.17 m^3 scale (dotted lines in Fig. 28), respectively.

The data of the fermentation performance control and the pH-value (Fig. 28 A and C) showed usual developments within a fermentation. The extract and pH-values decreased during time, whereas yeast growth was observable until 60 h and 50 h, respectively. It can be seen that the cell concentration started to decline close to the point of increased extract degradation. Hence, cell growth was decreased and the energy was used mostly for the conversion of carbohydrates to ethanol and CO_2. The pH-value instead stagnated at this time point. Both fermentations can be compared well since both data sets showed very similar levels for all these three parameters during fermentation.

In the 0.15 m^3 scale, changes in the redox potential, DCO_2, and DO at 25 h of fermentation time might have been caused by a short power loss of the sensor probe for several seconds. The challenge in the experiment with 0.17 m^3 instead was the low room temperature (~12.5 °C) of the fermentation hall during winter due to a lacking air conditioning. For the fermentations with top fermenting yeast a temperature of about 21 °C was aimed. Consequently, the vessel jacket was flushed with hot water at 25 h (Fig. 27) in order to accelerate the fermentation. This probably affected the other parameters as well temporarily. The redox potential in the 0.17 m^3 scale is not rising during the main fermentation phase (~25 h – 75 h) as in the 0.15 m^3 scale. The pH-value drops faster as well, i.e. with a steeper slope in the 0.17 m^3 scale. Since both parameters depend on the temperature, the differences to the 1st experiment (0.15 m^3) might be of physical nature but could also indicate a higher metabolic activity and oxygen consumption at higher temperatures.

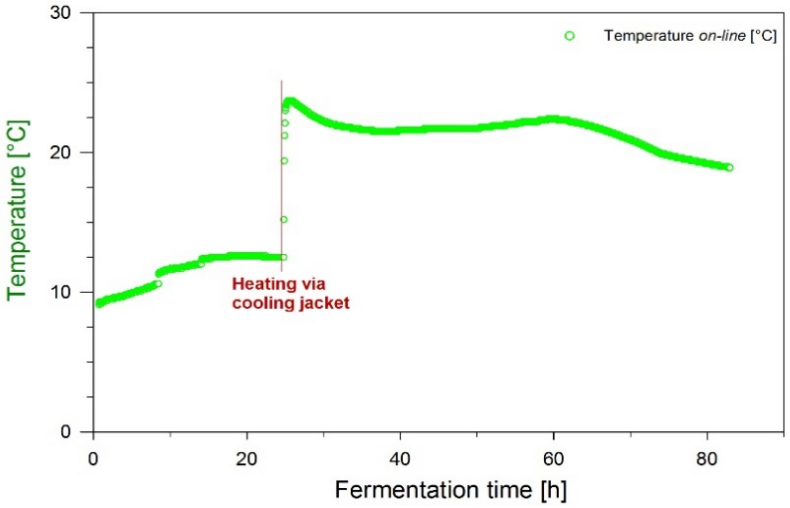

Fig. 27: Temperature monitoring in the 0.17 m^3 (pilot) scale.

In the 0.17 m^3 scale fermentation (2nd experiment), the sensors were moved to four defined positions within 4 min as explained in 4.2.4.1. Data gained during movements of the sensors (instationary conditions) between the positions are indicated with stars in Fig. 28. Sensor responses on the movement at the 0.17 m^3 scale were observed at 55 and 75 h for the redox potential, expressed by a sudden increase of 15 and 60 mV, respectively. For the DO-value, a sudden increase by 10, 5, and 10 % saturation at 40, 55, and 75 h, respectively was seen. Since the positions were changed quite fast (each 1 min), it cannot be clearly said whether the differences in the parameter values during the corresponding time frame are caused by spatial gradients in the vessel or by the movement of the sensor unit itself combined to a slow sensor response (e.g. for the pH-value > 1 min). Hence, spatial gradients were not detected in the pilot scale under these experimental conditions with the miniaturized sensor unit. (The time frames were elongated for later experiments).

The accuracy and long-term stability (~ 100 h without recalibration) of the sensors for redox potential, pH-value, DO, and temperature was satisfactory (Fig. 28). The fermentation course can be well monitored by the sensor unit. This was proven with the *off-line* controls (e.g. pH-value) and the measurement in standard solutions after the experiments.
For the investigation of the sensor stability during time, the maximum deviation of the sensor data for a minimum record time of 1 h (or longer) was determined. Measurement data of the redox potential electrode indicated deviations between 0.5 and 4.5 mV at a range between -200 and +200 mV during a recording time of 3 - 60 min. The pH-values correlated well with the *off-line* measurements (Fig. 28 C). Deviations of 0.004 - 0.09 pH-units were determined during 5 to 6 h of measurement. For the DCO_2 sensor, deviations between 0.03 and 0.5 g L^{-1} were measured during monitoring periods between 2.5 min and 9 h. The test of the DO sensor between 1 and 10 h revealed deviations between 0.65 and 5 %, only. Very low deviations of < 0.1 °C were determined for the temperature during more than 10 h measurements. In summary, the deviations during long-term application were low for all measured parameters. It must be considered, however, that the miniaturized sensors in the unit were exchanged before this experiment. Hence, they were applied for the first time and did not have defects due to clogging or toxification of an electrolyte from former applications.

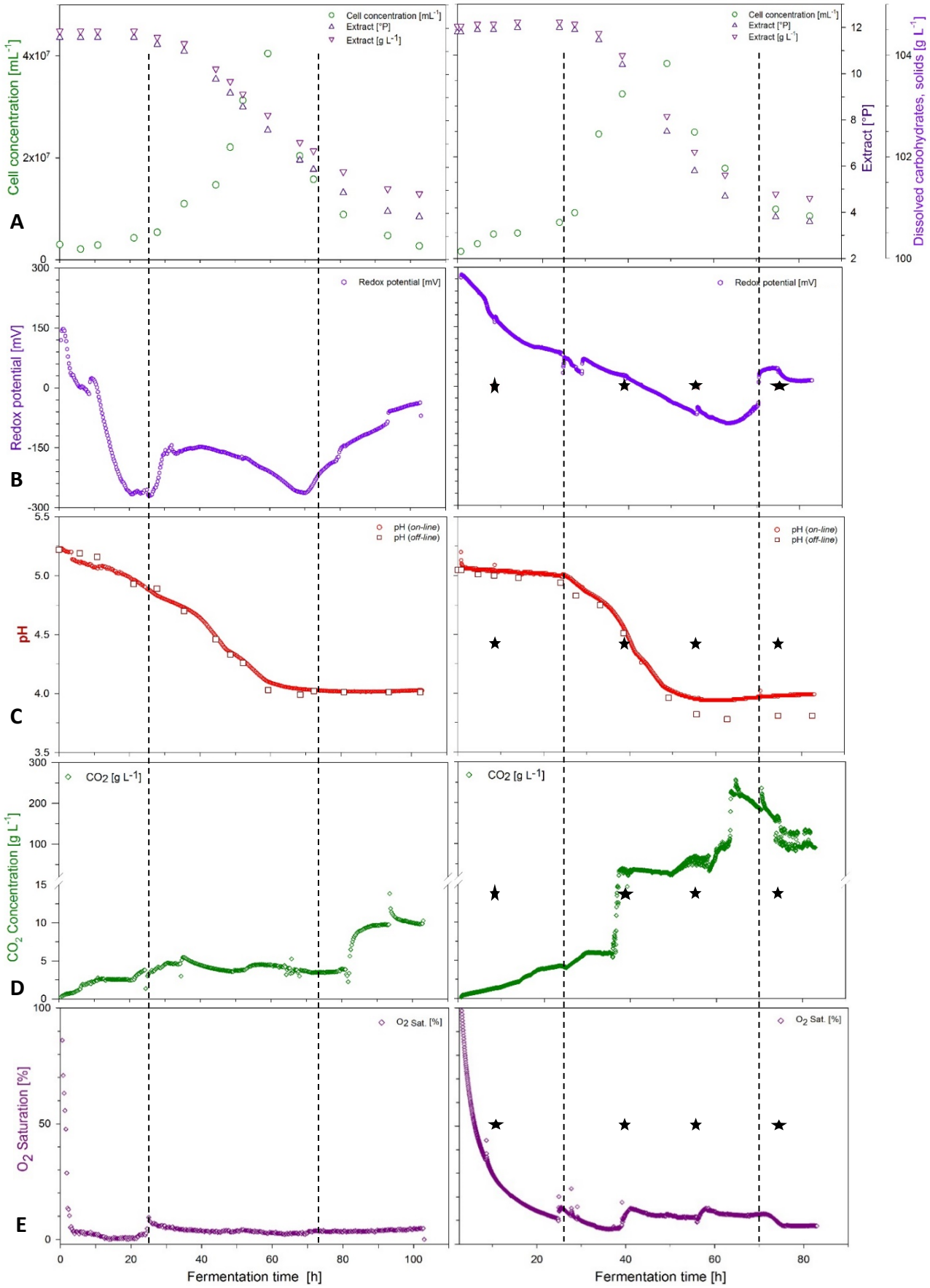

Fig. 28: Measurement of fermentation parameters in the pilot scale with top fermenting yeast. Left column: 0.15 m^3, right column: 0.17 m^3. A: *Off-line* fermentation performance control (cell count, pH-value, extract), B: redox potential, C: pH-value, D: DCO_2, E: DO. Main fermentation phase signed by vertical dot lines, sensor movements by black stars.

The influence of the operation time for the DCO_2 sensor is shown in Fig. 28. Usual values during a beer fermentation without any surplus pressure are in the range of 2 - 5 g L^{-1}. In the 1st experiment, the sensor worked accurately up to 80 h (Fig. 28 D, left). In the 2nd experiment, reasonable values were reached only up to 30 h (without sensor exchange or recalibration) (Fig. 28 D, right). Since the volume of the electrolyte is quite small with respect to the high DCO_2 concentrations that are reached during the fermentation, it is toxified after a certain time of exposure to these high concentrations. The optimal measurement range of this sensor is also quite low with a range of 0 - 200 mg L^{-1}. Hence, it would need to be exchanged already after 1-2 days or the electrolyte volume need to be increased.

The redox sensor represents very well the different phases during a beer fermentation. At the onset of the fermentation, the redox potential is high due to elevated dissolved oxygen concentrations (Fig. 28). During the main fermentation phase, the redox values are lower or even decrease constantly due to higher metabolic activity and oxygen consumption. Further, different metabolites that influence the oxidation-reduction ratio are synthesized. At the end of the fermentation, the redox potential increases again. Cell lysis and the release of substances that increase the redox potential might be a reason for this change at the bottom part of the fermenter. At the top of the fermenter close to the surface instead, hydrophobic substances might accumulate, which increase the redox potential as well. Since this was an open fermentation, diffusion of atmospheric oxygen can also not be prevented.

5.1.2.3. Mobile Multi-Parameter Measurements in industrial Scale (3 m^3, 24 m^3, 170/199 m^3)

For applications in industrial scale, a new housing unit for the sensors from HM was developed and constructed (4.1). Both sensor housing units from KSI and HM were applicable directly in the liquid phase until a fermentation volume of 24 m^3 (see Table 14), using cables of 5 m lengths for data transfer and providing data of five parameters.
As indicated in 5.1.1., however, the miniaturized sensors showed low accuracy, longer sensor response times and a non-linear drift after long-term and repeated use without recalibration. For some sensors (e.g. DCO_2), only a complete exchange of the sensor and a repair of the membrane or exchange of the electrolyte would increase the accuracy. This is not suitable for the monitoring of long-time fermentation processes due to hygienic restrictions and the lack of measurement data in case of sensor exchange. Further, it is financially of disadvantage. In the pilot scale (0.15 - 0.17 m^3) experiments, sufficient accuracy for all sensors and a stable operation for 100 h fermentation time was achieved for most of the miniaturized sensors. The reason is that the sensor unit was equipped with new miniaturized sensors before these two experiments, i.e. they were applied for the 1st time.
Therefore, only data obtained by measurements with the with the unit for housing the commercially available sensors (HM) are presented in the following for the scales ≤ 3 m^3. Further, higher distances of > 5 m, however, could be overcome only with the HM Arc-System, using sensors with an integrated pre-amplifier for a stable signal transfer through cables, which need to be as long as approx. 25 m.

The question to be answered by the *on-line* sensor technique was whether gradients appeared in the in the liquid phase of the investigated fermentation tanks. In order to display adequate scaling, all processes presented in the following were divided into the different phases: Filling phase, fermentation phase, (diacetyl rest in the 170/199 m^3 scale), and cooling phase as described in 4.2.3, Table 6. A special focus during gradient determination was set on the time frames, in which the sensors were moved. Since the process is a slow process and quasi stationary, time spaces between two close moving frames can be at least estimated.

Table 14: Overview of equipment and experiments for the application in industrial fermentation tanks.

Scale	Tank form	Sensor Equipment	pH-value KSI	Redox KSI	DO KSI	dCO_2 KSI	Temp. KSI	Pres-sure KSI	pH-value HM	Redox pot. HM	DO HM
3 m^3	CCT	Sensor unit KSI & HM sensor unit	✔	✔	✔	✔	✔	✔	✔	✔	✔
3 m^3	CCT	Sensor unit KSI & HM sensor unit, 5 m cable	✔	✔	✔	✔	✔	✔	✔	✔	✔
24 m^3	CCT	Sensor unit KSI & HM sensor unit, 5 m cable	✔	✔	✔	✔	✔	✔	✔	✔	✔
199 m^3	CCT	HM sensor unit, 25 m cable							✔	✔	✔
170 m^3	CCT	HM sensor unit, 25 m cable							✔	✔	✔

In the following, two different methods for data presentation for the 3 m^3 and 170/199 m^3 scale are shown. In Fig. 30 - Fig. 33 and Fig. 36 as well as Fig. 38 - Fig. 41 and Fig. 44 - Fig. 47 the results of the monitoring of the main fermentation phase are displayed as a plot over time. Since the filling, diacetyl rest, and cooling phase show very different conditions, these are excluded from the graphs in order to display adequate scaling for the main fermentation phase. The light blue bars indicate time frames, in which the sensor unit was positioned to all different heights with measuring breaks of 20 min (3 m^3) and 6 min (170/199 m^3 scale) at each position (i.e. movement frames). The exact time frames are displayed in appendix A, Table 20. The time of the movement itself and for stabilization are excluded from the data points.

In the presentation of the time development, however, it is difficult to determine the exact gradient size comparing all positions of one movement frame with each other and to distinguish between time-dependent and - also small - spatial gradients. Further, the visual evaluation of the color transitions is challenging. An improved method and data presentation for the determination of gradients was obtained by the mathematical calculation of the differences between all positions, respectively (see Fig. 34, Fig. 35 and Fig. 42, Fig. 43).

To obtain these graphs, firstly the mean values for every position were calculated based on the data gained at one position and time point, respectively. The time of the movement itself and for stabilization were excluded from the data points. In the next step, the differences between the mean values of all positions, i.e. of each position against all others, within one movement frame were calculated. One movement / measurement frame (where quasi-stationary conditions were assumed) was the time, which was needed to move the sensor unit once to each position and measure for 6 min (170/199 m^3 scale) or 20 min (3 m^3 scale). This allows for the differentiation between spatial and time-dependent gradients. Due to the graphical display of the gradient size (clustered according to the size and represented by different colors) at a defined time point, the known sensor accuracy and data trends before or after a movement frame can be well distinguished from the measurement data and taken into account during evaluation. This is not feasible if the single sensor measurement data are displayed over time. Since the mean values are used in the 2nd method, single outlier values, which might be detected as gradients, are not considered. Due to the division into time frames and the display of the differences in height rather than the measurement values, the filling and cooling phase could be included in the graphs (Fig. 34, Fig. 35; Fig. 42, Fig. 43) without increasing the scaling range.

Mobile Multi-Parameter Measurements in industrial Scale: 3 m³

For the correct interpretation of the monitored data and as reference method, a fermentation performance control was performed during the experiments once a day as described for the 0.15 and 0.17 m³ scale (5.1.2.2). The sampling point, however, was located at one single position. The data, shown in Fig. 29, prove that the fermentations followed a usual course with decreasing extract and pH-values during time and an increase in the yeast concentration until 90 h and 57 h in the 3 m³ scale, respectively. Metabolic activity decreases at these time points, indicated by the decreased amount of yeast cells at the sampling port due to sedimentation below it and a stagnation of the drop of the pH-value, caused by the decreased CO_2 release and decreased formation of carboxylic acids. Similar levels for all three parameters during fermentation in both experiments of the 3 m³ scale show the reproducibility and allow for the comparison of both fermentations.

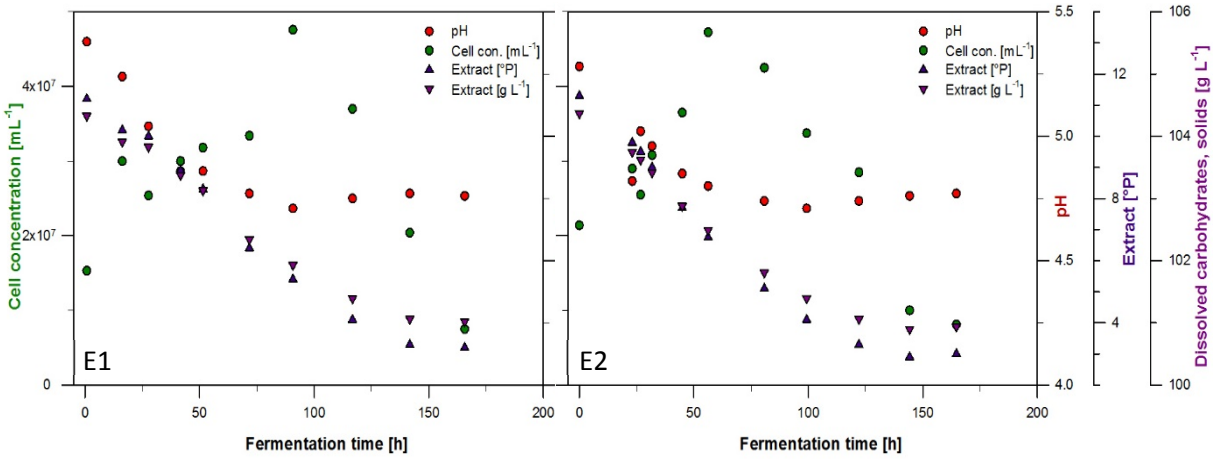

Fig. 29: Fermentation performance control (*off-line*) in the 3 m³ scale: cell concentration, pH-value, extract. Left: experiment 1 (E1), right experiment 2 (E2).

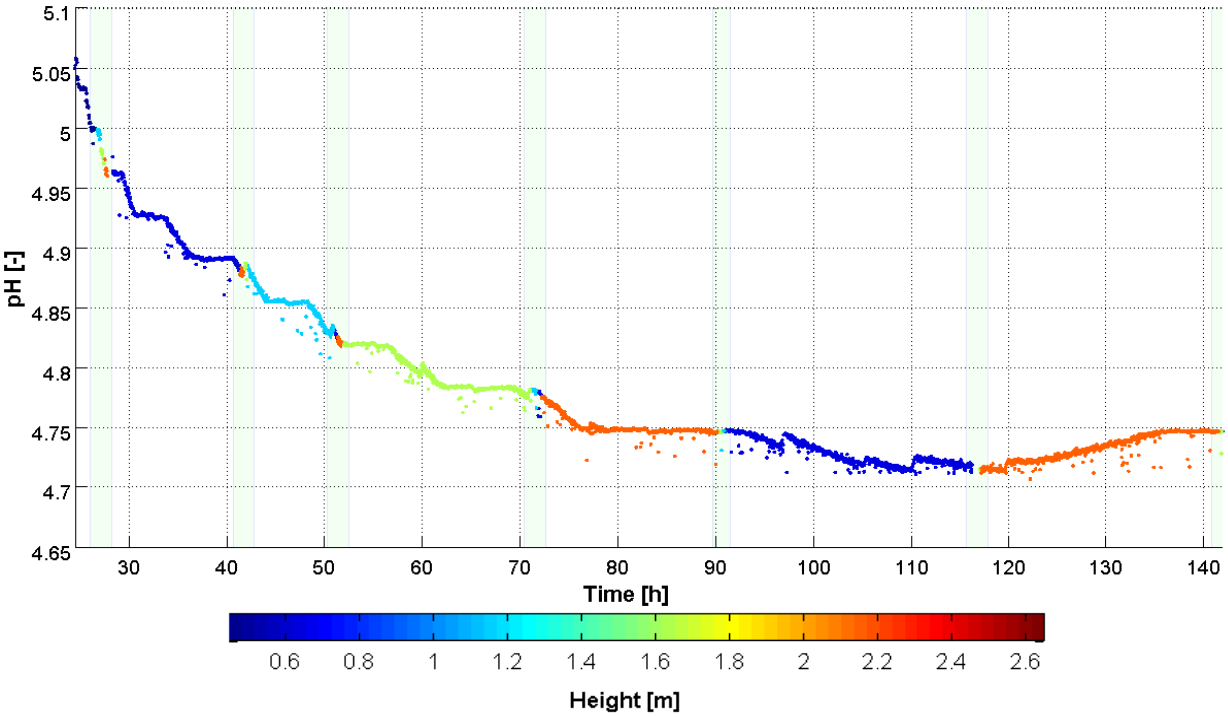

Fig. 30: Monitoring of the pH-value during the main fermentation in the 3 m³ scale (experiment 1). Filling and cooling phase excluded.

The parameters redox potential, pH-value, DO, and temperature were monitored simultaneously with both the KSI and HM sensor unit at six different heights of the reactor (Table 7 in 4.2.4.1). In comparison to the scale at 170 m^3, however, the sensors could not be moved with such a high frequency (mostly one to two times per day) due to the limited accessibility of the brewery. Further, the sensors were kept 20 min at each position for measurement in the 3 m^3 scale (only 6 min with the HM sensors in the 170/199 m^3 scale) since the miniaturized sensors had a longer response time. Hence, small spatial gradients of a short life time might not have been detected.

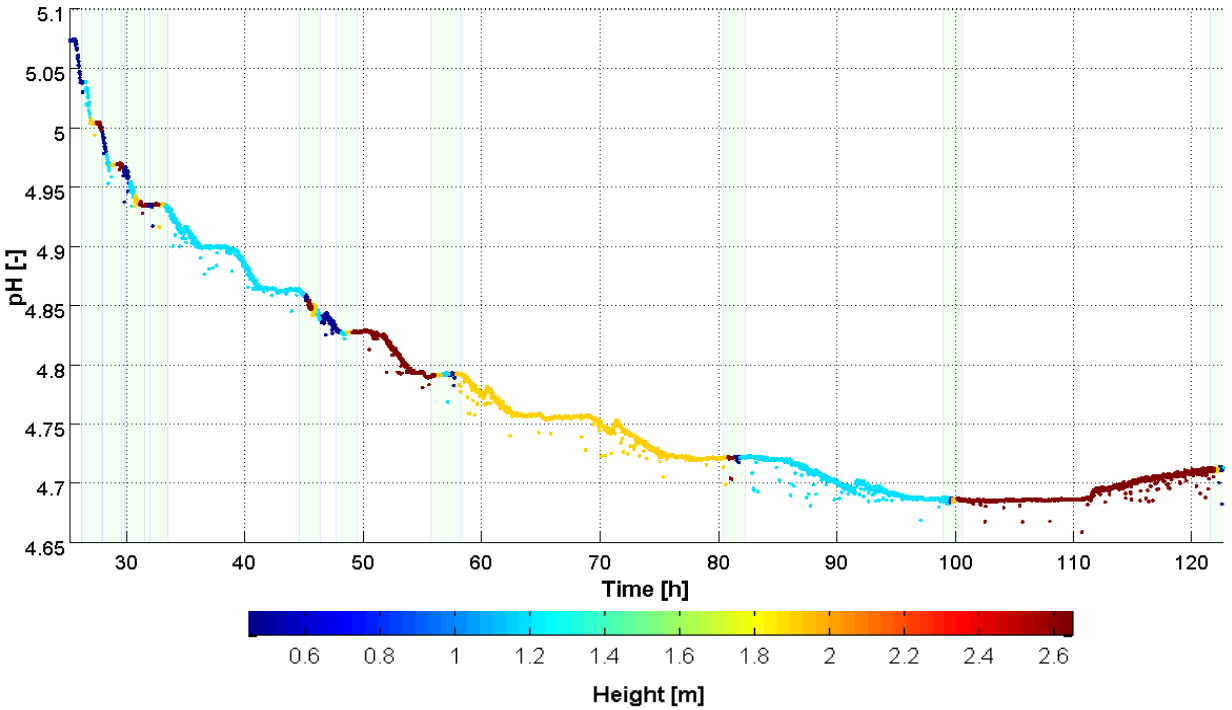

Fig. 31: Monitoring of the pH-value during the main fermentation in the 3 m^3 scale (experiment 2). Filling and cooling phase excluded.

In Fig. 30 and Fig. 31 as well as Fig. 32 and Fig. 33, the pH-value and the redox potential course during time for experiment one and two in the 3 m^3 scale are displayed. The sudden increasing redox values at 30, 32, and 57 h on one position might have been caused by a more vigorous movement of the sensor unit.

As stated above (page 82), these graphs give information about the fermentation course during time. For the investigation of the complete process time and the appearance of small gradients, however, an alternative data evaluation and presentation method was used (see Fig. 34, Fig. 35). The gradients were represented by different colors according to their size and displayed in the respective measurement windows (explained in detail on page 82). Due to the same low gradient size (pH < 0.05, redox potential < 0.5 mV) and connected fermentation time, the measurement frames 3 - 5 and 6 - 9 in Fig. 34 as well as 6 - 7 and 10 - 12 in Fig. 35 are displayed as one block, respectively. During the filling process (24.5 and 25.2 h), measurements were performed only at the first two positions due to the low filling volume.

It can be seen that - apart from the fermentation onset - only small gradients were detected during fermentation. Gradients along the tank height below 0.05 pH-units (max. 0.03) and 5 mV were detected during the complete 1st experiment after 28 h, indicating a good mixing due to natural convection (CO_2 bubble formation) and quasi-homogenous conditions (Fig. 34). Spatial gradients in the

redox potential of maximum 9.4 mV were measured at three positions during the onset of the fermentation between 26.1 and 28.2 h in the 1st experiment. Even at the start of the cooling procedure (141.7 h), the fluid flow was not affected negatively regarding the even distribution of the measured parameters.

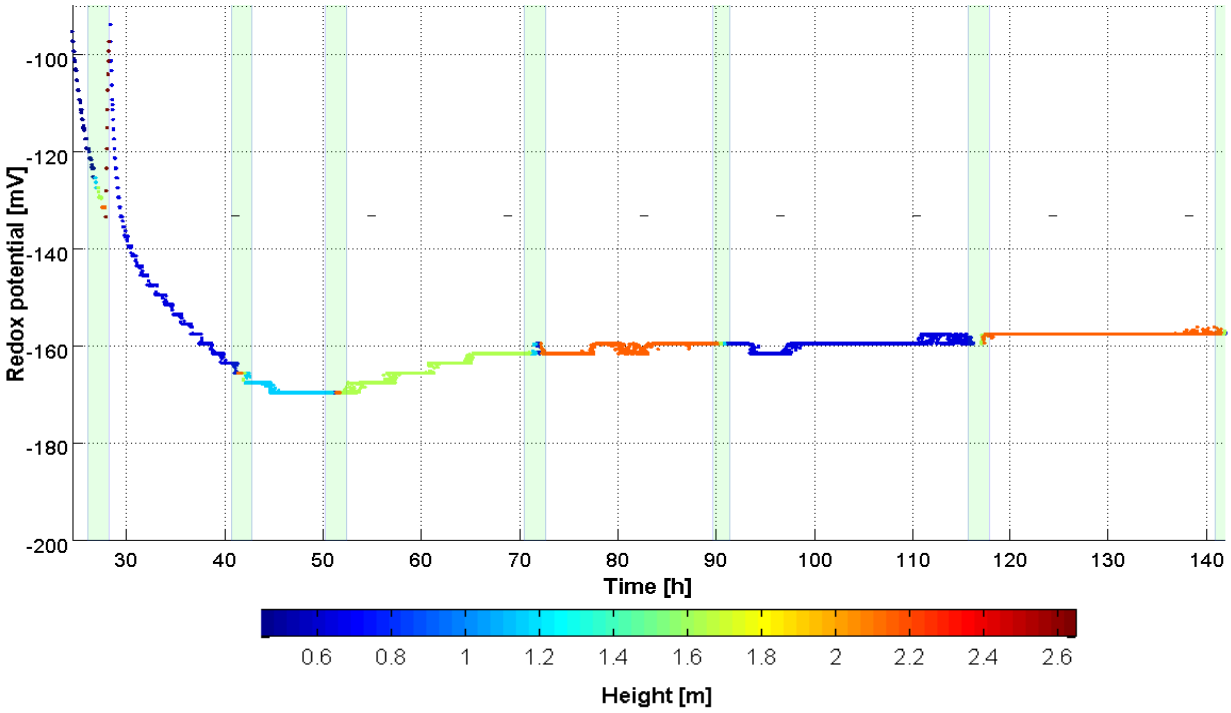

Fig. 32: Monitoring of the redox potential during the main fermentation in the 3 m³ scale (experiment 1). Filling and cooling phase excluded.

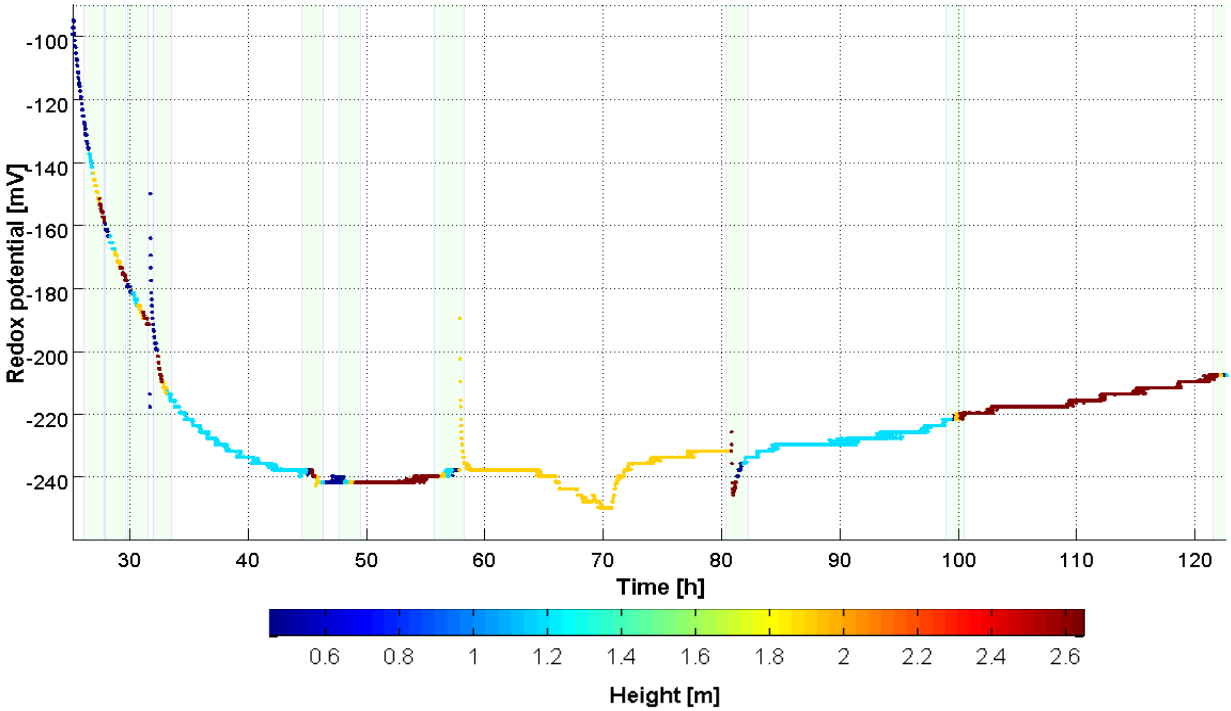

Fig. 33: Monitoring of the redox potential during the main fermentation in the 3 m³ scale (experiment 2). Filling and cooling phase excluded.

In the 2nd experiment, the determined gradients in the pH-value were below 0.05 pH-units (max. 0.04 at the fermentation onset) as well during the complete fermentation time considering all positions (Fig. 35). In the redox potential, however, a maximum spatial gradient of 23 mV (20 - 30 mV range) was

measured between 26.2 and 27.9 h between position one (0.65 m) and four (2.15 m). During the further fermentation course, gradients in the range between 5 and 7 mV as well as 7 and 20 mV were measured. A sudden gradient of 10 mV to 20 mV in the range of -100 to -250 mV might have an impact on the cell metabolic activity. During the cooling phase (start at 122.5 h) instead, no significant gradients were measured.

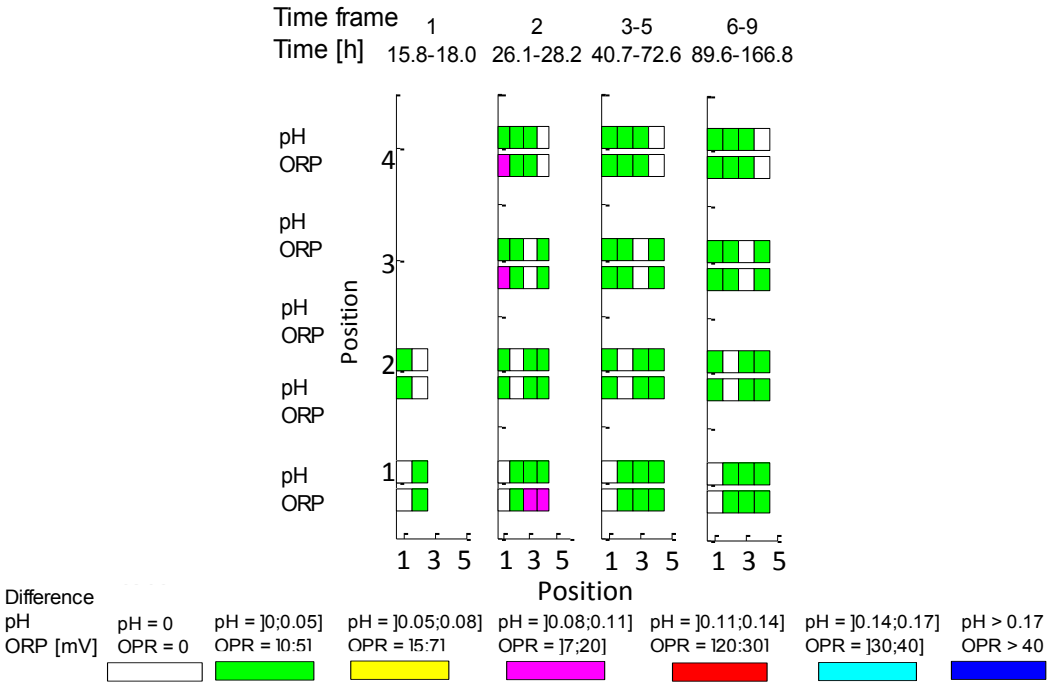

Fig. 34: Investigation of the mixing quality in the 3 m^3 scale (experiment 1).
Filling (with the 2nd batch) and cooling phase are included. Displayed are the differences (color bar) between the mean values in the pH-value and redox potential (ORP) of all positions within one movement frame (frames: 1 - 9). Positions: see Table 7.

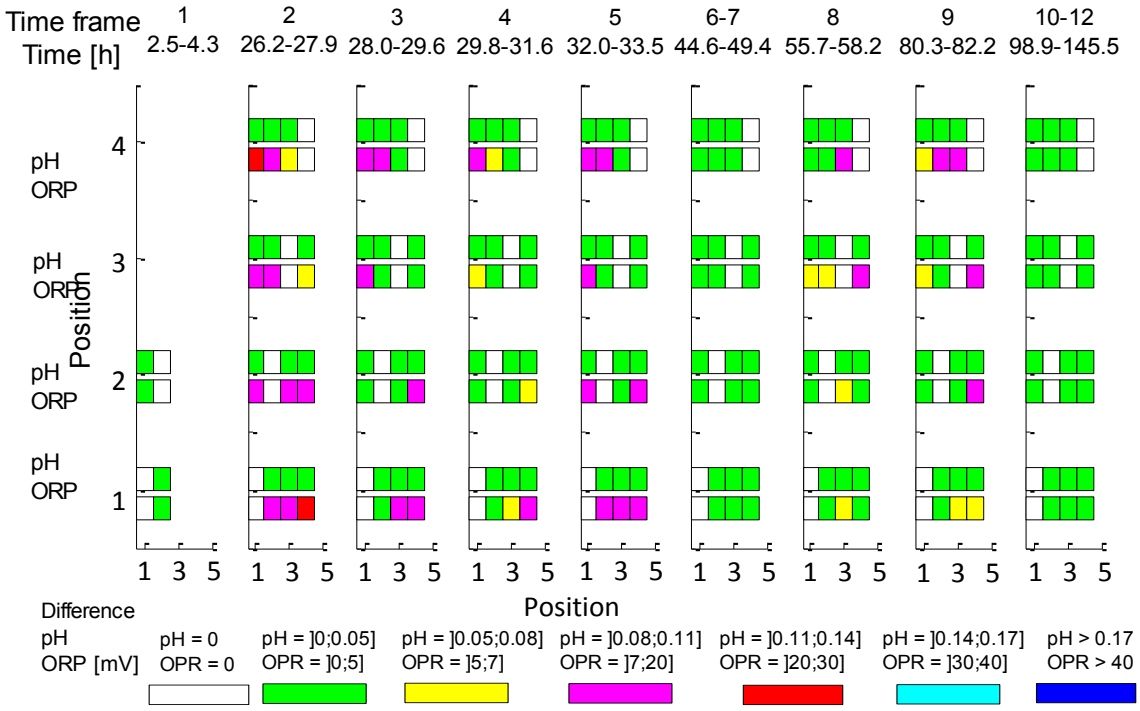

Fig. 35: Investigation of the mixing quality in the 3 m^3 scale (experiment 2).
Filling and cooling phase are included. Displayed are the differences (color bar) between the mean values in the pH-value and redox potential (ORP) of all positions within one movement frame (frames: 1 - 12). Positions: see Table 7.

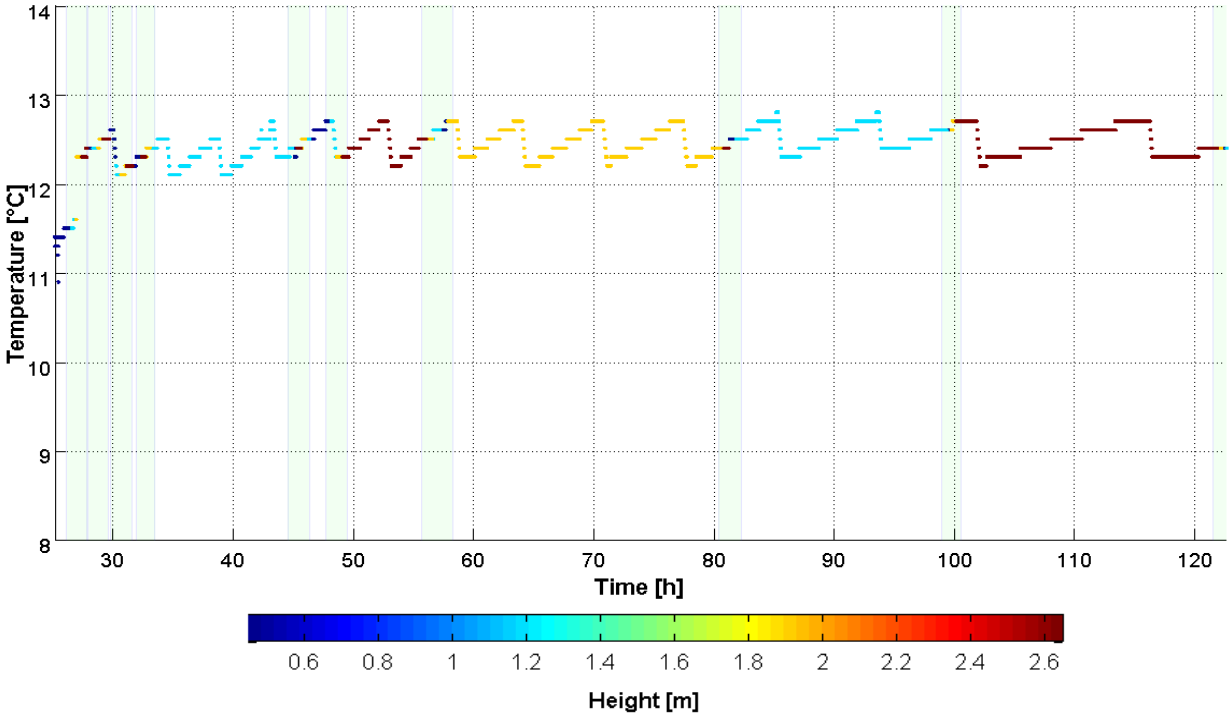

Fig. 36: Monitoring of the temperature in the 3 m^3 scale (experiment 2).
Filling and cooling phase excluded.

The DO-values in both experiments decreased to nearly zero right after the filling with the second batch was finished. They remained negligible, independent from the sensor position (see Fig. B 1 and Fig. B 2 in appendix B). Hence, this parameter was not any more of interest for the measurement of gradients in the investigated brewing fermentations.

The temperature was monitored in the 2nd experiment in the 3 m^3 scale (Fig. 36). Hence, it can be assumed that no temperature gradients along different heights of the reactor were measured that exceed the usual fluctuations.

Based on these results, it can be concluded that the pH-value and the redox potential are of interest in these fermentation processes for the investigation of gradient appearance. This was the case also for the 170/199 m^3 scale.

Mobile Multi-Parameter Measurements in industrial Scale: 170/199 m^3

In the largest scale, two experiments with the same medium and strain were performed (see 4.2.2). Due to the large volume, the tank was filled with seven (1st experiment) and six (2nd experiment) batches. The parameters redox potential, pH-value, DO, and temperature were monitored simultaneously with the HM sensor unit at six different heights of the reactor (Table 7 in 4.2.4.1).

The 1st process differed from the 2nd one concerning the onset of the fermentation (see 4.2.3, Table 6). After the filling was completed in the 2nd experiment, the tank was flushed with CO_2 twice for 5 min (13.0 - 13.1 h and 13.45 - 13.54 h) in order to support mixing of the batches. Measurements were conducted between the two steps.
The temperature for each batch during the filling in the 1st experiment was between 10 and 11 °C, whereas for the 2nd experiment 16 °C were aimed for each batch. In both experiments however, the

target temperature was set to 10.5 °C and reached in less than 30 min after each batch was filled in. In contrast to the 1st experiment, one batch less was added to the fermentation. Hence, the temperature for each batch was slightly higher in the 2nd experiment to achieve a similar fermentation progress during filling and at the fermentation onset as for the 1st experiment.
Further, in the 1st experiment a lot of foam was produced due to insufficient sealing of the openings at the tank dome, which served as entrance for the rope and cables, and some of the tank content was spilling out of the tank dome. The transfer of a certain volume (for more details see page 59) might have influenced the fluid flow pattern at this time point and the hours afterwards and must be considered during the analysis of the mixing quality. Further, the measurement frequency was reduced around this time (50 - 55 h). The action of transfer is indicated with a red line in the corresponding graphs.

In contrast to the 3 m^3 and 24 m^3 scale, the brewery was accessible 24 h daily for eight of ten process days. Hence, sampling and sensor positioning were conducted with higher frequency, i.e. up to three times for *off-line* sampling (including samples for the fermentation performance control and six times for positioning per day (see 4.2.4.2). Only during the diacetyl rest (see Table 6), the movement of the sensors was restricted due to inaccessibility of the brewery.

Analogously to the former experiments, a fermentation performance control was performed during the processes (three times per day), confirming a usual fermentation course. The extract and pH-values were decreasing during the fermentation course and the highest cell concentration at the sampling port could be observed in the middle of the fermentation at 80 h (1st experiment) and 110 h (2nd experiment) (Fig. 37). The two fermentations were well comparable due to the similar levels for all three parameters during the complete fermentation time.

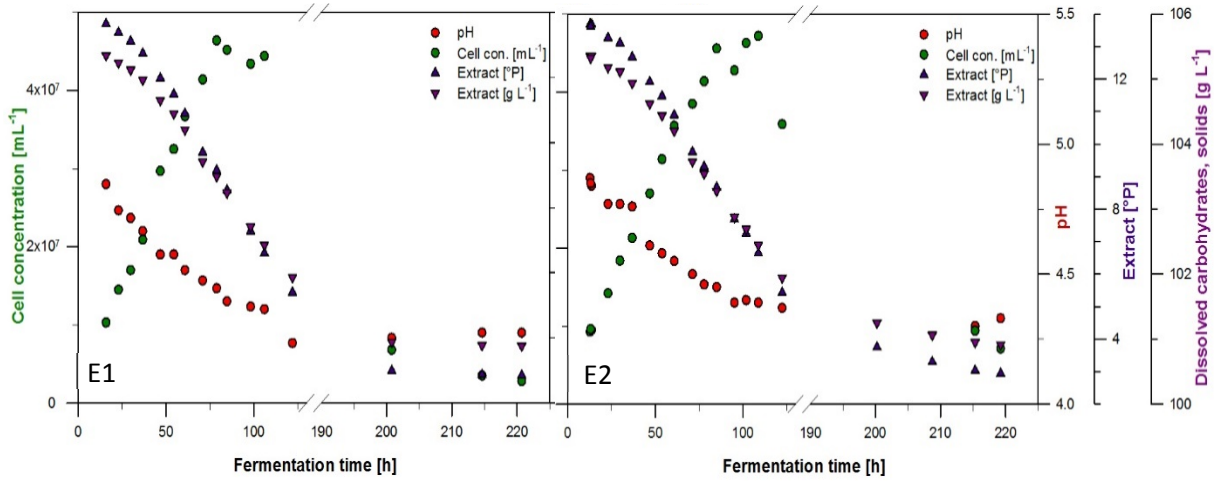

Fig. 37: Fermentation performance control in the 170/199 m^3 scale (*off-line)*: cell concentration, pH-value, extract. Left: experiment 1, right: experiment 2.

For the 170/199 m^3 scale, the pH-value and the redox potential courses during the fermentation time are displayed in Fig. 38, Fig. 40 for the 1st and in Fig. 39, Fig. 41 for the 2nd experiment. The dark red data points at the fermentation onset in both fermentations are data from the 7th position at 17.4 m. This position was tested instead of the 1st position during filling but resulted to be not suitable since the sensor unit was probably located in the foam layer. These data are not further discussed.

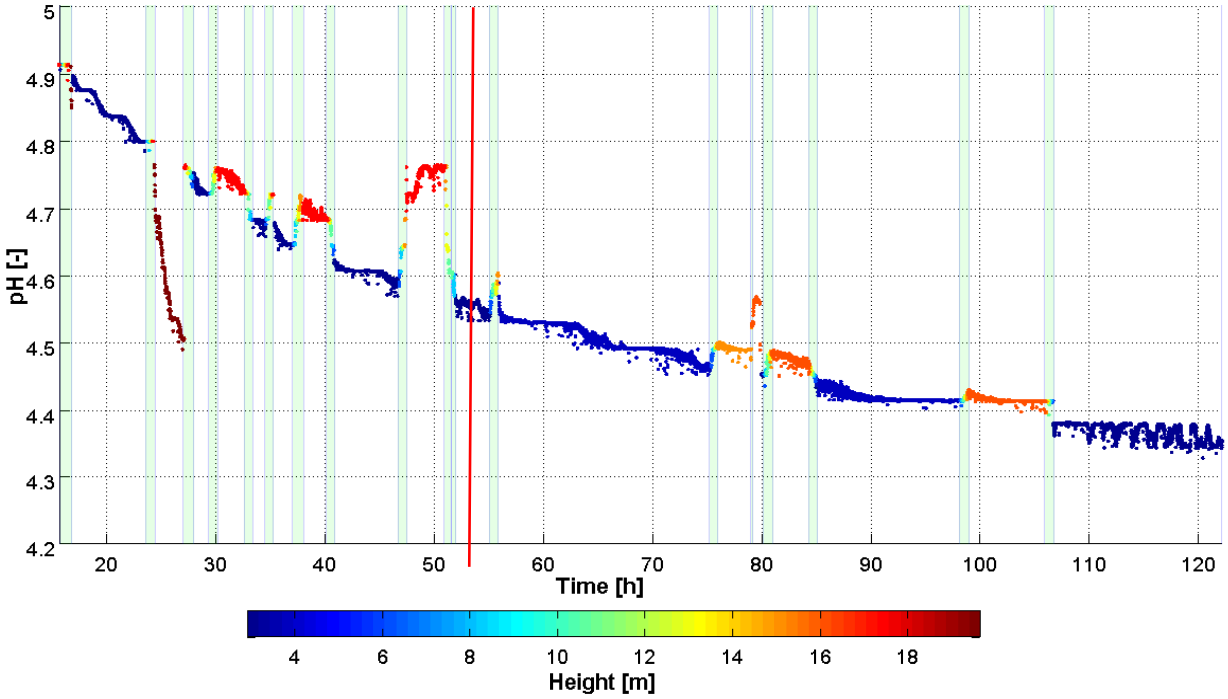

Fig. 38: Monitoring of the pH-value in the 170/199 m^3 scale (experiment 1).
Filling, diacetyl rest, and cooling phase excluded. The red line indicates the time point of the transfer of 13.5 m^3 to another tank due to foam formation.

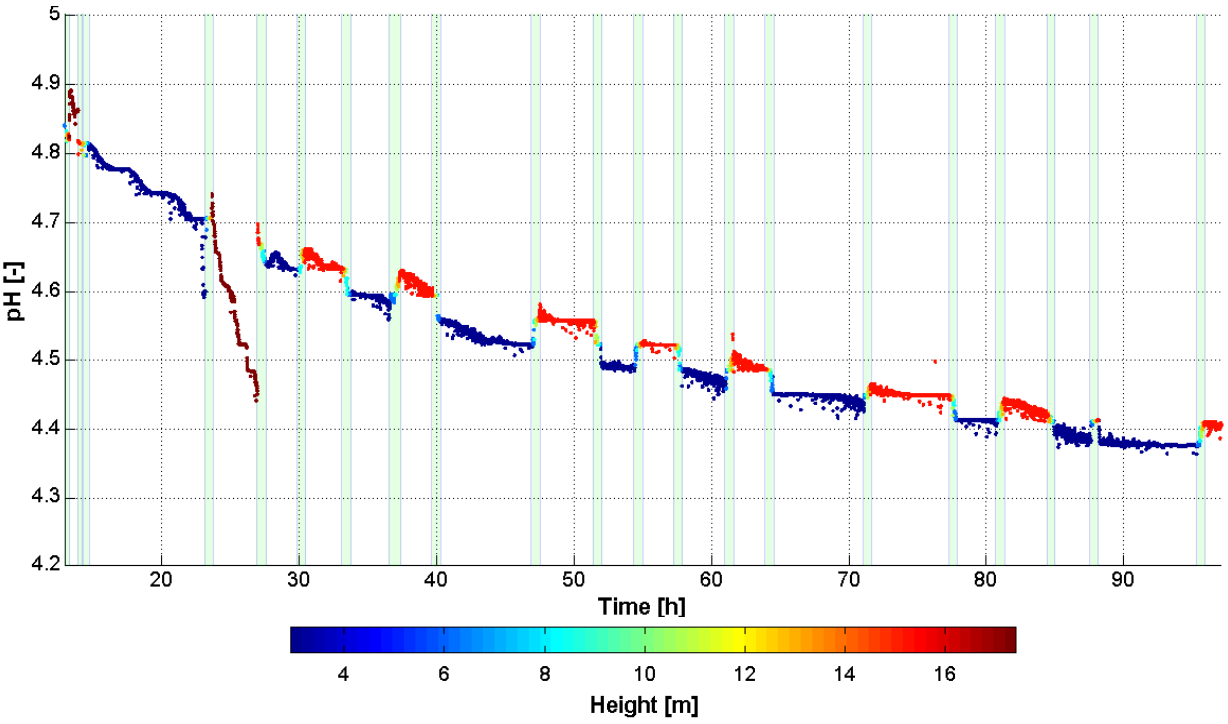

Fig. 39: Monitoring of the pH-value in the 170/199 m^3 scale (experiment 2).
Filling, diacetyl rest, and cooling phase excluded.

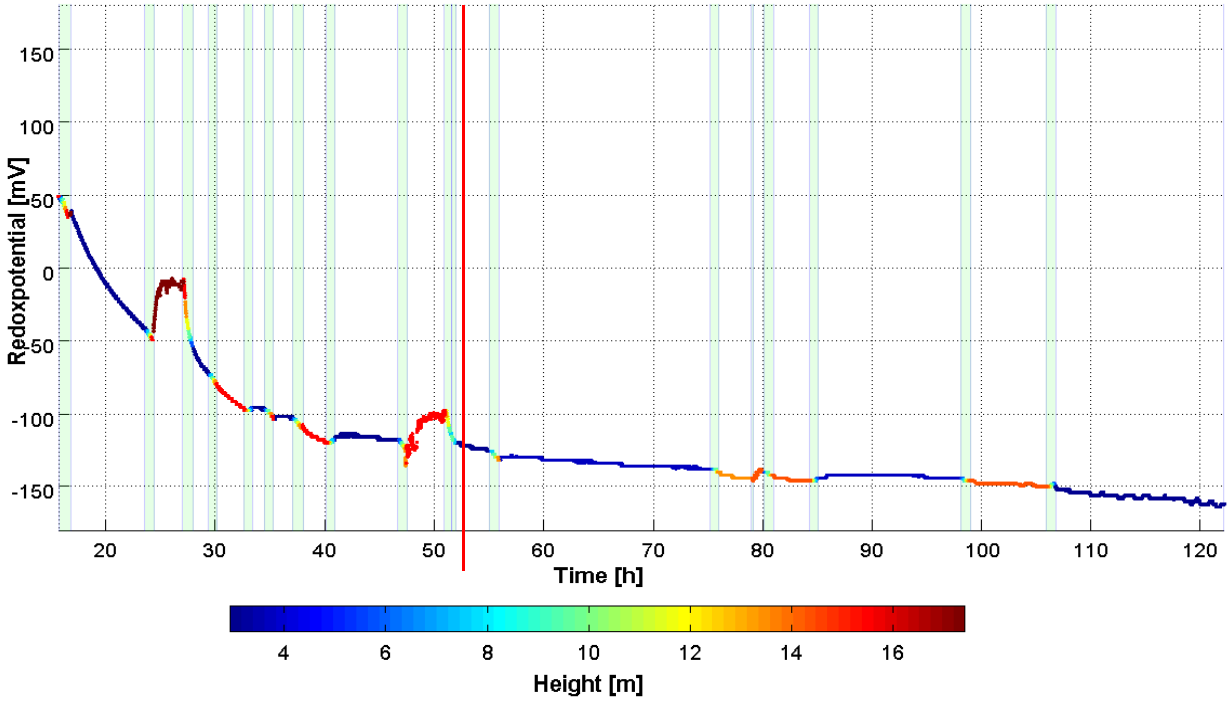

Fig. 40: Monitoring of the redox potential in the 170/199 m^3 scale (experiment 1).
Filling, diacetyl rest, and cooling phase excluded. The red line indicates the time point of the transfer of 13.5 m^3 to another tank due to foam formation.

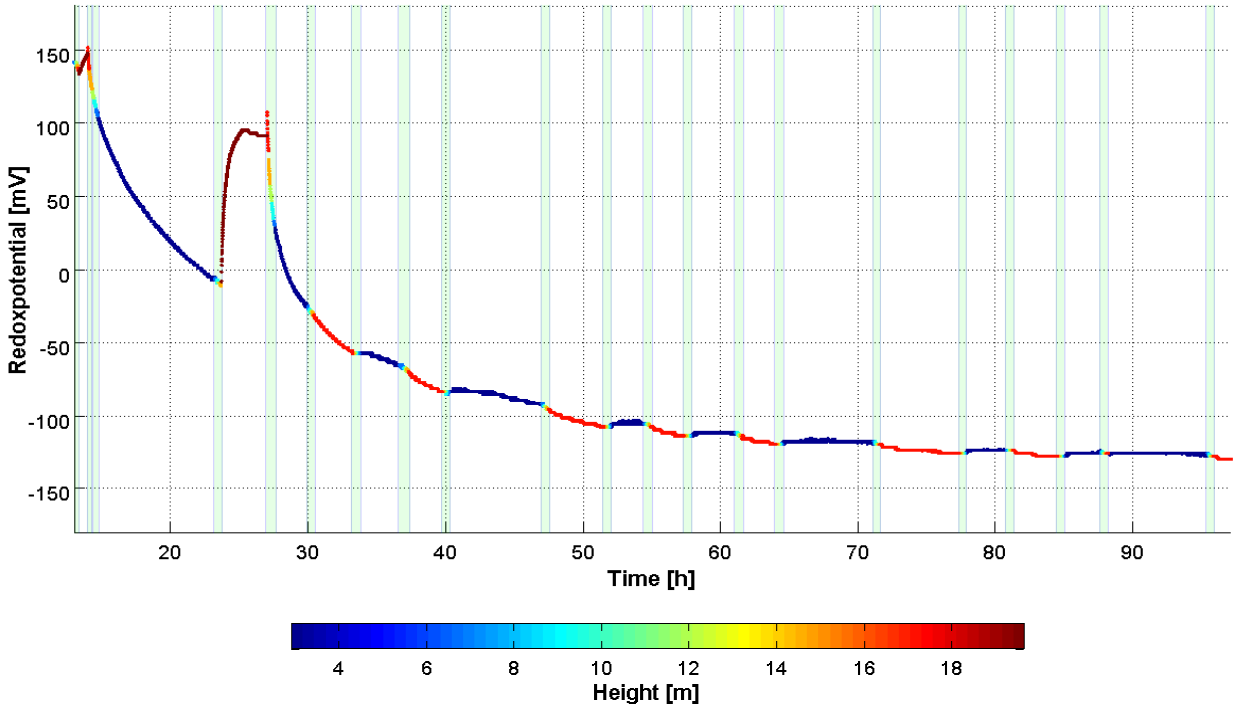

Fig. 41: Monitoring of the redox potential in the 170/199 m^3 scale (experiment 2).
Filling, diacetyl rest, and cooling phase excluded.

For the investigation of all process phases and the appearance of small gradients, the suggested alternative method for data evaluation and presentation was used as explained above (page 82). The results are presented in Fig. 42 and Fig. 43 with gradients clustered according to their size (represented by the color bar).

During the filling process at the fermentation onset, measurements were performed at 17.4 m height instead of the 1st position (see page 88). Since the measurement frames 6 - 7, 14 - 22 and 24 - 25 in Fig. 42 as well as 8 - 25 and 27 - 33 in Fig. 43 show the same low gradient range (pH < 0.05, redox potential < 0.5 mV), they were displayed as one block, respectively.

In contrast to the 3 m^3 scale, larger gradients existed during fermentation in the pH-value and the redox potential, especially at the onset of the fermentation. In the larger scale, these appeared also at later stages of the fermentation and during the cooling phase (205.4 / 205.8 h).

During the filling process, the maximum spatial gradients (along the tank height) were detected with 0.19 pH-units and even 110 mV for the redox potential in the 1st experiment, whereas in the 2nd experiment the difference for the pH-value was higher with 0.47 pH-units and the one for the redox potential lower with 78 mV. Here, the "bubbling" method in the 2nd experiment for 2 x 5 min has to be considered, which might have influenced both parameters due to the CO_2 addition. These results show that additionally to the fermentation course, the filling process can be monitored in *real-time*. By this, the mixing velocity of the different batches can be determined already during the filling process and approaches for optimization can be found.

In the main fermentation of the 1st experiment, gradients of maximum 0.17 for the pH-value and 20 mV for the redox potential were measured in the movement frame between 50.09 and 51.5 h (in Fig. 42). This was the time, in which the foam was spilling over the tank, some of the volume had to be transferred (53.6 h - 53.7 h), and the measurement frequency had to be reduced (see page 59). Other interesting time frames with gradients were determined at 15.8 - 16.8 h, 27 - 28 h, and 46.7 - 47.5 h.
The maximum spatial gradient in the 2nd experiment during the main fermentation phase was 66 mV for the redox potential at 26.9 - 27.7 h (Fig. 43). Further interesting time frames regarding the appearance of gradients in the redox potential were 14.4 - 14.8 h and 122.3 – 123 h. The latter phase was in the middle of the diacetyl rest (97 - 204 h) and might have consequently be influenced by the increase in temperature of 2 °C. Gradients in the pH-value during the main fermentation instead, were determined only between 23.1 and 23.8 h of maximum 0.09 - 0.11 pH-units.

At the end of the fermentation, the tank was cooled down activating different cooling zones in order to stop the fermentation and provoke yeast sedimentation to the tank conus (cooling phase). This led to superpositions due to temperature gradients, and hence, also to an uneven distribution of other parameters. This can be seen in the 1st experiment at 204 h, where the pH-value showed gradients above 0.17 pH-units along the tank height. For the 2nd experiment, this cannot be clearly determined since at the start of the cooling phase no measurement was conducted.

The detected gradients in the 170/199 m^3 scale are of relevance, especially those measured during the 2nd experiment in the main fermentation phase. A sudden gradient of 40 mV or higher for the redox potential in a quite narrow range of 50 to -150 mV will have an impact on the cell's metabolic activity. This might be true also for a difference of 0.11 pH-units.
Most of the time, however, the tank was quite well mixed regarding the investigated parameters. This shows that even large-scale fermentation tanks with a rather high height-to-diameter ratio (20 m x 4.45 m) can be well mixed due to natural convection, which is mainly caused by CO_2 bubble formation.

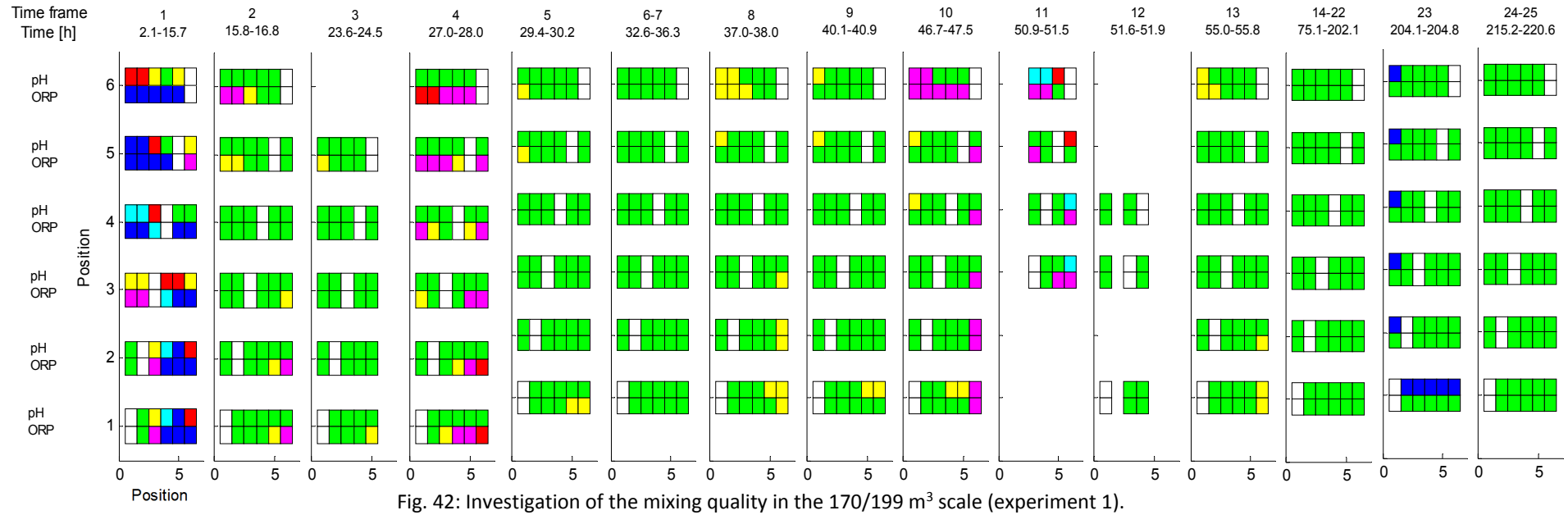

Fig. 42: Investigation of the mixing quality in the 170/199 m^3 scale (experiment 1).
Filling, diacetyl rest, and cooling phase are included. Displayed are the differences (color bar) between the mean values in the pH-value and redox potential (ORP) of all positions within one movement frame (frames: 1 -25). Positions: see Table 7. Transfer of volume between 53.6 h and 53.7 h.

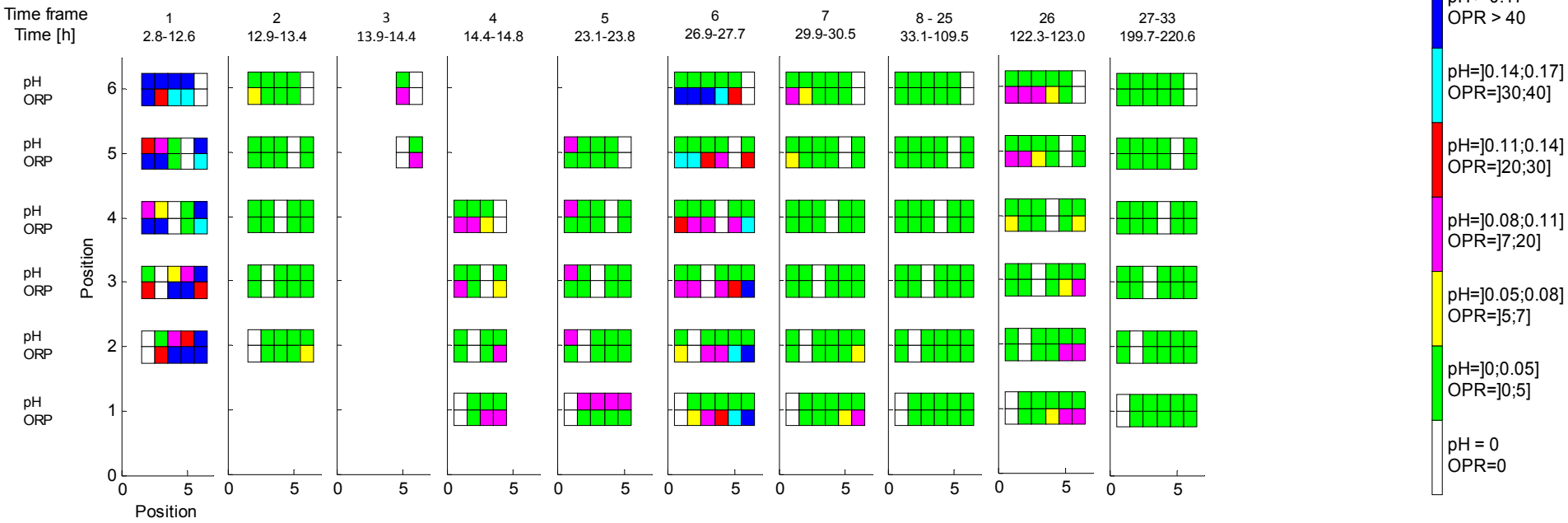

Fig. 43: Investigation of the mixing quality in the 170/199 m^3 scale (experiment 2). Filling, diacetyl rest, and cooling phase are included. Displayed are the differences (color bar) between the mean values of the pH-value and redox potential (ORP) of all positions within one movement frame (frames: 1 - 33). Positions: see Table 7. Between 13.0 and 13.09 h as well as 13.47 and 13.45 h the "bubbling" process was performed. Measurements were conducted between the two "bubbling" phases at position 3 - 6, the time frames 3 and 4 belong together.

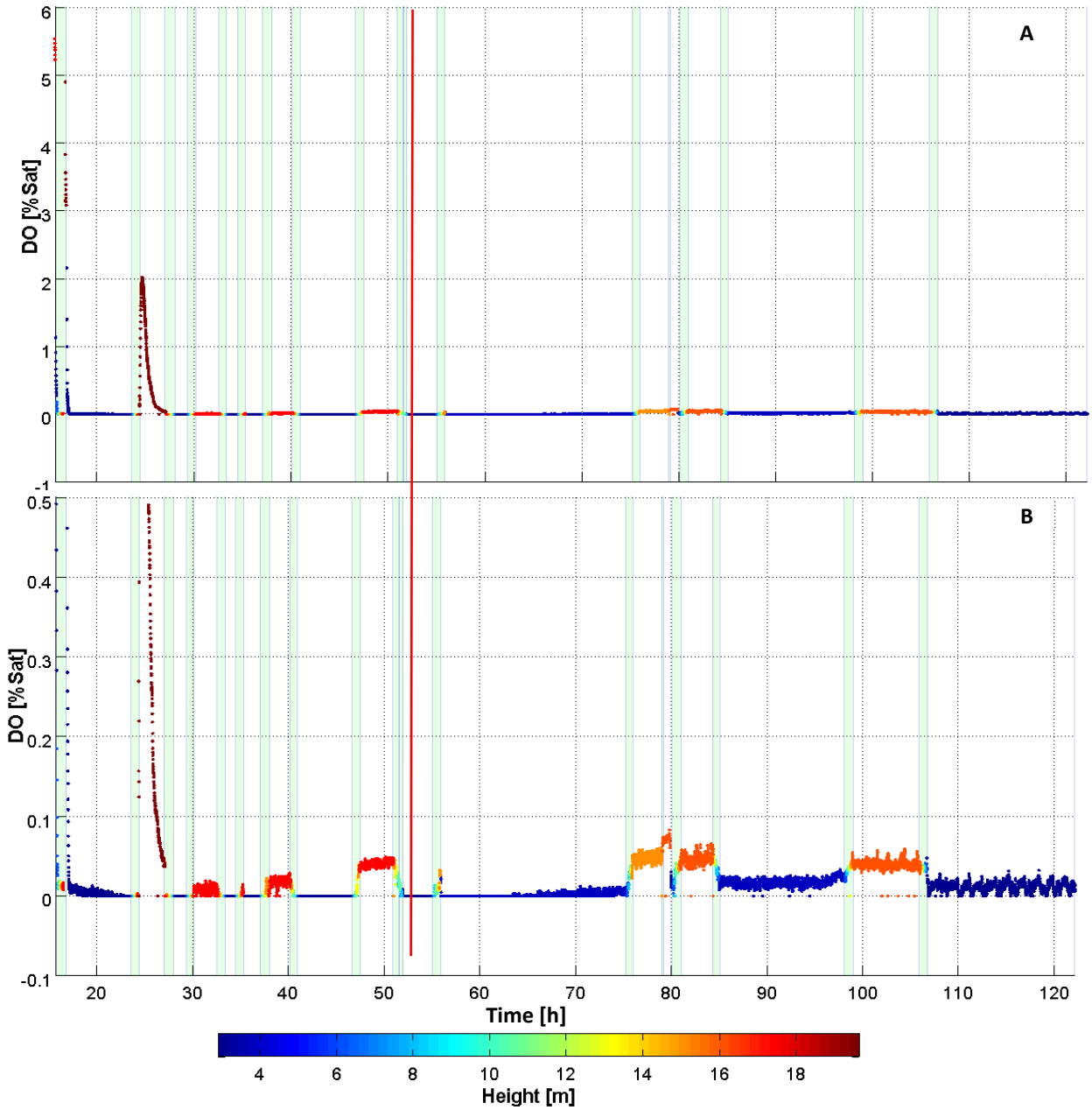

Fig. 44: Monitoring of the DO-value in the 170/199 m^3 scale (experiment 1).
Filling, diacetyl rest, and cooling phase excluded. The red line indicates the time point of the transfer of 13.5 m^3 to another tank due to foam formation. A: Scala including all data points; B: Zoom.

The course of the DO-value during the fermentations is presented in Fig. 44 and Fig. 45. The dark red data points at about 25 h in both fermentations are data from the 7th position at 17.4 m, which was not suitable since the sensor unit was probably located in the foam layer.

After the filling with 6 / 7 batches, the DO-values decreased in both experiments to nearly 0 % saturation (In the higher resolution (Fig. 44 B and Fig. 45 B), however, traces of oxygen were detectable with about 0.05 % in the 1st and 0.2 % in the 2nd experiment. Spatial gradients between the different positions were very small.

Hence, the information presented in literature concerning the anaerobic character of a brewing process (also at the onset of the fermentation) was proven by *real-time* and *in-situ* measurements. This shows the suitability of the applied sensor for the measurement of traces of oxygen. This is of special interest in other process steps in the brewery, e.g. the bottling, where oxygen should be completely avoided.

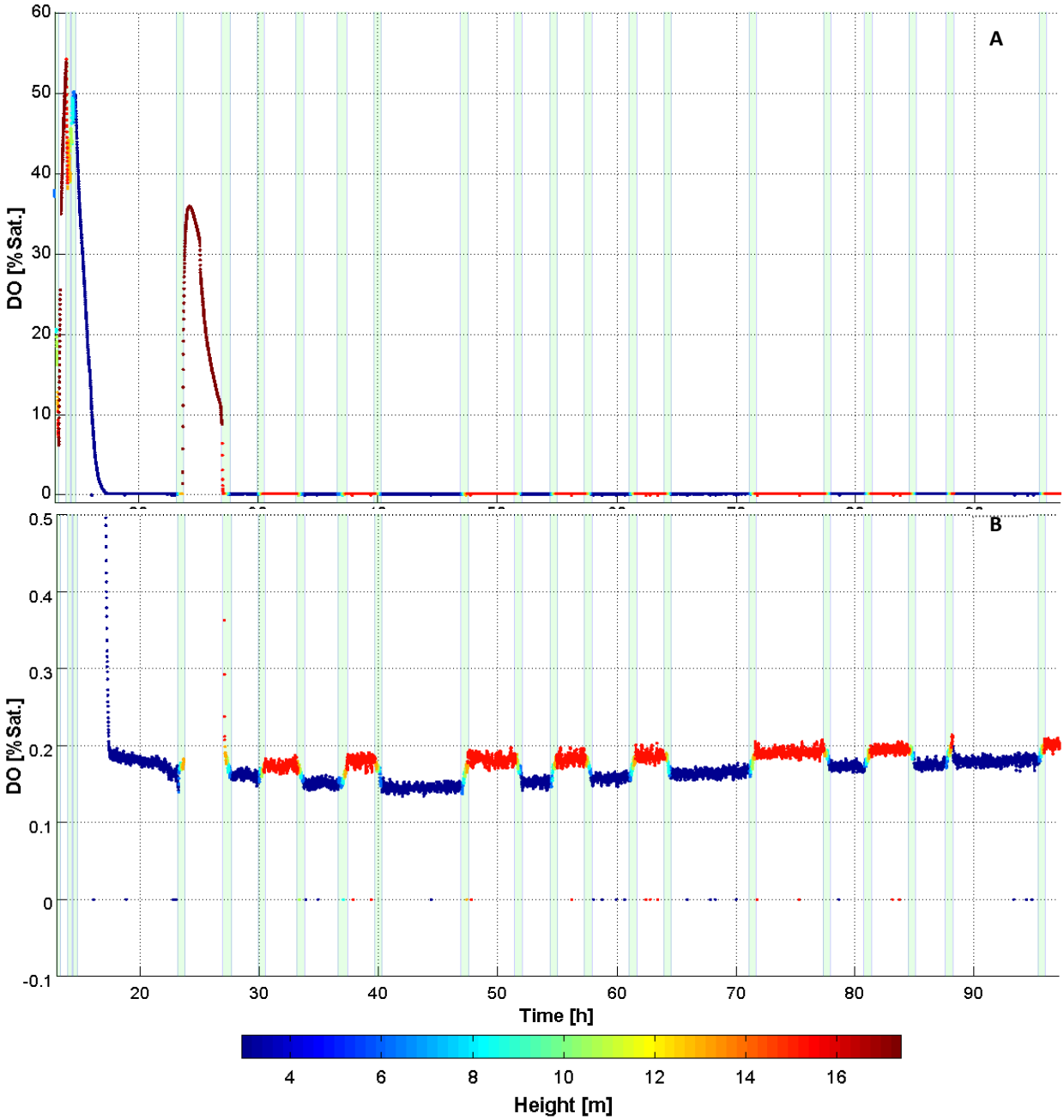

Fig. 45: Monitoring pf the DO-value in the 170/199 m^3 scale (experiment 2).
Filling, diacetyl rest, and cooling phase excluded. A: Scala including all data points; B: Zoom.

The temperature monitoring for the 170/199 m^3 scale is presented in Fig. 46 and Fig. 47, respectively. The dark red data points in both fermentations are data from the 7th position at 17.4 m, which was not suitable since the sensor unit was probably located in the foam layer.

The maximum gradients along the fermenter height were 0.4 °C in the 1st experiment, e.g. at about 27.5 and 51.5 h. These time points are consistent with the appearance of gradients regarding the pH-value and redox potential. In the 2nd experiment instead, the maximum gradient size was measured with 0.3 °C, e.g. at about 47 and 61 h. The 2nd fermentation was started with a higher temperature (about 16 °C) and decreased later to the level of the 1st one. The higher temperature differences during time might have influenced the fluid flow and temperature distribution.

The influence of cooling system, however, is larger than the detected gradients as it was seen also in the other scales. Hence, it cannot be clearly said whether temperature gradients along the reactor height existed.

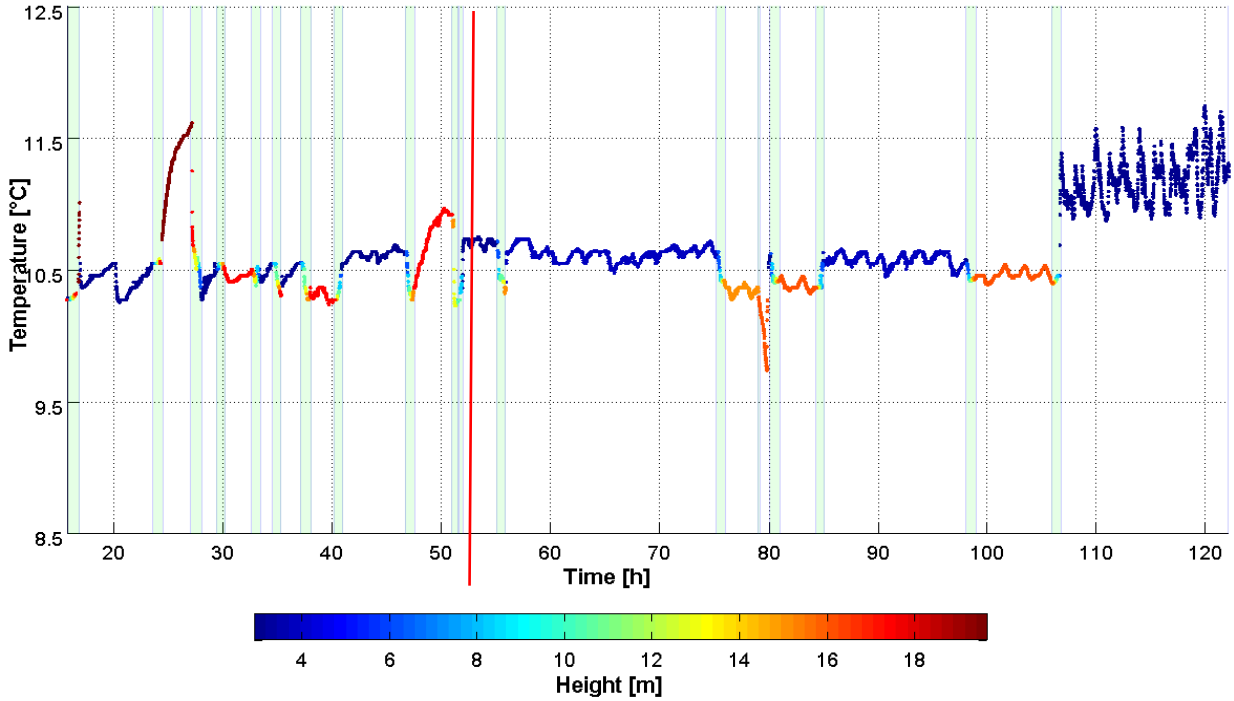

Fig. 46: Monitoring of the temperature in the 170/199 m^3 scale (experiment 1).
Filling, diacetyl rest, and cooling phase excluded. The red line indicates the time point of the transfer of 13.5 m^3 to another tank due to foam formation.

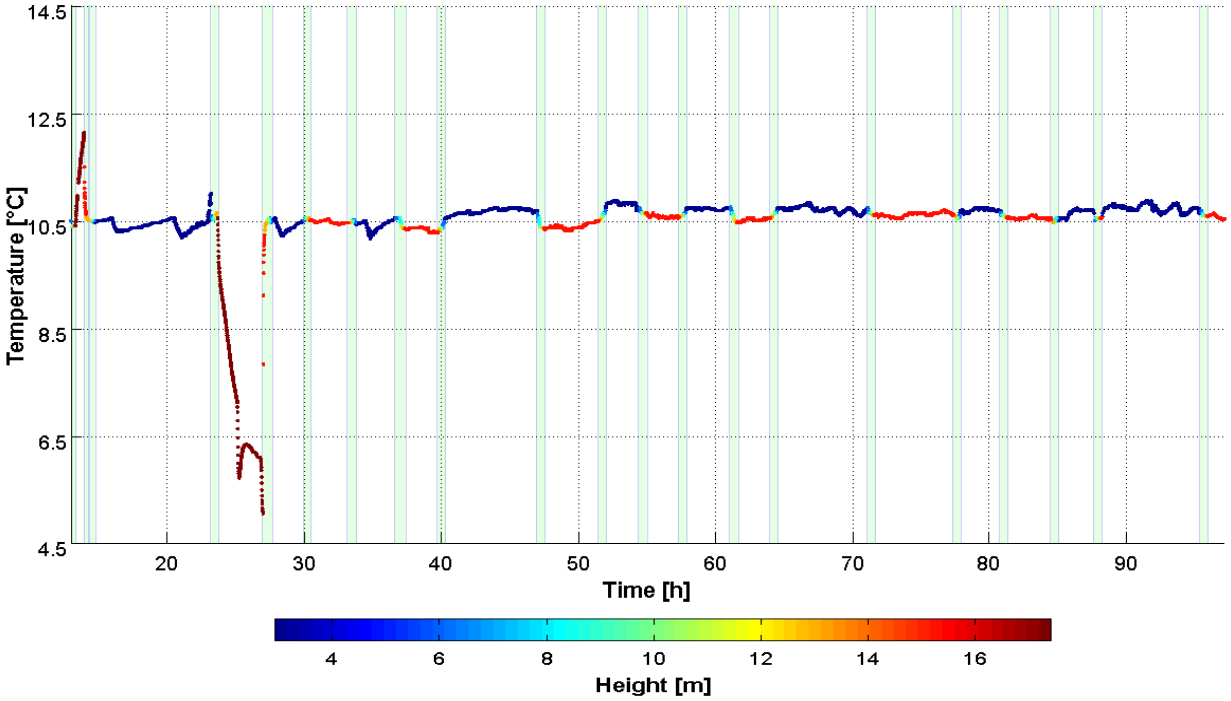

Fig. 47: Monitoring of the temperature in the 170/199 m^3 scale (experiment 2).
Filling, diacetyl rest, and cooling phase excluded.

Mobile Multi-Parameter Measurements in industrial Scale: 24 m³

In the tanks of 24 m³ volume, the height was the same as in the 3 m³. The difference was the tank diameter with 3 m instead of 1.5 m. Hence, the question was whether the different H/D ratio influenced the appearance of gradients.
Apart from the raw material, yeast strain and temperature profile, the process also differed at the onset of the fermentation. After 27 h of fermentation time (including the first 9 h of filling) the complete volume was transferred from tank 1 into tank 3 for the main fermentation. Due to a defect electronic part in the HM interface system, the sensor acquisition could be started only at 70 h of the complete fermentation time. Of the miniaturized system, the pressure sensor (see 5.1.2.1) and the temperature sensor provided reliable data.

The results are displayed for the temperature profile (KSI sensor) in the tank in Fig. 48 as well as for the redox potential and the pH-value (HM sensors) in Fig. 49. The data points are reduced to the time frames, in which the sensors were moved along the height. The mean values for each position with consideration of the sensor response and stabilization time are displayed.
The temperature profile during the complete fermentation time did not show spatial gradients. When looking closer to the time of the onset of the fermentation right after the filling, instead, gradients of up to 0.9 °C between the positions were determined until a fermentation time of about 17 h (Fig. 48 B). After this time the gradients disappear due to sufficient mixing by the natural convection as it was detected also in the 3 m³ scale.
Gradients of up to 20 mV in the redox potential were determined at the end of the fermentation (130 h) along the tank height (Fig. 49 A). These are larger than the maximum gradients in the same fermentation phase in the 170/199 m³ scale (maximum 15 mV) and the 3 m³ scale (5 mV).
The maximum gradients in the pH-value in the 24 m³ scale were determined to be 0.09 pH-units at around 70 h (Fig. 49 B). This gradient was also slightly higher than the one of the 3 m³ and 170/199 m³ scale with maximum 0.05 pH-units.

Since the important phase of the fermentation onset and main phase were missing, more experiments for validation are necessary. It seems, however, that in comparison to the 3 m³ and 170/199 m³ scale with a higher H/D ratio the gradients for the pH-value and redox potential at a certain time point were larger in the 24 m³. This can be explained by the larger diameter of the tank, i.e. a lower H/D ratio, which might negatively influence the convection or fluid flow. The experiments in this scale also provided information about the applicability of the sensors in an industrial process within a cooled environment and the challenges. Based on this, the technique was improved for the application in larger tanks that are installed outdoor.

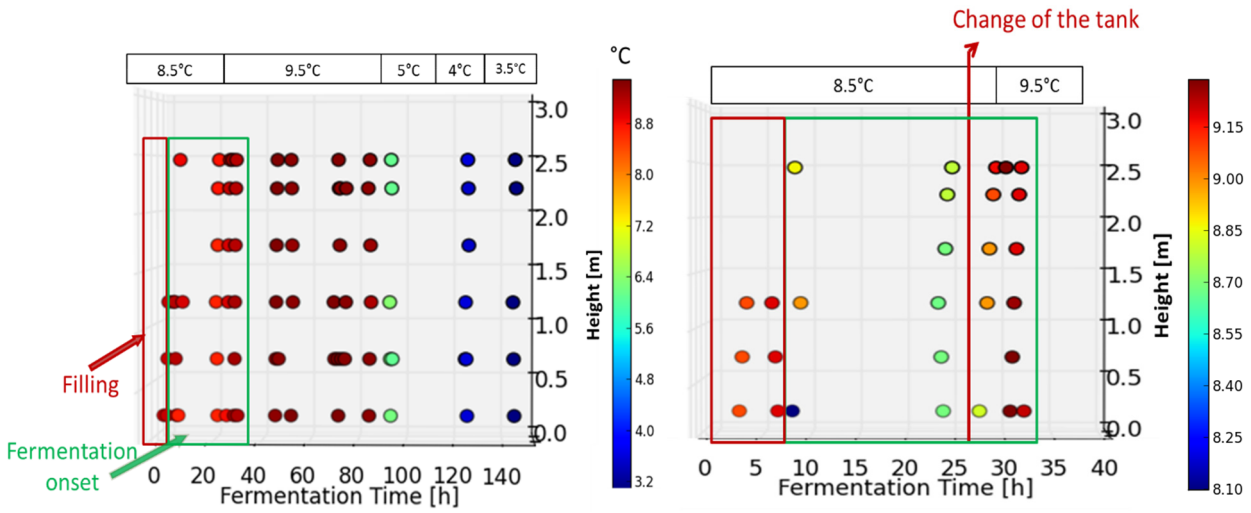

Fig. 48: Temperature profile at different positions in a fermentation of 24 m^3 volume (mean values). Cooling phase excluded. A: complete fermentation time; B: Zoom of the filling process and onset of the fermentation. At the change of the tank, the complete fermentation volume was transferred via pipes from one tank to another.

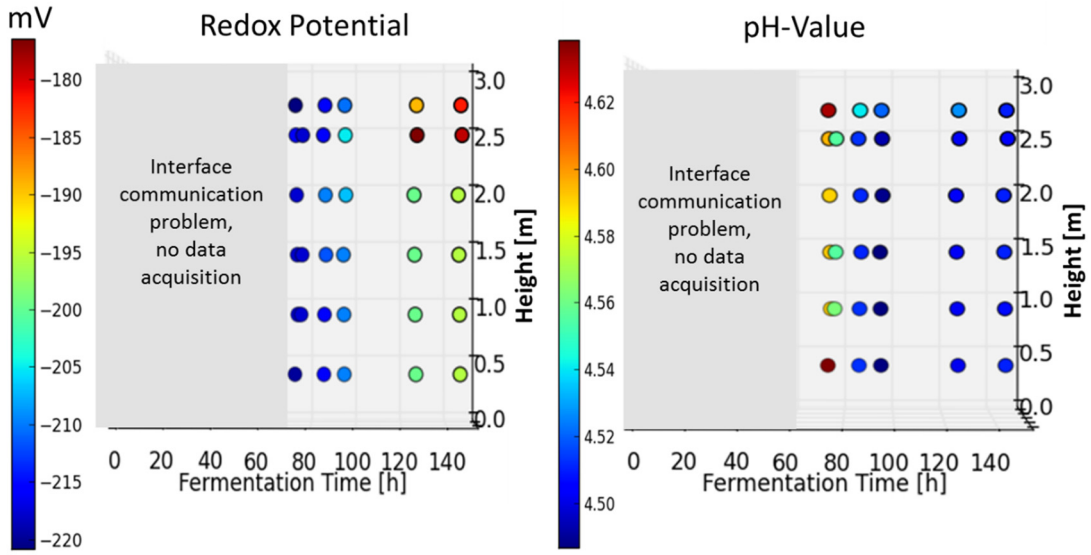

Fig. 49: Redox potential and pH-value at different positions in a fermentation of 24 m^3 volume (mean values). Cooling phase excluded. A: redox potential; B: pH-value.

5.2. *Off-line* Monitoring of Brewing Processes in different Scales

Additionally to the fermentation performance control for every process, *off-line* samples were taken for the determination of the following concentrations:

- extracellular carbohydrates,
- extra- and intracellular main carbon metabolites, and
- total and free sterol content.

These data are important for process understanding as well and were correlated to the *on-line* data for the scale of 3 m^3 and 170/199 m^3, respectively (see 5.3).

5.2.1. Analysis of extracellular Carbohydrates

The concentrations of selected carbohydrates were analyzed by HPLC-RID. The results for extracellular maltotriose, maltose, galactose, fructose, and glucose are presented in Fig. 50 (3 m^3 scale) and Fig. 51 (170/199 m^3 scale, 1st and 2nd experiment). Due to the fast conversion of carbohydrates in the cell and the long sample preparation for the determination of intracellular concentrations, the latter could not be detected for the carbohydrates.

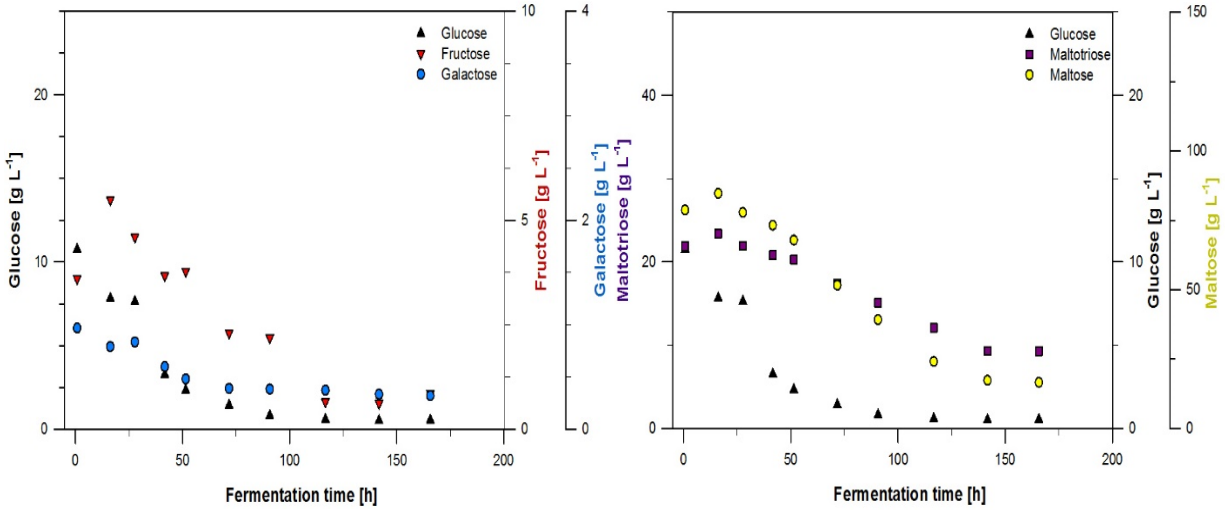

Fig. 50: Extracellular carbohydrate concentrations during a fermentation in the 3 m^3 scale.

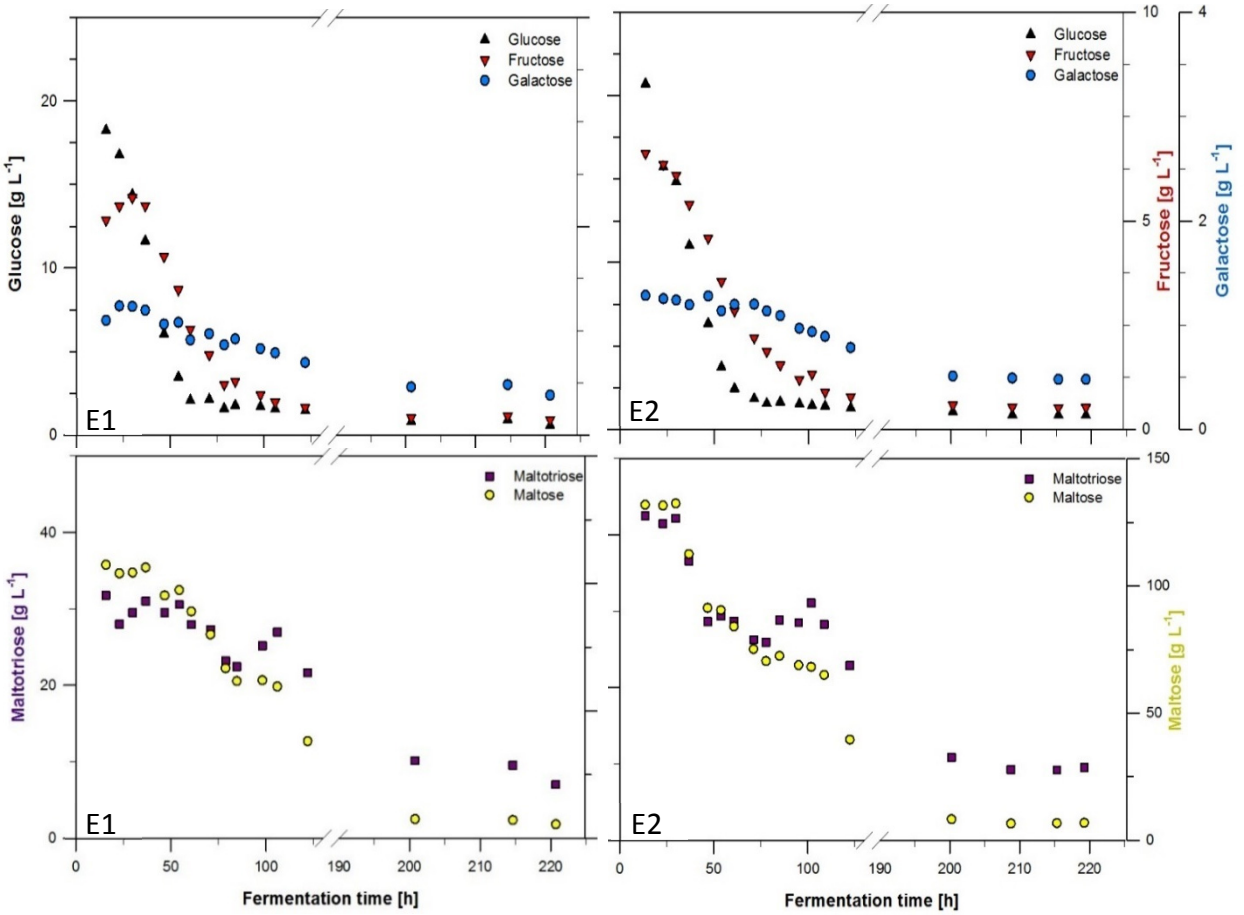

Fig. 51: Extracellular carbohydrate concentrations during a fermentation in the 170/199 m^3 scale. Left: experiment 1 (E1), right: experiment 2 (E2).

The carbohydrate analysis resulted in typical values for a beer fermentation and presents typical degradation courses for all experiments. At first, the monosaccharide glucose is consumed and converted, which can be seen in the steep slope (Fig. 50, Fig. 51). This is followed by fructose, and galactose as well as saccharose (data not shown) and finally by maltose and maltotriose.

According to this order, maltotriose and maltose show the highest values during fermentation. Since maltose is the main carbohydrate in the wort, it showed the highest concentration in all experiments with maximum levels at the onset of the fermentation between 85 g L^{-1} (3 m^3) and 110 - 130 g L^{-1} (170/199 m^3). For maltotriose, concentrations of 24 g L^{-1} (3 m^3) and 32 - 44 g L^{-1} (170/199 m^3) were determined. Galactose, fructose and glucose concentrations were much lower with 5, 1, and 11 g L^{-1} in the 3 m^3 scale and 1.2, 5.5 - 6.5, and 18 - 21 g L^{-1} in the 170/199 m^3 scale, respectively.

It can be seen that the carbohydrate concentrations are higher in the 170/199 m^3 scale, which can be explained by the different starting conditions concerning the higher extract and lower pH-values (see fermentation performance control (Fig. 29, Fig. 37).

5.2.2. Analysis of main Carbon Metabolites

Analogously to the carbohydrates, selected extra- and intracellular main carbon metabolites, namely: ethanol, acetaldehyde, pyruvate, glycerin, acetate, and malate are displayed for the 3 m^3 scale in Fig. 52, for the 170/199 m^3 scale in Fig. 53 (1st experiment) and in Fig. 54 (2nd experiment). All substances were analyzed by HPLC-RID as described in the materials and methods section. The break in the fermentation time in the 170/199 m^3 scale represents a time frame, in which the brewery was not accessible and hence, no samples were taken.

The steps of the alcoholic fermentation after glycolysis are represented well in the upper row of Fig. 52, Fig. 53, and Fig. 54, respectively (A: extracellular, B: intracellular). In all fermentations, the extracellular and intracellular concentrations of the intermediate pyruvate were decreasing with fermentation time (higher slope extracellularly), whereas the extracellular ethanol concentration was increasing. The maximum ethanol concentration in the 3 m^3 scale was 37.3 g L^{-1}, whereas the in the 170/199 m^3 scale only 25 - 26 g L^{-1} were reached. The intracellular ethanol concentrations remained very low or were not even detectable in the 170/199 m^3 scale. This might be due to a fast conversion inside the cell, which cannot be detected, and due to evaporation during sample preparation. The maximum extracellular pyruvate concentration at the onset of the fermentation only varied by 1.5 g L^{-1} between the two scales, the minimum concentration at the end of the fermentation by 0.5 g L^{-1}. At the intracellular level, no significant changes were detected between the 3 m^3 scale and the 1st experiment of the 170/199 m^3 scale. Only the 2nd experiment in the large scale revealed slightly (about 1 g L^{-1}) higher intracellular maximum and lower intracellular minimum concentration values, which might have been caused by the different filling procedure in the 2nd experiment or simply by the sample preparation. Therefore, it can be neglected.
The extra- and intracellular concentration of the intermediate acetaldehyde stayed nearly constant in all fermentations or in both scales with very low levels of 0.2 - 0.25 g L^{-1} and 0.07 - 0.1 g L^{-1}, respectively. In the lower graphs of Fig. 52 - Fig. 54 it can be seen that the concentrations of acetate and malate remained low as well. The extracellular acetate concentration was 0.1 g L^{-1}, the intracellular concentration 0.05 g L^{-1} in average for all three fermentations or both scales. The extracellular malate concentrations were in all fermentations about 0.3 g L^{-1} at the onset of the fermentation. In the smaller

scale, however, the extracellular concentration rises until the end of the fermentation to 0.5 g L^{-1}. The intracellular concentrations were determined to be between 0.17 - 0.3 g L^{-1} for the 3 m^3 scale and the 170/199 m^3 scale (only 1st experiment). Different intracellular values for malate were calculated for the 2nd experiment in the 170/199 m^3 scale, which oscillated between 0.6 and 0.9 g L^{-1} (Fig. 52 B, lower row).
Glycerin was accumulating during the fermentation and increasing especially extracellularly. Maximum extracellular concentrations of 2.5 g L^{-1} for the larger scale and 3.8 g L^{-1} for the smaller scale were determined at the end of the fermentation. The maximum intracellular levels were much lower with 0.5 g L^{-1} (3 m^3) and 1 - 1.4 g L^{-1} (170/199 m^3).

The higher maximum values in the 3 m^3 scale of extracellular ethanol, pyruvate, and glycerin might be caused by the higher fermentation temperature (2 °C) in the 3 m^3 scale, which accelerated the fermentation leading to a faster conversion of carbohydrates and formation of metabolites. Further, the starting conditions concerning extract and pH-value were different as it can be seen by the fermentation performance controls (Fig. 29 and Fig. 37). The small difference in the extract at the fermentation start, however, cannot explain the large difference in the maximum ethanol concentration at the end of the fermentations of both scales. According to the balling formula and the measured extract, the fermentations in both scales should reach an ethanol content of about 50 - 51 g L^{-1}. Since an enzymatic determination of ethanol with a Cedex Bio Analyzer (Roche Diagnostics International Ltd, Germany) also gave similar results, it is likely that ethanol was evaporating during sample preparation and/or analysis. Besides this, the scale and geometry itself, the mixing quality and hydrostatic pressure have an influence on the metabolic activity of the yeast as well.

Since in the 170/199 m^3 scale *off-line* analyses of two experiments with similar conditions could be analyzed, the reproducibility of the analysis methods as well as the *on-line* measurements could be tested. The data development, i.e. the degradation, synthesis and accumulation of carbohydrates (Fig. 51) and main carbon metabolites (Fig. 53, Fig. 54) as well as the synthesis and conversion of sterols (Fig. 56) was very similar in both experiments. Hence, the reproducibility was proven, which is important for the subsequent data correlation.

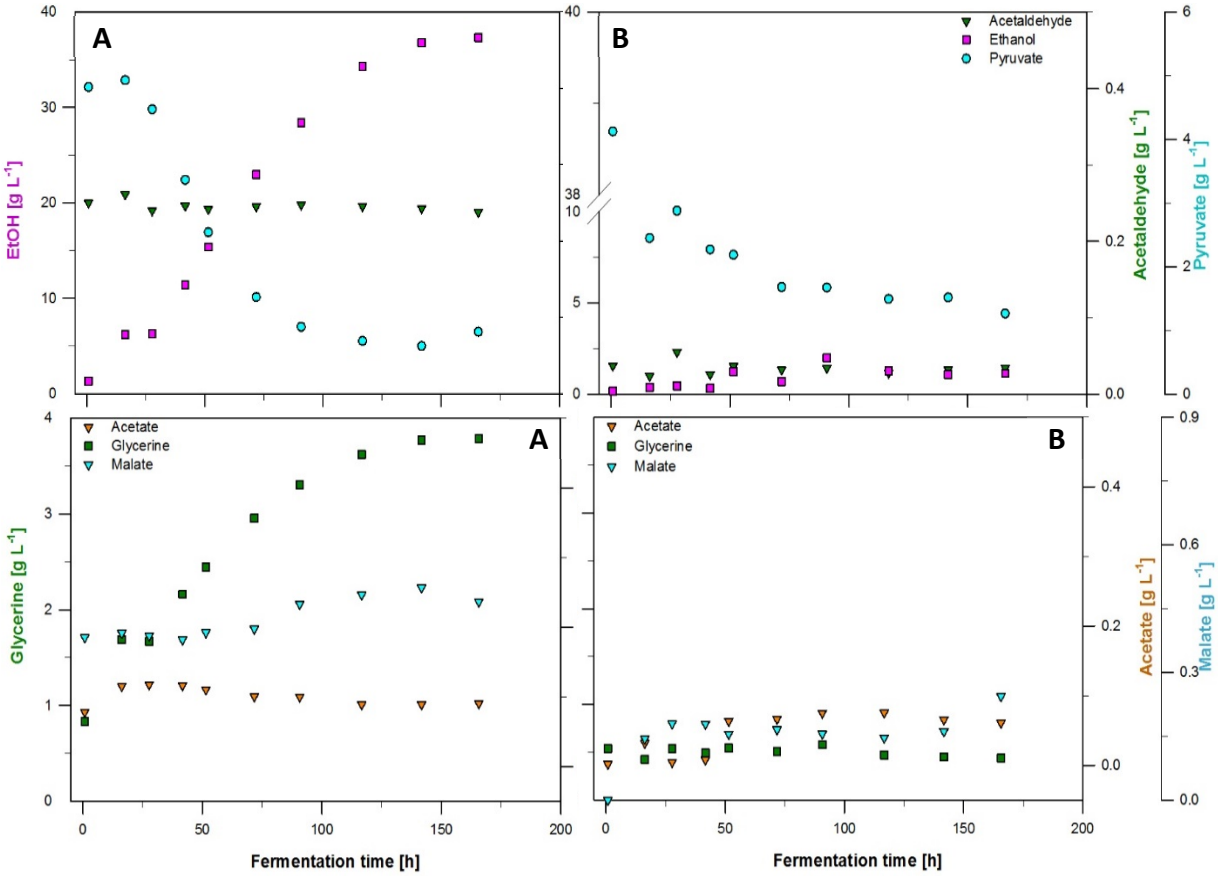

Fig. 52: Main carbon metabolite concentrations during a fermentation in the 3 m^3 scale, experiment 1. A: extracellular, B: intracellular.

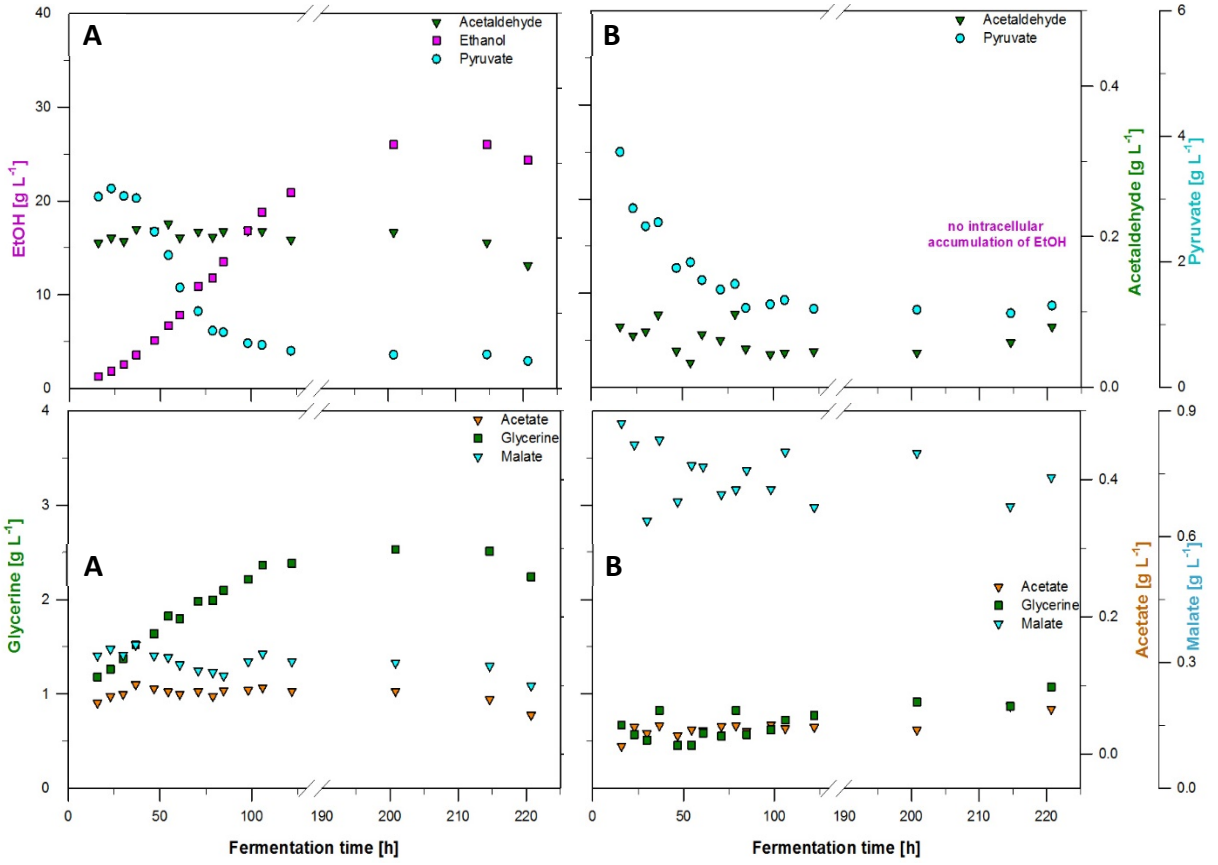

Fig. 53: Main carbon metabolite concentrations during a fermentation in the 170/199 m^3 scale, experiment 1. A: extracellular, B: intracellular.

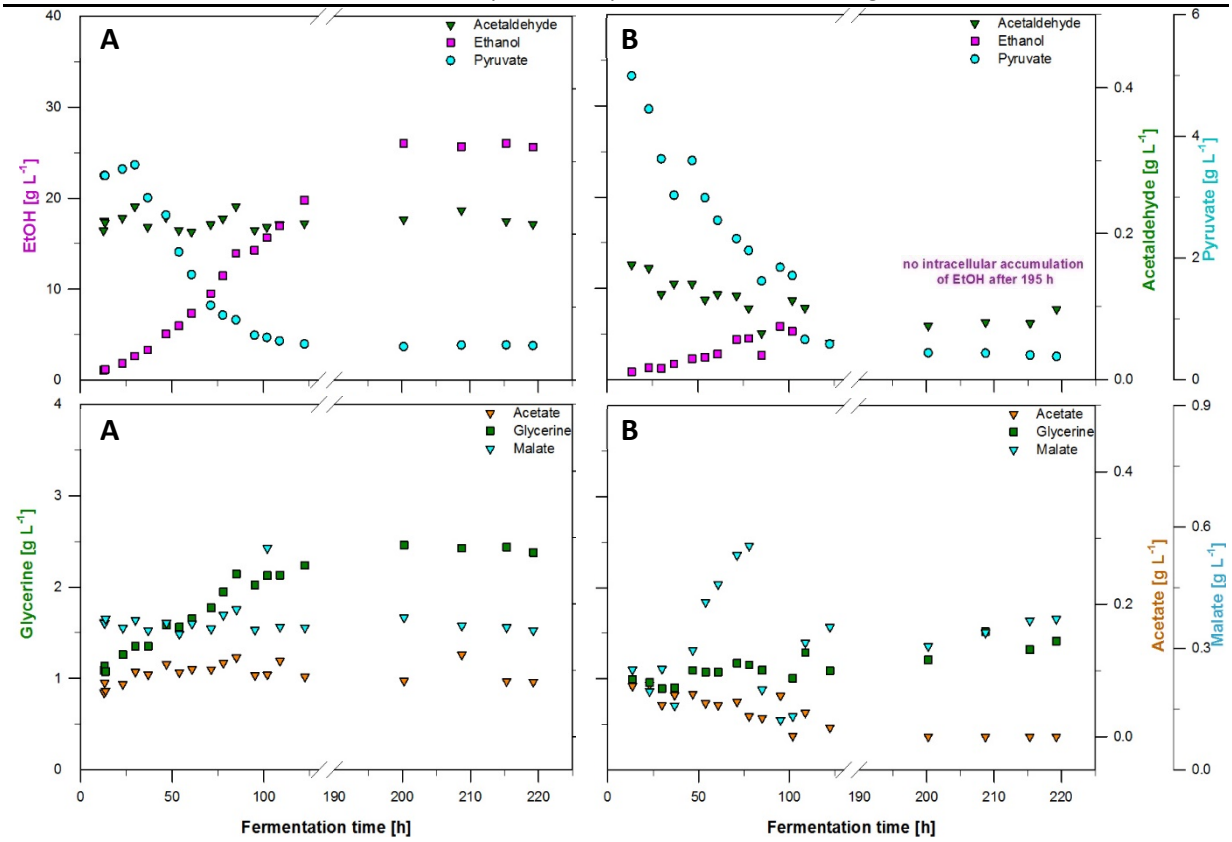

Fig. 54: Main carbon metabolite concentrations during a fermentation in the 170/199 m^3 scale, experiment 2. A: extracellular, B: intracellular.

5.2.3. Analysis of the Sterol Content

Sterols are of high importance for the membrane integrity, fluidity, and transport through it (see 2.1.2.3). The content of esterified sterols can be calculated based on the difference of the total and the free sterol content.

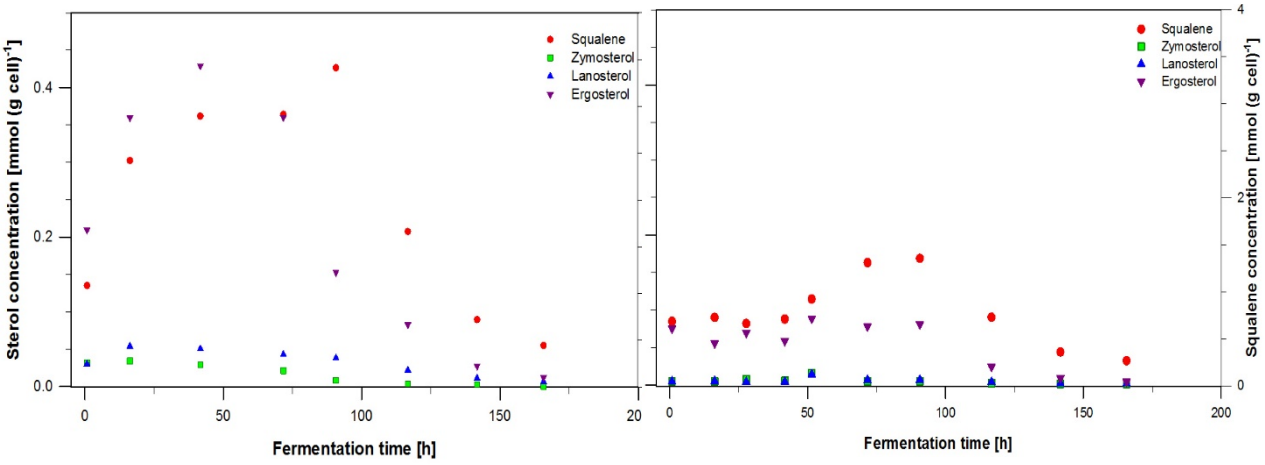

Fig. 55: Squalene and sterol content (total, free) in the 3 m^3 scale.
Left: total sterol content, right: free sterol content (total – free = esterified sterol content).

In the larger scale of 170/199 m^3 (Fig. 56), all sterol concentrations are about 10-fold lower than in the 3 m^3 scale (Fig. 55). This might be explained with the different fermentation conditions across the different scales, the different number of batches during filling, and concomitant aeration procedures

at the onset of fermentations (Fig. 29, Fig. 37). The high extract content at the onset of the fermentation in the 170/199 m^3 scale might have provoked a higher oxygen demand by the yeast cells, which was then not available for sterol synthesis.

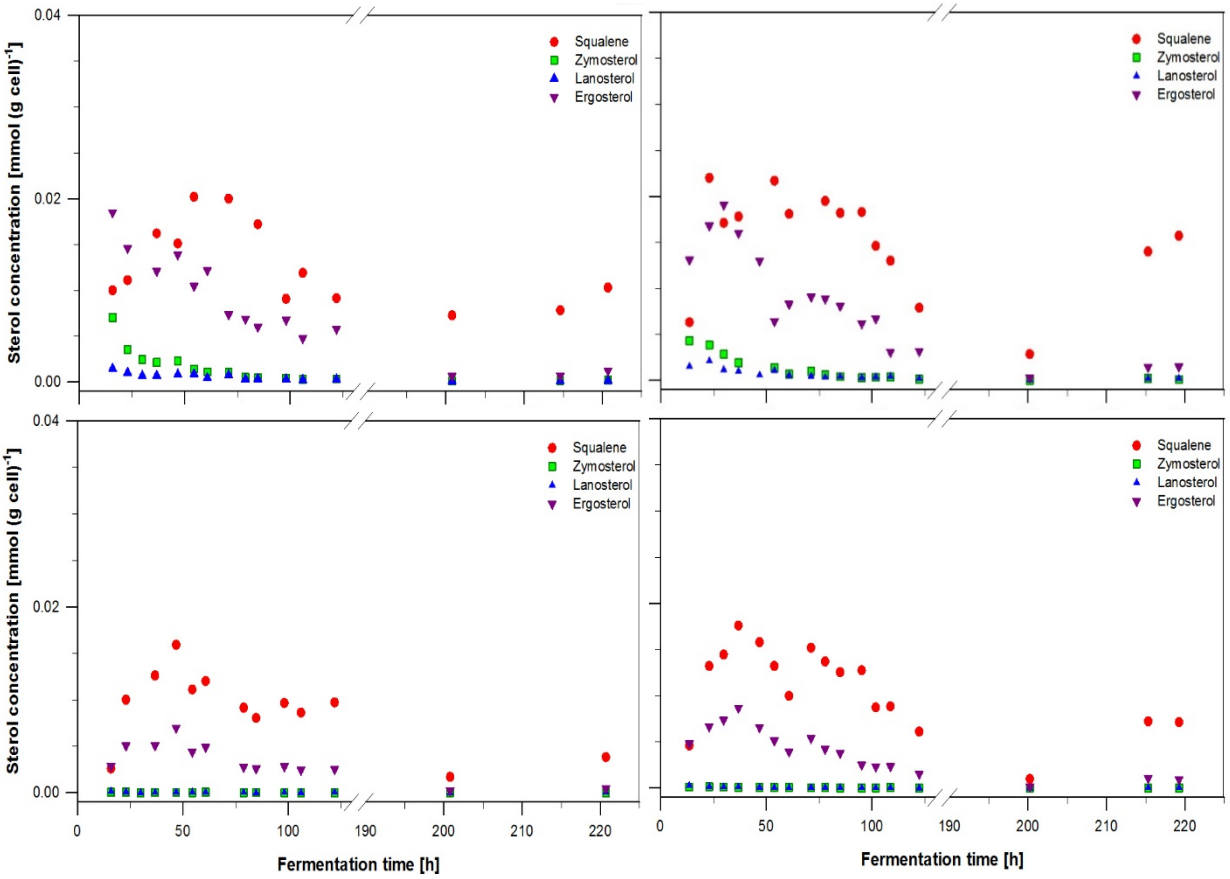

Fig. 56: Squalene and sterol content (total, free) from two experiments in the 170/199 m^3 scale. Upper row: total sterol content, lower row: free sterol content (total – free = esterified sterol content). Left: experiment 1, right: experiment 2.

In the larger scale of 170/199 m^3 (Fig. 56), all sterol concentrations are about 10-fold lower than in the 3 m^3 scale (Fig. 55). This might be explained with the different fermentation conditions across the different scales, the different number of batches during filling, and concomitant aeration procedures at the onset of fermentations (Fig. 29, Fig. 37). The high extract content at the onset of the fermentation in the 170/199 m^3 scale might have provoked a higher oxygen demand by the yeast cells, which was then not available for sterol synthesis.

Total and free squalene, i.e. the precursor, which cannot be esterified, is accumulating in all experiments in both scales in the 1st part of the process, although in different amounts and until different time points: ca. 90 h in the 3 m^3 and 50 - 60 h in the 170/199 m^3 scale. It is degraded in the following (Fig. 55, Fig. 56). Accumulation is observable in 170/199 m^3 scale at the end, probably due to oxygen depletion (Fig. 56). This might have happened as well in the smaller scale, but samples were not available at the end of the fermentation.

Ergosterol is the final product in the sterol biosynthesis in yeast. Free ergosterol can be used for the integration into the cell membrane and its stabilization. The total ergosterol content at the 3 m^3 scale decreases after about 50 h but reaches levels below 0.1 mmol (g cell)$^{-1}$ only after 125 h. The content of free ergosterol instead remains at a level of about 0.1 mmol (g cell)$^{-1}$ until 100 h. Hence, ergosterol

synthesis for membrane stabilization proceeds for a long time although at low level after 100 - 125 h. In the 170/199 m^3 scale, the total ergosterol content is decreasing continuously (in case of E1) and after 30 h (in case of E2) to a level of about 0.01 mmol (g cell)$^{-1}$ in the 170/199 m^3 scale. The content of free ergosterol remains stable at around 0.01 mmol (g cell)$^{-1}$. The decrease of the sterol content is a typical indicator for oxygen limitation time, which was detectable with the *on-line* measurements.

The intermediates lano- and zymosterol (total and free content) remain at a very low level in all three fermentations, indicating a fast conversion towards other sterols.

5.3. Correlation of *on-line* and *off-line* Data measured in the 3 m^3 and 170/199 m^3 Scale

A correlation analysis was conducted with the *on-line* and *off-line* data in two industrial scales (3 m^3 and 170/199 m^3) in order to quantify data dependencies on a statistical basis.

The *on-line* data included the sensor measurements of the pH-value, redox potential, DO-value, and temperature; the *off-line* data included the concentrations of carbohydrates, main carbon metabolites, and sterols. The exact data set composition for the different experiments is explained in the materials & methods section (4.4). Two methods were applied:

1) PCA and
2) PLS regression of *off-line data* predicted by *on-line* data.

Before the analyses with methods 1) and 2), the variables were standardized or z-transformed, obtaining variables with an expected value $\mu = 0$ and a variance $\sigma^2 = 1$ (see section 4.4). This was performed in case the parameter distribution between the experiments differed. For method 3), selected data (carbohydrates) of one scale were chosen and not z-transformed. This allows a continuous prediction during fermentation time of the selected substances for this process.

For all methods, the *on-line* and *off-line* data of the complete process, i.e. including filling diacetyl rest, and cooling phase, were used for calculation. In the 3 m^3 scale during the 2nd experiment, only *on-line* measurements were performed in order to increase the frequency of the movements of the sensor probes and investigate the sensor performance, without focusing on the *off-line* sampling and sample preparation in the 2nd experiment in the 3 m^3 scale. Hence, loading plots and PLS regression were generated only for the data set (*on-line* and *off-line* values) of the 1st experiment and no model validation was performed.

5.3.1. Principal Component Analysis (PCA)

The 1st step of the multivariate data analysis was a PCA for the reduction of data dimensions and the identification of variables containing similar information. Since for this work the visualization of the contribution of predictor (*A*) and response (*B*) variables to the PCs is of importance, a loading plot presentation was chosen (see section 4.4). It shows the data distribution and provides information about data patterns and similarities. Variables with high absolute values are identifiable and sensitive, the ones with low values, i.e. close to the point of origin, are of less importance for the respective PC.

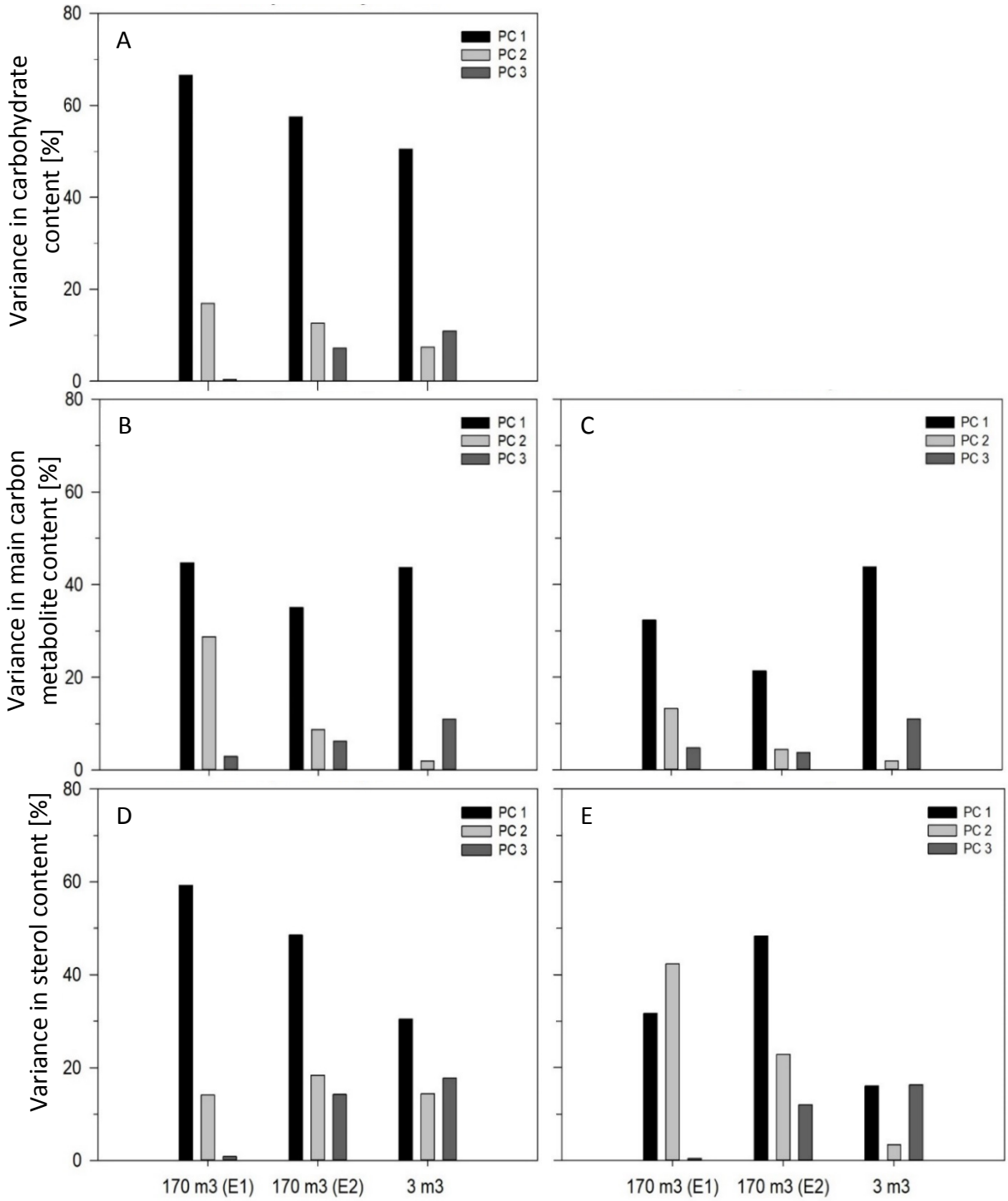

Fig. 57: Variance [%] in the following *off-line* data explained by PC 1, PC 2 or PC 3 for the different fermentations (see x-Axis): E = experiment. A: Extracellular carbohydrate concentration; B: Extracellular main carbon metabolite concentration; C: Intracellular main carbon metabolite concentration; D: Total sterol content; E: Free sterol content.

The loadings as displayed in the figures Fig. 58 - Fig. 61 include:

1. Loading plots of *on-line* data and data from *off-line* carbohydrate concentration analysis (extracellular),
2. Loading plots of *on-line* data and data from *off-line* main carbon metabolites analysis (extra- and intracellular), and
3. Loading plots of *on-line* data and data from *off-line* sterol content analysis (total and free sterol content).

In these loading plots, *A* defines the *on-line* sensor data (i.e. the pH-value, DO-value, redox potential, and temperature) and *B* the *off-line* data (concentrations of carbohydrates and main carbon metabolites as well as the sterol content).

The PCA determined two PCs that explain the variance in the *off-line* data sufficiently. The percentages for PC 3 instead were lower than for PC 1 and PC 2 in most cases, especially in the 170/199 m^3 scale as shown in Fig. 57. The loading plots for (*off-line*) data, which were not even described by PC 2 with a contribution higher than 10 % of the value, are shown in the appendix B (iii, page 178) and not further considered.

5.3.1.1. Loading Plots for Carbohydrates

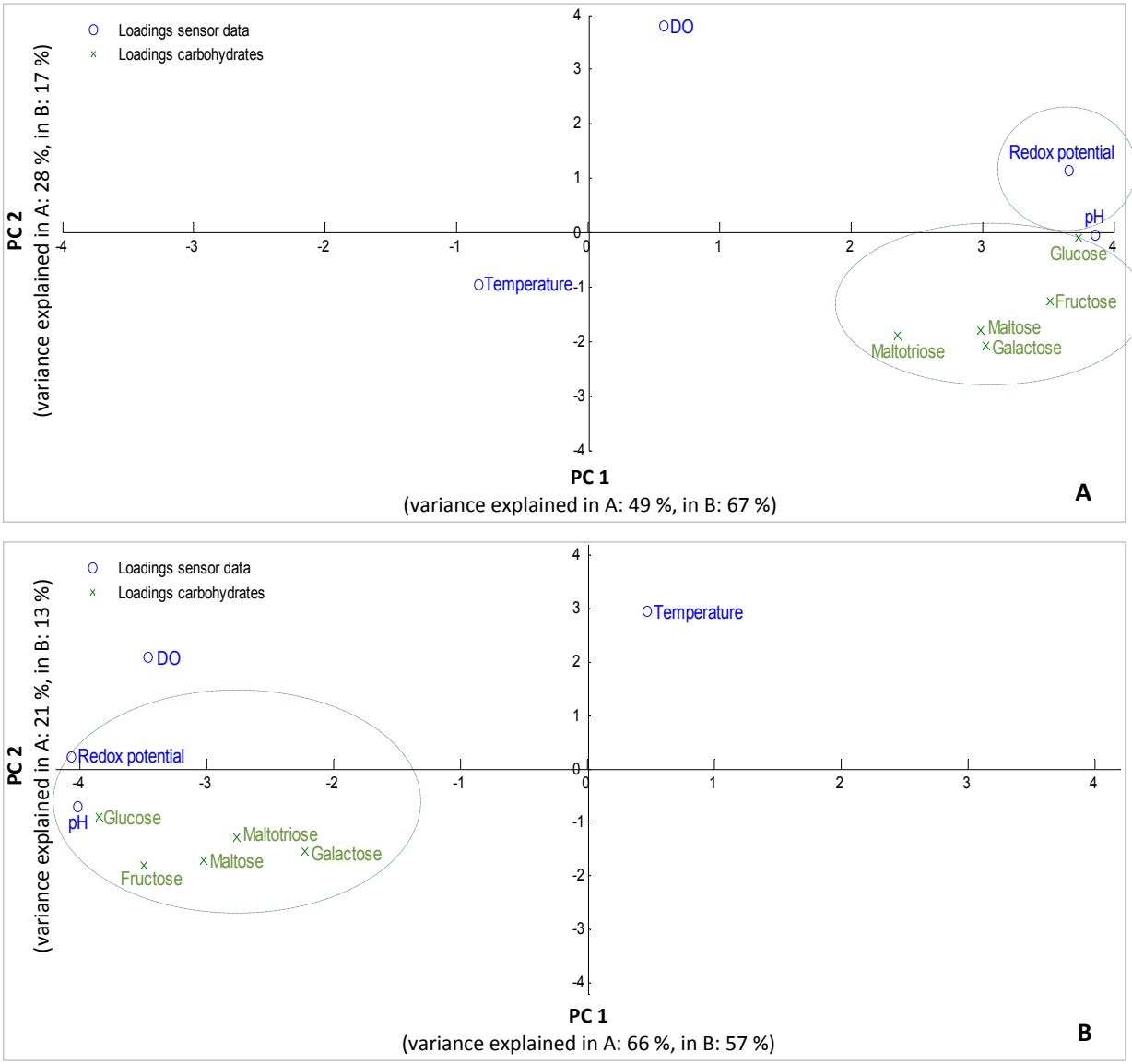

Fig. 58: Loadings of the *on-line* sensor data vs. the concentration of extracellular carbohydrates in the 170/199 m^3 scale. A: experiment 1; B: experiment 2. Presented are the loadings of the sensor data (blue circles) and the concentrations of extracellular metabolites (green crosses).

The following extracellular carbohydrates were investigated by PCA for both scales: glucose, fructose, galactose, maltose, and maltotriose. For the corresponding loadings in the 3 m^3 scale, the 2nd PC

contributes to less than 10 % to the variance in the *off-line* data and is therefore insignificant (Fig. 57 A, appendix B iii). The variance explained by PC 2 in the 170/199 m^3 scale is rather low but sufficient to analyze corresponding loadings (Fig. 58 A, B).

The loadings of the sensor data and the carbohydrate concentrations in the 1st and 2nd experiments in the 170/199 m^3 scale show values with opposed prefixes regarding PC 1. The calculation, however, was performed equally for both fermentations and the course of the parameters (*on-line* and *off-line*) during fermentation was very similar. Hence, the absolute values and the formation of clusters are similar in both fermentations, except of the DO value. One explanation for these results could be the different onset of the fermentations as stated in 4.2.3.

It can be seen that the cluster of the redox potential and pH-value are in close relation to the cluster of all analyzed carbohydrates. All parameter loadings show high values in the PCA regarding PC 1 in the 170/199 m^3 scale, especially concerning fructose and glucose. This indicates that the two *on-line* parameters (absolute values of pH and redox potential) and the *off-line* data (carbohydrate concentration) are well described and significant. The temperature instead, is of less importance for this component.

5.3.1.2. Loading Plots of main Carbon Metabolites

The correlation analyses of the following extracellular main carbon metabolites with the *on-line* sensor data are presented for pyruvate, acetaldehyde, acetate, glycerin, and ethanol in Fig. 59. The variance in the *off-line* main carbon metabolite concentrations in the 3 m^3 scale described by PC 2 met the stipulated limit of 10 % for the extracellular concentrations, which is however still low (Fig. 57 B, Fig. 59 A). For the extracellular main carbon metabolites in the 170/199 m^3 scale (1st experiment) instead, nearly 30 % contribution to the variance by PC 2 was determined (Fig. 57 B, Fig. 59 B). For the intracellular concentrations, only 13 % were calculated (Fig. 57 C, Fig. 59 C). The contribution to variances by PC 2 for the extracellular and intracellular main carbon metabolites in the 170/199 m^3 scale (2nd experiment) as well as for the intracellular concentrations in the 3 m^3 scale (1st experiment) were below 10 % (Fig. 57 B - C, Fig. B 7) and therefore not significant for prediction.

The analysis of the loading values and their relations reveals that the loadings for pyruvate and those for the pH-value and redox potential are of a high (absolute) value regarding PC 1 in both scales (Fig. 59 A, Fig. 59 B, C). Their close location in the plot indicates the relation between the parameters. The formation of pyruvate in the glycolysis undergoes several oxidation and reduction steps and is therefore related to the redox potential. This is in turn related to the pH-value (Nernst equation).
The loadings of the extracellular ethanol and glycerin content in the 3 m^3 scale and 170/199 m^3 scale (only 1st experiments) show high values (especially for PC 1), indicating their significance (Fig. 59 A, B). The values of these two parameters, however, show opposed prefixes to the loading values of the DO measurements in the 170/199 m^3 scale for PC 1. This might be explained by the biochemical reactions during alcoholic fermentation, which do not require oxygen for the formation of ethanol.
The temperature and acetaldehyde can be clustered (Fig. 59 A, B), showing higher significance for PC 2 for the extracellular part in the 3 m^3 scale and 170/199 m^3 scale (only 1st experiment). The close relation between the two parameters might originate from the temperature dependence of the alcohol dehydrogenase, which catalyzes the conversion of acetaldehyde to ethanol (Dickenson and Dickinson, 1975). Also the reaction from pyruvate to acetaldehyde might be temperature-dependent.

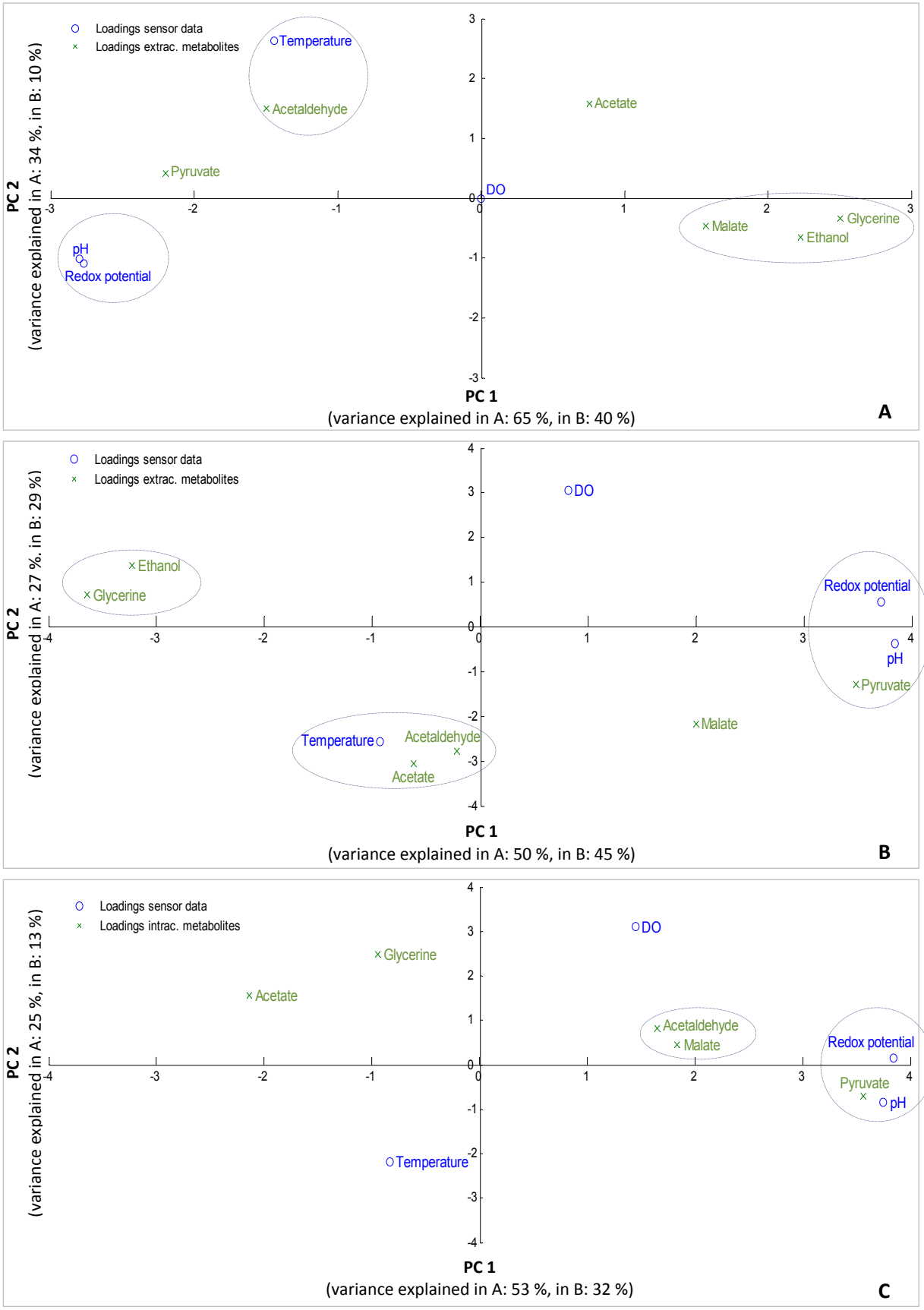

Fig. 59: Loadings of the *on-line* sensor data vs. the concentrations of main carbon metabolites. A: 3 m^3 scale, experiment 1, extracellular; B: 170/199 m^3 scale, experiment 1, extracellular; C: 170/199 m^3 scale, experiment 1, intracellular. Presented are the loadings of the sensor data (blue circles) and the concentrations of extracellular main carbon metabolites (green crosses).

5.3.1.3. Loading Plots for Sterols

The PCs obtained by the PCA of the total and free sterol content and the *on-line* sensor data are presented in Fig. 60 and Fig. 61: squalene, zymosterol, lanosterol, ergosterol. The contribution of PC 2 for the total content is very similar in the 3 m^3 and 170/199 m^3 scale experiments (Fig. 57 D, Fig. 60). The contribution of PC 2 for the prediction of the free sterol content was higher in the 170/199 m^3 scale experiments, whereas in the smaller scale, PC 2 had nearly no contribution (Fig. 57 E, Fig. 61):

The distance of the loadings from the origin in the 3 m^3 scale indicates that all total sterol concentrations and all *on-line* parameters except the DO value are significant (Fig 1A). The loading factors of the precursor squalene, the intermediate lanosterol, and the product ergosterol are closely grouped in a cluster in the 3 m^3 scale (Fig. 60 A). The values of the grouped sterols are negatively correlated to the pH / redox potential-values concerning PC 2.
All parameters are significant in the 170/199 m^3 scale for the total sterol content analysis. The loadings of the pH / redox potential-values and several total sterol concentrations form a cluster, which shows a much higher significance for PC 1 in comparison to PC 2 (Fig. 60 B, C). Interestingly, the squalene concentration seems to develop independently from the other parameters in both experiments (Fig. 60 B, C), probably due to the regulation within the sterol synthesis at the conversion form squalene to lanosterol.
The loadings of the temperature differed between both experiments in the 170/199 m^3 scale. Since the temperature profile in one experiment between both PCAs, i.e. the total and free sterol concentration analysis, was rather similar, the loading values are probably alternated due to a low sensitivity of this parameter (Fig. 60 B, C and Fig. 61 A, B). The same alternation of loadings is seen for the DO measurements in the two experiments in the 170/199 m^3 scale for both PCAs.
As expected, the changes in the loading values for the DO value develop similar in the PCAs for both free and total sterols within one experiment. The differences between both experiments were probably caused by the release of a certain amount of foam through an open hole within the first 50 h in the 1st experiment, followed by changes in pressure. This might have influenced the convection movement including the distribution of parameters like the DO as it was determined by the *on-line* sensor measurements (Fig. 44). This effect is evident since oxygen is essential during sterol biosynthesis.

The loadings of the free lanosterol content show much higher significance for PC 1 than for PC 2 in both experiments in the 170/199 m^3 scale. The loadings of the pH-value and redox potential, however, have similar values to lanosterol and can therefore be clustered (Fig. 61 A, B). Interestingly, the order of the loading values of the free sterol content is nearly the same as for the total sterol content for both PCs.
The significance is decreasing for PC 1 and increasing for PC 2 with the following order: zymosterol, lanosterol, ergosterol, and squalene for the total sterol content as well as lanosterol, zymosterol, ergosterol, and squalene for the free sterol content. The high absolute loading values in PC 1 for the intermediates and the pH / redox potential-values show their significance in the process. Squalene as the precursor and ergosterol as the end product of the sterol biosynthesis instead have similar values for PC 2. The loading values of the intermediates zymosterol and lanosterol content, are the compounds among all sterols, which are most closely related to the development of the pH-value and redox potential. This represents the process course, in which the amount of sterol intermediates remained at a nearly constant level in contrast to the precursor and product.

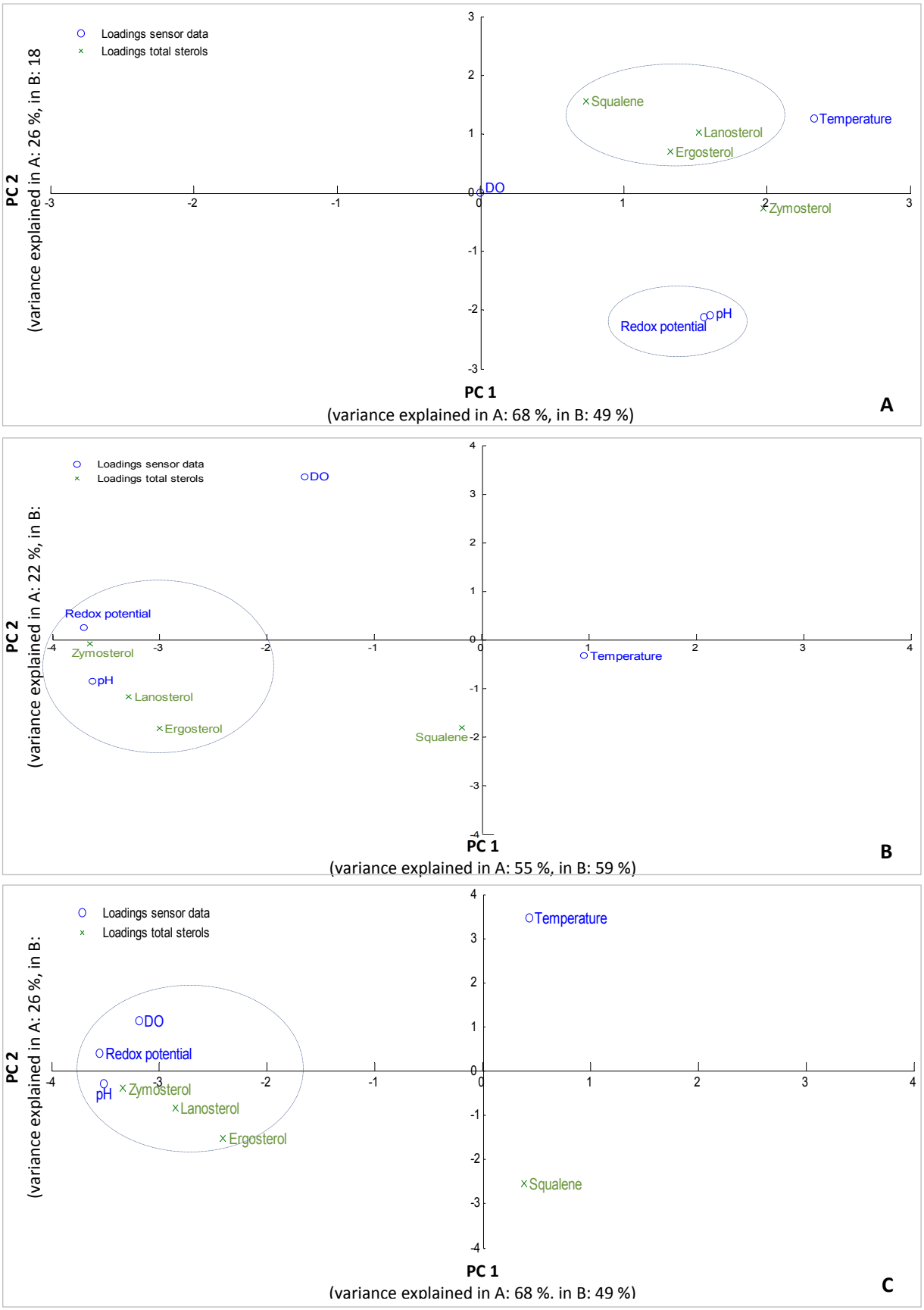

Fig. 60: Loadings of the *on-line* sensor data vs. the total sterol content.
A: 3 m^3 scale, experiment 1; B: 170/199 m^3 scale, experiment 1; C: 170/199 m^3 scale, experiment 2. Presented are the loadings of the sensor data (blue circles) and the concentrations of total sterols (green crosses).

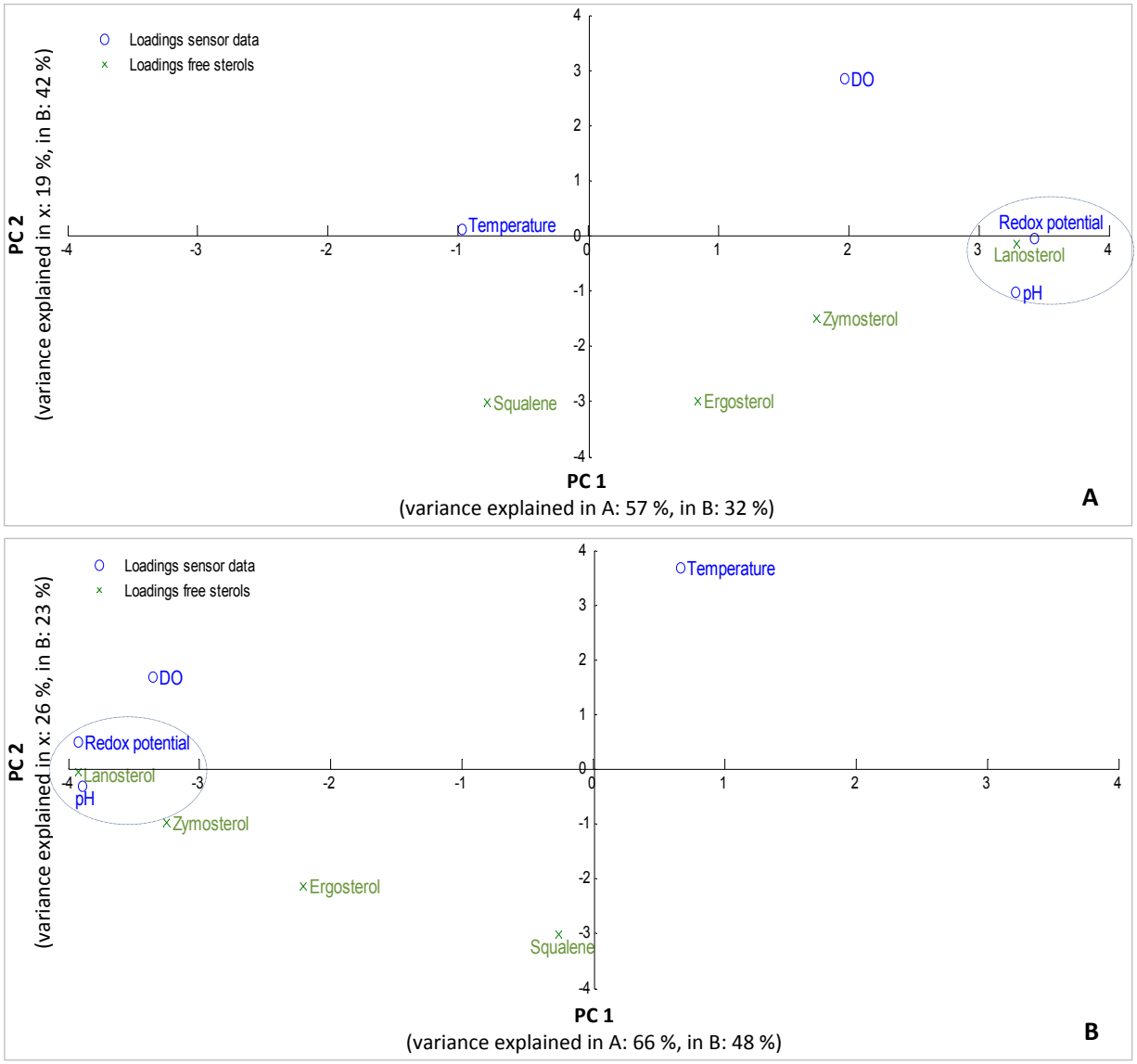

Fig. 61: Loadings of the *on-line* sensor data vs. the free sterol content measured in A: the 170/199 m^3 scale, experiment 1, B: the 170/199 m^3 scale, experiment 2. Presented are the loadings of the sensor data (blue circles) and the concentrations of free sterols (green crosses).

5.3.2. Partial Least Square (PLS) Regression

The PLS regression was the 2nd step of the multivariate data analysis in order to analyze correlations between *on-line* and *off-line* data and evaluate the prediction capability, i.e. identify outliers. The PLS was performed with two PCs. The selection of regression plots was based on the PCA results in 5.3.1. PLS was performed separately for the following metabolites:

1. A cross-validation of *on-line* data to *off-line* carbohydrate concentrations (extracellular),
2. A cross-validation of *on-line* data to *off-line* main carbon metabolite concentrations (extra- and intracellular),
3. A cross-validation of *on-line* data to *off-line* sterol contents (total and free sterol content),
4. A validation of the correlation model of the cross-validations of the 2nd experiment (for carbon- & keto acids, aldehydes and alcohols, carbohydrates, and sterols, respectively) with the data set of the 1st experiment in the 170/199 m^3 scale.

Compared to the 3 m^3 scale, a better correlation was achieved in the 170/199 m^3 scale in nearly all cases (Fig. 62 - Fig. 66). Interestingly, the 1st experiment of this scale, during which a certain amount of foam was released through an open hole within the first 50 h, shows even a better correlation than the 2nd experiment. This can be related to the changes in movement or mixing of the fermenter volume under different pressure. A different mixing quality also affects the distribution of parameters, including those that have not been measured *on-line*, like nutrient or metabolite concentrations. The mixing quality analyses based on the *on-line* data measurements (Fig. 42 and Fig. 43) also revealed differences between the two experiments concerning both the time points of the appearance of gradients and their extent.

Best correlation between the *on-line* measured parameters pH-value, redox potential, DO-value, and temperature was achieved for the carbohydrate concentrations. All correlation coefficients that are not presented in the following are given in the appendix B, iv.

Glucose was well correlated in the 170/199 m^3 scale and still satisfactory in the 3 m^3 scale (0.76). The 2nd best correlation was achieved for fructose in the 170/199 m^3 scale (Table 15). For maltose and galactose as well as for all carbohydrates in the 3 m^3 scale, correlation coefficients lower than 0.8 were determined. For maltotriose in the 170/199 m^3 scale, the coefficients were even below 0.7. The reason in case of maltotriose and maltose might be the very high initial concentrations of both substrates, which require additional manual dilution steps for analysis and might still touch the linear range limits of the analysis instrument (HPLC).

Table 15: Coefficients for the correlation of extracellular carbohydrate concentrations with *on-line* sensor data (Fig. 62). E = experiment. E1 on E2 represents the validation of the model developed with the data set of E2 with the independent data set of E1 in the 170/199 m^3 scale.

	199 m^3 scale, E1	**170 m^3 scale, E2**	**170 m^3 scale, E1 on E2**
Glucose	0.93	0.92	0.88
Fructose	0.93	0.91	0.80

Good correlations were found for the total and the free sterol content of zymosterol, lanosterol, and ergosterol in the 1st experiment of the 170/199 m^3 scale (Table 16). In the 2nd experiment of this scale, however, they were lower except of the free zymosterol content. The reasons for these differences between the two experiments of the same scale are elucidated in the previous section of PCA, beside the different fermentation conditions described in the methods section.

Table 16: Coefficients for the correlation of total and free sterol content with *on-line* sensor data (Fig. 65, Fig. 66). E = experiment.

	199 m^3 scale, E1, total	**170 m^3 scale, E2, total**	**199 m^3 scale, E1, free**	**170 m^3 scale, E2, free**
Zymosterol	0.95	0.87	0.44	0.72
Lanosterol	0.88	0.62	0.81	0.59
Ergosterol	0.87	0.68	0.90	0.96

Concerning the main carbon metabolites, the correlations to the *on-line* data were not satisfactory. For the extracellular concentrations, correlation coefficients higher than 0.7 were determined only for glycerin in all experiments and in the 170/199 m^3 scale also for pyruvate and ethanol (Table 17, Fig. 63). A reason for the mostly low correlation for the intracellular main carbon metabolites ($R^2 < 0.5$), except for pyruvate (Table 18, Fig. 64), could be the long and tedious sample preparation after inactivation with $HCLO_4$, which harbours many error sources as described in the discussion section.

Table 17**:** Coefficients for the correlation of the concentrations of extracellular main carbon metabolites with *on-line* sensor data
(Fig. 63). E1 on E2 represents the validation of the model developed with the data set of E2 with the independent data set of E1 in the 170/199 m3 scale.

	3 m^3 scale. E1	**199 m^3 scale. E1**	**170 m^3 scale. E2**	**170 m^3 scale. E1 on E2**
Glycerin	0.71	0.92	0.80	0.88
Pyruvate		0.92	0.83	0.74
Ethanol		0.82	0.66	0.72

Table 18: Coefficients for the correlation of the concentrations of intracellular main carbon metabolites with *on-line* sensor data
(Fig. 64). E = experiment. E1 on E2 represents the validation of the model developed with the data set of E2 with the independent data set of E1 in the 170/199 m^3 scale.

	3 m^3 scale, E1	**199 m^3 scale, E1**	**170 m^3 scale, E2**	**170 m^3 scale, E1 on E2**
Pyruvate	0.88	0.88	0.84	0.81
Malate	0.89			

5.3.2.1. Cross-Validation of the carbohydrates

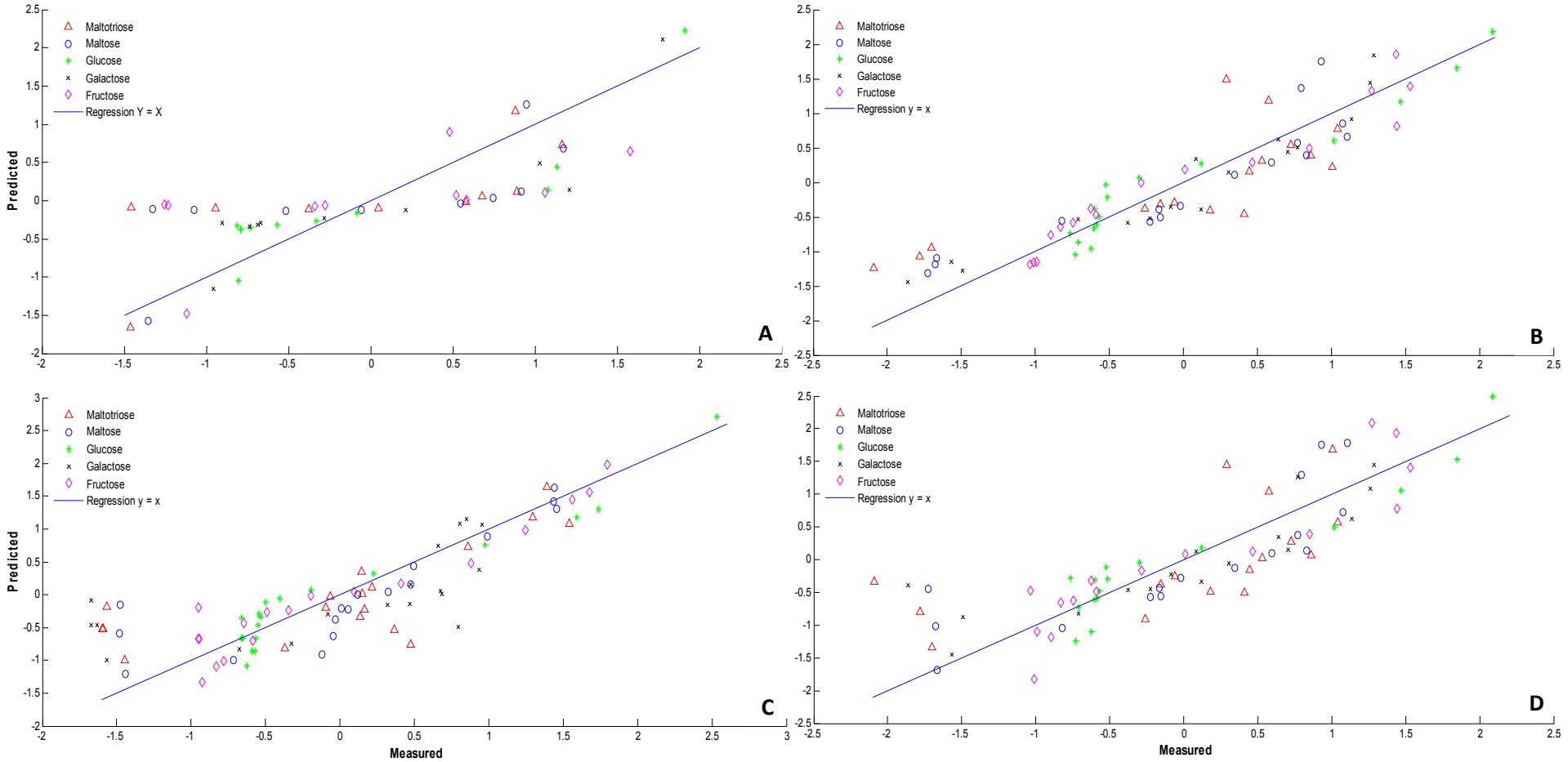

Fig. 62: Cross-validation of the extracellular carbohydrate concentration.
A: 3 m^3 scale, experiment 1; B: 170/199 m^3 scale, experiment 1; C: 170/199 m^3 scale, experiment 2. D: Validation of the regression model in the 170/199 m^3 scale with independent data from the same scale. The predicted values are based on the PLS regression of the *on-line* and *off-line* data of the 2nd experiment, measured values are based on the extracellular carbohydrate concentration data of the 1st experiment.

5.3.2.2. Cross-Validation of the Concentrations of Main Carbon Metabolites

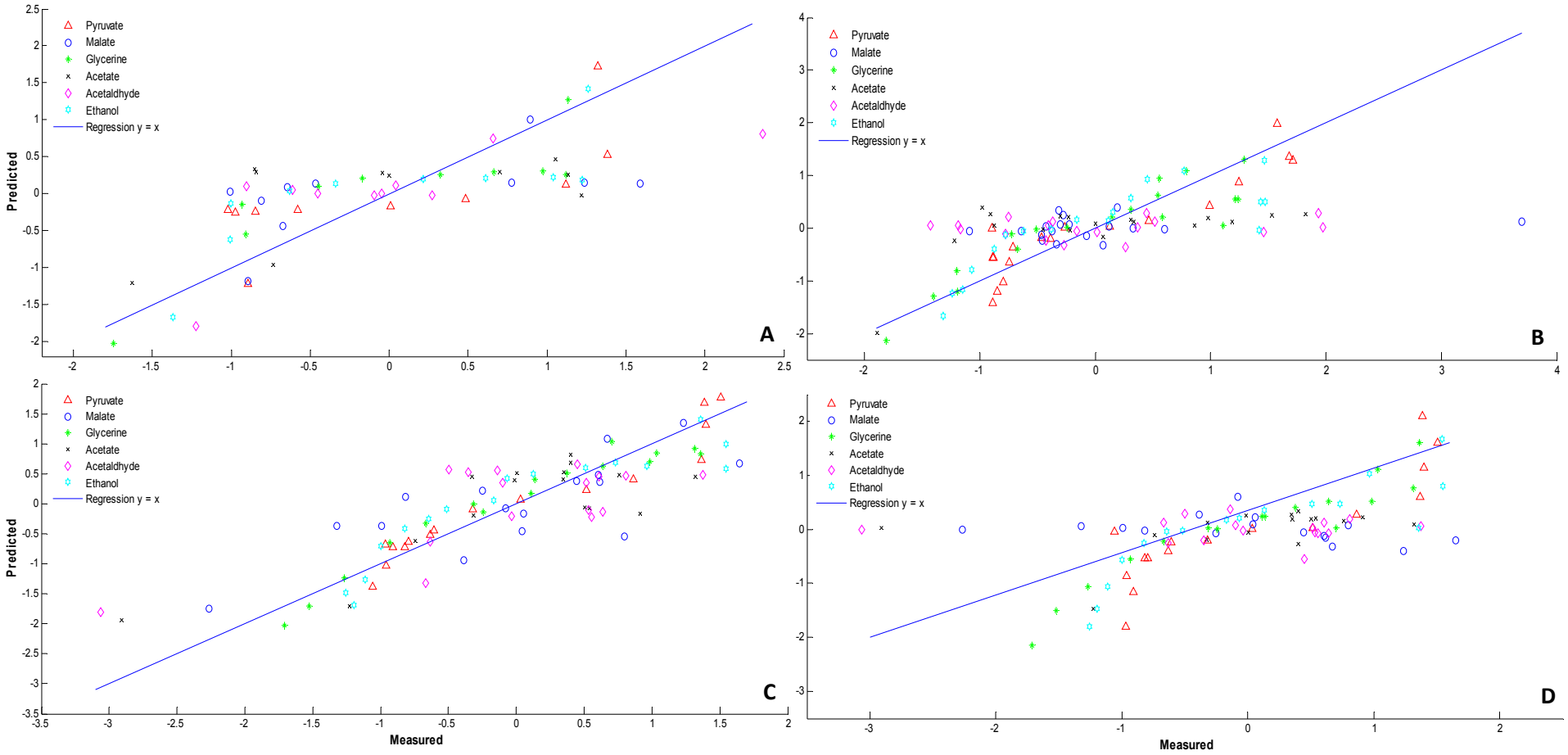

Fig. 63: Cross-validation of the concentrations of extracellular main carbon metabolites.
A: 3 m^3 scale, experiment 1; B: 170/199 m^3 scale, experiment 1; C: the 170/199 m^3 scale, experiment 2. D: Validation of the regression model in the 170/199 m^3 scale with independent data from the same scale. The predicted values are based on the PLS regression of the *on-line* and *off-line* data of the 2nd experiment, measured values are based on the extracellular carbohydrate concentration data of the 1st experiment.

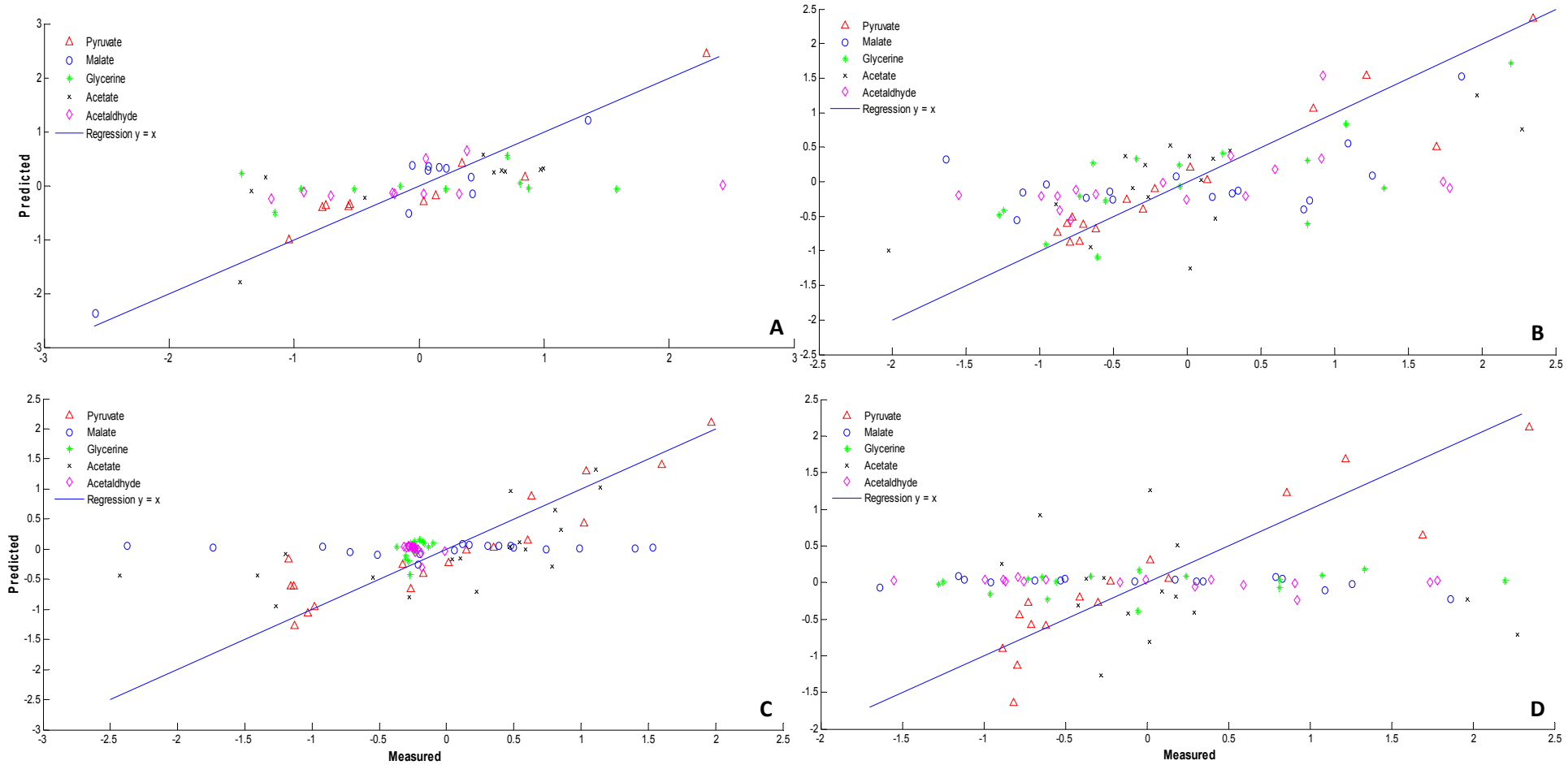

Fig. 64: Cross-validation of the concentrations of intracellular main carbon metabolites.
A: 3 m^3 scale, experiment 1; B: 170/199 m^3 scale, experiment 1; C: the 170/199 m^3 scale, experiment 2. D: Validation of the regression model in the 170/199 m^3 scale with independent data from the same scale. The predicted values are based on the PLS regression of the *on-line* and *off-line* data of the 2nd experiment, measured values are based on the extracellular carbohydrate concentration data of the 1st experiment.

5.3.2.3. Correlation of the off-line Data: Sterols

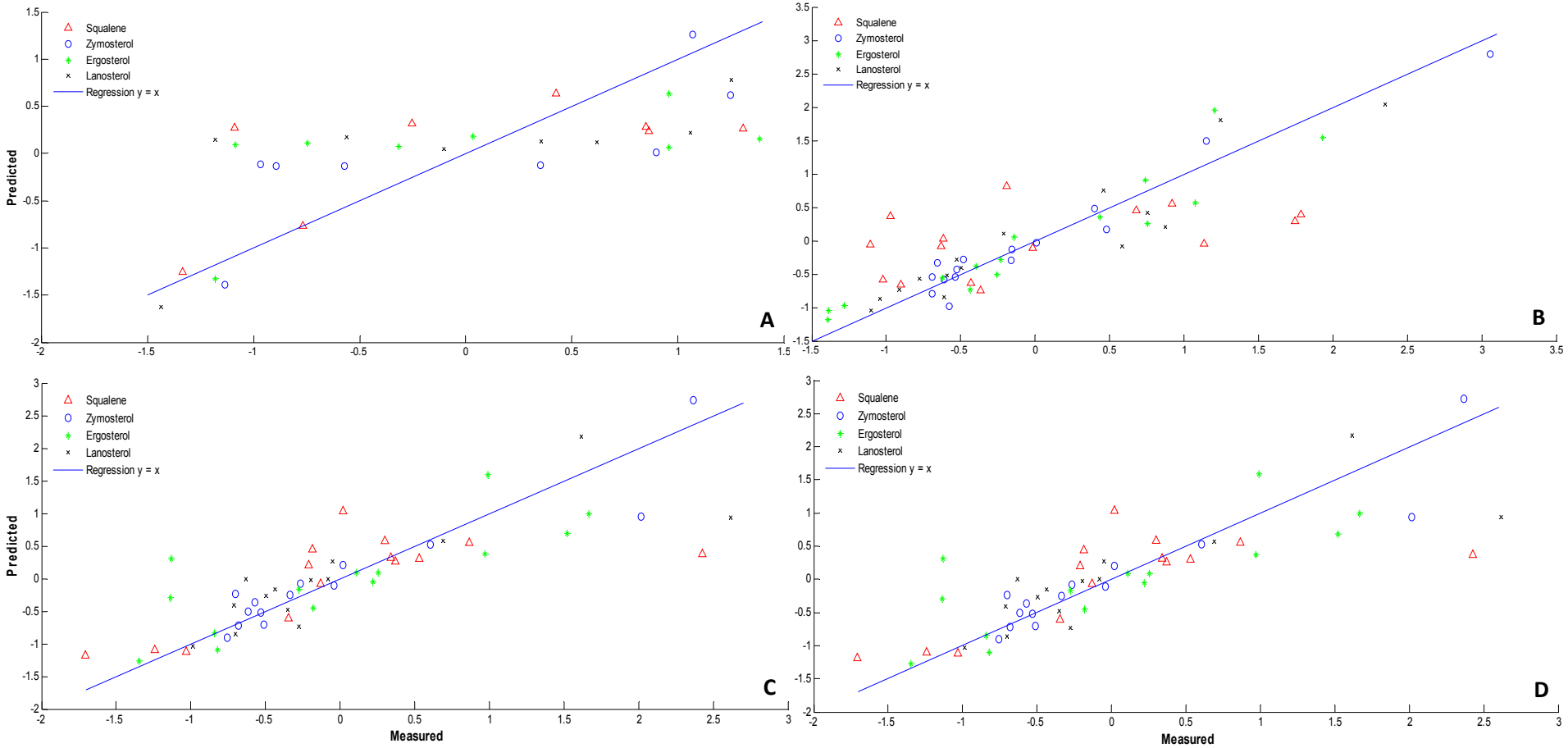

Fig. 65: Cross-validation of the total sterol content.
A: the 3 m^3 scale, experiment 1; B: the 170/199 m^3 scale, experiment 1; C: the 170/199 m^3 scale, experiment 2. D: Validation of the regression model in the 170/199 m^3 scale with independent data from the same scale. The predicted values are based on the PLS regression of the *on-line* and *off-line* data of the 2nd experiment, measured values are based on the extracellular carbohydrate concentration data of the 1st experiment.

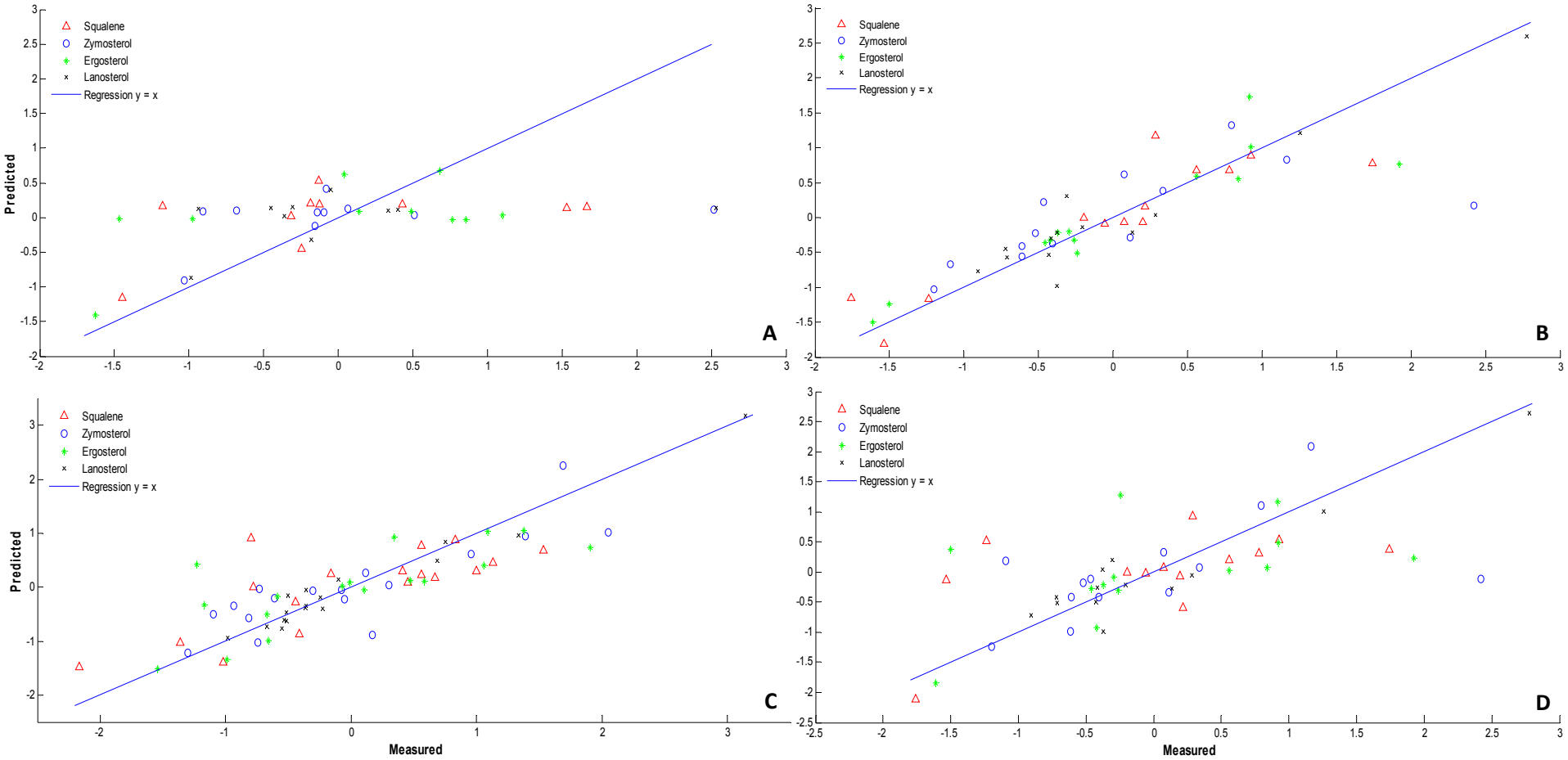

Fig. 66: Cross-validation of the free sterol content.
A: 3 m^3 scale, experiment 1; B: 170/199 m^3 scale, experiment 1; C: 170/199 m^3 scale, experiment 2. D: Validation of the regression model in the 170/199 m^3 scale with independent data from the same scale. The predicted values are based on the PLS regression of the *on-line* and *off-line* data of the 2nd experiment, measured values are based on the extracellular carbohydrate concentration data of the 1st experiment.

5.3.2.4. Partial Least Square (PLS) Regression of selected Carbohydrates in the 170/199 m³ Scale

Since the correlation of carbohydrates to the *on-line* data showed high correlation, these substances were investigated separately for each carbohydrate by PLS regression in order to compare predicted and measured values during the fermentation course. The results are displayed in Fig. 67 and Fig. 68, the corresponding regression plots (measured vs. predicted) are displayed in appendix B (Fig. B 3, Fig. B 4). For this analysis, two PCs were used analogously to 5.3.1 and 5.3.2.

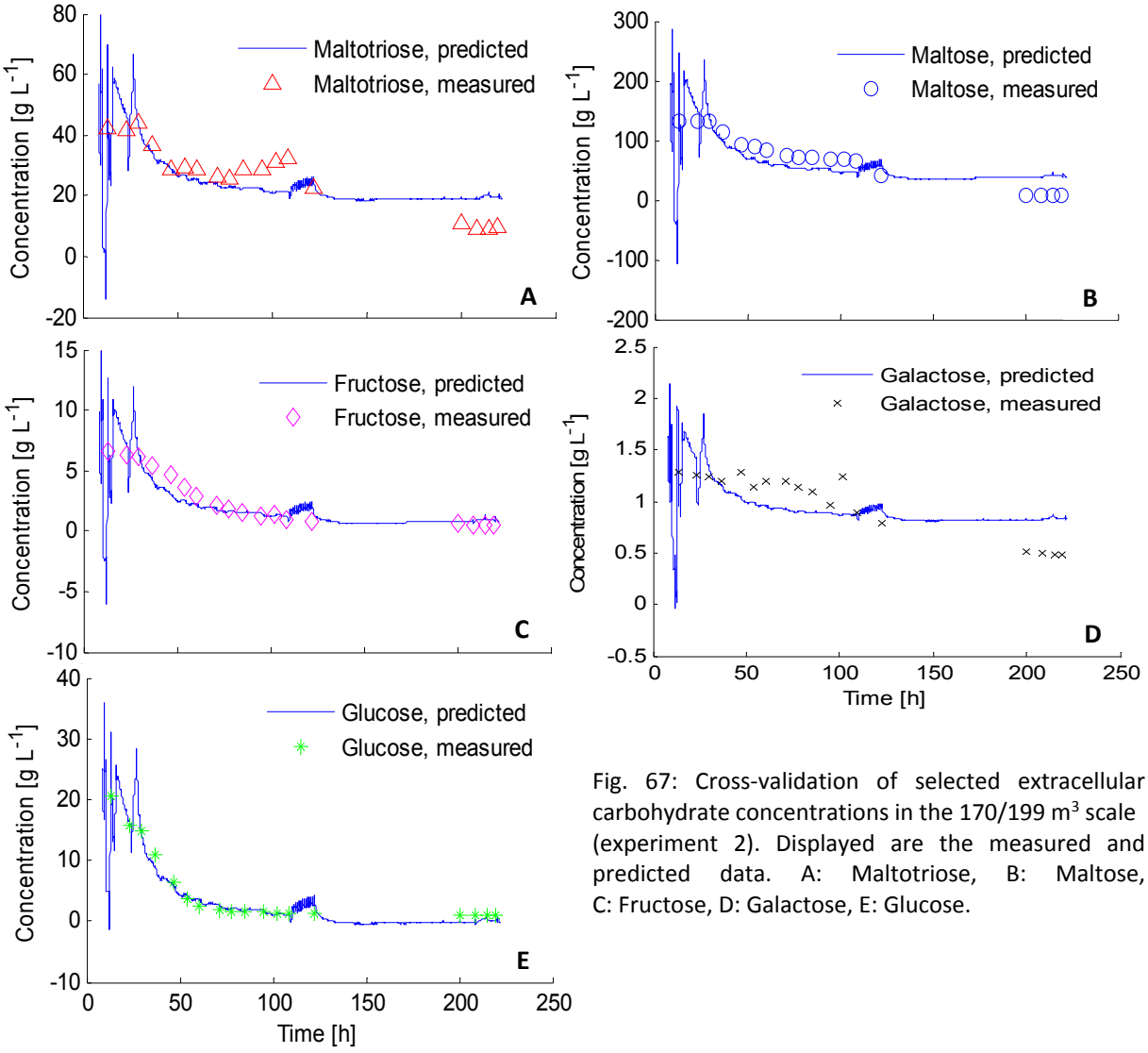

Fig. 67: Cross-validation of selected extracellular carbohydrate concentrations in the 170/199 m³ scale (experiment 2). Displayed are the measured and predicted data. A: Maltotriose, B: Maltose, C: Fructose, D: Galactose, E: Glucose.

The data show that maltotriose, maltose, glucose, galactose, and fructose can be predicted very well and galactose less accurately by the *on-line* data. The predicted values differ from the measured values at the end of the fermentation. This might be caused by the tank cooling, which started at 205 h. The correlation coefficients for this cross-validation can be seen in Table 19.

Even the validation of the model with the *off-line* data concerning the carbohydrate concentration of the 1st experiment with the same settings showed good agreement (Fig. 68). Hence, this model is suitable for the prediction of the extracellular carbohydrate content in similar fermentation processes. It can be improved by excluding the filling and cooling phases.

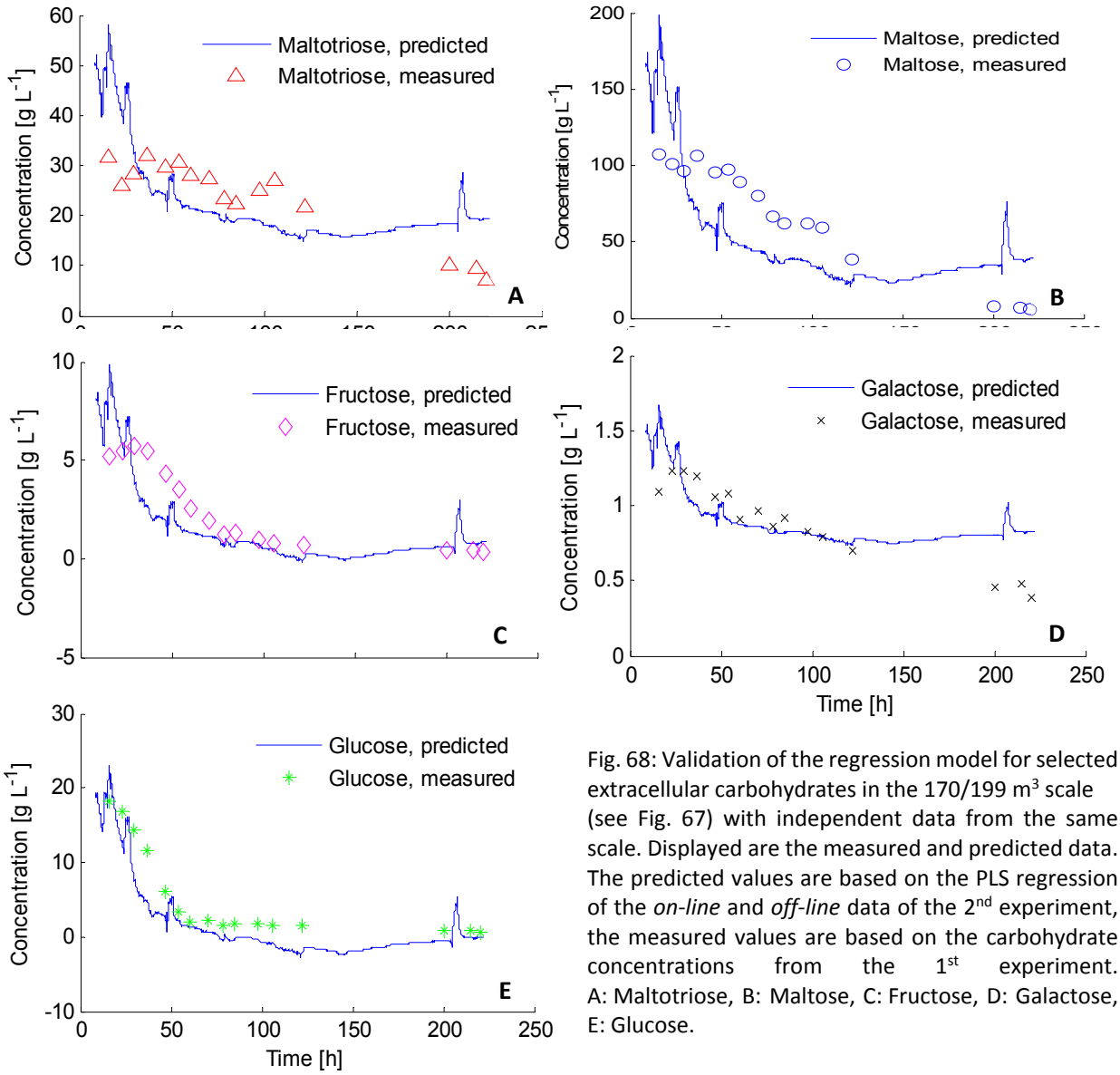

Fig. 68: Validation of the regression model for selected extracellular carbohydrates in the 170/199 m^3 scale (see Fig. 67) with independent data from the same scale. Displayed are the measured and predicted data. The predicted values are based on the PLS regression of the *on-line* and *off-line* data of the 2nd experiment, the measured values are based on the carbohydrate concentrations from the 1st experiment. A: Maltotriose, B: Maltose, C: Fructose, D: Galactose, E: Glucose.

Table 19: Coefficients for the correlation of selected extracellular carbohydrate concentrations (not z-transformed) with *on-line* sensor data at the 170/199 m^3 scale (Fig. 67, Fig. 68).

	170 m^3 scale, E2	**170 m^3 scale, E1 on E2**
Maltotriose	0.63	-0.71
Maltose	0.72	-0.16
Glucose	0.97	0.69
Galactose	0.37	0.19
Fructose	0.89	0.29

6. Discussion

6.1. Innovation Potential of the Measurement Technology

A key element of the developed technique is the simultaneous multi-position and multi-parameter measurement for the detection of gradients in the core of the liquid phase of large-scale processes. The applicability in unstirred large-scale brewing tanks with a volume of up to 200 m^3 was proven. With some adaptions, the technique can be installed at various tanks, independently of the tank geometry or size. The positions of the sensors in vertical direction can be flexibly chosen. Hence, it can be applied in industrial processes without tank retrofitting.

6.1.1. Multi-Position Approach

Multi-position measurements are necessary to obtain not only local information but a representative measurement in large-scale processes (Garcia et al., 1993). By multi-position temperature measurements, Schuch determined temperature gradients of up to 2 °C along the tank height during the main fermentation in a tank, in which the liquid surface was not in contact with a cooling zone. This tank had a fermentation volume of 380 m^3, an area covered by cooling zones of 40 % and a height to diameter (H/D) ratio of 4, whereas the two other investigated tanks had the following features, respectively: 100 m^3 volume, 30 % covered area, and a H/D ratio of 4 as well as 450 m^3 volume, 100 % covered area, and a H/D ratio of 2 (Schuch, 1996b). Up to 12 temperature sensors and sampling ports were installed at different positions in both, vertical and horizontal direction. Further, the temperature gradients in height were larger if only one cooling zone instead of at least two zones were integrated (Schuch, 1996d). Hence, the necessity of multi-position measurements increases with a smaller area covered by cooling zones. The formation of temperature gradients also depends on the tank H/D ratio. They were found to be larger with a lower H/D ratio (Schuch, 1996b; Wan, 1995).
In contrast to the mobile technique developed in this thesis, however, the sensor positions were fixed in Schuch's experiments and the tank had to be retrofitted. This is not feasible in industrial brewing processes and hinders the application of the technique in other processes. Further, only one parameter instead of several in parallel could be measured *on-line* in the studies of Schuch and co-authors.

If multi-position measurements cannot be conducted, CFD techniques can be used to estimate the fluid flow in a reactor instead (Sun and Norton, 2007; Yuan et al., 2009). These techniques, however, do not consider and are not able to estimate kinetic or physiological parameters as well as mass transfer rates, which might be also altered by heterogeneities in the liquid phase (Delvigne et al., 2017; Haringa et al., 2017) (see also 2.2.4.1). Further, small gradients are difficult to detect with this technique. CFD techniques as a single method will therefore not replace multi-position *real-time* and *in-situ* measurements but can be a useful complementary tool. They should be, however, combined with kinetic models to form hybrid models, which consider cell consumption and synthesis rates and therefore population heterogeneities.

Sampling for *at-line* or *off-line* analysis at different positions is also preferable in order to obtain representative data and identify critical and representative zones for the bulk liquid phase (Schwill-Miedaner, 2016). For example, a locally limited diacetyl analysis in a heterogeneous tank entails the

risk of too long or too short fermentation times since diacetyl is an indicator for the maturation grade (Schwill-Miedaner, 2011). This might lead to quality losses if samples are not representative. It is known, and was also seen in our studies, that larger gradients appear with higher frequency during the filling and tank cooling. A gradient in cell count and temperature at the end of the fermentation and during cooling is even aimed in order stop the fermentation and force the yeast cells to sediment in the vessel cone for harvesting. Sampling at only one position, however, will lead to wrong assumptions about the concentration of different metabolites in the complete tank volume (Schuch, 1996b).
Schuch integrated sampling tubes at the same positions as the temperature sensors (see page 121). Samples for the *off-line* determination of the extract and ethanol content, pH-value, vicinal diketone concentrations, and cell concentrations were taken during the main fermentation phase, maturation, and cold storage. In the extract and ethanol content, no significant gradients during the main fermentation were detected in three different tanks systems (100 m^3, 380 m^3, 450 m^3). The gradients in the pH-value were close to the detection limit and independent on the tank height in this phase. This shows that a multi-position measurement of these three parameters is not necessary for this process.
For diacetyl and pentanedione instead, gradients of up to 0.2 mg L^{-1} were detected, which is higher than the taste limit of 0.1 mg L^{-1}. Therefore, it is significant and worth to monitor at multiple positions. The cell count was differing as well between the positions (in vertical and horizontal direction) with up to 10 Mio cells mL^{-1} at day two in 380 m^3 and nearly 39 Mio cells mL^{-1} at day four in 450 m^3. Since cells in suspension show a better fermentation performance due to the better availability of nutrients and oxygen (at the fermentation onset), sampling and measurements at various positions is very important. Therefore, it would be a huge benefit if *on-line* sensors were available for the cell count and total diacetyl content, which can be integrated into the mobile multi-parameter sensor unit for locally flexible measurements.
In a 30 m^3 scale fed-batch cultivation with *S. cerevisiae*, the formation of glucose gradients at different feeding positions (top or bottom) was investigated. Samples for glucose analysis were taken continuously at three different positions (0.97, 3.90, 6.35 m) by a rapid sampling system. As expected, the gradients were larger when feeding was supplied in the poorly mixed zone above the top impeller than in the well mixed zone close to the impeller located at the bottom of the tank (Larsson et al., 1996). This shows as well that installing a sampling port only at one of these positions will lead to wrong assumptions concerning the mixing quality and parameter distribution in the tank. An *on-line* glucose sensor, which is suitable for the integration into the developed multi-position sensor unit, would allow for the monitoring of the glucose distribution in the core of the liquid phase in large-scale reactors, also in fed-batch cultivations, and could replace insufficient *off-line* analyses.

Sampling at different positions was not feasible in this work since retrofitting of the tanks would have been necessary, which is difficult for brewing tanks. Due to the small gradients determined in the different investigated scales, however, and the rather slow process in comparison to bacterial processes, these processes can be assumed as quasi-homogeneous. Hence, the data obtained from sampling at one spot and subsequent *at-line* and *off-line* analysis were correlated with the multi-position *on-line* data as presented in the results section.
Since the sensors in the mobile sensor unit can be easily exchanged by screwing, parameters can be added. As soon as suitable sensors for *in-situ* application are available for parameters that are still analyzed *off-line* after sampling (e.g. glucose, cell count, ethanol and diacetyl content), they can be easily integrated in the unit for mobile multi-parameter measurements.

6.1.2. Multi-Parameter Measurements

Multi-parameter measurements are needed for an improved understanding of scale up-related issues. The temperature or pH-value do not provide sufficient information about complex interactions in the process. Many of the studies, in which gradients were investigated in large-scale fermentation processes, focused on single parameters, e.g. temperature (Wan, 1995) or DCO_2 (Shardlow, 1972), or on a single *on-line* (temperature) and several *off-line* parameters such as the pH-value, extract, cell count, alcohol and diacetyl content (Schuch, 1996b). Further, these parameters were monitored only at a few fixed positions (see section 4.2.1), which required retrofitting of the tank. Due to the inflexibility, the data cannot be obtained at every height or position of the tank for representative measurements.

A system towards both multi-position and multi-parameter monitoring similar to the approach of Schuch (1996b) - but with a higher number of investigated positions - was developed by Maule and co-authors (1976). In a CCT with a volume of about 164 m^3, 13 different positions were accessible via a "sampling tree". This consisted of a central trunk and eight branches, each equipped with a resistance temperature sensor and sampling pipes. The samples were collected in a vacuum chamber for pH-value, cell count, and extract analysis. Gradients in the pH-value, cell count or extract were not detected, neither in lateral nor in vertical direction (Maule, 1976).
By this "sampling tree" construction, Maule examined the optimal position for a temperature sensor. Without external cooling zones, the yeast activity in this region led to higher temperatures, especially in the cone where yeast cells are accumulating. If the temperature sensor is installed only in such a zone, there is a risk of overcooling the whole tank due to the wrong temperature estimation. Hence, temperature sensors should be installed between the cooling jackets and at different heights. The correct temperature profile of the tank can be controlled adequately in order to avoid layering and overcooling of local parts, if following such a strategy (Maule, 1976). The benefit of several cooling zones, distributed across the tank surface, was discussed also by other authors (Schuch, 1996b; Unterstein, 1986; Wan, 1995). Unterstein stated that each zone should be equipped with a temperature sensor, which is installed 30 - 35 cm below the cooling zone. The temperature sensors should have an accuracy of ± 0.25 °C. The number of cooling zones and the area of the cylindrical part of the tank that is covered by cooling zones mainly depends on the tank diameter. The covered area shall be larger with increasing tank diameter. For example, a tank with an inner diameter of 3 m and a total height of 8.8 m should have an area covered with cooling zones of nearly 27 %, whereas with an inner diameter of 8 m and a total tank height of 23.4 m about 72 % of the area shall be covered with cooling systems. Very important is the cooling zone at the tank conus for yeast sedimentation in order to prevent further fermentation activity at the end of the fermentation.

These studies show that the multi-parameter approach was partially realized in former developments. Apart from the temperature, however, the data of the other parameters are obtained only by *at-line* or *off-line* measurements instead of *real-time*/*on-line* monitoring. Further, the fixed positions of the sensors and sampling pipes do not allow locally flexible and geometry - independent measurements as it can be performed with the mobile multi-parameter sensor probe as developed in the presented work. As stated above, the modular construction of the housing unit allows for a fast and easy sensor exchange. Hence, there is a great potential in future for the integration of more process parameters that cannot yet be measured *on-line.* This can be realized as soon as sensors, suitable for *in-situ* application and data transfer across long distances, are available.

6.2. Technical Features, Applicability, and Limits of the Sensor Technique

The developed measurement technique can be applied in various unstirred processes and different tank geometries as proven in this thesis. With the integration of a guide bar, also stirred processes can be assessed. In parts, modular structures are already realized, e.g. for the integration of commercially available sensors in the housing unit, as they can be exchanged one by one by screwing. The complete mobile multi-parameter sensor technique, however, including the construction for positioning, data acquisition, and data visualization cannot be applied without trained personnel or support by the developers, yet.

For the utilization in industry, the mobile multi-parameter sensor system must be applicable as a plug-and-play-system. This means that every single unit, i.e. the winch rope and its installation at the top of the tank, the integration of the measurement technique (sensors, cables, connection to the acquisition program), and the program for data evaluation and visualization must be of modular structure and easy to adapt to different tank dimensions. This will allow for a fast implementation for each kind of process without an adaption of the constructions for each individual tank.

In this thesis, gradients for *on-line* parameters in horizontal or radial direction could not be investigated. For the investigation of the complete liquid phase, further developments towards a measuring technique that is applicable in both vertical and horizontal direction as well as the construction of a multi-position sampling system is necessary.

Measurement stability and accuracy of the sensors is of basic importance. Measurement errors must be considered for gradient determination. Therefore, it is essential to know the detection limits, response times, and measurement stability or drift during time of the applied sensor techniques.
The two developed mobile multi-parameter systems are characterized by different dis-/advantages as displayed in Table 3. The main drawback of the miniaturized sensors is their measurement instability and drift behavior during long-term applications in complex medium, e.g. brewing wort.

More than four experiments with a duration of several days (up to 170 h) were performed for testing the stability and drift (see 4.1.1.). From the results it was seen that the commercially available sensors showed a higher measurement accuracy and stability as well as lower drift than the miniaturized sensors during all tested long-term applications in complex brewing media (see 5.1.1 for more details). Even a data transfer across long distances (cable length of up to 30 m) did not affect these measurements with the commercially available sensors.
The maximum sensor accuracy is determined by the technical specifications of the sensors and the corresponding calibration standard solutions (see 5.1.1). In case of the multiple application of the miniaturized sensors, the drift was higher than the accuracy of the sensors and therefore the limiting parameter concerning the suitability of the sensors for long-term applications in complex brewing media.

The loss in measurement stability and gain in sensor drift can be explained by the fact that the miniaturized sensors are equipped with sensor membranes of a very small diameter, which are sensible to clogging. Further, a very low electrolyte volume (e.g. for sensors of the DCO_2-, pH-value, redox potential) is applied, which entails the risk of toxification. Hence, they are more sensible to harsh environment in long-term applications, e.g. in brewing media with high CO_2 formation (≤ 5g L^{-1}).

Interestingly, accurate and stable measurements were obtained with the miniaturized sensors for the DCO_2-value, pH-value, redox potential, and temperature in a biogas process during a period of up to 30 days (Enseleit et al., 2017). Since the temperature and pressure measurements of the miniaturized sensors are based on resistivity, they provided stable measurements also in a brewing process. This was proven for up to 190 h in brewing fermentations in the laboratory scale. Further, the very first application of the miniaturized sensors right after the exchange by the KSI showed a lower drift and provided stable measurement data during a complete yeast fermentation in the laboratory scale (Fig. 28). Hence, the miniaturized sensors are suitable for a limited number of applications. The miniaturization can be of advantage for certain applications, where accessibility is given only for small devices and if many parameters have to be measured in parallel (Päßler et al., 2010; Sachse et al., 2015).

For the application in this project, however, the miniaturized sensors unit was not suitable since the sensors can only be exchanged by the supplier. This would have been necessary after each fermentation or even in between and was therefore not feasible. The disadvantages of the larger sensor unit, namely the lower number of integrable sensors and the higher weight, are of far less importance than the measurement stability. Further, the maximum distance that can be overcome with the miniaturized sensors for data transfer is 5 m. Hence, it was applicable only until the 24 m^3 scale with a tank height of 3 m. Due to the small size, there is no space to integrate a pre-amplifier in the sensors. Hence, the signal is amplified only after data transfer outside of the tank. The commercially available sensors are equipped with such a pre-amplifier.
Therefore, only data obtained with the commercially available sensors, integrated into the large housing unit, are presented in this thesis after the 0.15 - 0.17 m^3 scale (Fig. 30 - Fig. 49).
Gradients along the tank height that are below the measurement accuracy or the threshold determined by the calibration solutions cannot be regarded as gradients (see also 5.1.1). Gradients above these values regarding the accuracy could be determined and well differentiated with the commercially available sensors. The reason for the accuracy range for the pH sensor (± 0.02 – 0.05) is the time that is necessary for the diffusion of protons into the glass membrane and the intrusion of lithium and sodium ions. Since changes occur continuously during the process and the liquid is permanently in motion, the pH electrode is not always in equilibrium with the surrounding volume. Further, a small temperature influence especially at low temperatures on the pH measurement could be determined, despite the integrated temperature compensation. Without external influence due to electrolyte contamination or drift during long-term applications, the highest measurement accuracy for the pH sensor is equivalent to the accuracy of the standard solutions for the pH-value.

The measured values for the pH, redox potential, and DO were also well distinguishable from the drift during time, which was rather low (see 5.1.1). Concerning the temperature, the influence of the cooling system was higher than the maximum accuracy of the temperature sensors of ± 0.2 °C. Hence, the measured temperature gradients are not considered to be relevant for the process during the main fermentation phase. This shows that the determination of small local gradients in fermenters equipped with cooling jackets is challenging. More relevant instead, is the overall temperature course during time as well during the cooling phase at the end of the fermentation.

6.3. Formation of Gradients

In large-scale processes, the formation of gradients might occur, especially in unstirred processes leading to an uneven distribution of substrate, oxygen, carbon dioxide or temperature (Nienow et al., 2011). Hence, the question in this work was, whether these gradients assumed and discussed in literature exist in the large-scale, unstirred and (mostly) anaerobic brewing processes.
If gradients exist, the influence of oscillating conditions on cells has to be investigated for better process understanding and optimization. This was performed by several research groups as explained in more detail in the introduction section. Examples are scale-down reactor systems, consisting of several compartments with different fermentation conditions (Lemoine et al., 2016; Marbà-Ardebol et al., 2017) or the application of different feeding profiles in a mini bioreactor platform in order to investigate stress responses in form of metabolic shifts or specific gene expressions by GFP measurements (Lejeune et al., 2013). Additionally to the scale-down approach, the interactions between the fluid flow and cell physiology can be investigated by the application of CFD in combination to kinetic models (Delvigne et al., 2017).

Currently, no multi-position and multi-parameter measurements are applied in the brewing industry. The developed techniques, described in 4.1.2, were applied in retrofitted tanks under experimental, not under production conditions. Further, only the temperature was investigated *on-line.* Even nowadays, only the temperature, pressure and / or pH-value is monitored *on-line* in these processes and mostly at a single position.

For the determination of gradients in the presented study, the following parameters were investigated in different scales concerning their distribution along the tank height: pH-value, redox potential, DO concentration, and temperature as well as pressure and DCO_2 concentration with the miniaturized system. The following similarities and differences existed between the different presented scales regarding their process conditions: All processes were conducted without mechanical mixing and without aeration after pitching. Differences between the scales, however, were quite a few: The tank geometry, the number of batches during filling and the corresponding aeration steps, the temperature regulation systems (cooling jackets), the applied yeast strains, the original gravity as well as the remaining extract, and the start and final pH-value. Further, the “bubbling” method in the 2nd experiment in the 170/199 m^3 scale at the onset of the fermentation (see 4.2.3), i.e. the insertion of additional CO_2 at the tank bottom for improved mixing has to be considered during data evaluation. The strong foam formation due to an insufficient sealing of an opening at the tank dome in the 1st experiment has to be regarded as well since this might have led to different pressure conditions influencing the fluid flow in the reactor.

No large gradients were detected in the experiments. The detected ones were temporary and present only in certain fermentation phases. The good mixing can be ascribed to the convection movement inside the tank. An upward movement of liquid in the center of the tank is caused by raising gas bubbles and heat formation due to yeast activity. The rising bubbles grow due to further CO_2 uptake by diffusion and decreasing hydrostatic pressure with increasing height (Boulton and Quain, 2001d). At the top of the tank, the liquid is guided to the tank wall, where cooling jackets generate temperature gradients leading to a downward movement of the liquid, with a lower mixing efficiency though (Garcia et al., 1993). The good mixing by natural convection was also shown in a study of Garcia et al., who analyzed the pH-value, the cell dry weight, carbohydrates, and ethanol concentrations at six different

heights of an unstirred fermentation tank with 9.5 L volume (García et al., 1994). During the main fermentation phase, no differences in the parameter concentrations at different heights could be found. The CO_2 released from the fermenter volume was analyzed by a thermic mass flow device. These analyses showed that the agitation, caused by rising CO_2 bubbles, is sufficient to mix the complete fermenter volume during the main fermentation phase. Further, by this method the mixing power of the fermenter could be determined from the amount of released CO_2, including the following parameters: the medium volume (m^3), the gas production rate (m3 (m^3 $s)^{-1}$), the medium density (kg $(m^3)^{-1}$), the atmospheric pressure (m of column medium), and the fermenter height (m) (García et al., 1994).

In literature, it is reported that mixing in large-scale fermentation tanks based on natural convection is enhanced if CCTs with a H/D ratio of 3:1 or 4:1 are used (Hoggan, 1977; Ulenberg et al., 1972). With increasing H/D eight to diameter ratio, parameters such as the temperature (Wan, 1995) or the cell concentration (Schuch, 1996a) were found to be more homogenously distributed in brewing fermentation tanks. This is caused by the increasing number of asymmetric, disordered and instable turbulent flows at higher H/D ratio (Wan, 1995). Shardlow and co-authors measured the DCO_2 concentration at three different heights (4.6 m, 10 m, 16.5 m) in a *S. cerevisiae* fermentation of 242 m^3 and 491 m^3 volume with a H/D ratio of 3.5:1. Only small gradients of maximum 0.8 % (vol/vol) could be determined only on the 3rd day during a fermentation of eight days in total (Shardlow, 1972). This shows that the distribution of DCO_2 is well distributed along the tank height with the correct ratio. It would be interesting, however, to proof this for more positions and at different diameters.

6.3.1. The DO-Value

It is known from literature that the oxygen is consumed and the process becomes anaerobic very fast in in brewing fermentations, i.e. in the first 2-3 h (Kucharczyk and Tuszyński, 2017). The *on-line* measurements in this work prove this with a drastic decline in most cases within the first 1-3 h after the tank filling was finished to nearly zero in all investigated scales, independently of the sensor position. Only in the 1st experiment of the 170/199 m^3, where half a batch had to be transferred to another tank due to the release of foam through an unsealed hole in the tank dome, a peak in the DO value was seen at later stages. This shows the fast response of the DO sensor, providing reliable measurements. Due to these low values, a gradient formation in dissolved oxygen cannot occur.

More important to consider are oxidative stress for yeast cells during propagation or oxidation reactions after the fermentation, e.g. during beer maturation and filling (Annemüller and Manger, 2009e; Paumi et al., 2017). It was found that oxygen stress, induced by lidocaine concentrations of 5 - 30 mM or H_2O_2 concentrations of 1 - 20 mM can alter the activity of several enzymes of the carbohydrate metabolism based on changes on the proteome level. By this, glycolytic pathways and subsequently energy generation as well as the redox balance are negatively influenced (Boone et al., 2016).

The importance of oxygen during propagation and pitching, e.g. for sterol biosynthesis is discussed in detail in the correlation analysis of the oxygen and the sterol content (section 6.4.3). Further, protection mechanisms against oxidative stress and ROS are discussed in 6.3.3.

6.3.2. The pH-Value

For the pH-value, gradients of maximum 0.4 pH-units in the 3 m^3 scale and 0.17 pH-units in the 170/199 m^3 scale were determined in our studies during the onset of the fermentation and main fermentation phase.
If cells are exposed to sudden pH gradients, although they are small, stress responses might be generated. Stress responses were observed in form of morphological changes, i.e. filamentous growth, in the yeast *Yarrowia lipolytica* as a response to perturbations in the pH-value (Timoumi et al., 2017).
High pH levels, e.g. a pH-value of 8.0 or 9.0, can inhibit cell growth since the available energy is needed for the down regulation of the intracellular pH-value, e.g. by active transport mechanisms (Peña et al., 2015). Sudden changes towards alkaline conditions can lead to stress responses in budding *S. cerevisiae* on the genetic expression level (Roque et al., 2016; Serra-Cardona et al., 2015). Higher levels of calcium were detected at a pH-value above 7.0., activating the protein phosphatase calcineurin. This triggers the binding of the transcription factor (Crz1) to calcineurin/Crz1 responsive gene promoters in the nucleus. Several genes involved in glucose and trehalose metabolism were found to be influenced by calcineurin / Crz1 (Roque et al., 2016). The latter is also known to be involved in stress regulation (Virgilio et al., 2017).
Changes on the genetic level due to pH perturbations were also detected by Rajkumar and co-authors (2016). They developed synthetic, inducible promotors that are activated at low pH-values (≤ 3) in yeast. For optimal growth under metabolic acid stress, about 129 genes are necessary (Shin et al., 2016). Changes in gene expression as a stress response do not only occur at acidic or alkaline stress. They are a response form in yeast to many different stress conditions, e.g. temperature shocks, oxidizing and reducing agents, osmotic pressure, amino acid starvation or nitrogen source depletion, etc. (Gasch et al., 2000).
The protection against inhibitory effects of substances by the adjustment of the pH-value was studies by Marini and co-authors (1961). They could prevent the inhibition of the glycolysis in *S. cerevisiae* by nystatin with the adjustment of the pH-value to around 5.8. These studies show the importance of the correct pH-value for a stable operation of a fermentation process.

For stress responses and cell regulation, the intracellular pH-value (pH_i) also plays an important role since it influences many intracellular biochemical and metabolic pathways, such as membrane lipid synthesis (Aabo et al., 2011; Barbosa et al., 2015). It was found that a rapid decrease in the pH_i indirectly leads to the repression of genes responsible for membrane phospholipid synthesis (Young et al., 2010). This can occur, when the cells experience oscillating extracellular pH-values as they might occur in large-scale processes. The pH_i-value itself is regulated by the activation of the plasma membrane ATPase proton pump (Pma1) with ATP molecules from the glucose metabolism (Elsutohy et al., 2017; Mahmoud et al., 2017). This fungal specific proton pump is of high importance since it allows the cells to maintain a neutral pH_i-value also under high extracellular acid stress by pumping protons out of the cell (Ferreira et al., 2001; Shin et al., 2016). In our experiments, very small amounts of glucose were present until the end of the fermentation as well as di-and tri-saccharides. Hence, the substrate for ATP generation during glycolysis was present all time. The proton pumps, activated by ATP molecules, were probably compensating the small gradients in the pH-value that were detected.

During most of the fermentation time in the 170/199 m^3 scale, however, the determined pH gradients were below the long-term measurement accuracy or even below the accuracy determined by the calibration solutions. Since also the drift during long time application was determined to be very low

in pre-experiments (maximum 0.03 pH-units after about 220 h), the maximum gradient value between the different heights in these time frames can be assumed to be in the range of 0.02 - 0.05 pH-units. Additionally, the temperature influences the pH measurement and calibration and cannot completely be compensated (Okamura et al., 2014; Tauber, 2010). Hence, very small gradients cannot be distinguished from the values determined by the limits of the measurement technology.

6.3.3. The Redox Potential

The redox potential is influenced by the amount of oxidizing and reducing agents and compounds, e.g. the ratio of NAD^+/NADH, FAD/$FADH_2$, $NADP^+$/NADPH, glutathione/glutathione disulfide (GSH/GSSG), and reactive oxygen species (ROS) (Vevea et al., 2013). A low potential is related to a higher content of reducing substances and vice versa. Among the reducing agents, the fast reducing ones have the highest impact in the brewing process (Burkert, 2005). Further, antioxidants are important for the beer quality and beer aging processes since even low concentrations of oxygen can form highly reactive oxygen species (ROS). Beers with a low antioxidant potential often have a pallid taste and insufficient flavor quality (Kunz et al., 2014).
Changes in the intracellular metabolism can also change the redox balance in extracellular parts, influencing different cellular processes such as proliferation (Banerjee, 2012). Other cell functions that are influenced by changes in the redox potential are: signal transduction, DNA and RNA synthesis, protein synthesis, enzyme activation, and cell cycle regulation (Liu et al., 2017). Wort is a very complex medium and many substances can be altered by oxygen. Hence, it is difficult to determine exactly, which chemical reactions and which cellular processes contribute to alterations of the extracellular redox potential and to what extend (Burkert, 2005).

Sudden changes in the redox potential might influence the energy metabolism of the cell, which on the other site has an impact on many cell functions and also on the substrate stability (Burkert, 2005). With an increase of reducing agents in the medium, the cell viability and vitality decrease since the ability to transfer electrons gets lost (Banerjee, 2012; Burkert, 2005). Already a change of 30 mV in the intracellular redox potential can lead to a 10-fold shift in the equilibrium between the dithiol containing proteins (reduced) and disulfide containing proteins (oxidized) (Banerjee, 2012).
In the industrial scale of 170/199 m^3, gradients in the redox potential of 66 mV at the fermentation onset were determined. Most of the time in all investigated scales, however, they were determined to be of maximum 20 mV or lower. During the filling process, gradients of up to 110 mV were reached in the 170/199 m^3, where six to seven batches were inserted one after the other. These gradients on the extracellular level at the onset of the fermentation might have had an impact on the chemical equilibrium as described above. There might have been, however, also stress regulatory mechanisms.

In the 170/199 m^3 scale experiments, the redox potential decreased by about 200 mV and 280 mV during the complete fermentation time. In contrast, it was reported that the reduction level decreases while the redox potential increases. The decrease in the reduction power is explained with the assimilation of reducing substances by the yeast cells, the decrease in the total polyphenol content, and the precipitation of these substances by changes in the pH-value as they occur during the brewing process (Burkert, 2005).
The different results can be explained by the different carbohydrate composition, pH levels, and temperature of the conducted fermentations. Kunz and co-authors stated that the reducing potential of young beer depends on the temperature, pH-value, and the composition of wort concerning di-, tri,

and monosaccharides. At a low pH-value (pH = 4.2), the reducing power of the different carbohydrates decreases in the following order: isomaltulose, fructose, maltotriose, and maltose. The reducing power of glucose is very low since low pH-values inhibit the formation of the open-chain aldehyde structure. At higher temperatures (80 / 90°C) as they occur in wort boiling, the reducing potential of maltotriose was determined to be higher than for maltose (Kunz et al., 2011).

In case of stress induced by reduction or oxidation reactions, redox regulation systems are essential for cell protection. In yeast cells, this is realized by amino acids or small peptides, such as cysteine and glutathione or thioredoxin, which regulate the redox potential in different intracellular compartments, interacting with each other. They also have an impact on the status of redox-sensitive macromolecules and can protect against oxidative stress (Banerjee, 2012; Herrero et al., 2008; Shelton et al., 2005). In *S. cerevisiae,* enzymes protect the cells against reactive oxygen species (ROS). These can act directly as ROS detoxifiers or those that act as redox regulators of protein thiols and by this support to maintain the redox balance (Herrero et al., 2008). Responses to ROS stress further include the direct alteration of kinases and transcription factors as well as indirect changes of cysteine-rich redox-sensitive proteins by the construction of intra- or inter-molecular disulfide bond between the corresponding cysteines (Adler et al., 1999).

Since the DO value in anaerobic processes rather depletes after a short time, it is difficult to use this parameter for fermentation control. It was observed during cultivations with *S. cerevisiae* and a glucose feed concentration below 200 g L^{-1} that the redox potential turned from negative to positive values at the moment when glucose was completely utilized. Hence, the redox potential is suitable for fermentation control (Feng et al., 2012).
Liu et al. also discussed the utilization of the redox potential as monitoring parameter for process control in high gravity fermentations (Liu et al., 2016). According to their investigations in 1 L fermentations with *S. cerevisiae SPSC01* and a glucose concentration of either 260 or 300 g L^{-1}, a redox potential value below -200 mV indicates anaerobic conditions with low cell concentrations and yeast viability. In an aerobic fermentation, levels for the redox potential above -50 mV are present combined to biomass increase and high yeast viability. Hence, the range between -200 mV and -50 mV is used for monitoring of micro-aerobic fermentation processes. The redox potential-controlled high gravity fermentation showed the highest ethanol production and optimal glucose utilization.
A similar strategy was applied in a high gravity ethanol fermentation with *S. cerevisiae* NP 01 using sweet sorghum juice with 300 g L^{-1} of total sugar in a 2 L bioreactor (Khongsay et al., 2014). The redox potential was controlled in order to improve ethanol production while optimally using the carbohydrates. The fermentation performance was compared applying no control and control at -100 mV and -150 mV. The best performance was determined at -150 mV with an ethanol production of 134.35 ± 1.67 g L^{-1} (productivity: 2.80 ± 0.03 g L^{-1} h^{-1}). In contrast, the not controlled process reached lower values of only 115.34 ± 2.01 g L^{-1} (productivity: 2.14 ± 0.05 g L^{-1} h^{-1}). Hence, also the fermentation time was reduced in the controlled process by 6 h.
By using inulin as a substrate, high ethanol concentrations can be reached if a redox potential based control is applied in *K. marxianus* (Gao et al., 2016). At a redox potential of -130 mV, which is in the range of the values determined in this study, a high cell viability was determined, leading to a high ethanol concentration and productivity with values of 97.7 g L^{-1} and 2.04 g L^{-1}, respectively. A residual sugar concentration of only 3 g L^{-1} was measured. This group detected differences in the Emden-Meyerhof-Pathway (EMP) and pentose phosphate pathway (PPP) at different values of the redox potential. The carbon flux into the EMP pathway per hour raised due to a higher glucose and fructose

uptake rate at higher redox potential levels. By this, the flux into the PPP increased as well, leading to a higher biomass formation due to the enhanced synthesis of DNA, RNA, lipids, and proteins. Since in the EMP pathway pyruvate - a precursor of ethanol - is synthesized, the formation of ethanol is also enhanced at higher redox potential levels. Additionally, the high carbon flux from the PP pathway back into the EMP pathway at the nodes of fructose-6-phosphate and glycerinaldehyde-3-phosphate increases ethanol formation (Gao et al., 2016). These results correlate with the findings in our studies, in which at the beginning of the fermentation higher redox potential levels (-100 mV in the 3 m^3 scale and 50 to 150 mV in the 170/199 m^3 scale) were determined and the carbohydrate uptake and the ethanol formation were faster than at later fermentation stages with lower redox potential values (-160 to -240 mV in the 3 m^3 scale and -140 to -150 mV in the 170/199 m^3 scale).

6.3.4. The Temperature

The optimal fermentation temperature differs between different yeast strains as explained in the introduction section. The fermentation temperature is important since it influences yeast growth and metabolic activity, biochemical processes, and the fluid flow in a fermenter (Annemüller and Manger, 2009a; Merritt, 1966). Further, the temperature has an impact on the productivity, yield, protein expression, viability and vitality (Choudhary et al., 2016; Li et al., 2001). It was shown that the efficiency of the energy metabolism in the cell, which influences the biomass yield, is temperature-dependent (Zakhartsev et al., 2015). The impact of the temperature is often based on temperature-dependent enzymatic activities (Da Cruz, 2013).

Also the fatty acid content and composition can be influenced by the temperature due to different enzymatic activities. It was found that the total fatty acid composition of *Candida* strains grown at different temperatures differed. The strains grown at 10 °C showed much higher amounts of linoleic acid and lower amounts of oleic acid than those grown at 25°. These strains, however, showed similar contents of total lipids and phosphatides, and similar phosphatide and neutral lipid compositions (Kates and Baxter, 1962). The gradients determined in our studies along the tank height (maximum 0.4 °C) are neglectable in comparison to the applied temperature ranges in the cited study. Additionally, the influence of the cooling systems has to be considered as stated in 2.2.2 and 6.2.

Further, the temperature has a great impact on the composition of volatile flavor compounds, which influence the beer quality (Hiralal et al., 2014; Kanellaki et al., 2014; Olaniran et al., 2011). One of the critical metabolic parameters is the unwanted flavor compound diacetyl, which is produced to a higher extend at higher temperatures. This is also valid for the propagation (Marais, 2010). In order to improve the beer flavor, novel yeast strains were designed that possess a higher tolerance towards low temperatures (Nikulin et al., 2018).

Thermotolerance can be induced by various factors besides heat stress, the cultivation medium and yeast strain. These include certain chemicals, ethanol, sorbic acid, osmotic dehydration, and low external pH-values (Coote et al., 1991; Piper, 1993). The tolerance towards high temperatures in *S. cerevisiae* was found to be the highest at an external pH-value of 4.0. Further investigations revealed that heat tolerance was dependent on the (intracellular) ATPase activity, triggered by the intracellular pH-value (Coote et al., 1991). Heat shock tolerance is further supported by higher intracellular levels of the carbohydrate storage compounds trehalose and glycogen, also known as heat-shock proteins (e.g. > 10 % of biomass dry weight) (Boulton and Quain, 2001a). The thermotolerance can also be increased by genetic and metabolic engineering (Choudhary et al., 2016).

6.3.5. Summary: Gradients in cylindroconical Brewing Tanks

The detected spatial gradients in the investigated brewing processes were rather small. In contrast, spatial substrate (glucose) gradients of up to 40 mg L^{-1} were detected in a fed-batch yeast cultivation of 30 m^3, using three different sampling ports distributed along the reactor height. The magnitude was obviously dependent on the feed position and badly or well mixed reactor zones (Larsson et al., 1996). Gradients of the same magnitude (up to 40 mg L^{-1}) of glucose gradients were detected in a stirred fed-batch *Escherichia coli* cultivation in a 12 m^3 bioreactor with a H/D ratio of 2.5. Aeration was realized by a ring sparger and three Rushton turbines were used for mixing. Samples for glucose measurement were taken at the bottom, middle, and top of the fermenter. The gradients were the highest in the area around the feeding port (top or bottom) (Bylund et al., 1998). This might lead to overflow metabolism, which should be avoided by the fed-batch technique. In simulations of a substrate-limited, aerated yeast fermentation of 22 m^3, gradients in the glucose concentration of even up to 80 mg L^{-1} near the top (feeding zone) and 5 mg L^{-1} at the bottom were determined (Haringa et al., 2017). Unfortunately, information about the magnitude of gradients concerning the parameters measured during this thesis, e.g. pH-value and redox potential, are missing for yeast fed-batch processes.

The gradients in the 3 m^3 scale during this study were determined to be slightly higher than in the 170/199 m^3 scale. One reason might be the placement and number of the active cooling zones, which were two in the 3 m^3 scale and three in the 170/199 m^3 scale. When activated separately at different time points they influence the temperature profile inside the tanks leading to temporary and local temperature gradients, which are not detectable with the presented technique. These gradients provoke an improved convection movement compared to the small scale and finally, a better mixing. Further, the lower H/D ratio in the 170/199 m^3 scale and the sharp conical fermenter bottom enhance the movement of natural convection (Böttcher and Meironke, 2012; Hoggan, 1977), as described above.

The comparison of the gradient formation between the two fermentation processes in the 170/199 m^3 scale did not show any differences, although in the 2nd experiment the tank was flushed with CO_2 via the tank bottom (“bubbling”) after the filling of the tank with several batches was completed. This indicates that no CO_2 addition is necessary to support the natural convection and mixing of the different batches. Based on these results, this standard procedure was removed, saving time and energy. Further, the entrances at the tank dome for the rope and cable hose of the measurement technique were not sealed in the 1st experiment. Hence, a lot of foam was produced and some of the tank content was spilling out of the tank dome. This led to temporary gradient formation in the *on-line* values at around 50 h, probably due to changes in the pressure, which might have influenced the fluid flow and therefore the amounts of cells kept in suspension and the distribution of nutrients (Nienow et al., 2010; Zdaniewicz et al., 2016). These changes, however, could not be proven by measurements.

It also has to be considered that the influence of differences in the natural raw material and the yeast quality during pitching between the batches cannot be distinguished by the measurement technique from other influences. The fermentation performance control and the analysis of *off-line* parameters did not show significant differences in comparison to the 2nd experiment as well, which could have been related clearly to this event.

Important during the evaluation of gradients is the cell response to inhomogeneous conditions. Different strains might accept different minimum gradient levels as a kind of threshold before cell

stress is caused, and a cell response can be observed. Many other fermentation parameters can further affect the cell vitality and therefore, their ability to handle stress conditions. Hence, the cell responses to stress / oscillating conditions can vary.

6.4. *Off-line* Measurements and Correlation Analysis

Beside the stress caused by oscillating conditions, inadequate levels of different parameters (Budroni et al., 2017; Zhao and Bai, 2009) can provoke various stress responses. Among others, these parameters include the *on-line* parameters measured in this study: pH-value, redox potential, temperature, and DO value (see 6.3.). Hydromechanical stress (Daub et al., 2014), hydro-osmotic stress (Rodríguez-González et al., 2017) and substrate gradients (Larsson et al., 1996) as well as substrate limitation or excess (Broach, 2012; Honigberg and Lee, 1998; Zhang and Cao, 2017) are other factors that affect cell viability and vitality. Hydro-osmotic and partial carbon dioxide pressure in the brewing process can influence yeast growth and reproduction as well as the formation of metabolic products, e.g. the amount of alcohols and esters or the DCO_2 concentration during fermentation (Schönberger et al., 2016).

Since many of these factors influence the metabolic activity, protein transport and folding, phosphorylation or other cell functions (Larsson et al., 1996), the concentration of the metabolites analyzed in this study might have also been affected.

In the investigated processes, not many - and if, only small - spatial gradients were determined due to natural convection. These quasi-homogenous conditions allowed the correlation of the *off-line* data obtained by samples taken at only one position with the multi-position *on-line* data at a position close to the sampling port. In the results section, it is demonstrated that the best correlation between *on-line* and *off-line* data was achieved for the extracellular carbohydrates and the sterol content. In contrast, the results concerning the extracellular main carbon metabolites were not satisfactory. For the intracellular main carbon metabolites, no correlations were found at all, although small gradients during the time course were determined, e g. for pyruvate and acetaldehyde. Reasons for this are given in the error analysis regarding the sample preparation (6.4.1.)

6.4.1. Error Analysis

In order to correctly interpret the *off-line* measured data and conduct correlation analysis, possible errors of sample preparation and analysis method have to be discussed.

The sample preparation for the extracellular carbohydrate analysis was the fastest in comparison to the main carbon metabolites sterols. It only consisted of the following steps: filtration of the supernatant, freezing and dilution. Further, no volatile compounds were included, which might have evaporated during the sample preparation. Hence, the number of error sources was low. Since the carbohydrates of interest were present in high concentrations during the whole brewing process, the detection limit of the HPLC was not a limiting factor. The only challenge was the compound separation on the HPLC column due to peak overlapping of the different polysaccharides.

The sample preparation for the extracellular main carbon metabolite analysis was the same as for the carbohydrates. These samples, however, contained volatile compounds of interest, which might have evaporated. Hence, variations in the time of sample preparation could influence the final result.
In order to obtain the intracellular section of main carbon metabolites, many different steps such as inactivation of the metabolic activity, cell disruption, and separation of the metabolites were necessary, which contained the risk of manual errors. The risk of evaporation was even more significant for the intracellular section since the sample preparation according to the protocol took about 35 - 40 min.
For the extra- and intracellular part, the small amount of some substances with values close to or below the detection limit of the available HPLC instrument were challenging. The complex beer matrix further hampered the evaluation of HPLC data since substances were not always clearly separable. Therefore, the correlation of these data will not be discussed in detail in the following.

The sterol sample preparation included even more steps than the preparation for the intracellular main carbon metabolite analysis and lasted longer but did not require any actions directly at the experiment spot, apart from freezing. The steps were performed completely under laboratory conditions. Further, no volatile compounds were included in the analysis. One challenge here was the low cell density in brewing processes compared to yeast fermentations in the laboratory scale, which affected the signal intensity of the GC-FID.

6.4.2. Correlation between extracellular Carbohydrate Concentrations and *on-line* measured Parameters

Oxygen is present only at the onset of the fermentation as described above. In this stage and during propagation oxygen can cause stress as discussed in 6.3.1.
The PCA and loading analysis showed that the DO value has a significance for both PCs in the 170/199 m^3 scale. This shows the influence of the dissolved oxygen on the extracellular carbohydrate concentration at the onset of the fermentation. Since oxygen is important for sterol biosynthesis and membrane functionality (see 6.4.3), it indirectly influences the secretion of carbohydrates through the cell membrane. In the investigated processes, the course of the carbohydrate concentrations during time as well as for the course of the DO value correspond to those reported in the literature (Annemüller and Manger, 2009a). Hence, the impact of the present oxygen was of positive nature.

The pH-value and oscillations in the pH-value do not only influence several features during fermentation as the yeast growth or production rate but also morphological changes (Peña et al., 2015; Timoumi et al., 2017) and the carbohydrate metabolism (Roque et al., 2016; Serra-Cardona et al., 2015). Details concerning the various stress responses are described in 6.3.2.
In our studies, the time-dependent pH changes during the main fermentation were in accordance to the target values and those known from literature, indicating a stable fermentation process. The PCA revealed that the pH-value is closely related to the carbohydrate concentrations in large-scale processes, especially to glucose and fructose. These are the carbohydrates that are utilized at first and therefore even more dependent on fermentation conditions, including the pH-value. Hence, in case of sudden disturbances by local pH gradients the carbohydrate metabolism can be easily affected. These gradients might be formed in horizontal direction, which is not yet accessible with the developed technique.

The PCA of the extracellular carbohydrate concentrations further showed that the loadings of the pH-value and the redox potential can be clustered due to similar loading values. Hence, the influence on the carbohydrate content is similar for both *on-line* parameters and can be explained by their chemical relation.
The redox potential is an indicator for the metabolic activity (Kukec et al., 2002) and can therefore be used as a control parameter (see 6.3.3). Many enzymes require cofactors for the conduction of different redox reactions since they function as electron carriers. In carbohydrate metabolism, the cofactor NADH – formed during glycolysis - is an essential reducing substance for catabolism (Liu et al., 2017). Further, many enzymes are influenced by different reducing and oxidizing agents, such as glutathione and thioredoxin and pH-value altering substances (Liu et al., 2017). Hence, the redox potential is dependent on certain enzyme activities but also has an impact on many enzymes involved in different metabolic activities, including the carbohydrate catabolism. The influence can be seen in the PCA by the similar loading values of the redox potential and the extracellular carbohydrate concentrations.

The fermentation temperature influences many metabolic activities in yeast including the carbohydrate degradation and utilization as presented in 6.3.4. Thermotolerant strains can be of advantage in industrial production. At higher fermentation temperatures (about 40 °C), a more efficient carbohydrate utilization was achieved by the simultaneous saccharification and fermentation in thermotolerant yeast strains (Choudhary et al., 2016). By this, the product yield in lignocellulosic biomass fermentation was increased.
The PCA for the 170/199 m^3 scale revealed that the temperature is only significant for PC 2 in one experiment. Hence, the temperature does not seem to have a great impact on the carbohydrate conversion at the applied fermentation temperatures. In literature it is also reported that lower fermentation temperatures are preferable for most yeast strains to avoid losses in metabolic activity. Heat stress should be avoided or the cells must be adapted stepwise to build up thermotolerance.
The PLS regressions analysis showed that the extracellular carbohydrate content of glucose and fructose correlated very well with the *on-line* data measured in the 170/199 m^3 scale. These regression models include the pH- and DO-value, redox potential beside the temperature. Hence, all parameters contribute and influence the metabolic conversion of carbohydrates and their secretion by intracellular transport mechanisms.

6.4.3. Correlation between Sterol Content and *on-line* measured Parameters

The brewing process becomes anaerobic only several hours after tank filling as described above in the discussion of the *on-line* parameters. Since oxygen is important for sterol biosynthesis (Hu et al., 2017), changes in the DO value could be seen in the sterol content, as investigated in the 3 m^3 and 170/199 m^3 scale. The available oxygen for each single cell might be higher for longer time than the measured values in the broth. The described accumulation of squalene after 50 h and 90 h as well as in the end of the 170/199 m^3 scale, however, indicate oxygen limitation and consequently an impaired activity of the enzymes involved in the post-squalene steps of the ergosterol biosynthesis. The content of the other investigated sterols (zymosterol, lanosterol, ergosterol) instead decreases at later fermentation stages at very low DO levels. In literature, the amount of dissolved oxygen required for sterol biosynthesis is reported to be between 0.1 and 0.3 mg $(g\ cell)^{-1}$ for yeast fermentations and can be up to 0.5 mg $(g\ cell)^{-1}$ in high gravity fermentations (Rosenfeld et al., 2003). During pitching, an aeration

of 4 – 8 ppm should be adjusted depending on the strain and original gravity (Annemüller et al., 2011; Hoggan, 1977).

A lack in available sterols can cause a higher number of cells with impaired vitality (Kucharczyk and Tuszyński, 2017; Verbelen et al., 2009b), e.g. cells with instable membranes or affected transmembrane transport of nutrients and products, such as ethanol. Since some products are toxic to the cells, a high sterol availability and thus membrane integrity is of importance for the cell viability as well. Kodedová et al. deleted several genes involved in ergosterol biosynthesis (ERG 2 – 6) and observed an increased sensitivity to hyperosmotic stress and a lower resistance to antifungal drugs. This emphasizes the importance of the enzymes involved in sterol synthesis for yeast vitality and stress management (Kodedová and Sychrová, 2015).
The sterol content in connection to available oxygen is also related to the aroma profile of beer, e.g. concerning the concentration of esters (Thiele, 2006) or acetaldehyde and higher alcohols (Kucharczyk and Tuszyński, 2017). It was reported that an addition of oxygen during the stationary phase in a medium with an ergosterol and oleic acid excess increased the specific fermentation rate and cell viability. On the other side, the fermentation time was decreased (Rosenfeld et al., 2003).

The PCA of this work also shows the relation of the sterol content to the DO values in the large-scale of 170/99 m^3 (0). The loadings of the DO value are closely located to the loadings of the pH-value and redox potential and the intermediates zymosterol and lanosterol for the total and free part (Fig. 56). This relation can be explained by the high oxygen requirement of 10 O_2 molecules for the steps until the synthesis of zymosterol (Maczek, 2009; Rosenfeld et al., 2003). This theory is further strengthened when comparing both experiments at the large-scale (170/199 m^3), of which only in the 1st one a disturbance due to the release of foam through an unsealed opening in the tank dome occurred. Apart from the high foam formation, the transfer of about 13.5 m^3 through the lower part of the tall tank at about 54 h might have changed the pressure in the tank and therefore influenced the amount of DCO_2. Consequently, the amount of rising bubbles in the tank might have changed as well leading to a different mixing behavior and parameter distribution, such as the amount of DO in the beginning of the process or nutrients and other metabolites. This can be seen in the PCA since the values of the DO loadings are different between the two experiments, especially concerning the free sterol content. The precursor squalene and the product ergosterol instead, are not related to the DO value but contribute to the second component with a higher amount than the intermediates, indicating their importance for the correlation analysis and model setup based on their metabolic relevance. The DO value in the 3 m^3 scale was zero during the whole time and can therefore not be correlated.

It can be seen that the course (accumulation or decrease) of ergosterol in the 3 m^3 scale and after 50 h in the 170/199 m^3 scale for the total content is similar to this of squalene.
According to the literature, the ergosterol content should decrease at lower oxygen availability (as shown by the *on-line* DO measurements), while squalene should accumulate since the pre-squalene pathways do not require oxygen (Hu et al., 2017). At lower fermentation temperatures (< 12 °C) as they were applied in the presented fermentations, however, the main carbon metabolism is decelerated. This leads to a slower conversion of squalene to ergosterol and could explain the delayed decrease in ergosterol. Investigation with hybrids of *S. cerevisiae* and *S. eubayanus* revealed that the concentrations of ergosterol was dependent on the fermentation temperature (tested at 10 and 20 °C) and the strain composition (Krogerus et al., 2017).
Another explanation for similar values of ergosterol to squalene in the experiments (after about 50 h for the total sterol content in the 170/199 m^3 scale) could be the esterification of ergosterol as a

storage compound since this step does not require oxygen (Boulton and Quain, 2001b). This hypothesis is supported by the difference between the determined total and free ergosterol content as this equals the content of esterified sterols. It was especially large in the 3 m^3 scale with up to 0.4 mmol (g cell)$^{-1}$. The levels of total and free squalene content instead, are mostly the same since squalene cannot be esterified due to the lacking hydroxyl group (Maczek, 2009). Differences for squalene in the smaller scale might be caused by the complex sterol sample preparation. With fermentation time, the content of esterified ergosterol is decreasing in the 3 m^3 scale, indicated by the decrease of the difference between total and free ergosterol content. It was revealed in a study that in case of the inhibition of sterol esterification the sterol biosynthesis is impaired as well, leading to a decrease of the total intracellular sterol content (Arthington-Skaggs et al., 1996).
Furthermore, the expression of certain enzymes, involved at the different steps of the ergosterol biosynthesis (see Fig. 3) might be affected by various process conditions like pressure, osmotic stress, high DCO_2 levels, or oxygen and nutrient limitation. Oxygen depletion during propagation and pitching is a challenge in the anaerobic brewing process. Higher expression levels of certain enzymes important for sterol biosynthesis, e.g. ERG1 (squalene epoxidase) and ERG11 (Lanosterol 14-alpha-demethylase), were observed in an *S. cerevisiae* ale yeast strain only during oxygenation, resulting in higher ergosterol contents (Verbelen et al., 2009a). The yeast was fermented in deaerated sterile wort (DO < 0.5 mg L^{-1}, 12 °P) at 22 °C in 2 L tubes (75 cm tall, 8 cm inner diameter). Before pitching, the yeast was pre-oxygenated for 1, 2, 3, 5, and 8 h in a membrane loop reactor at 20 °C, in which 3 L of the yeast suspension were circulated for the denoted time at 750 mL min^{-1}, respectively. The target oxygen concentration of 8 mg L^{-1} in the yeast suspension was reached by the supply of oxygen with a membrane sparger. The relation between ergosterol biosynthesis and ERG1 under aerobic conditions was confirmed by another group, who down-regulated this enzyme, leading to the accumulation of the precursor squalene (Garaiová et al., 2014).
The group of Garaiová (2014) achieved even higher levels of squalene under anaerobic conditions by the depletion of ergosterol. This phenomenon is explained with the feedback inhibition of the pre-squalene pathway by ergosterol. Hence, higher levels of ergosterol in the presented results of this thesis might have led to a decrease in squalene. Further, squalene can also be utilized as carbon source and metabolized for maintenance under anaerobic conditions (Bhattacharjee et al., 2001).
Changes in the lipid fraction in the yeast strain *S. carlsbergensis* as a stress response to stress conditions during fermentation were investigated with yeast cells reused one, two, and three times in an industrial brewing process. The ergosterol content increased from originally 0.40 mg g^{-1} of DCW without re-pitching to 0.64 mg g^{-1} of DCW after the 3rd usage, indicating an adaptation of the sterol composition to stress parameters (Rupčić et al., 2010).

Beside the influence of oxygen on the sterol and unsaturated fatty acid synthesis, it has an impact on the cell vitality, stress regulation, and fermentation performance as elucidated in the introduction. The exposure too high levels of oxygen in the further fermentation course, however, can be of disadvantage due to high cell growth and low ethanol production (Briggs et al., 2004). An aeration of 0.2 vvm can be regarded as over supplementation (Liu et al., 2016). Over aeration during propagation can also influence the fermentation performance at later stage because the propagated yeast tends to form high levels of foam (Hoggan, 1977). It was also shown by electrochemical measurements that a second aeration or extensive aeration at the beginning of the process can damage the substrate and hence influence the redox potential in the final beer and its quality (Burkert, 2005).

The relation of the pH-value and alteration of the sterol composition due to stress adaption was shown by Kamthan et al. An adaption to a low pH-value (2.8) and the acquisition of tolerance towards the inorganic acid HCl by the alteration of the sterol composition was also observed in *S. cerevisiae* (Fletcher et al., 2017). By this mechanism, acidophilic yeasts are able to produce the ATP amount required for growth by respiration at high glucose concentrations and low pH-values (Fletcher et al., 2015). In case of acetic acid stress (50 mM at pH = 4.0), changes in membrane lipid and sterol composition can be ascribed to changes in phosphorylation of different phosphoproteins involved in lipid and sterol metabolism (Guerreiro et al., 2017).

The PCA showed that the loadings of the pH-value and the redox potential have similar values, indicating their close relation and similar influence on the sterol content. The importance of the redox potential for the maintenance of anaerobic conditions and the relation to the pH-value is discussed above (section 6.3.3).

The temperature also affects the sterol biosynthesis. The PLS regression analysis revealed, that the correlation of the sterol content to the *on-line* data set (pH-value, redox potential, DO, temperature) in the 170/199 m^3 scale showed much better correlation (see below). The reason might be the lower fermentation temperature in the larger scale, indicating that the temperature has an impact on sterol formation or more precise, on the enzyme activity and stress management involved in sterol biosynthesis.
The results of the following two studies also showed a connection. A change in sterol composition, from ergosterol to fecosterol, was detected by Caspeta et al. at high temperature (≥ 40 °C) in strains with improved growth and ethanol production (Caspeta et al., 2014). These changes were caused by enhanced expression of genes connected to sterol biosynthesis and mutations in the genes of the membrane associated enzyme (C-5 sterol desaturase). Of special importance for the development of thermo-tolerance are changes in the sterol metabolism. Since sterols are essential for the regulation of membrane fluidity and lipid composition, connected functions such as vesicular sorting and transport, cytoskeleton organization, asymmetric growth, and the activity of membrane bound enzymes are affected as well by high temperatures. Hence, they require fast stress adaption by altering the sterol composition (Caspeta et al., 2014).
An increased tolerance towards high or very low temperatures, high ethanol concentrations, and low pH-values in a fission yeast when the expression of the C-5 sterol desaturase was increased (Kamthan et al., 2017). The enzyme expression level and hence, also the level in tolerance increased by about 5-fold at either exposure to low pH conditions (pH = 3.0 instead of 5.2) after 4 - 6 h or with a temperature shift from 23 to 4 °C after 6 h. These are conditions are similar to those of the brewing process and might be the explanation for adaption of the yeast cells to these conditions and increased tolerance to these harsh conditions.

In the PLS regressions analysis, the sterol content correlated well with the measured *on-line* data, especially concerning the 1st experiment of the 170/199 m^3 scale. The reasons for the good correlations, especially in the 1st experiment, are described above for the PCA. Good correlations were also found in the second experiment for the free ergosterol content, which is of special importance for the membrane integrity and fluidity. Since these regression models include the pH- and DO value, redox potential, and temperature, their correlation to ergosterol indicates the relation of the sterol biosynthesis to the mentioned process parameters. Further, these parameters influence enzyme activity also concerning sterol biosynthesis - and intracellular transport mechanisms.

The locus of sterol biosynthesis differs from their final deposition in yeast cells. Free sterols are synthesized in the plasma membrane, with ergosterol showing the highest concentration (Zinser et al., 1993). Esterification of sterols instead, takes place in the endoplasmic reticulum and they are stored in lipid particles. This requires intramembrane transport of the steryl esters, which is influenced by the presence of unsaturated fatty acids. Since these are oxygen-dependent (Boulton and Quain, 2001b), it is likely that the DO-value, monitored *on-line,* influences the sterol transport mechanisms, including related enzyme activities.

Nevertheless, more investigations concerning the relation of the sterol content and process parameters are necessary. A correlation analysis considering each single *on-line* parameter would give more information concerning the predictability. Further, more sterol intermediates should be included in the analysis in order to follow the sterol biosynthesis and the relation to other parameters in more detail., e.g. to identify potential limitations.

7. Conclusion

This thesis presents the development of mobile multi-parameter sensor tools and proves their applicability in unstirred large-scale brewing tanks with a volume of up to 200 m^3. A new approach of this technique is the mobile application of multiple sensors directly in the core of the liquid phase of large-scale reactors. This improves process monitoring and increases the knowledge about heterogeneities and critical reactor zones. The identification of critical process phases was shown for the filling phase in the 170/199 m^3 scale. The brewery eliminated a process step after the filling phase based on the results obtained by the mobile sensor technique.

The determined spatial gradients in the investigated brewing processes were - in contrast to the expectations - rather small, even in the largest scale. In contrast, spatial substrate (glucose) gradients of up to 40 - 80 mg L^{-1} were detected in stirred industrial-scale fed-batch processes and simulations with yeast and bacteria (see 6.3). Hence, the natural convection movement in cylindroconical brewing vessels, which is mainly caused by CO_2 bubble formation and temperature gradients, is sufficient for mixing large-scale reactors.

The mobile multi-parameter sensor technology is not yet easily applicable for any kind of reactor. The constructions for the installation of the technique on the tank dome were adapted for each tank individually. Hence, the system must be optimized for plug-and-play-applications in industry. All parts of the sensor monitoring tool must be modularized and simplified in order to facilitate a fast integration into various tanks with different accessibilities. Further, for the investigation of the liquid phase in radial direction, a monitoring and sampling technique that is applicable in both, vertical and horizontal direction, is required.

The determination of the influence of local gradients on the cell and thus, the process, is of high importance as presented in the scientific background section. The correlation analysis for the identification of parameter dependencies, conducted in this thesis, is a first step towards this. There is, however, a great potential for the application of other process analytical tools.

8. Outlook

Beside the optimization of the mobile multi-parameter sensor tool towards a plug-and-play-solution, there is more potential for improvement. The integration of more than three commercially available sensors into the large sensor housing unit would be beneficial. The stainless steel area between the sensors could be reduced. Further, the unit could be longer for the application in large-scale reactors. Thus, additional sensors could be integrated with an offset (below or above) to the existing unit since in the scale of several 100 m^3 a few centimeters of distance are not significant. An increase in diameter is disadvantageous for the application in closed tanks as the technique hast to be inserted through permanently installed openings with a limited diameter.

Sensors suitable for the integration into submergible units and the application in large-scale tanks, which requires a data transfer across long distances, are still not available for many parameters. Anyhow, sensors for the viable biomass and optical density are currently under development towards this purpose (ARC-Series from Hamilton Germany GmbH) and are hopefully available soon.

A fourth sensor, suitable for the integration in such a mobile sensor unit, is already available for conductivity measurements. Monitoring of this parameter is of interest for mixing and homogenization processes. It was already applied in biogas fermenters, providing information about the relative spatial ion distribution in the fermenter.
The development of sensors for *in-situ* DCO_2 determination of higher concentrations (e.g. like in the brewing process) is very challenging. Sensor developing companies try this already for several years. Such a sensor would be of great benefit, not only for the brewing industry but also for other ethanol producing fermentations, e.g. the production of biofuels, or in cell culture.

By using a guide bar, the developed technique can also be applied in stirred processes in future. It is further applicable in reactors that are mixed by air circulation systems instead of mechanical agitation with a stirrer, e.g. in bubble columns or air lift reactors as well as in reactors with the Vogelbusch system, which are equipped with a gassing hollow stirrer at the reactor bottom for air sparging.

A wireless data transfer would be also a great advantage in future. This is, however, a big challenge in processes with high gas formation like the brewing process since gas bubbles hinder the signal to propagate through the liquid as it was shown for the localization system based on ultrasound signals. The identification of a new approach for a localization system is also a future task.

For the application of the sensor technique in processes with larger gradients, such as fed-batch processes, a multi-position sampling is essential. Data correlation in this thesis using *off-line* data from a single sampling point was only feasible because the tanks were determined to be quasi-homogenous. If this is not the case, samples must be collected at various positions, preferably close to the sensor location. A multi-position sampling system was already developed for biogas plants. This system, however, requires retrofitting of the fermenters, which is not feasible for food or beverage production tanks due to the risk of contamination and good manufacturing practice regulations. Hence, it must be a system, which is insertable via permanently installed tank openings.

In some experiments in the 3 m^3 scale of this work, cell physiological and vitality analyses were performed by four parameter flow cytometry (data not shown). The application of such technique, however, requires short distances between sampling site and instrument. This was not given for most

of the experiments in this thesis. In order to increase the knowledge about the impact of heterogeneities or other stress inducing factors on the cell physiology and vitality, it would be of great benefit to have such devices installed close to the production site.

Regarding the multivariate data analysis, the consideration of single *on-line* parameters during correlation analysis would give more information about the predictability of *off-line* data. Model-based methods, such as CFD and kinetic models, can be applied in future and compared to the experimental data obtained in this thesis.

References

Aabo, T., Glückstad, J., Siegumfeldt, H. and Arneborg, N., 2011. Intracellular pH distribution as a cell health indicator in *Saccharomyces cerevisiae*. J R Soc Interface, 8(64): 1635-1643.

Abdel-Banat, B.M.A., Hoshida, H., Ano, A., Nonklang, S. and Akada, R., 2010. High-temperature fermentation: how can processes for ethanol production at high temperatures become superior to the traditional process using mesophilic yeast? Appl Microbiol Biot, 85(4): 861-867.

Aber-Instruments, 2015. Understanding viable cell biomass in SUB using *in-line* capacitance for PAT control (Webinar). Aber-Instruments Ltd.

Adams, W.J., 2006. Markets - beer in Germany and the United States. J Econ Perspect, 20(1): 189-205.

Adler, V., Yin, Z.M., Tew, K.D. and Ronai, Z., 1999. Role of redox potential and reactive oxygen species in stress signaling. Oncogene, 18(45): 6104-6111.

Aït-Sahalia, Y. and Xiu, D., 2017. Principal component analysis of high frequency data. Journal of the American Statistical Association: 51 pp.

Åkesson, M., Hagander, P. and Axelsson, J.P., 2001. Avoiding acetate accumulation in *Escherichia coli* cultures using feedback control of glucose feeding. Biotechnol Bioeng, 73(3): 223-230.

Al Khamici, H., Hossain, K., Cornell, B. and Valenzuela, S., 2016. Investigating sterol and redox regulation of the ion channel activity of CLIC1 using tethered bilayer membranes. Membranes, 6(4): 51-64.

Alford, J.S., 2006. Bioprocess control: Advances and challenges. Computers and Chemical Engineering, 30(10–12): 1464-1475.

Alpha-Laval, 2003. Rotary jet advantages - using Iso-Mix technology in breweries.

Alpha-Laval, 2010. Mixing in beer fermenters with Alfa Laval Iso-Mix rotary jet mixers

Alupoaei, C.E. and Garcia-Rubio, L.H., 2005. An interpretation model for the UV-VIS spectra of microorganisms. Chem Eng Commun, 192(2): 198-218.

Alupoaei, C.E. and García-Rubio, L.H., 2004. Growth behavior of microorganisms using UV-Vis spectroscopy: *Escherichia coli*. Biotechnol Bioeng, 86(2): 163-167.

Alupoaei, C.E., Olivares, J.A. and Garcia-Rubio, L.H., 2004. Quantitative spectroscopy analysis of prokaryotic cells: Vegetative cells and spores. Biosensors and Bioelectronics, 19(8): 893-903.

Amanullah, A., Buckland, B.C. and Nienow, A.W., 2004. Chapter 18: Mixing in the fermentation and cell culture industries, Handbook of Industrial Mixing: Science and Practice. John Wiley & Sons, Inc., pp. 1071-1170.

Anderson, J.D., 2009. Part I. In: J.F. Wendt (Editor), Computational Fluid Dynamics - An Introduction, Part I. Springer-Verlag, Rhode-Saint-Genèse, Belgium, pp. 333.

Anderson, R.G. and Kirsop, B.H., 1974. The control of volatile ester synthesis during the fermentation of wort of high specific gravity. Journal of the Institute of Brewing, 80(1): 48-55.

Annemüller, G., Manger, H.-J. and Lietz, P., 2011. The yeast in the brewery - management, pure yeast cultures, propagation. Versuchs- u. Lehranstalt f. Brauerei (VLB).

Annemüller, G. and Manger, H.J., 2009a. Beer fermentation and maturation: Basics, technology, industrial manufacturing equipment (Original: Gärung und Reifung des Bieres: Grundlagen, Technologie, Anlagentechnik). VLB Berlin, PR- und Verlagsabteilung.

Annemüller, G. and Manger, H.J., 2009b. Chapter 1.1.: Sub-processes of beer fermentation and storage (Original: Teilprozesse der Biergärung und -reifung), Beer Fermentation and Maturation: Basics, Technology, Industrial Manufacturing Equipment (Original: Gärung und Reifung des Bieres: Grundlagen, Technologie, Anlagentechnik). VLB Berlin, PR- und Verlagsabteilung.

Annemüller, G. and Manger, H.J., 2009c. Chapter 1.3.: Conventional fermentation and maturation and modern large-scale technologies (Original: Klassische Gärung und Reifung und moderne Großtanktechnologie), Beer Fermentation and Maturation: Basics, Technology, Industrial

Manufacturing Equipment (Original: Gärung und Reifung des Bieres: Grundlagen, Technologie, Anlagentechnik). VLB Berlin, PR- und Verlagsabteilung.

Annemüller, G. and Manger, H.J., 2009d. Chapter 2.12: Yeast harvest (Original: Hefeernte), Beer Fermentation and Maturation: Basics, Technology, Industrial Manufacturing Equipment (Original: Gärung und Reifung des Bieres: Grundlagen, Technologie, Anlagentechnik). VLB Berlin, PR- und Verlagsabteilung.

Annemüller, G. and Manger, H.J., 2009e. Chapter 3: Conversion of substances and changes during the fermentation (Original: Stoffumwandlungen und Veränderungen während der Gärung), Beer Fermentation and Maturation: Basics, Technology, Industrial Manufacturing Equipment (Original: Gärung und Reifung des Bieres: Grundlagen, Technologie, Anlagentechnik). VLB Berlin, PR- und Verlagsabteilung.

Annemüller, G. and Manger, H.J., 2009f. Chapter 4: By-products of fermentation and maturation and their importance for the beer quality (Original: Nebenprodukte der Gärung und Reifung und ihre Bedeutung für die Qualität des Bieres), Beer Fermentation and Maturation: Basics, Technology, Industrial Manufacturing Equipment (Original: Gärung und Reifung des Bieres: Grundlagen, Technologie, Anlagentechnik). VLB Berlin, PR- und Verlagsabteilung.

Annemüller, G. and Manger, H.J., 2009g. Chapter 5: Important technological and technical parameters for the regulation of the fermentation and storage (Original: Wichtige technologische und technische Einflussfaktoren zur Steuerung der Gärung und Reifung), Beer fermentation and maturation: Basics, technology, industrial manufacturing equipment (Original: Gärung und Reifung des Bieres: Grundlagen, Technologie, Anlagentechnik). VLB Berlin, PR- und Verlagsabteilung.

Annemüller, G. and Manger, H.J., 2009h. Chapter 6: Classical procedures of fermentation and maturation (Original: Klassische Verfahren der Gärung und Reifung), Beer Fermentation and Maturation: Basics, Technology, Industrial Manufacturing Equipment (Original: Gärung und Reifung des Bieres: Grundlagen, Technologie, Anlagentechnik). VLB Berlin, PR- und Verlagsabteilung.

Annemüller, G. and Manger, H.J., 2009i. Chapter 8: Optimization of the discontinuous fermentation by the application of cylindroconical tanks (Original: Optimierung der diskontinuierlichen Gärung durch die Anwendung von zylindrokonischen Tanks), Beer Fermentation and Maturation: Basics, Technology, Industrial Manufacturing Equipment (Original: Gärung und Reifung des Bieres: Grundlagen, Technologie, Anlagentechnik). VLB Berlin, PR- und Verlagsabteilung.

Annemüller, G. and Manger, H.J., 2009j. Chapter 11: Top fermenting beers and characteristics of top fermentation (Original: Obergärige Biere und Besonderheiten der Obergärung), Beer Fermentation and Maturation: Basics, Technology, Industrial Manufacturing Equipment (Original: Gärung und Reifung des Bieres: Grundlagen, Technologie, Anlagentechnik). VLB Berlin, PR- und Verlagsabteilung.

Apetrei, C. et al., 2010. Combination of an e-nose, an e-tongue and an e-eye for the characterisation of olive oils with different degree of bitterness. Anal Chim Acta, 663(1): 91-97.

Arnoux, A.S., Belloy, L., Esteban, G., Teissier, P. and Ghommidh, C., 2004. *On-line* monitoring of lactic acid bacteria by an impedance sensor, 9th International Congress on Engineering and Food, Montpellier, France.

Arnoux, A.S., Preziosi-Belloy, L., Esteban, G., Teissier, P. and Ghommidh, C., 2005. Lactic acid bacteria biomass monitoring in highly conductive media by permittivity measurements. Biotechnol Lett, 27(20): 1551-1557.

Arthington-Skaggs, B.A., Crowell, D.N., Yang, H., Sturley, S.L. and Bard, M., 1996. Positive and negative regulation of a sterol biosynthetic gene (ERG3) in the post-squalene portion of the yeast ergosterol pathway. Febs Lett, 392(2): 161-165.

Ault, R.G., 1965. Spoilage bacteria in brewing - a review. Journal of the Institute of Brewing, 71(5): 376-391.

Badotti, F. et al., 2008. Switching the mode of sucrose utilization by *Saccharomyces cerevisiae*. Microb Cell Fact, 7: 4-15.

Bailey, R.B. and Parks, L.W., 1975. Yeast sterol esters and their relationship to the growth of yeast. J Bacteriol, 124(2): 606-612.

Bamforth, C., 2016. Brewing Materials and Processes: A Practical Approach to Beer Excellence. Elsevier Science, 341 pp. pp.

Bamforth, C.W., 2006. 8.3 Propagation, Brewing: New Technologies. Woodhead Pub.

Banerjee, R., 2012. Redox outside the box: Linking extracellular redox remodeling with intracellular redox metabolism. J Biol Chem, 287(7): 4397-4402.

Barbosa, A.D. et al., 2015. Lipid partitioning at the nuclear envelope controls membrane biogenesis. Mol Biol Cell, 26(20): 3641-3657.

Batchuluun, E., Mansberger, I., Rauh, C. and Delgado, A., 2014. Optimization of fermentation and maturation phases in beer production by adaptive flow design, 10th International Trends in Brewing, Genth, Belgium.

Batchuluun, E., Mansberger, I., Rauh, C., Lopez-Ramirez, E. and Delgado, A., 2011. Optimization of fermentation and maturation phases in beer production by the use of adaptive flow design, Congress about Laser Methods in Fluid Measurement Techniques (Original: "Fachtagung Lasermethoden in der Strömungsmesstechnik"), Ilmenau, Germany, pp. 7 pp.

Becker, T., Enders, T. and Delgado, A., 2002. Dynamic neural networks as a tool for the *on-line* optimization of industrial fermentation. Bioproc Biosyst Eng, 24(6): 347-354.

Becker, T. et al., 2007. Future aspects of bioprocess monitoring. In: R. Ulber and D. Sell (Editors), White Biotechnology. Advances in Biochemical Engineering/Biotechnology. Springer Berlin Heidelberg, pp. 249-293.

Becker, T. and Krause, D., 2010. Softsensor systems - mathematics as a bonding element to the process course (Original: Softsensorsysteme – Mathematik als Bindeglied zum Prozessgeschehen). Chemie Ingenieur Technik, 82(4): 429-440.

Becker, T., Mitzscherling, M. and Delgado, A., 2001. Ultrasonic velocity – a noninvasive method for the determination of density during beer fermentation. Eng Life Sci, 1(2): 61-67.

Becker, T. and Tippmann, J., 2016. 500 Years of purity law - process technology for beer by Prof. Dr.-Ing. Thomas Becker and Dr.-Ing. Johannes Tippmann, Professorial chair of brewing and beverage technology, Technical University Munich. Chemie Ingenieur Technik, 88(12): 1847-1847.

Bhattacharjee, P., Shukla, V.B., Singhal, R.S. and Kulkarni, P.R., 2001. Studies on fermentative production of squalene. World Journal of Microbiology and Biotechnology, 17(8): 811-816.

Birle, S., Hussein, M.A. and Becker, T., 2015. *On-line* yeast propagation process monitoring and control using an intelligent automatic control system. Eng Life Sci, 15(1): 83-95.

Bisson, L.F., Coons, D.M., Kruckeberg, A.L. and Lewis, D.A., 1993. Yeast sugar transporters. Critical Reviews in Biochemistry and Molecular Biology, 28(4): 259-308.

Blagovic, B., Rupcic, J., Mesaric, M., Georgiu, K. and Maric, V., 2001. Lipid composition of brewer's yeast. Food Technol Biotech, 39(3): 175-181.

Blanco, C.A., de la Fuente, R., Caballero, I. and Rodríguez-Méndez, M.L., 2015. Beer discrimination using a portable electronic tongue based on screen-printed electrodes. J Food Eng, 157(Supplement C): 57-62.

Bockisch, A. et al., 2014. *In-situ* investigation of the liquid phase in industrial yeast fermentations with mobile multi-parameter sensors. Chemie Ingenieur Technik, 86(9): 1582-1582.

Boone, C.H.T., Grove, R.A., Adamcova, D., Braga, C.P. and Adamec, J., 2016. Revealing oxidative damage to enzymes of carbohydrate metabolism in yeast: An integration of 2D DIGE, quantitative proteomics, and bioinformatics. Proteomics, 16(13): 1889-1903.

Borkmann, K., Müke, O., Manger, H.-J., Annemüller, G. and Schade, W., 1978. About the fermentation and maturation technology in stand-alone large-scale fermenters (Original: Zur Technologie der Gärung und Reifung im freigebauten Großraumfermenter). Brauwissenschaft, 31(3).

Boswell, C.D., Nienow, A.W., Gill, N.K., Kocharunchitt, S. and Hewitt, C.J., 2003a. The impact of fluid mechanical stress on *Saccharomyces cerevisiae* cells during continuous cultivation in an

agitated, aerated bioreactor; its implication for mixing in the brewing process and aerobic fermentations. Food and Bioproducts Processing, 81(1): 23-32.

Boswell, C.D., Nienow, A.W. and Hewitt, C.J., 2002. Studies on the effect of mechanical agitation on the performance of brewing fermentations: Fermentation rate, yeast physiology, and development of flavor compounds. J Am Soc Brew Chem, 60(3): 101-106.

Boswell, C.D., Varley, J., Boon, L., Hewitt, C.J. and Nienow, A.W., 2003b. Studies on the impact of mixing in brewing fermentation - Comparison of methods of effecting enhanced liquid circulation. Food and Bioproducts Processing, 81(C1): 33-39.

Böttcher, K. and Meironke, H., 2012. Determining of velocity fields during real and experimental simulated beer fermentations by UDV and LDA. Proceedings in Applied Mathematics and Mechanics (PAMM), 12(1): 559-560.

Boulton, C. and Nordkvist, M., 2011. Improved management of large capacity fermentations, 13th Africa Section Conference - Uganda 2011, Uganda.

Boulton, C. and Nordkvist, M., 2014. A stable platform for control of fermentation, 11th International Trends in Brewing Symposium - VitalSensors Ghent, Belgium.

Boulton, C. and Quain, D., 2001a. Chapter 2.2: Beer types. In: C. Boulton and D. Quain (Editors), Brewing Yeast and Fermentation Blackwell Science Ltd.

Boulton, C. and Quain, D., 2001b. Chapter 3.5.: Synthesis of sterols and unsaturated fatty acids. In: C. Boulton and D. Quain (Editors), Brewing Yeast and Fermentation Blackwell Science Ltd.

Boulton, C. and Quain, D., 2001c. Chapter 3.7: Formation of flavour compounds. In: C. Boulton and D. Quain (Editors), Brewing Yeast and Fermentation Blackwell Science Ltd.

Boulton, C. and Quain, D., 2001d. Chapter 5.1: General properties of fermentation Vessels. In: C. Boulton and D. Quain (Editors), Brewing Yeast and Fermentation Blackwell Science Ltd.

Boulton, C.A., 1991. Developments in brewery fermentation. Biotechnology and Genetic Engineering Reviews, 9(1): 127-181.

Brányik, T., Vicente, A., Cruz, J.M. and Teixeira, J., 2002. Continuous primary beer fermentation with brewing yeast immobilized on spent grains. Journal of the Institute of Brewing, 108(4): 410-415.

Brányik, T., Vicente, A.A., Dostálek, P. and Teixeira, J.A., 2005. Continuous beer fermentation using immobilized yeast cell bioreactor systems. Biotechnol Progr, 21(3): 653-663.

Briggs, D.E., Boulton, C.A., Brookes, P.A. and Stevens, R., 2004. Chapter 15: Beer maturation and treatment, Brewing Science and Practice. Woodhead Publishing Limited, Cambridge.

Brischwein, M. et al., 2003. Functional cellular assays with multi-parametric silicon sensor chips. Lab Chip, 3(4): 234-240.

Broach, J.R., 2012. Nutritional control of growth and development in yeast. Genetics, 192(1): 73-105.

Brown, D.G. and Jaffé, P.R., 2001. Effects of nonionic surfactants on the UV/visible absorption of bacterial cells. Biotechnol Bioeng, 74(6): 476-482.

Budroni, M., Zara, G., Ciani, M. and Comitini, F., 2017. *Saccharomyces* and *non-Saccharomyces* starter yeasts. In: M. Kanauchi (Editor), Brewing Technology. InTech, Rijeka, pp. Ch. 04.

Buhligen, F. et al., 2014. Analysis of aging in lager brewing yeast during serial re-pitching. J Biotechnol, 187: 60-70.

Burkert, J., 2005. Evaluation of beer quality by different reduction classes. (Original: Beurteilung der Bierqualität anhand unterschiedlicher Reduktonklassen). Doctoral Thesis, Technische Universität München, München, 248 pp.

Bylund, F., Collet, E., Enfors, S.-O. and Larsson, G., 1998. Substrate gradient formation in the large-scale bioreactor lowers cell yield and increases by-product formation. Bioprocess Engineering, 18(3): 171-180.

Caballero, B., Finglas, P.M. and Toldrá, F., 2016. Encyclopedia of food and health. Choice: Current Reviews for Academic Libraries, 53(8): 1146-1147.

Caballero, I., Blanco, C.A. and Porras, M., 2012. Iso-alpha-acids, bitterness and loss of beer quality during storage. Trends Food Sci Tech, 26(1): 21-30.

Carvell, J. et al., 2016. Monitoring live biomass in disposable bioreactors. Biopharmaceutical Fill and Finish: Technical and Operating Challenges for the Latest Formulations and Devices. BioProcess International

Caspeta, L. et al., 2014. Altered sterol composition renders yeast thermotolerant. Science, 346(6205): 75-78.

Castritius, S., Geier, M., Jochims, G., Stahl, U. and Harms, D., 2012. Rapid determination of the attenuation limit of beer using middle-infrared (MIR) spectroscopy and a multivariate model. J Agr Food Chem, 60(25): 6341-6348.

Ceriotti, L. et al., 2007. *On-line* monitoring of BALB/3T3 metabolism and adhesion with multi-parametric chip-based system. Anal Biochem, 371(1): 92-104.

Cernuda, C. et al., 2017. Improved quantification of important beer quality parameters based on nonlinear calibration methods applied to FT-MIR spectra. Anal Bioanal Chem, 409(3): 841-857.

Chang, Q., Randers-Eichhorn, L., Lakowicz, J.R. and Rao, G., 1998. Steam-Sterilizable, Fluorescence Lifetime-Based Sensing Film for Dissolved Carbon Dioxide. Biotechnology Progress, 14(2): 326-331.

Chen, L.Z., Nguang, S.K., Li, X.M. and Chen, X.D., 2004. Soft sensors for *on-line* biomass measurements. Bioproc Biosyst Eng, 26(3): 191-195.

Chen, X., Hussein, M. and Becker, T., 2017. Determination of bubble size distribution in gas–liquid two-phase systems via an ultrasound-based method. Eng Life Sci, 17(6): 653-663.

Cheng, C., Zhang, M., Xue, C., Bai, F. and Zhao, X., 2017. Development of stress tolerant *Saccharomyces cerevisiae* strains by metabolic engineering: New aspects from cell flocculation and zinc supplementation. Journal of Bioscience and Bioengineering, 123(2): 141-146.

Chicoye, E., Helbert, J.R. and Rice, J.F., 1978. Accelerated fermentation of lager beer. Google Patents.

Choudhary, J., Singh, S. and Nain, L., 2016. Thermotolerant fermenting yeasts for simultaneous saccharification fermentation of lignocellulosic biomass. Electron J Biotechn, 21: 82-92.

Claßen, J., Aupert, F., Reardon, K.F., Solle, D. and Scheper, T., 2017. Spectroscopic sensors for *in-line* bioprocess monitoring in research and pharmaceutical industrial application. Anal Bioanal Chem, 409(3): 651-666.

Clementschitsch, F. and Bayer, K., 2006. Improvement of bioprocess monitoring: development of novel concepts. Microb Cell Fact, 5: 19-30.

Colen, L. and Swinnen, J., 2016. Economic growth, globalisation and beer consumption. Journal of Agricultural Economics, 67(1): 186-207.

Cutaia, A.J., Reid, A.-J. and Speers, R.A., 2009. Examination of the relationships between original, real and apparent extracts, and alcohol in pilot plant and commercially produced beers. Journal of the Institute of Brewing, 115(4): 318-327.

Da Cruz, A.L.B., 2013. Temperature Impact on Yeast Metabolism: Insights from Experimental and Modeling Approaches (book).

Dack, R.E., Black, G.W., Koutsidis, G. and Usher, S.J., 2017. The effect of Maillard reaction products and yeast strain on the synthesis of key higher alcohols and esters in beer fermentations. Food Chem, 232(Supplement C): 595-601.

Daoud, I.S. and Searle, B.A., 1990. *On-line* monitoring of brewery fermentation by measurement of CO_2 evolution rate. Journal of the Institute of Brewing, 96(5): 297-302.

Daub, A. et al., 2014. Characterization of hydromechanical stress in aerated stirred tanks up to 40 m^3 scale by measurement of maximum stable drop size. Journal of Biological Engineering, 8(1): 1-14.

de Kok, S., Kozak, B.U., Pronk, J.T. and van Maris, A.J.A., 2012. Energy coupling in *Saccharomyces cerevisiae*: selected opportunities for metabolic engineering. FEMS Yeast Research, 12(4): 387-397.

Delafosse, A. et al., 2015. Euler–Lagrange approach to model heterogeneities in stirred tank bioreactors – Comparison to experimental flow characterization and particle tracking. Chem Eng Sci, 134: 457-466.

Delbrück, M., 1898. About the progresses in the fermentation chemistry in the last decades (Original: Über die Fortschritte der Gährungschemie in den letzten Decennien). European Journal of Inorganic Chemistry, 31(2): 1913-1925.

Delente, J., Akin, C., Krabbe, E. and Ladenburg, K., 1969. Fluid dynamics of anaerobic fermentation. Biotechnol Bioeng, 11(4): 631-646.

Delvigne, F., Takors, R., Mudde, R., van Gulik, W. and Noorman, H., 2017. Bioprocess scale-up/down as integrative enabling technology: from fluid mechanics to systems biology and beyond. Microb Biotechnol, 10(5): 1267-1274.

Dequin, S., 2001. The potential of genetic engineering for improving brewing, wine-making and baking yeasts. Appl Microbiol Biot, 56(5-6): 577-88.

Deutscher-Brauer-Bund-e.V., 2018. The brewing process from brewing to bottling.

Díaz-Garćıa, J., Costa-Fernández, J.M., Bordel-García, N. and Sanz-Medel, A., 2001. Room-temperature phosphorescence fiber-optic instrumentation for simultaneous multi-position analysis of dissolved oxygen. Analytica Chimica Acta, 429(1): 55-64.

Dickenson, C.J. and Dickinson, F.M., 1975. A study of the pH and temperature dependence of the reactions of yeast alcohol dehydrogenase with ethanol, acetaldehyde and butyraldehyde as substrates. Biochem J, 147(2): 303-311.

Difford's-Guide, Heineken brewery. Difford's-Guide.

Domingos, J.M.B. et al., 2018. Cheese whey integrated valorisation: Production, concentration and exploitation of carboxylic acids for the production of polyhydroxyalkanoates by a fed-batch culture. Chem Eng J, 336: 47-53.

Dragone, G., Mussatto, S.I. and Almeida e Silva, J.B., 2007. High gravity brewing by continuous process using immobilised yeast: Effect of wort original gravity on fermentation performance. Journal of the Institute of Brewing, 113(4): 391-398.

Elsutohy, M.M. et al., 2017. *Real-time* measurement of the intracellular pH of yeast cells during glucose metabolism using ratiometric fluorescent nanosensors. Nanoscale, 9(18): 5904-5911.

Endress&Hauser, 2015. Level detection for liquids employing the vibration measurement principle Report), Flow control networks.

Enfors, S.O. et al., 2001. Physiological responses to mixing in large-scale bioreactors. J Biotechnol, 85(2): 175-185.

Engan, S., 1972. Wort composition and beer flavour. II. The influence of different carbohydrates on the formation of some flavour components during fermentation. Journal of the Institute of Brewing, 78(2): 169-173.

Enseleit, U. et al., 2017. Spatial monitoring of the liquid phase with multi-parameter sensors in industrial-scale fermenters. Technisches Messen, 84(10): 620-627.

Esbensen, K. et al., 2004. Fermentation monitoring using multisensor systems: feasibility study of the electronic tongue. Anal Bioanal Chem, 378(2): 391-395.

Esslinger, H.M., 2009. Handbook of Brewing In: H.M. Eßlinger (Editor), Process, Technology, Markets. Wiley-VCH Verlag GmbH & Co. KGaA, Weinheim.

Faria-Oliveira, F.b., Puga, S.n. and Ferreira, C.l., 2013. Chapter 23: Yeast: World's finest chef. In: I. Muzzalupo (Editor), Food Industry. InTech, Rijeka.

Feng, S., Srinivasan, S. and Lin, Y.-H., 2012. Redox potential-driven repeated batch ethanol fermentation under very-high-gravity conditions. Process Biochem, 47(3): 523-527.

Ferreira, A.P., Vieira, L.M., Cardoso, J.P. and Menezes, J.C., 2005. Evaluation of a new annular capacitance probe for biomass monitoring in industrial pilot-scale fermentations. J Biotechnol, 116(4): 403-409.

Ferreira, T., Mason, A.B. and Slayman, C.W., 2001. The yeast pma1 proton pump: a model for understanding the biogenesis of plasma membrane proteins. J Biol Chem, 276(32): 29613-29616.

Fletcher, E. et al., 2017. Evolutionary engineering reveals divergent paths when yeast is adapted to different acidic environments. Metabolic Engineering, 39: 19-28.

Fletcher, E., Feizi, A., Kim, S.S., Siewers, V. and Nielsen, J., 2015. RNA-seq analysis of *Pichia anomala* reveals important mechanisms required for survival at low pH. Microb Cell Fact, 14(1): 143-154.

Folz, R. and Tyrell, T., 2011. Fermentation tests with improved EBC fermentation modules. Brauerei Forum International VLB Edition: 10-11.

Food-and-Drug-Administration, U.S.D.o.H.a.H.S., 2004a. Guidance for industry: PAT - a framework for innovative pharmaceutical development, manufacturing, and quality assurance, Rockville.

Food-and-Drug-Administration, U.S.D.o.H.a.H.S., 2004b. Pharmaceutical CGMPs for the 21st century - a risk based approach, Rockville.

Fraser, H.B., Moses, A.M. and Schadt, E.E., 2010. Evidence for widespread adaptive evolution of gene expression in budding yeast. Proceedings of the National Academy of Sciences, 107(7): 2977-2982.

Gao, J. et al., 2016. Application of redox potential control to improve ethanol productivity from inulin by consolidated bioprocessing. Process Biochem, 51(10): 1544-1551.

Garaiová, M., Zambojová, V., Šimová, Z., Griač, P. and Hapala, I., 2014. Squalene epoxidase as a target for manipulation of squalene levels in the yeast *Saccharomyces cerevisiae*. FEMS Yeast Research, 14(2): 310-323.

Garcia, A.I., Garcia, L.A. and Diaz, M., 1993. Mixing in unstirred batch fermenters. Chemical Engineering Journal and Biochemical Engineering Journal, 51(3): B57-B61.

García, A.I., Pandiella, S.S., García, L.A. and Díaz, M., 1994. Mechanism for mixing and homogenization in beer fermentation. Bioprocess Engineering, 10(4): 179-184.

Garn, M., Gisin, M., Thommen, C. and Cevey, P., 1989. A flow injection analysis system for fermentation monitoring and control. Biotechnol Bioeng, 34(4): 423-428.

Gasch, A.P. et al., 2000. Genomic expression programs in the response of yeast cells to environmental changes. Mol Biol Cell, 11(12): 4241-4257.

Ge, X., Kostov, Y. and Rao, G., 2003. High-stability non-invasive autoclavable naked optical CO_2 sensor. Biosensors and Bioelectronics, 18(7): 857-865.

GEA, 2017. ECO-FERM: Optimized quality and higher capacity in the fermenting cellar.

Geier, D., Whitehead, I., Birle, S. and Becker, T., 2016. Zukunftsweisende Methoden der Prozessführung bei der Bierherstellung. Chemie Ingenieur Technik, 88(12): 1880-1890.

Gélinas, P., 2010. Mapping Early Patents on Baker's Yeast Manufacture. Comprehensive Reviews in Food Science and Food Safety, 9(5): 483-497.

Gélinas, P., 2014. Fermentation Control in Baker's Yeast Production: Mapping Patents. Comprehensive Reviews in Food Science and Food Safety, 13(6): 1141-1164.

George, S., Larsson, G. and Enfors, S.-O., 1993. A scale-down two-compartment reactor with controlled substrate oscillations: Metabolic response of *Saccharomyces cerevisiae*. Bioprocess Engineering, 9(6): 249-257.

Georgy, K., 2015. Low-oxygen brewing process ensures high quality. Brauwelt International, 33(1/15): 3 pp.

Ghasemi-Varnamkhasti, M. et al., 2011. Potential application of electronic nose technology in brewery. Trends Food Sci Tech, 22(4): 165-174.

Ginovart, M., Prats, C., Portell, X. and Silbert, M., 2011. Exploring the lag phase and growth initiation of a yeast culture by means of an individual-based model. Food Microbiol, 28(4): 810-817.

Gnoth, S., Jenzsch, M., Simutis, R. and Lubbert, A., 2007. Process analytical technology (PAT): batch-to-batch reproducibility of fermentation processes by robust process operational design and control. J Biotechnol, 132(2): 180-186.

Gomez-Tejedor, J.A., Castro-Palacio, J.C. and Monsoriu, J.A., 2014. The acoustic Doppler effect applied to the study of linear motions. Eur J Phys, 35(2).

Gonzalez Viejo, C., Fuentes, S., Torrico, D., Howell, K. and Dunshea, F.R., 2018. Assessment of beer quality based on foamability and chemical composition using computer vision algorithms, near infrared spectroscopy and machine learning algorithms. J Sci Food Agr, 98(2): 618-627.

Guerreiro, J.F., Mira, N.P., Santos, A.X.S., Riezman, H. and Sá-Correia , I., 2017. Membrane phosphoproteomics of yeast early response to acetic acid: Role of Hrk1 kinase and lipid biosynthetic pathways, in particular sphingolipids. Front Microbiol, 8(1302).

Guilliermond, A., 1920. The yeasts: Culture, identification, and microbiology. John Wiley and Sons, Inc., Chapman an Hall Limited, New York, London, 448 pp.

Hamilton_Company, 2011. VisiFerm DO Arc 120 - Data sheet.

Hamilton_Company, 2012a. Arc pH and ORP sensors - Manual.

Hamilton_Company, 2012b. Arc sensors - Brochure.

Hamilton_Company, 2012c. pH measurement in *Escherichia coli* fermentation with EasyFerm Food.

Hamilton_Company, 2014a. Conducell 4USF Arc - Manual.

Hamilton_Company, 2014b. VisiFerm DO Family - Manual.

Hamilton_Company, 2015. *On-line* data, *real-time* decisions - viable and total cell density sensors.

Hamilton_Company, 2016a. Conducell 4USF Arc 120 - Specification Sheet.

Hamilton_Company, 2016b. EasyFerm Plus Arc 120 - Specification sheet.

Hamilton_Company, 2016c. EasyFerm Plus ARC ORP 120 - Specification Sheet

Hamilton_Company, 2016d. VisiFerm DO Arc 120 - Specification sheet.

Hänel, D., 2004. Molecular Gas Dynamics (Book). In: P.D.-I.D. Hänel (Editor). Springer Verlag Berlin, Heidelberg, New York, Duisburg.

Hansen, E.C., 1896. Practical studies in fermentation: Being contributions to the life history of microorganisms. E.& F.N. Spon; Spon & Chamberlain, London; New York, 5-10 pp.

Haringa, C., 2017. Through the organism's eyes: The interaction between hydrodynamics and metabolic dynamics in industrial-scale fermentation processes. Doctoral Thesis, Technische Universiteit Delft, Delft, 245 pp.

Haringa, C., Deshmukh, A.T., Mudde, R.F. and Noorman, H.J., 2017. Euler-Lagrange analysis towards representative down-scaling of a 22 m^3 aerobic *S. cerevisiae* fermentation. Chem Eng Sci, 170: 653-669.

Haringa, C. et al., 2016. Euler-Lagrange computational fluid dynamics for (bio)reactor scale down: An analysis of organism lifelines. Eng Life Sci, 16(7): 652-663.

Hashimoto, T., Maruhashi, T., Yamaguchi, Y., Hida, Y. and Oka, K., 2012. The effect on fermentation by-products of the amino acids in wort. Proceedings of the World Brewing Congress. Technical Session 16: Yeast III Session. Master Brewers Association of the Americas (MBAA).

Haukeli, A.D. and Lie, S., 1978. Conversion of α-acetolactate and removal of diacetyl - a kinetic study. Journal of the Institute of Brewing, 84(2): 85-89.

Hauptmann, P., Hoppe, N. and Püttmer, A., 2002. Application of ultrasonic sensors in the process industry. Measurement Science and Technology, 13(8): 73-83.

Hayduck, F., 1915. Yeast production process without or only a low alcohol production (Original: Verfahren der Hefefabrikation ohne oder nur mit geringer Alkoholerzeugung), Germany.

Hayduck, F., 1920. Max Delbrück. Reports of the German association of chemistry (Original: Berichte der deutschen chemischen Gesellschaft) (A and B Series), 53(4): 47-62.

He, Y. et al., 2014. Wort composition and its impact on the flavour-active higher alcohol and ester formation of beer – a review. Journal of the Institute of Brewing, 120(3): 157-163.

Henning, B. and Rautenberg, J., 2006. Process monitoring using ultrasonic sensor systems. Ultrasonics, 44, Supplement: 1395-1399.

Herrero, E., Ros, J., Bellí, G. and Cabiscol, E., 2008. Redox control and oxidative stress in yeast cells. Biochimica et Biophysica Acta (BBA) - General Subjects, 1780(11): 1217-1235.

Herwig, C., 2010. Process analytical technology in the biotechnology (Original: Prozessanalytische Technologie in der Biotechnologie). Chemie Ingenieur Technik, 82(4): 405-414.

Hewitt, C.J. and Nienow, A.W., 2007. The scale-up of microbial batch and fed-batch fermentation processes, Adv Appl Microbiol. Academic Press, pp. 105-135.

Hinkle, P.C., 2005. P/O ratios of mitochondrial oxidative phosphorylation. Biochimica et Biophysica Acta (BBA) - Bioenergetics, 1706(1): 1-11.

Hiralal, L., Olaniran, A.O. and Pillay, B., 2014. Aroma-active ester profile of ale beer produced under different fermentation and nutritional conditions. Journal of Bioscience and Bioengineering, 117(1): 57-64.

Hoggan, J., 1977. Aspects of fermentation in conical vessels. Journal of the Institute of Brewing, 83(3): 133-138.

Honda, H. and Kobayashi, T., 2004. Industrial application of fuzzy control in bioprocesses. Advances in Biochemical Engineering/Biotechnology, 87: 151-171.

Honigberg, S.M. and Lee, R.H., 1998. Snf1 kinase connects nutritional pathways controlling meiosis in *Saccharomyces cerevisiae*. Molecular and Cellular Biology, 18(8): 4548-4555.

Hough, J.S., Briggs, D.E., Stevens, R. and Young, T.W., 1982. Brewery fermentations, Malting and Brewing Science: Volume II, Hopped Wort and Beer. Springer US, Boston, MA, pp. 644-686.

Hu, Z. et al., 2017. Recent advances in ergosterol biosynthesis and regulation mechanisms in *Saccharomyces cerevisiae*. Indian Journal of Microbiology, 57(3): 270-277.

Ihunegbo, F.N., Madsen, M., Esbensen, K.H., Holm-Nielsen, J.B. and Halstensen, M., 2012. Acoustic chemometric prediction of total solids in bioslurry: A full-scale feasibility study for *on-line* biogas process monitoring. Chemometr Intell Lab, 110(1): 135-143.

Institute-of-Brewing, 1976. The institute of brewing - Sections Cambidge Meeting. Journal of the Institute of Brewing, 82(5): 255-263.

Intelmann, D. et al., 2009. Structures of storage-induced transformation products of the beer's bitter principles, revealed by sophisticated NMR spectroscopic and LC-MS techniques. Chemistry - a European Journal, 15(47): 13047-13058.

Janzen, N.H., Schmidt, M., Krause, C. and Weuster-Botz, D., 2015. Evaluation of fluorimetric pH sensors for bioprocess monitoring at low pH. Bioprocess and Biosystems Engineering, 38(9): 1685-1692.

Jeevarajan, A.S., Vani, S., Taylor, T.D. and Anderson, M.M., 2002. Continuous pH monitoring in a perfused bioreactor system using an optical pH sensor. Biotechnology and Bioengineering, 78(4): 467-472.

Jenkins, C.L., Kennedy, A.I., Hodgson, J.A., Thurston, P. and Smart, K.A., 2003. Impact of serial re-pitching on lager brewing yeast quality. J Am Soc Brew Chem, 61(1): 1-9.

Jenzsch, M., Simutis, R., Eisbrenner, G., Stückrath, I. and Lübbert, A., 2006. Estimation of biomass concentrations in fermentation processes for recombinant protein production. Bioproc Biosyst Eng, 29(1): 19-27.

Jimenez-Jorquera, C., Orozco, J. and Baldi, A., 2010. ISFET based microsensors for environmental monitoring. Sensors (Basel), 10(1): 61-83.

Johnson, A., 1987. The control of fed-batch fermentation processes - A survey. Automatica, 23(6): 691-705.

Jolliffe, I.T. and Cadima, J., 2016. Principal component analysis: a review and recent developments. Philosophical Transactions: Series A - Mathematical, Physical, and Engineering Sciences, 374(2065): 16 pp.

Jumo, 2011. ISFET pH combination electrode, Type 201050.

Junker, B.H., 2004. Scale-up methodologies for *Escherichia coli* and yeast fermentation processes. Journal of Bioscience and Bioengineering, 97(6): 347-364.

Junne, S., Klingner, A., Kabisch, J., Schweder, T. and Neubauer, P., 2011. A two-compartment bioreactor system made of commercial parts for bioprocess scale-down studies: Impact of oscillations on *Bacillus subtilis* fed-batch cultivations. Biotechnology Journal, 6(8): 1009-1017.

Juresic, G.C., Popovic, S., Skara, J., Glad, M. and Blagovic, B., 2017. Effect of environmental stress factors and recycling on the lipid composition of brewer's yeast mitochondria. Kem Ind, 66(9-10): 475-480.

Kamthan, A., Kamthan, M. and Datta, A., 2017. Expression of C-5 sterol desaturase from an edible mushroom in fisson yeast enhances its ethanol and thermotolerance. Public Library of Science (Plos) One, 12(3): 20 pp.

Kanellaki, M., Bekatorou, A. and Koutinas, A.A., 2014. Low-temperature production of wine, beer, and distillates using cold-adapted yeasts. In: P. Buzzini and R. Margesin (Editors), Cold-adapted Yeasts: Biodiversity, Adaptation Strategies and biotechnological Significance. Springer Berlin Heidelberg, Berlin, Heidelberg, pp. 417-439.

Kapral, D., 2008. Stratified fermentation - causes and corrective Actions. Master Brewers Association of the Americas (MBAA), Technical Quartely, 45(2): 115-120).

Karakuzu, C., Türker, M. and Öztürk, S., 2006. Modelling, *on-line* state estimation and fuzzy control of production scale fed-batch baker's yeast fermentation. Control Engineering Practice, 14(8): 959-974.

Kariminiaae-Hamedaani, H.R., Shahrokhi, M. and Roostaazad, R., 2005. Experimental evaluation of batch and continuous production of baker's yeast under computer controlled pH. Iranian Journal of Chemistry and Chemical Engineering - International English Edition, 24(2): 43-49.

Käß, F., Junne, S., Neubauer, P., Wiechert, W. and Oldiges, M., 2014. Process inhomogeneity leads to rapid side product turnover in cultivation of *Corynebacterium glutamicum*. Microb Cell Fact, 13: 10 pp.

Kates, M. and Baxter, R.M., 1962. Lipid composition of mesophilic and psychrophilic yeasts (*Candida* species) as influenced by environmental temperature. Canadian Journal of Biochemistry and Physiology, 40(9): 1213-1227.

Kell, D.B., Samworth, C.M., Todd, R.W., Bungard, S.J. and Morris, J.G., 1987. *Real-time* estimation of microbial biomass during fermentations, using a dielectric probe. Stud Biophys, 119(1-3): 153-156.

Kessler, R., Hergeth, W.-D., Maiwald, M. and ACHEMA, 2012. ACHEMA 2012 Trends Report: Process Analytical Technology: The Way to Knowledge-based Production (Original: ACHEMA 2012 Trendbericht: Prozessanalytik: Der Weg zur wissensbasierten Produktion), 11 pp., ACHEMA.

Kessler, R.W., 2012. Process analytics: strategies and case studies in industrial practice (Original: Prozessanalytik: Strategien und Fallbeispiele aus der industriellen Praxis). Wiley-VCH Verlag GmbH, Weinheim.

Kessler, R.W. and Becker, T., 2010. Process analytic: Indispensable tool for efficient processes (Original: Prozessanalytik: Unverzichtbares Werkzeug für effiziente Prozesse). Chemie Ingenieur Technik, 82(4): 359-359.

Kessler, W., 2006. Introduction into the multivariate data analysis (Original: Einführung in die multivariate Datenanalyse), Multivariate Data Analysis (Multivariate Datenanalyse). Wiley-VCH Verlag GmbH & Co. KGaA, pp. 1-20.

Khongsay, N., Lin, Y.-H., Laopaiboon, P. and Laopaiboon, L., 2014. Improvement of very-high-gravity ethanol fermentation from sweet sorghum juice by controlling fermentation redox potential. J Taiwan Inst Chem E, 45(2): 302-307.

Kiefer, J., Ebel, N., Schlucker, E. and Leipertz, A., 2010. Characterization of *Escherichia coli* suspensions using UV/VIS/NIR absorption spectroscopy. Analytical Methods, 2(2): 123-128.

Kielhorn, E. et al., 2015. Multi-position sensor technology and lance-based sampling for improved monitoring of the liquid phase in biogas processes. Energy and Fuels, 29(7): 4038-4045.

Kiss, B. and Németh, A., 2015. Monitoring of fermentations with *on-line* capacitance sensor. International Journal of Current Research, 7(12): 23881-23886.

Klein, T., Schneider, K. and Heinzle, E., 2013. A system of miniaturized stirred bioreactors for parallel continuous cultivation of yeast with *on-line* measurement of dissolved oxygen and off-gas. Biotechnol Bioeng, 110(2): 535-542.

Klug, L. and Daum, G., 2014. Yeast lipid metabolism at a glance. FEMS Yeast Research, 14(3): 369-388.

Knabben, I. et al., 2010. *On-line* determination of viable biomass up to very high cell densities in *Arxula adeninivorans* fermentations using an impedance signal. J Biotechnol, 149(1–2): 60-66.

Knabben, I., Regestein, L., Schauf, J., Steinbusch, S. and Buchs, J., 2011. Linear correlation between *on-line* capacitance and *off-line* biomass measurement up to high cell densities in *Escherichia coli* fermentations in a pilot-scale pressurized bioreactor. J Microbiol Biotechn, 21(2): 204-211.

Kobayashi, M., Shimizu, H. and Shioya, S., 2007. Physiological analysis of yeast cells by flow cytometry during serial re-pitching of low-malt beer fermentation. Journal of Bioscience and Bioengineering, 103(5): 451-456.

Kobi, D., Zugmeyer, S., Potier, S. and Jaquet-Gutfreund, L., 2004. Two-dimensional protein map of an "ale"-brewing yeast strain: proteome dynamics during fermentation. FEMS Yeast Research, 5(3): 213-30.

Kodedová, M. and Sychrová, H., 2015. Changes in the sterol composition of the plasma membrane affect membrane potential, salt tolerance and the activity of multidrug resistance rumps in *Saccharomyces cerevisiae*. Public Library of Science (Plos) One, 10(9): 19 pp.

Kondakci, T. and Zhou, W.B., 2017. Recent applications of advanced control techniques in food industry. Food Bioprocess Tech, 10(3): 522-542.

Krogerus, K., Seppänen-Laakso, T., Castillo, S. and Gibson, B., 2017. Inheritance of brewing-relevant phenotypes in constructed Saccharomyces cerevisiae × Saccharomyces eubayanus hybrids. Microb Cell Fact, 16: 66.

Krommenhoek, E.E. et al., 2008. Lab-scale fermentation tests of microchip with integrated electrochemical sensors for pH, temperature, dissolved oxygen and viable biomass concentration. Biotechnol Bioeng, 99(4): 884-892.

Kronlöf, J., Härkönen, T., Hartwall, P., Home, S. and Linko, M., 1998. Main fermentation with immobilized yeast 22nd Congress of European Brewery Convention, Zürich, pp. 355 - 362.

Kronlöf, J. and Linko, M., 1992. Production of beer using immobilized yeast encoding α-acetolactate decarboxylase. Journal of the Institute of Brewing, 98(6): 479-491.

Kucharczyk, K. and Tuszyński, T., 2017. The effect of wort aeration on fermentation, maturation and volatile components of beer produced on an industrial scale. Journal of the Institute of Brewing, 123(1): 31-38.

Kukec, A., Berovic, M., Celan, S. and Wondra, M., 2002. The role of *on-line* redox potential measurement in Sauvignon blanc fermentation. Food Technol Biotech, 40(1): 49-55.

Kunz, T., Frenzel, J., Wietstock, P.C. and Methner, F.J., 2014. Possibilities to improve the antioxidative capacity of beer by optimized hopping regimes. Journal of the Institute of Brewing, 120(4): 415-425.

Kutyla-Olesiuk, A., Wawrzyniak, U.E., Ciosek, P. and Wroblewski, W., 2014. Electrochemical monitoring of citric acid production by Aspergillus niger. Analytica Chimica Acta, 823: 25-31.

Kutyla-Olesiuk, A., Zaborowski, M., Prokaryn, P. and Ciosek, P., 2012. Monitoring of beer fermentation based on hybrid electronic tongue. Bioelectrochemistry, 87: 104-113.

Lapin, A., Müller, D. and Reuss, M., 2004. Dynamic behavior of microbial populations in stirred bioreactors simulated with Euler−Lagrange methods: Traveling along the lifelines of single cells. Ind Eng Chem Res, 43(16): 4647-4656.

Lara, A.R., Galindo, E., Ramírez, O.T. and Palomares, L.A., 2006. Living with heterogeneities in bioreactors. Mol Biotechnol, 34(3): 355-381.

Larsson, G. et al., 1996. Substrate gradients in bioreactors: origin and consequences. Bioprocess Engineering, 14(6): 281-289.

Lei, H. et al., 2013. Effects of Lys and His supplementations on the regulation of nitrogen metabolism in lager yeast. Appl Microbiol Biot, 97(20): 8913-8921.

Lei, H. et al., 2016. Fermentation performance of lager yeast in high gravity beer fermentations with different sugar supplementations. Journal of Bioscience and Bioengineering, 122(5): 583-588.

Lei, H., Zhao, H., Yu, Z. and Zhao, M., 2012. Effects of wort gravity and nitrogen level on fermentation performance of brewer's yeast and the formation of flavor volatiles. Appl Biochem Biotech, 166(6): 1562-1574.

Lejeune, A., Frank, D. and Thonart, P., 2013. Physiological response of yeast to process perturbations: A mini-bioreactor approach. Cerevisia, 38(1): 15-19.

Lemoine, A. et al., 2016. Performance loss of *Corynebacterium glutamicum* cultivations under scale-down conditions using complex media. Eng Life Sci, 16(7): 620-632.

Lemoine, A., Maya Martínez-Iturralde, N., Spann, R., Neubauer, P. and Junne, S., 2015. Response of *Corynebacterium glutamicum* exposed to oscillating cultivation conditions in a two- and a novel three-compartment scale-down bioreactor. Biotechnol Bioeng, 112(6): 1220-1231.

Lewis, M. and Powell, J., 2017. Yeast for mathematicians: A ferment of discovery and model competition to describe data. B Math Biol, 79(2): 356-382.

Li, Z. et al., 2001. Low-temperature increases the yield of biologically active Herring antifreeze protein in *Pichia pastoris*. Protein Expression and Purification, 21(3): 438-445.

Lin, J., Jia, B., Shan, S.-s. and Xu, S.-a., 2014. Fed-batch fermentation with glucose syrup as an adjunct for high-ethanol beer brewing. Journal of the Institute of Brewing, 120(4): 426-432.

Lin, Z. et al., 2017. High-efficiency acetone-butanol-ethanol production and recovery in non-strict anaerobic gas-stripping fed-batch fermentation. Appl Microbiol Biot, 101(21): 8029-8039.

Lindner, P., 1893. The single culture in the hanging drop. Aged cells in fresh wort. Abnormal cell forms and formation of transverse walls in industrial yeasts. (Original: Die Einzelkultur im hängenden Tropfen. Gealterte Zellen in frischer Würze. Abnormale Zellformen und Querwandbildungen bei Betriebshefen.). Wochenschrift für Brauerei (WsB), 10: 1554-1357.

Lindner, P., 1895. Microscopic process control in the fermentation industry: with an introduction into pure yeast culture, infection and yeast science, for students and practicioners. (Original: Mikroskopische Betriebskontrolle in den Gärungsgewerben: mit einer Einführung in die Hefenreinkultur, Infektionslehre und Hefenkunde, für Studierende und Praktiker bearbeitet). Verlagsbuchhandlung Paul Parey, 365 pp.

Liu, C.-G., Hao, X.-M., Lin, Y.-H. and Bai, F.-W., 2016. Redox potential driven aeration during very-high-gravity ethanol fermentation by using flocculating yeast. Sci Rep-Uk, 6: 25763-25769.

Liu, C.-G., Qin, J.-C. and Lin, Y.-H., 2017. Fermentation and Redox Potential. In: D.A. Jozala (Editor), Fermentation Processes. InTech.

Liu, C.-G., Xue, C., Lin, Y.-H. and Bai, F.-W., 2013. Redox potential control and applications in microaerobic and anaerobic fermentations. Biotechnology Advances, 31(2): 257-265.

Lloyd, W.J.W., 1986. Adjuncts. Journal of the Institute of Brewing, 92(4): 336-345.

Lodolo, E.J., Kock, J.L.F., Axcell, B.C. and Brooks, M., 2008. The yeast *Saccharomyces cerevisiae* – the main character in beer brewing. FEMS Yeast Research, 8(7): 1018-1036.

Louthander, D., Bachinger, T., Gawronski, M. and Martensson, P., 2009. Sensor device, system and method for monitoring an anaerobic digestion process. In: SENSET-AB (Editor), European Patent Office, SE.

Luyben, K.C.A.M., 1997. Fermentation dynamics and fermenter design, 6th Convention of the institute of brewing (SA Section), Durban, pp. 37-46.

Maczek, J., 2009. Metabolic Modelling: Comparative analysis of the sterol biosynthesis. Doctoral Thesis, Technische Universität Berlin, 156 pp.

Maczek, J., Junne, S., Nowak, P. and Goetz, P., 2006. Metabolic flux analysis of the sterol pathway in the yeast *Saccharomyces cerevisiae*. Bioproc Biosyst Eng, 29(4): 241-52.

Mahmoud, S. et al., 2017. TOR complex 1 regulates the yeast plasma membrane proton pump and pH and potassium homeostasis. Febs Lett, 591(13): 1993-2002.

Maiwald, M., 2010. Process analytics as an instrument for information management in the chemical and pharmaceutical industry (Original: Prozessanalytik als Instrument des Informationsmanagements in der Chemischen und Pharmazeutischen Industrie). Chemie Ingenieur Technik, 82(4): 383-390.

Makushok, T., Alves, P., Huisman, Stephen M., Kijowski, Adam R. and Brunner, D., 2016. Sterol-rich membrane domains define fission yeast cell polarity. Cell, 165(5): 1182-1196.

Marais, L.M., 2010. The effect of yeast propagation temperature on diacetyl reduction: An in-process study at Spendrups brewery. Chalmers University of Technology (Chalmers tekniska högskola. Institutionen för kemi- och bioteknik), Gothenburg.

Marbà-Ardebol, A.M., Bockisch, A., Neubauer, P. and Junne, S., 2017. Sterol synthesis and cell size distribution under oscillatory growth conditions in Saccharomyces cerevisiae scale-down cultivations. Yeast, 11 pp.

Marbà-Ardebol, A.M., Turon, X., Neubauer, P. and Junne, S., 2016. Application of flow cytometry analysis to elucidate the impact of scale-down conditions in *Escherichia coli* cultivations. Afinidad, 73(573): 7-15.

Marini, F., Arnow, P. and Lampen, J.O., 1961. The effect of monovalent cations on the inhibition of yeast metabolism by nystatin. Microbiology, 24(1): 51-62.

Marschall, L., 2000. In the shadow of chemical synthesis - industrial biotechnology in Germany 1900-1970 (Original: Im Schatten der Chemischen Synthese - Industrielle Biotechnologie in Deutschland). Campus Verlag, Frankfurt / Main, 385 pp.

Marshall, E.M. and Bakker, A., 2004. Chapter 5: Computational fluid mixing, Handbook of Industrial Mixing: Science and Practice. John Wiley & Sons, Inc., pp. 257-343.

Martin, S., Bosch, J., Almcnar, J. and Posada, J., 1975. Large outdoor sphero-conical tanks: A new realization on lagering and fermentation processes, 15th Proceedings of the European Brewery Convention Congress. Elsevier Amsterdam, Nice, pp. 301-310.

Mas, S., Ossard, F. and Ghommidh, C., 2001. *On-line* determination of flocculating *Saccharomyces cerevisiae* concentration and growth rate using a capacitance probe. Biotechnol Lett, 23(14): 1125-1129.

Maule, D.R., 1976. Cylindroconical tanks - a study of cooling jacket performance. The Brewer, 64: 140-144.

Maule, D.R., 1986. A century of fermenter design. Journal of the Institute of Brewing, 92(2): 137-145.

McKellar, R.C. et al., 2002. Use of the electronic nose and gas chromatography-mass spectrometry to determine the optimum time for aging of beer. Master Brewers Association of the Americas (MBAA), Technical Quaterly, 39(2): 99-105.

McLeod, G. et al., 2009. A comparison of variate pre-selection methods for use in partial least squares regression: A case study on NIR spectroscopy applied to monitoring beer fermentation. J Food Eng, 90(2): 300-307.

Meironke, H., 2007. Characterization of the impluse and heat transport in cylindroconical tanks during fermentation, maturation and storage by means of laser optical and ultrasound measurement technologies - Dissertation (Original: Charakterisierung des Impuls- und Wärmetransports in zylindrokonischen Tanks während der Gärung, Reifung und Lagerung mittels laseroptischer und Ultraschall Messtechniken). Monsenstein und Vannerdat, Münster.

Meironke, H., 2014a. Experimental studies of convection flow during the fermentation process of beer by means of ultrasonic doppler velocimetry 9th International Symposium on Ultrasonic Doppler Methods for Fluid Mechanics and Fluid Engineering. Ubertone, Strasbourg.

Meironke, H., 2014b. Thermofluidynamics of the multiphase flow inside cylindroconical fermenters with different scales. Materials Science, Engineering and Chemistry (MATEC) Web of Conferences, Vol. 18.

Meironke, H. and Böttcher, K., 2014. Experimental investigation of parameters, influencing velocity fields during beer fermentation. Key Engineering Materials, 597: 37-45.

Merritt, N.R., 1966. The influence of temperature on some properties of yeast. Journal of the Institute of Brewing, 72(4): 374-383.

Mettler-Toledo-GmbH-Process-Analytics, 2004. pH measurement - *In-line* monitoring in breweries, Last visited: 07.01.18 (http://www.mt.com/de/en).

Min-hua, Z., Zong-jun, L., Hong, W., Wen-yong, L. and Ding-he, Z., 2013. Fed-batch culture of high cell-density oleaginous yeast trichosporon fermentans HWZ004. Journal of South China University of Technology (Natural Science Edition), 41(10): 47 - 52, 65.

Mishima, K., Mimura, A. and Takahara, Y., 1991. *On-line* monitoring of cell concentrations during yeast cultivation by dielectric measurements. Journal of Fermentation and Bioengineering, 72(4): 296-299.

Mo, C.Q. and Bard, M., 2005. Erg28p is a key protein in the yeast sterol biosynthetic enzyme complex. J Lipid Res, 46(9): 1991-1998.

Moilanen, P., Laakkonen, M. and Aittamaa, J., 2005. Modelling fermenters with CFD. In: P. Luis and E. Antonio (Editors), Computer Aided Chemical Engineering. Elsevier, pp. 709-714.

Moonjai, N., Verstrepen, K.J., Delvaux, F.R., Derdelinckx, G. and Verachtert, H., 2002. The effects of linoleic acid supplementation of cropped yeast on its subsequent fermentation performance and acetate ester synthesis. Journal of the Institute of Brewing, 108(2): 227-235.

Mross, S., Zimmermann, T., Winkin, N., Kraft, M. and Vogt, H., 2015. Integrated multi-sensor system for parallel *in-situ* monitoring of cell nutrients, metabolites and cell mass in biotechnological processes. Procedia Engineering, 120: 372-375.

Narziss, L. and Back, W., 2016. Brewing science and brewing technology (Original: Brauwissenschaft und Brauereitechnologie). Chemie Ingenieur Technik, 88(12): 1869-1879.

Nathan, L., 1930. Improvements in the fermentation and maturation of beers, part I & II. Journal of the Institute of Brewing, 36(6): 538-544.

Nayyar, A., Walker, G., Wardrop, F. and Adya, A.K., 2017. Flocculation in industrial strains of *Saccharomyces cerevisiae*: role of cell wall polysaccharides and lectin-like receptors. Journal of the Institute of Brewing, 123(2): 211-218.

Nery, E.W. and Kubota, L.T., 2016. Integrated, paper-based potentiometric electronic tongue for the analysis of beer and wine. Anal Chim Acta, 918(Supplement C): 60-68.

Neubauer, P. and Junne, S., 2010. Scale-down simulators for metabolic analysis of large-scale bioprocesses. Current Opinion in Biotechnology, 21(1): 114-121.

NewBrunswickScientific, 2008. Using redox measurements to control an anaerobic yeast fermentation. Biotechniques, 45(6): 670-671.

Nienow, A.W., McLeod, G. and Hewitt, C.J., 2010. Studies supporting the use of mechanical mixing in large-scale beer fermentations. Biotechnol Lett, 32(5): 623-633.

Nienow, A.W., Nordkvist, M. and Boulton, C.A., 2011. Scale-down/scale-up studies leading to improved commercial beer fermentation. Biotechnology Journal, 6(8): 911-925.

Nikulin, J., Krogerus, K. and Gibson, B., 2018. Alternative Saccharomyces interspecies hybrid combinations and their potential for low-temperature wort fermentation. Yeast, 35(1): 113-127.

Nordkvist, M., Boulton, C. and Nienow, A., 2011. Moving jets mix up the food and drink industry. The Chemical Engineer(834): 36-38.

Okabe, M., Katoh, M., Furugoori, F., Yoshida, M. and Mitsui, S., 1992. Growth and fermentation characteristics of bottom brewer's yeast under mechanical stirring. Journal of Fermentation and Bioengineering, 73(2): 148-152.

Okamura, K. et al., 2014. Colorimetric pH measurement for seawater samples using a three light-emitting diodes detector and a calibration method for temperature dependence. Anal Sci, 30(12): 1135-1141.

Olaniran, A.O., Maharaj, Y.R. and Pillay, B., 2011. Effects of fermentation temperature on the composition of beer volatile compounds, organoleptic quality and spent yeast density. Electron J Biotechn, 14(2).

Owicki, J.C. et al., 1994. The light-addressable potentiometric sensor - principles and biological applications. Annu Rev Bioph Biom, 23: 87-113.

Palermo, G., Piraino, P. and Zucht, H.-D., 2009. Performance of PLS regression coefficients in selecting variables for each response of a multivariate PLS for omics-type data. Advances and Applications in Bioinformatics and Chemistry, 2: 57-70.

Pangborn, R.M., Lewis, M.J. and Tanno, L.S., 1977. Sensory quantification of bitterness and flavor of beer during storage. Journal of the Institute of Brewing, 83(4): 244-250.

Päßler, S., Herrmann, S., Vonau, W. and Bertau, M., 2010. Optimization of biochemical engineering processes by means of a sensor-supported microbioreactor (Original: Optimierung bioverfahrenstechnischer Prozesse mittels sensorgestütztem Mikrobioreaktor). Technisches Messen, 77: 24-30.

Paumi, C., Chowning, S., Schwarze, T. and Fugate, D., 2017. Role of glutathione in yeast growth and fermentation for beer and wine production (Poster). In: C. Paumi (Editor), University Presentation Showcase Event no. 26, Kentucky University, pp. 1.

Peña, A., Sánchez, N.S., Álvarez, H., Calahorra, M. and Ramírez, J., 2015. Effects of high medium pH on growth, metabolism and transport in *Saccharomyces cerevisiae*. FEMS Yeast Research, 15(2): fou005, 13 pp.

Peris, M. and Escuder-Gilabert, L., 2013. *On-line* monitoring of food fermentation processes using electronic noses and electronic tongues: A review. Anal Chim Acta, 804: 29-36.

Petrova, S., Kostov, Y., Jeffris, K. and Rao, G., 2006. Optical ratiometric sensor for alcohol measurements. Anal Lett, 40(12): 715-727.

Pfeiffer, T. and Morley, A., 2014. An evolutionary perspective on the Crabtree effect. Frontiers in Molecular Biosciences, 1: 17 pp.

Ploier, B., Daum, G. and Petrovič, U., 2014. Molecular mechanisms in yeast carbon metabolism: Lipid metabolism and lipidomics. In: J. Piškur and C. Compagno (Editors), Molecular Mechanisms in Yeast Carbon Metabolism. Springer Berlin Heidelberg, Berlin, Heidelberg, pp. 169-215.

Poelmans, E. and Swinnen, J.F.M., 2012. A brief economic history of beer.

Poghossian, A., Lüth, H., Schultze, J.W. and Schöning, M.J., 2001. (Bio-)chemical and physical microsensor arrays using an identical transducer principle. Electrochim Acta, 47(1–2): 243-249.

Porro, D., Vai, M., Vanoni, M., Alberghina, L. and Hatzis, C., 2009. Analysis and modeling of growing budding yeast populations at the single cell level. Cytometry Part A, 75A(2): 114-120.

Powell, C.D. and Diacetis, A.N., 2007. Long term serial re-pitching and the genetic and phenotypic stability of brewer's yeast. Journal of the Institute of Brewing, 113(1): 67-74.

Pragati, K. and Sharma, H.K., 2012. Concept of computational fluid dynamics (CFD) and its applications in food processing equipment design. Food Processing and Technology, 3(1): 138-145.

Ragazzo-Sanchez, J.A., Chalier, P., Chevalier-Lucia, D., Calderon-Santoyo, M. and Ghommidh, C., 2009. Off-flavours detection in alcoholic beverages by electronic nose coupled to GC. Sensors and Actuators B: Chemical, 140(1): 29-34.

Raines, M.B., 2009. Yeast propagation and maintenance: principles and practices Maltose-Falcons, pp. 23 pp.

Rajkumar, A.S. et al., 2016. Engineering of synthetic, stress-responsive yeast promoters. Nucleic Acids Res, 44(17): e136, 12 pp.

Rathore, A.S., Bhambure, R. and Ghare, V., 2010. Process analytical technology (PAT) for biopharmaceutical products. Anal Bioanal Chem, 398(1): 137-154.

Read, E.K. et al., 2010. Process analytical technology (PAT) for biopharmaceutical products: Part I. concepts and applications. Biotechnol Bioeng, 105(2): 276-284.

Rees, E.M.R. and Stewart, G.G., 1999. Effects of magnesium, calcium and wort oxygenation on the fermentative performance of ale and lager strains fermenting normal and high gravity worts. Journal of the Institute of Brewing, 105(4): 211-218.

Reid, G.L., Ward, H.W., Palm, A.S. and Muteki, K., 2012. Process analytical technology (PAT) in pharmaceutical development. American Pharmaceutical Review.

Restaino, O.F. et al., 2013. High cell density cultivation of a recombinant *E. coli* strain expressing a key enzyme in bioengineered heparin production. Appl Microbiol Biot, 97(9): 3893-3900.

Ring, J. et al., 2012. The Metabolism beyond programmed Cell Death in Yeast. Exp Cell Res, 318(11): 1193-1200.

Rodríguez-González, M. et al., 2017. Role of the Sln1-phosphorelay pathway in the response to hyperosmotic stress in the yeast *Kluyveromyces lactis*. Molecular Microbiology, 104(5): 822-836.

Roque, A., Petrezsélyová, S., Serra-Cardona, A. and Ariño, J., 2016. Genome-wide recruitment profiling of transcription factor Crz1 in response to high pH stress. BioMed Central (BMC) Genomics, 17(1): 662 pp.

Rosenfeld, E., Beauvoit, B., Blondin, B. and Salmon, J.M., 2003. Oxygen consumption by anaerobic *Saccharomyces cerevisiae* under enological conditions: effect on fermentation kinetics. Appl Environ Microb, 69(1): 113-21.

Rupčić, J., Jurešić, G.Č. and Blagović, B., 2010. Influence of stressful fermentation conditions on neutral lipids of a *Saccharomyces cerevisiae* brewing strain. World Journal of Microbiology and Biotechnology, 26 (29)(7 (10)): 1331-1336.

Sachse, S. et al., 2015. On the use of electrochemical multi-sensors in biologically charged media. J Sens Sens Syst, 4(2): 295-303.

Saerens, S. and Swiegers, J.H., 2017. Production of low-alcohol or alcohol-free beer with *Pichia kluyveri* yeast strains. Google Patents.

Saerens, S.M. et al., 2008a. Parameters affecting ethyl ester production by *Saccharomyces cerevisiae* during fermentation. Appl Environ Microb, 74(2): 454-61.

Saerens, S.M., Delvaux, F.R., Verstrepen, K.J. and Thevelein, J.M., 2010. Production and biological function of volatile esters in *Saccharomyces cerevisiae*. Microb Biotechnol, 3(2): 165-77.

Saerens, S.M., Verbelen, P.J., Vanbeneden, N., Thevelein, J.M. and Delvaux, F.R., 2008b. Monitoring the influence of high-gravity brewing and fermentation temperature on flavour formation by analysis of gene expression levels in brewing yeast. Appl Microbiol Biot, 80(6): 1039-1051.

Sara Teixeira de, M.-S., Wanderley de, S. and Juliany, C.F.R., 2015. Sterol biosynthesis pathway as an alternative for the anti-protozoan parasite chemotherapy. Current Medicinal Chemistry, 22(18): 2186-2198.

Schelter, M., Zosel, J., Oelßner, W. and Mertig, M., 2014. A novel method for measuring dissolved gases in liquids. Sensors and Actuators B: Chemical, 193 (Supplement C): 113-120.

Schmidt-Hager, J. et al., 2017. New device for biomass monitoring in shake flask Culture: Development of an analytical unit based on the SFR Shake Flask Reader, PreSens Precision Sensing GmbH, Regensburg.

Schocker, A. and Kleinert, T., 2010. Integration of process analytical technology into process control: Examples from industrial application at BASF (Original: Integration der Prozessanalysentechnik in die Prozessführung: Beispiele aus der industriellen Praxis bei BASF). Chemie Ingenieur Technik, 82(4): 391-404.

Schönberger, C. et al., 2016. Selected chapters of brewing technology (Original: Ausgewählte Kapitel der Brauereitechnologie). Fachverlag Hans Carl.

Schuch, C., 1996a. Distribution of bottom fermenting yeast cells in cylindrochonical tanks (Original: Verteilung untergäriger Hefezellen in zylindrokonischen Tanks). Brauwelt, 44: 6 pp.

Schuch, C., 1996b. Motional processes in a cylindrochonical tank during fermentation and maturation (Original: Bewegung im zylindrokonischen Tank während Gärung und Reifung). VDI Reihe (146): 121 pp.

Schuch, C., 1996c. Sampling in cylindroconical tanks (Original: Probenahme in zylindrokonischen Tanks). Brauwelt, 17-18: 788-806.

Schuch, C., 1996d. Temperature distribution in cylindrochonical tanks (Original: Temperaturverteilung in zylindrokonischen Tanks). Brauwelt, 17/18: 594-597.

Schuch, C. and Denk, V., 1996. The visualization of the fluid flow in a model of a cylindro-conical tank (Original: Die Visualisierung von Strömungen in einem Modell eines zylindrokonischen Tanks). Mon.schr. Brauwiss., Heft 3/4: 98-103.

Schwill-Miedaner, A., 2011. Chapter 14: Sampling. In: A. Schwill-Miedaner (Editor), Process Engineering in the Brewing Process (Original: Verfahrenstechnik im Brauprozess). Fachverlag Hans Carl, Nürnberg.

Schwill-Miedaner, A., 2016. The Importance of Sampling in the Brewing Process (Original: Die Bedeutung der Probennahme im Brauprozess). Chemie Ingenieur Technik, 88(12): 1946-1954.

Semkiv, M.V., Dmytruk, K.V., Abbas, C.A. and Sibirny, A., 2016. Activation of futile cycles as an approach to increase ethanol yield during glucose fermentation in *Saccharomyces cerevisiae*. Bioengineered, 7(2): 106-111.

Semkiv, M.V., Dmytruk, K.V., Abbas, C.A. and Sibirny, A.A., 2014. Increased ethanol accumulation from glucose via reduction of ATP level in a recombinant strain of *Saccharomyces cerevisiae* overexpressing alkaline phosphatase. BioMed Central (BMC) Biotechnology, 14:42: 9 pp.

SensAction, 2017. LiquidSens, Last visited: 15.12.17. http://www.sensaction.de/en/.

Sensotech-GmbH, 2017. LiquiSonic® Plato and Brix. Sensotech-GmbH, Magdeburg-Barleben, Germany.
Serra-Cardona, A., Canadell, D. and Ariño, J., 2015. Coordinate responses to alkaline pH stress in budding yeast. Microbial Cell, 2(6): 182-196.
Shardlow, P.J., 1972. The choice and use of cylindroconical fermentation vessels. Master Brewers Association of the Americas (MBAA), Technical Quaterly, 9(1): 1-5.
Shelton, M.D., Chock, P.B. and Mieyal, J.J., 2005. Glutaredoxin: Role in reversible protein S-glutathionylation and regulation of redox signal transduction and protein translocation. Antioxidants & Redox Signaling, 7(3-4): 348-366.
Shin, J.J. et al., 2016. Systematic identification of genes involved in metabolic acid stress resistance in yeast and their potential as cancer targets. Disease Models and Mechanisms, 9(9): 1039-1049.
Slouka, C. et al., 2017. Low-frequency electrochemical impedance spectroscopy as a monitoring tool for yeast growth in industrial brewing processes. Chemosensors, 5(3): 24 pp.
Smart, K.A., 2007. Brewing yeast genomes and genome-wide expression and proteome profiling during fermentation. Yeast, 24(11): 993-1013.
Sohoni, S.V. et al., 2015. Optimization of high cell density fermentation process for recombinant nitrilase production in *E. coli*. Bioresource Technol, 188: 202-208.
Speers, R.A. and Stokes, S., 2009. Effects of vessel geometry, fermenting volume and yeast re-pitching on fermenting beer. Journal of the Institute of Brewing, 115(2): 148-150.
Statista, S.B., 2018a. Number of breweries in Germany according to their production per year between 2005 and 2016. (Anzahl der Braustätten in Deutschland nach Gesamtjahreserzeugung in den Jahren 2005 bis 2016). Last visited: 18.01.2018. http://de.statista.com/statistik/daten/studie/29613/umfrage/braustaetten-nach-jahreserzeugung/.
Statista, S.B., 2018b. Proportion of small breweries at beer production in Germany between 2005 and 2016. (Original: Anteil von Kleinbrauereien am Bierausstoß in Deutschland in den Jahren 2005 bis 2016). Last visited: 18.01.18. http://de.statista.com/statistik/daten/studie/294715/umfrage/anteil-von-kleinbrauereien-am-bierausstoss-in-deutschland/.
Steinweg, C., 2016. Digital Communication in Algae Cultivation, Karlsruhe Institute of Technology.
Stenholm, K. and Home, S., 1999. A new approach to limit dextrinase and its role in mashing. Journal of the Institute of Brewing, 105(4): 205-210.
Stewart, G.G., 2006. Studies on the uptake and metabolism of wort sugars during brewing fermentations, 43. Master Brewers Asociation of the Americas, Madison, WI, United States of America, 5 pp.
Stewart, G.G., 2016. *Saccharomyces* species in the production of beer. Beverages, 2(4): 34-52.
Stewart, G.G., Hill, A.E. and Russell, I., 2013. 125th anniversary review: Developments in brewing and distilling yeast strains. Journal of the Institute of Brewing, 119(4): 202-220.
Steyer, J.P., Bouvier, J.C., Conte, T., Gras, P. and Sousbie, P., 2002. Evaluation of a four year experience with a fully instrumented anaerobic digestion process. Water Sci Technol, 45(4-5): 495-502.
Steyer, J.P., Genovesi, A. and Harmand, J., 2001. Advanced monitoring and control of anaerobic wastewater treatment plants: fault detection and isolation. Water Sci Technol, 43(7): 183-190.
Stippl, V.M., Delgado, A. and Becker, T.M., 2004. Development of a method for the optical *in-situ* determination of pH-value during high-pressure treatment of fluid food. Innov Food Sci Emerg, 5(3): 285-292.
Subramanian, G., 2017. Continuous Biomanufacturing: Innovative Technologies and Methods. Wiley-VCH Verlag GmbH & Co. KGaA, Weinheim, Germany, 587 pp.
Sun, D.-W. and Norton, T.s., 2007. An overview of CFD applications in the food industry, Computational Fluid Dynamics in Food Processing. Contemporary Food Engineering. CRC Press, pp. 1-41.
Suomalainen, H., 1981. Yeast esterases and aroma esters in alcoholic beverages. Journal of the Institute of Brewing, 87(5): 296-300.
Suomalainen, H. and Lehtonen, M., 1979. The production of aroma compounds by yeast. Journal of the Institute of Brewing, 85(3): 149-156.

Swinnen, J.F.M., 2012. The economics of beer. Eur Rev Agric Econ, 39(3): 537-537.

Tang, W. et al., 2017. A 9-pool metabolic structured kinetic model describing days to seconds dynamics of growth and product formation by *Penicillium chrysogenum*. Biotechnol Bioeng, 114(8): 1733-1743.

Tauber, G., 2010. Industrial pH measurement - contribution of temperature to measurement uncertainty. Technisches Messen, 77(3): 150-155.

Teng, E., L., W. and Chiat, L.M., 2016. Simulation of a bioreactor with an improved fermentation kinetics – fluid flow model. Science and Technology, 24(1): 137-163.

Thiele, F., 2006. Influence of yeast vitality and fermentation parameters on metabolites and flavour stability (Original: Einfluss der Hefevitalität und der Gärparameter auf die Stoffwechselprodukte der Hefe und auf die Geschmacksstabilität). Doctoral Thesis, Technische Universität München, München, 232 pp.

Thungon, P.D., Kakoti, A., Ngashangva, L. and Goswami, P., 2017. Advances in developing rapid, reliable and portable detection systems for alcohol. Biosensors and Bioelectronics, 97: 83-99.

Tietgens, H., John, G.T. and Bettenbrock, K., 2017. CO_2, O_2, and biomass monitoring in *Escherichia coli* shake flask culture: Following glucose–glycerin diauxie *on-line*. BioProcess International: 1 pp.

Timoumi, A. et al., 2017. Dynamic behavior of *Yarrowia lipolytica* in response to pH perturbations: dependence of the stress response on the culture mode. Appl Microbiol Biot, 101(1): 351-366.

Tremblay, V.J. and Tremblay, C.H., 2005. The U.S. brewing industry: Data and economic analysis. MIT Press, 379 pp.

Ulenberg, G.H., Gerritson, H. and Huisman, J., 1972. Experiences with a giant cylindrico-conical tank. Master Brewers Association of the Americas (MBAA), Technical Quaterly, 9(3): 117-122.

Umbreit, W.W., 1960. Advances in applied microbiology, 2. Academic Press Inc., New York and London, 383 pp.

Unrean, P. and Nguyen, N.H.A., 2013. Optimized fed-batch fermentation of *Scheffersomyces stipitis* for efficient production of ethanol from hexoses and pentoses. Appl Biochem Biotech, 169(6): 1895-1909.

Unterstein, K., 1986. Cylindroconical fermentation and storage tanks (Original: Zylindrokonische Gär- und Lagertanks). Brauwelt, 1. Halbjahr.

Uttamlal, M. and Walt, D.R., 1995. A fiberoptic carbon-dioxide sensor for fermentation monitoring. Bio-Technol, 13(6): 597-601.

Van de Walle, M., 2014. Beer statistics, 2015 edition. The Brewers of Europe.

Vanderhaegen, B., Neven, H., Verachtert, H. and Derdelinckx, G., 2006. The chemistry of beer aging – a critical review. Food Chem, 95(3): 357-381.

Verbelen, P.J., De Schutter, D.P., Delvaux, F., Verstrepen, K.J. and Delvaux, F.R., 2006. Immobilized yeast cell systems for continuous fermentation applications. Biotechnol Lett, 28(19): 1515-1525.

Verbelen, P.J., Depraetere, S.A., Winderickx, J., Delvaux, F.R. and Delvaux, F., 2009a. The influence of yeast oxygenation prior to brewery fermentation on yeast metabolism and the oxidative stress response. FEMS Yeast Research, 9(2): 226-239.

Verbelen, P.J., Saerens, S.M., Van Mulders, S.E., Delvaux, F. and Delvaux, F.R., 2009b. The role of oxygen in yeast metabolism during high cell density brewery fermentations. Appl Microbiol Biot, 82(6): 1143-1156.

Vevea, J.D., Alessi Wolken, D.M., Swayne, T.C., White, A.B. and Pon, L.A., 2013. Ratiometric biosensors that measure mitochondrial redox state and ATP in living yeast cells. Journal of Visualized Experiments (JoVE)(77): e50633, 12 pp.

Vial, C. and Stiriba, Y., 2013. Characterization of bioreactors using computational fluid dynamics, Fermentation Processes Engineering in the Food Industry. Contemporary Food Engineering. CRC Press, pp. 121-164.

Villanueva, S. et al., 2006. SPME coupled to an array of MOS sensors: Reduction of the interferences caused by water and ethanol during the analysis of red wines. Sensors and Actuators B: Chemical, 120(1): 278-287.

Villarreal, P. et al., 2016. Tolerance to ultraviolet radiation of psychrotolerant yeasts and analysis of their carotenoid, mycosporine, and ergosterol content. Curr Microbiol, 72(1): 94-101.

Virgilio, S., Cupertino, F.B., Ambrosio, D.L. and Bertolini, M.C., 2017. Regulation of the reserve carbohydrate metabolism by alkaline pH and calcium in *Neurospora crassa* reveals a possible cross-regulation of both signaling pathways. BioMed Central (BMC) Genomics, 18(1): 457-472.

Virkajärvi, I. and Kronlöf, J., 1998. Long-Term Stability of Immobilized Yeast Columns in Primary Fermentation. J Am Soc Brew Chem, 56(2): 70-75.

Virkajärvi, I., Lindborg, K., Kronlöf, J. and Pajunen, E., 1999. Effects of aeration on flavor compounds in immobilized primary fermentation. Mon.schr. Brauwiss., 52(1): 9-28.

Virkajärvi, I. and Pohjala, N., 2000. Primary Fermentation with Immobilized Yeast: Some Effects of Carrier Materials on the Flavour of the Beer. Journal of the Institute of Brewing, 106(5): 311-318.

Vojinović, V., Cabral, J.M.S. and Fonseca, L.P., 2006. Real-time bioprocess monitoring: Part I: *In-situ* sensors. Sensors and Actuators B: Chemical, 114(2): 1083-1091.

Vonau, W., Gerlach, F. and Herrmann, S., 2010. Sensor for detecting relative hydrogen value for e.g. food industry, has pH electrode, half cell and electrochemical reference electrode that are formed on planar substrate using planar technology, in: K.M. e.V. (Editor), German Patent and Trademark Office (Original: Deutsches Patent- und Markenamt), DE.

Vonau, W. and Guth, U., 2006. pH Monitoring: A review. Journal of Solid State Electrochemistry, 10(9): 746-752.

Vu and Viet Man Le, V., 2010. Using fed-batch fermentation in high-gravity brewing: Effects of nutritional supplementation on yeast fermentation performance, 17, 117-126 pp.

Vu, V. and Kim, K., 2009. High-cell-density fed-batch culture of *Saccharomyces cerevisiae* KV-25 using molasses and corn steep liquor. J Microbiol Biotechn, 19(12): 1603-1611.

Wackerbauer, K., 1969. The influence of cylindroconical fermentation vessels on bottom and top fermentation (Original: Der Einfluss von zylindro-konischen Gärgefäßen auf Untergärung und Obergärung). Monat Brauerei(22. Jahrgang): 370-375.

Wackerbauer, K., 1995. The Fermentation and Storage in vertical Tanks (Original: Die Gärung und Lagerung in stehenden Tanks). Monat Brauerei(28. Jahrgang): 38-44.

Wagner, T. et al., 2012. Light-addressable potentiometric sensors and light–addressable electrodes as a combined sensor-and-manipulator microsystem with high flexibility. Procedia Engineering, 47: 890-893.

Walker, G.M., 2004. Metals in yeast fermentation processes. Adv Appl Microbiol, 54: 197-229.

Walsh, R.M. and Martin, P.A., 1977. Growth of *Saccharomyces cerevisiae* and *Saccharomyces uvarum* in a temperature gradient incubator. Journal of the Institute of Brewing, 83(3): 169-172.

Wan, N., 1995. Investigations of the influence of bioprocess engineering parameters on the temperature distribution and the fermentation in cylindroconical tanks (Original: Untersuchungen über den Einfluss verfahrenstechnischer Parameter auf die Temperaturverteilung und auf die Gärung in zylindrokonischen Gärtanks), Technische Universiät Berlin, Berlin.

Wang, G. et al., 2015a. Integration of microbial kinetics and fluid dynamics toward model-driven scale-up of industrial bioprocesses. Eng Life Sci, 15(1): 20-29.

Wang, J., Wen, B., Xu, Q., Xie, X. and Chen, N., 2015b. Optimization of carbon source and glucose feeding strategy for improvement of L-isoleucine production by *Escherichia coli*. Biotechnology, Biotechnological Equipment, 29(2): 374-380.

Werner, C.F., 2014. Development of light-addressable potentiometric sensor systems and their applications in biotechnological environments. Doctoral Thesis, Philipps-Universität Marburg, Marburg/Lahn.

Werner, C.F. et al., 2011. Determination of the extracellular acidification of Escherichia coli by a light-addressable potentiometric sensor. physica status solidi (a), 208(6): 1340-1344.

Willaert, R., 2006. The Beer Brewing Process: Wort Production and Beer Fermentation, Handbook of Food Products Manufacturing. John Wiley & Sons, Inc., pp. 443-506.

Willaert, R., 2007. The beer brewing process: Wort production and beer fermentation. In: J.H. Hui (Editor), Handbook of Food Products Manufacturing. John Wiley & Sons, Inc., Brussel.

Willaert, R., 2012. Biochemistry of beer Fermentation, Food Biochemistry and Food Processing. Wiley-Blackwell, pp. 627-653.

Witham, K., 2015. Increasing boom: Mintel study: Growth tendency for craft beer in Germany (Original: Fortschreitender Boom: Mintel-Studie: Craft-Bier mit Wachstumstendenz in Deutschland). Brau Industrie (Sachon): 22-25.

Witkowska, E., Buczkowska, A., Zamojska, A., Szewczyk, K.W. and Ciosek, P., 2010. Monitoring of periodic anaerobic digestion with flow-through array of miniaturized ion-selective electrodes. Bioelectrochemistry, 80(1): 87-93.

Wolfbeis, O.S., 2005. Materials for fluorescence-based optical chemical sensors. Journal of Materials Chemistry, 15(27-28): 2657-2669.

Xiong, Z.-Q. et al., 2008. *Real-time* viable-cell mass monitoring in high-cell-density fed-batch glutathione fermentation by *Saccharomyces cerevisiae* T65 in industrial complex medium. Journal of Bioscience and Bioengineering, 105(4): 409-413.

Yamanè, T. and Shimizu, S., 1984. Fed-batch techniques in microbial processes, Bioprocess Parameter Control. Springer Berlin Heidelberg, Berlin, Heidelberg, pp. 147-194.

Yardley, Y.E., Kell, D.B., Barrett, J. and Davey, C.L., 2000. *On-line*, *real-time* measurements of cellular biomass using dielectric spectroscopy. Biotechnology and Genetic Engineering Reviews, 17: 3-35.

Young, B.P. et al., 2010. Phosphatidic acid is a pH biosensor that links membrane biogenesis to metabolism. Science, 329(5995): 1085-1088.

Younis, O.S. and Stewart, G.G., 1998. Sugar uptake and subsequent ester and higher alcohol production by *Saccharomyces cerevisiae*. Journal of the Institute of Brewing, 104(5): 255-264.

Yuan, Y., Xu, Y. and Liu, X., 2009. CFD modeling of subcooling process for beer fermentation liquid. Asia-Pacific Journal of Chemical Engineering, 4(1): 99-106.

Zak, S.H., 2003. Chapter 9: Neural networks, Systems and Control. Oxford University Press, Inc., New York, pp. 469-489.

Zakhartsev, M., Yang, X., Reuss, M. and Pörtner, H.O., 2015. Metabolic efficiency in yeast *Saccharomyces cerevisiae* in relation to temperature dependent growth and biomass yield. J Therm Biol, 52: 117-129.

Zdaniewicz, M., Poreda, A. and Tuszyński, T., 2016. Rotary jet head – a device for accelerating the fermentation process in brewing. Journal of the Institute of Brewing, 122(2): 317-321.

Zhang, N. and Cao, L., 2017. Starvation signals in yeast are integrated to coordinate metabolic reprogramming and stress response to ensure longevity. Current Genetics, 63(5): 839-843.

Zhao, X.Q. and Bai, F.W., 2009. Mechanisms of yeast stress tolerance and its manipulation for efficient fuel ethanol production. J Biotechnol, 144(1): 23-30.

Zinser, E., Paltauf, F. and Daum, G., 1993. Sterol composition of yeast organelle membranes and subcellular distribution of enzymes involved in sterol metabolism. J Bacteriol, 175(10): 2853-2858.

Zosel, J., Oelßner, W., Decker, M., Gerlach, G. and Guth, U., 2011. The measurement of dissolved and gaseous carbon dioxide concentration. Measurement Science and Technology, 22(7): 45 pp.

10 Theses

1. Monitoring of gradients during the filling allows for *real-time* adaption of this process phase, reducing time and energy losses. This was proven in the 170/199 m^3 scale since the brewery removed a time and energy consuming "bubbling" procedure after the filling process.

2. In large-scale brewing processes, no significant spatial gradients of the dissolved oxygen and temperature and were detected along the tank height. Hence, the natural convection by CO_2 bubble formation and temperature gradients is sufficient for mixing large volumes (proven for up to 170/199 m^3) in CCTs. If gradients exist temporarily, they are larger in tanks with a higher volume.

3. Significant gradients were detected for the redox potential with maximum 66 mV during the onset of the fermentation and for the pH-value with maximum 0.17 pH-units during the main fermentation in the 170/199 m^3 scale. The maximum gradients in the 3 m^3 were 0.04 units for the pH-value and 23 mV for the redox potential during the onset of the fermentation.

4. During the filling process, even larger gradients of up to 110 mV for the redox potential and 0.2 units for the pH-value were determined in the 170/199 m^3 scale.

5. Correlation analyses of *on-line* sensor data with *off-line* data from metabolite analysis showed that the carbohydrate concentrations, especially for glucose and fructose, correlated best with the *on-line* data with $R^2 > 0.9$, followed by the total sterol content.

6. Measurement stability and a low sensor drift during long-term application requires sensors with membranes that are resistant to clogging and electrolyte volumes of more than 2 mL in order to prevent toxification of the electrolyte by chemical compounds, e.g. CO_2. The applied miniaturized sensors (with a membrane diameter of a 3 - 4 mm) do not fulfil these requirements.

7. The pH-value, redox potential, temperature, and DO-value were monitored with commercially available sensors (tip diameter: 10 – 12 mm) in brewing fermentations of up to 220 h with a pressure of up to 1.9 bar without significant losses in the measurement stability or an increase in the sensor drift.

8. Miniaturized sensors based on resistance measurements, e.g. for the temperature and pressure measurement, also showed stability under harsh conditions such as complex media, high cell concentrations, and strong gas formation.

9. A stable data transfer across a distance of up to 30 m was realized by using commercially available sensors with integrated pre-amplifiers.

10. Localization of the sensor monitoring tools by ultrasound is challenging due to the strong gas bubble formation (CO_2) during the onset and main fermentation phase interrupting the emitted ultrasound signal.

Appendix A: Materials and Methods

i. Recording of *on-line* Sensor Measurements

Table 20: Movement time frames and corresponding positions in the 3 m^3 and 170/199 m^3 scale. (E= experiment.)

	3 m^3 scale, E1		3 m^3 scale, E2		199 m^3 scale, E1		170 m^3 scale, E2	
Time frame	**Posi-tions**	**Time [h]**	**Posi-tions**	**Time [h]**	**Posi-tions**	**Time [h]**	**Posi-tions**	**Time [h]**
1	1,2	15.834-17.177	1,2	2.538-4.273	1,2,3,4,5,6	2.126-14.746	2,3,4,5,6	2.827-12.636
2	1,2,3,4	26.053-27.808	1,2,3,4	26.177-27.863	1,2,3,4,5,6	15.754-16.418	2,3,4,5,6	12.906-13.327
3	1,2,3,4	40.658-42.768	1,2,3,4	27.956-29.622	1,2,3,4,5	23.572-24.162	5,6	14.04-14.30
4	1,2,3,4	50.253-52.406	1,2,3,4	29.846-31.568	1,2,3,4,5,6	27.275-28.005	1,2,3,4	14.382-14.779
5	1,2,3,4	70.406-72.606	1,2,3,4	31.980-33.515	1,2,3,4,5,6	28.013-30.045	1,2,3,4,5	23.146-23.662
6	1,2,3,4	89.605-91.370	1,2,3,4	44.556-46.335	1,2,3,4,5,6	32.725-33.380	1,2,3,4,5,6	27.022-27.677
7	1,2,3,4	115.56-117.70	1,2,3,4	47.720-49.443	1,2,3,4,5,6	34.478-35.15	1,2,3,4,5,6	29.899-30.489
8	1,2,3,4	140.63-142.83	1,2,3,4	55.660-58.207	1,2,3,4,5,6	37.027-37.797	1,2,3,4,5,6	33.127-33.799
9	1,2,3,4	164.55-166.80	1,2,3,4	80.332-82.171	1,2,3,4,5,6	40.247-40.912	1,2,3,4,5,6	36.553-37.405
10			1,2,3,4	98.889-100.43	1,2,3,4,5,6	46.657-47.378	1,2,3,4,5,6	39.650-40.297
11			1,2,3,4	121.39-122.92	3,4,5,6	50.992-51.517	1,2,3,4,5,6	46.886-47.541
12			1,2,3,4	143.72-145.47	1,2,3	51.574-51.943	1,2,3,4,5,6	51.376-52.024
13					1,2,3,4,5,6	54.991-55.835	1,2,3,4,5,6	54.343-54.974
14					1.5,2, 3,4,5,6	75.125-75.912	1,2,3,4,5,6	57.211-57.874
15					6, 6.5	78.894-79.083	1,2,3,4,5,6	60.947-61.603
16					1,2,3,4,5	80.009-80.812	1,2,3,4,5,6	63.873-64.520
17					1,2,3,4,5	84.376-84.885	1,2,3,4,5,6	70.986-71.592
18					1,2,3,4,5,6	97.971-98.766	1,2,3,4,5,6	77.213-77.820
19					1,2,3,4,5,6	105.895-106.649	1,2,3,4,5,6	80.622-81.261
20					1,2,3,4,5,6	121.956-122.702	1,2,3,4,5,6	84.326-84.933
21					1,2,3	200.533-200.836	1,2,3,4,5,6	87.465-88.079
22					1,2,3,4,5,6	201.369-202.090	1,2,3,4,5,6	95.225-95.831

23			1,2,3,4,5,6	204.155-204.802	1,2,3,4,5,6	101.32-101.92
24			1,2,3,4,5,6	215.217-215.865	1,2,3,4,5,6	106.07-106.57
25			1,2,3,4,5,6	219.821-220.577	1,2,3,4,5,6	108.77-109.40
26					1,2,3,4,5,6	122.27-123.00
27					1,2,3	199.67-199.98
28					1,2,3,4,5,6	201.01-201.60
29					1,2,3,4,5,6	203.87-204.50
30					1,2,3,4,5,6	207.88-208.50
31					1,2,3,4,5,6	214.66-215.27
32					6	218.90-218.96
33					1,2,3,4,5,6	219.90-220.51

ii. Carbohydrate Analysis with HPLC-RID

a. Chemicals and Materials for HPLC-Analysis and Sample Preparation for the Analysis of Carbohydrates

Table 21: Chemicals applied during sample preparation & analysis of carbohydrates by HPLC-RID.

Substance	Specifications	Supplier
Bi-dest. H_20 (for dilution, needle washing, and eluent)	Purity: 100 % (ISO 3696)	EASYpure II, Wilhelm Werner GmbH, Germany
Butanol	Purity: ≥ 99.8 %	Carl Roth GmbH, Germany
Fructose	Purity: > 99 %, water content: ≥ 0.5 %	AppliChem GmbH, Germany
Galactose	Purity: > 98 %, water content < 0.3 %	AppliChem GmbH, Germany
D-(+)-Glucose	Water free	Carl Roth GmbH, Germany
D-(+)-Maltose	Monohydrate ≥ 99 %	Sigma-Aldrich, Germany
Maltotriose	> 97 %, water < 5 %	AppliChem GmbH, Germany

Table 22: Standards and concentrations for the calibration (carbohydrate identification & quantification).

Standard	Concentration of master solution [g L^{-1}]	Concentrations for calibration [g L^{-1}]	Solvent
Fructose	20	0.05, 0.5, 1.0, 2.0, 4.0, 5.0, 10, 20	Bidest. H_2O
Galactose	10	0.075, 0.15, 0.3, 0.75, 1.5, 3, 6, 10	
D-(+)-Glucose	20	0.05, 0.1, 0.2, 0.5, 1.0, 1.5, 2.0, 3.0, 5.0, 10, 15, 20	
Maltose	20	0.1, 0.5, 1.0, 2.0, 3.0, 4.0, 5.0, 10, 15, 20	
Maltotriose	20	0.05, 0.5, 1.0, 2.0, 3.0, 5.0, 10, 20	
Saccharose	4	0.01, 0.05, 0.1, 0.5, 1.0, 2.0, 4.0	
Trehalose	4	0.05, 0.5, 1.0, 2.0, 4.0	

Table 23: HPLC vials and related materials used for HPLC analysis.

Item	Specifications	Supplier
Inlets	200 µL	VWR International
Screw caps	Black	
Septa 10A	Red	
Vials ND8	transparent glass, 2 mL	
Rotilabo®-syringe filters	0.8 µm pore size, CME, unsterile	Carl Roth GmbH, Germany

b. HPLC: Instrument Settings and Methods for Carbohydrate Analysis

All samples must be filtered with syringe filter (pore size: 0.8 µm) before analysis. In case of precipitation after thawing freezed samples they must be centrifuged again (10000 rpm, 10 min).
Instrument: Agilent Technologies 1200 Series (Agilent Technologies, Waldbronn, Germany) with degasser G1322A, isocratic pump G1310A, autosampler G1329A, column oven G1316A, and detector RID G1362A.

Column: Hyplex Ca^{2+} column (Varian, Agilent Technologies, Waldbronn, Germany), size: 300 x 7.7 mm, particle diameter: 8 µm.

The **instrument settings** are listed in the following:

Pump Settings

- **Control:**
  Column Flow: 0.25 mL min^{-1}
  Stoptime: 64.50 min
  Posttime: Off
- **Solvent A:**
  100 % bi-dest. H_2O
- **Pressure limits:**
  Min: 0 bar, max: 50 bar

Injection Program

1	DRAW 20 µL from sample, 1.0 mm offset
2	INJECT
3	DRAW 30 µL from vial 1, 1.0 mm offset
4	MIX 30 µL in air, twice, max. speed
5	EJECT 30 µL into seat
6	DRAW 30 µL from vial 3, 1.0 mm offset
7	MIX 30 µL in air, twice, max. speed
8	EJECT 30 µL into seat

Injection including needle washing:
Injection volume: 20.0 µL
Washing from Vial 1
Optimization: none

- **Auxiliary:**
  LDraw Speed: 200 µL min^{-1}
  Eject Speed: 200 µL min^{-1}
  Draw Position 1.0 mm

- **Time:**
  Stop time: 64.50 min as pump setting
  Post time: Off

Column Thermostat

Left temperature: 80.0 °C
Right temperature: Same as left
Enable analysis: With any Temperature
Store left temperature: Yes
Store right temperature: No

- **Time:**
  Stop time: 64.50 min as pump setting
  Post time: Off

RID Signals

- **Temperature:**
  Optical unit temperature: 40 °C
  Signal Polarity: Positive

- **Automatic purge:**
  Purge time: 1.00 min
  Wait time: 1.00 min

- **Time:**
  Stop time: 64.50 min as pump setting
  Post time: Off

- **Peak width:**
  Response time > 0.2 min (4s for standard substance)

- **Analog output:**
  Zero offset analog out: 5 %
  Attenuation analog out: $500*10^3$ nRIU

- **Automatic zero before analysis:**
  On

- **Automatic recycling after analysis:**
  Off

- **Signal details:** Available signals RID1 A

iii. Main Carbon Metabolite Analysis with HPLC-RID

a. Chemicals and Materials for HPLC-Analysis and Sample Preparation for the Analysis of Main Carbon Metabolites

Table 24: Chemicals applied during sample preparation & analysis of main carbon metabolites by HPLC-RID.

Substance	Specifications	Supplier
Bi-dest. H_20 (for dilution and needle washing)	Purity: 100 % (ISO 3696)	EASYpure II, Wilhelm Werner GmbH, Germany
Sulfuric acid	Purity: 95 -98 %, Conc. 5 mM	Carl Roth GmbH, Germany
Perchloric acid	Purity: 70 %	ROTIPURAN® Supra, Carl Roth GmbH, Germany
Acetaldehyde	Purity: ≥ 99.5 %	Fluka (Sigma Aldrich), Germany
Acetic acid	Purity: 100 %	Carl Roth GmbH, Germany
Butanol	Purity: ≥ 99.8 %	Carl Roth GmbH, Germany
Diacetyl	Purity: 97 %	Sigma-Aldrich, Germany
Ethanol absolute	Purity: > 99 %, water < 0.5 %	AnalaR NORMAPUR
Glycerin	Purity: ≥ 95.5 %, water free	Carl Roth GmbH, Germany
Iso-butanol	Purity: 99 %	Carl Roth GmbH, Germany
Lactate	Purity: 90 %	Sigma-Aldrich, Germany
Malate	Purity: ≥ 95.5 %	Merck KGaA, Germany
Methanol	Purity: 100 %	HiPerSolv Chromanorm®, VWR Sci., USA
Propanol	Purity: 99.8 %	LiChrosolv®/Merck Millipore, Germany
Propionic acid	Purity: ≥ 99 %	Carl Roth GmbH, Germany
Pyruvate	Concentration: > 98 %	Carl Roth GmbH, Germany
Succinate	Purity: 97 %	Sigma-Aldrich, Germany

Table 25: Standards and concentrations for the calibration (main carbon metabolite identification & quantification).

Standard	Concentration of master solution [g L^{-1}]	Concentrations for calibration [g L^{-1}]	Solvent
Acetaldehyde	2	0.01, 0.1, 0.5, 1.0, 1.5, 2.0	Bidest. H_2O
Acetic acid	4.0	0.165, 0.5, 1.0, 2.0, 4.0	
Butanol (internal standard during sample analysis)	1.0	0.1, 0.2, 0.5, 1.0	
Diacetyl	1.0	0.0001, 0.001, 0.01, 0.1, 0.5, 1.0	
Ethanol	none	0.1, 0.05, 1.0, 2.5, 5.0, 7.5, 10, 15, 20, 25, 30, 35, 40	
Glycerin	2.0	0.113, 0.281, 0.562, 1.125, 2.25	
Iso-butanol	2.0	0.001, 0.01, 0.1, 0.5, 1.0, 2.0	
Lactate	2.5	0.05, 0.1, 0.25, 0.5, 1.0, 1.25, 1.5, 2.0, 2.5	
Malate	0.5	0.05, 0.075, 0.1, 0.25, 0.5	
Methanol	2.0	0.05, 0.1, 0.5, 1.0, 1.5, 2.0	
Propanol	10	0.05, 0.1, 0.2, 0.3, 0.5, 1.0, 2.0, 5.0, 10	
Propionic acid	1.0	0.05, 0.1, 0.25, 0.5	
Succinate	1.0	0.075, 0.1, 0.25, 0.5, 0.75	
Pyruvate	10	0.05, 0.1, 0.25, 0.5, 1.0, 1.5, 2.0, 3.0, 5.0, 6.0, 8.0, 10	

Table 26: HPLC vials and related materials used for HPLC analysis.

Item	Specifications	Supplier
Inlets	200 µL	VWR International
Screw caps	black	
Septa 10A	red	
Vials ND8	transparent glass, 2 mL	
Rotilabo®-syringe filters	0.8 µm pore size, CME, unsterile	Carl Roth GmbH, Germany

b. HPLC: Instrument Settings and Methods for Main Carbon Metabolite Analysis

All samples must be filtered with syringe filter (pore size: 0.8 µm) before analysis. In case of precipitation after thawing freezed samples they must be centrifuged again (10000 rpm, 10 min).
Instrument: Agilent Technologies 1200 Series (Agilent Technologies, Waldbronn, Germany) with degasser G1322A, isocratic pump G1310A, autosampler G1329A, column oven G1316A, and detector RID G1362A.

Column: HyperREZ column carbohydrate H^+ (Thermo Fisher Scientific, USA), size: 300 x 7.7 mm, particle diameter: 8 µm.

The **instrument settings** are listed in the following:

Pump Settings

- **Control:**
  Column Flow: 0.5 mL min^{-1}
  Stoptime: 55.00 min
  Posttime: Off
- **Solvent A:**
  100 % 5 mM H_2SO_4
- **Pressure limits:**
  Min: 0 bar, max: 60 bar

Injection Program

1	DRAW 10 µL from sample, 5.0 mm offset
2	INJECT
3	DRAW 30 µL from vial 1, 1.0 mm offset
4	MIX 30 µL in air, twice, max. speed
5	EJECT 30 µL into seat
6	DRAW 30 µL from vial 3, 1.0 mm offset
7	MIX 30 µL in air, twice, max. speed
8	EJECT 30 µL into seat

Injection including needle washing:
Injection volume: 20.0 µL
Washing from Vial 1
Optimization: none

- **Auxiliary:**
  LDraw Speed: 200 µL min^{-1}
  Eject Speed: 200 µL min^{-1}
  Draw Position 0.3 mm

- **Time:**
  Stop time: 55.00 min as pump setting
  Post time: Off

Column Thermostat

Left temperature: 15.0 °C
Right temperature: Same as left
Enable analysis: With any Temperature
Store left temperature: Yes
Store right temperature: No

- **Time:**
  Stop time: 55.00 min as pump setting
  Post time: Off

RID Signals:

Temperature:
Optical unit temperature: 20 °C
Signal Polarity: Positive

- **Automatic purge:**
  Purge time: 1.00 min
  Wait time: 1.00 min

- **Time:**
  Stop time: 55.00 min as pump setting
  Post time: Off

- **Peak width:**
  Response time > 0.2 min (4s for standard substance)

- **Analog output:**
  Zero offset analog out: 5 %
  Attenuation analog out: $500*10^3$ nRIU

- **Automatic zero before analysis:**
  On

- **Automatic recycling after analysis:**
  Off

- **Signal details:** Available signals RID1 A

iv. Sterol Analysis with GC-FID

a. Chemicals and Materials applied for GC-Analysis and Sample Preparation

Table 27: Chemicals applied during sample preparation & analysis of sterols by GC-FID.

Substance	Specifications	Supplier
Chloroform	Purity: ≥ 99 % for GC	Sigma-Aldrich, Germany
Dichloromethane	Purity: ≥ 99.8 %	HiPerSolv CHROMANORM®, VWR Chemicals, Germany
Glass beads	Diameter: 0.5 mm	Carl Roth GmbH, Germany
Hydrochloric acid	Concentration: 25 %	Carl Roth GmbH, Germany
n-Hexane	Purity: 99 % for HPLC	Sigma-Aldrich, Germany
Iso-propanol	Purity: 100 % for HPLC	Sigma-Aldrich, Germany
Methanol	Purity: ≥ 99 % for GC	Carl Roth GmbH, Germany
Potassium hydroxide (KOH)	Concentration: ≥ 85 %	Carl Roth GmbH, Germany
Pyrogallol	MW = 126.11 g mol^{-1}	Sigma-Aldrich, Germany
Cholesterol	Purity: ≥ 99 %	Sigma-Aldrich, Germany, lot nr.: SLBC7554V
Ergosterol	Purity: ≥ 95 %	Sigma-Aldrich, Germany, lot nr.: BCBK4106V
Lanosterol	Purity: ≥ 93 %	Sigma-Aldrich, Germany, lot nr.: 091M5071V
Squalene	Purity: ≥ 98 %	Sigma-Aldrich, Germany, lot nr.: SLBD0500V
Zymosterol	Purity: ≥ 98 %	Avanti Polar Lipids, USA, lot nr.: 700068P

Table 28: Standard substances for sterol identification & quantification with GC-FID.

Standard	Concentration of master solution	Concentrations for calibration [mmol L^{-1}]	Solvent
Cholesterol (internal standard during sample analysis)	1 mg mL^{-1}	/	Chloroform
Ergosterol	50 mmol L^{-1}	0.1, 0.5, 1.5	Dichloromethane-Iso-propanol (1:1)
Lanosterol	100 mmol L^{-1}	0.1, 0.3, 0.7	Dichloromethane
Squalene	100 mmol L^{-1}	0.1, 0.5, 1.5	Chloroform
Zymosterol	1 mmol L^{-1}	0.1, 0.3, 0.7	Dichloromethane

Table 29: Temperature program for the sterol standard analysis by GC-FID.

Total time [min]	Heating rate [°C min^{-1}]	Temperature [°C]	Temperature const. [min]
0	0	150	2
2	15		
8,667	0	250	26.333
37	5		
45	0	290	7

Table 30: GC vials and related materials used for GC analysis.

Item	Specifications	Supplier
Inlets	200 µL	VWR International
Septa 10A	red, anti-volatile	
Screw caps	black	
Vials ND8	brown glass, 2 mL	

b. Sample preparation

The procedure for sample preparation for the analysis of the total and free sterol content (non-esterified) was the following (based on a protocol of Maczek and co-authors (2006):

Free sterol content:

1. The frozen samples were thawed quickly by using a microwave (Emerson Cube AR610 Microwave, maximum power level 2), placing the falcon tubes with loosed lids into glass beakers and shaking them from time to time to homogenize.
2. The OD_{600} was adjusted to 12 with deionized water (in most cases samples had an OD below 8 and had to be concentrated during the centrifugation procedure (step 3).
3. 20 mL of the sample were centrifuged at 2 °C with 6000 rpm for 6 min (Eppendorf 5810R (rotor F34-6-38)). The supernatant was discarded and the cell pellet washed briefly with 3 mL cold deionized water and centrifuged again. The washed cell pellet was then rapidly dissolved in 2 mL of cold deionized water
4. The sample was transferred into special capsules for milling. In order to disrupt the cells, 2 mL of a chloroform-methanol mixture (4:1, (≥ 99 %) Sigma-Aldrich, (≥ 99 %) Carl Roth GmbH, both Germany), 4 mL of glass beads (0.5 mm, Carl Roth GmbH, Germany), and 100 µL of an internal standard (1 mg mL^{-1} cholesterol in chloroform, both (≥ 99 %) Sigma-Aldrich, Germany) were added to the sample and the capsule was closed properly. The volume was mixed for 15 min at 30 Hz using the miller (Retsch MM 400).
5. For recovery of the glass beads, they were separated on a Nylon filter of 125 µm (Carl Roth GmbH, Germany) from the sample, which was caught in 50 mL Falcon tubes (VWR, Germany). In order to ensure that the compete sample is in the Falcon tube the capsules were rinsed with 1 mL chloroform and this volume was added to the beads stuck on the filter. Additionally, the glass beads on the filter were rinsed with 1 mL Chloroform.
6. The mixture in the Falcon tubes was then centrifuged for 15 min, 9000 rpm at 2 °C for phase separation (Eppendorf 5810R (rotor F34-6-38)). The lower chloroform phase was rapidly transferred into 100 mL round-bottom flask (Schott Duran flask, Germany), with lid, using a 5 mL pipette with plastic tips to reach the highest yield. This step was repeated once for a higher yield.
7. The chloroform was removed on a rotary evaporator (Büchi Rotavapor®) at 35 °C, a velocity at a level between 1 and 3, and under reflux with 280 mbar to 310 mbar according to the remaining volume.
8. The remaining sample in the round-bottom flask was dissolved in 750 µL 2-isopropanol (100 % for GC, VWR, Germany) and then incubated for 2 min in an ultrasonic bath (Bandelin Sonorex, Berlin). The volume was transferred in labelled Eppendorf tubes (VWR, Germany). In order to increase the yield this procedure was repeated and the sample transferred into the same tube. The vials were stored until analysis at -20 °C.
9. In order to concentrate the sample for a sufficient signal intensity in the GC-FID, a vacuum centrifuge (Bachofer, Reutlingen) was used. 1 mL of the sample was transferred into a labelled brown GC-vial (VWR International) and dried for about 40 – 60 min. The concentrate was dissolved in 200 µL iso-propanol, transferred to another labelled brown GC vial with inlet, and stored at -20 °C until analysis. The remaining 500 µL from the 1st vial were stored at -20 °C as a reserve.
10. The analysis by GC-FID was conducted as described in Appendix A, iv.c.

Total sterol content:

1. The frozen samples were thawed and washed as described for the free sterols in step 1 -3. The samples were transferred into 30 mL glass tubes (Pyrex Culture Tubes, 20x200 SVL SCRE) since the high temperature in the next steps would dissolve the plastic tubes.
2. 2.5 mL of 1N HCl (Carl Roth GmbH, Germany) and 100 µL of the internal standard cholesterol (1 mg mL^{-1} cholesterol in chloroform, both ≥ 99 %, Sigma-Aldrich, Germany) were added to the sample (glass pipettes for HCl). The sample was incubated for 20 min in boiling water with open lids.
3. Then the sample was cooled (on ice), 3 g of KOH ((>85 %) Carl Roth GmbH, Germany) were added step by step on ice (exothermic reaction!). When all KOH was dissolved, 12 mL of a methanolic solution of pyrogallol with a concentration of 0.25 g L^{-1} (Pyrogallol (MW=126.11 g mol^{-1}), Sigma-Aldrich, Germany; MeOH for GC (≥ 99 %), Carl Roth GmbH, Germany) were added using a glass pipette.
4. The mixture was incubated at 70 °C for 1:45 h in a water bath with the glass tube being covered with water until the sample filling level.
5. The tubes were cooled to room temperature, 15 mL n-Hexane were added to every sample using glass pipettes, and the tubes were shaken shortly by hand for mixing. The tubes were subsequently shaken with the rotor (Driver STR4 and STR4/5 holder, Stuart Scientific) for 15 min at step 4 (about 24 rpm).
6. The upper phase (= hexane phase) was transferred into a round-bottom flask (100mL) with lid, using a 5 mL pipette with plastic tips to reach the highest yield. The 6^{th} step was repeated and the upper phase was pipetted into the same round-bottom flask.
7. Hexane was removed on a rotary evaporator (Büchi Rotavapor®) at 35 °C, a velocity at a level between 1 and 3, and under reflux with 220 mbar to 310 mbar according to the remaining volume.
8. The next steps were performed as described for the free sterol content in step 8 and 10. Concentration of the sample was not necessary.

c. GC: Instrument Settings and Methods

Instrument: GC -2010 plus (Shimadzu, Germany), equipped with a flame ionization detector (FID) and autosampler AOC-20i (splitness mode). Needle washing with iso-propanol.

Capillary column: Wall coated open tubular fused silica (Varian, Germany), covered with dimethylpolysiloxane (DF = 0.12 µm coating CP-Sil5CB), length: 25 m, inner diameter: 250 µm. The autosampler AOC-20i was used for automated sample handling.

The following **temperature program** was set for the sterol identification and quantification in the brewing samples:

- The starting temperature of 150 °C was maintained for 2 min before it was heated at a rate of 15 °C per min to a temperature of 250 °C.
- After 37 min was heated with a final temperature of 290 °C at a rate of 5 °C per min, which was maintained for additional 7 min.
- The injector temperature was 290 °C, and the detector temperature 300 °C.

Injection volume: The injected sample volume was 0.5 µL for all investigations and 0.3 µL during the measurement of the standard solutions. The **Flow rate** was set to 30 mL min^{-1}.

Appendix B: Results

i. Additional Data from *on-line* Sensor Measurements (Chapter 5.1.2.3)

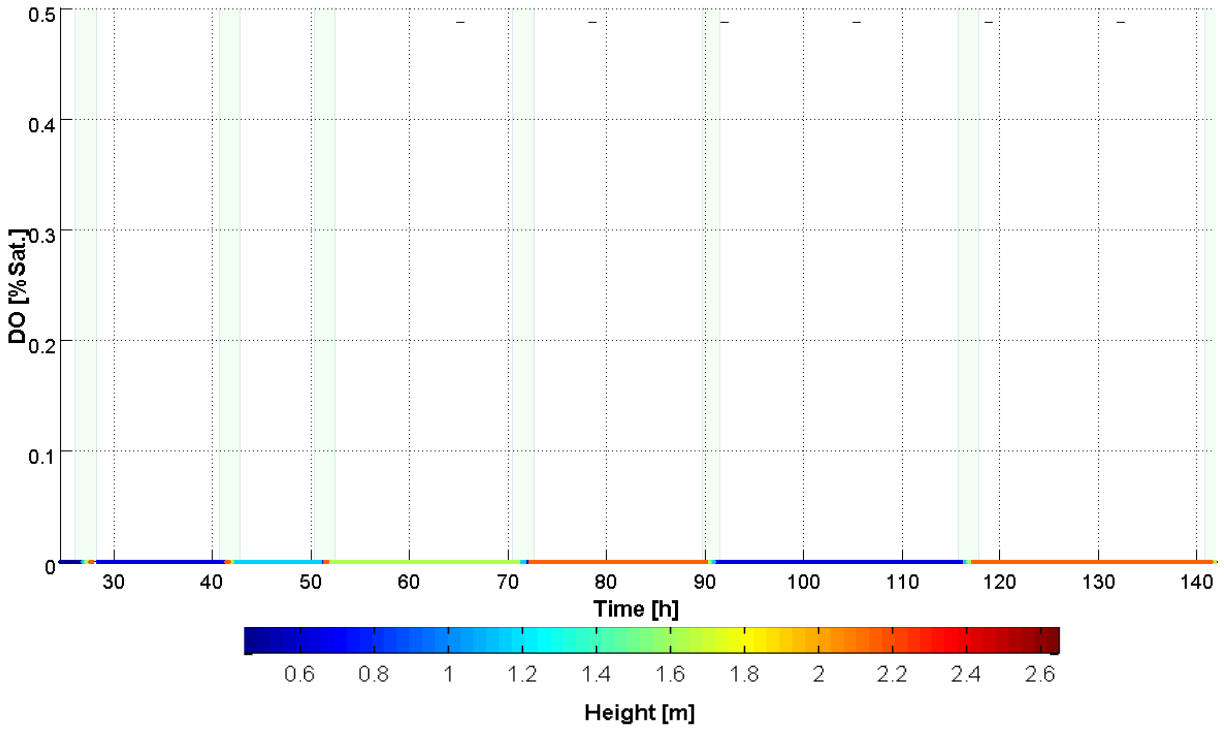

Fig. B 1: DO monitoring in the 3 m^3 scale (experiment 1).
Filling and cooling phase excluded.

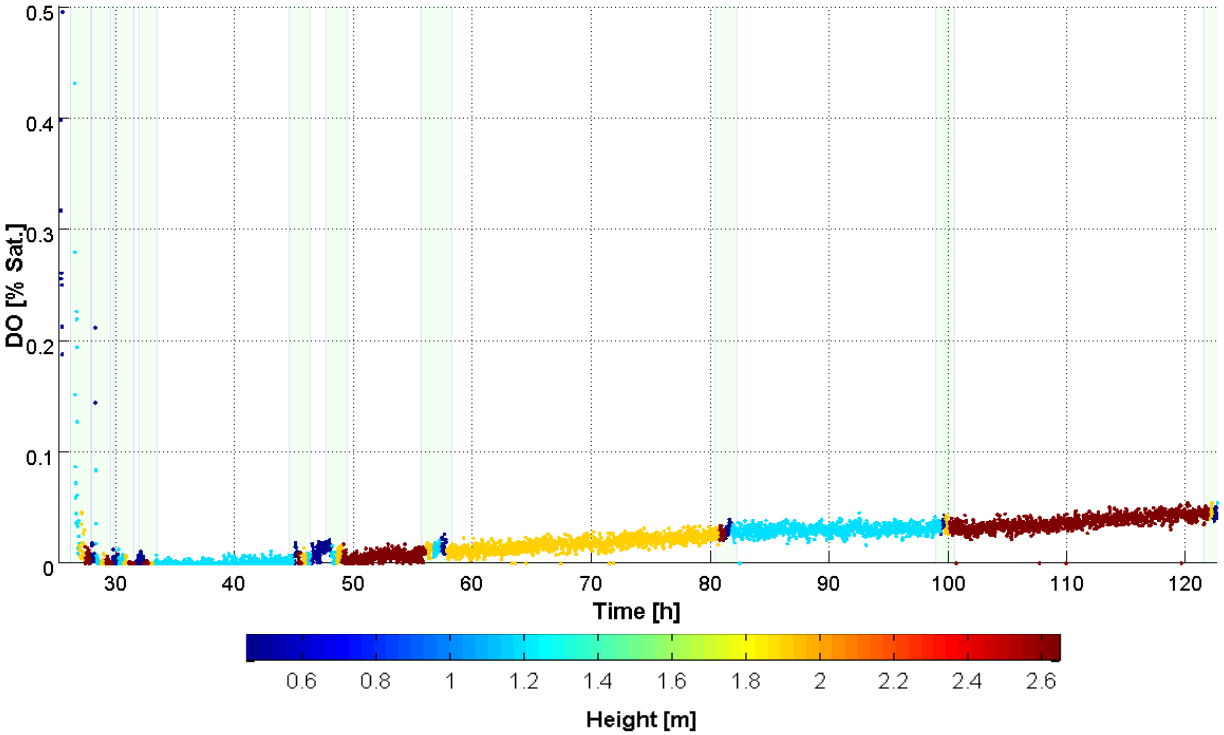

Fig. B 2: DO monitoring in the 3 m^3 scale (experiment 2).
Filling and cooling phase excluded.

ii. Regression Plots of Carbohydrates measured in the 170/199 m³ Scale (Chapter 5.3.2.4)

E = experiment. E 1 on E 2 represents the validation of the model developed with the data set of E2 with the independent data set of E1 in the 170/199 m³ scale.

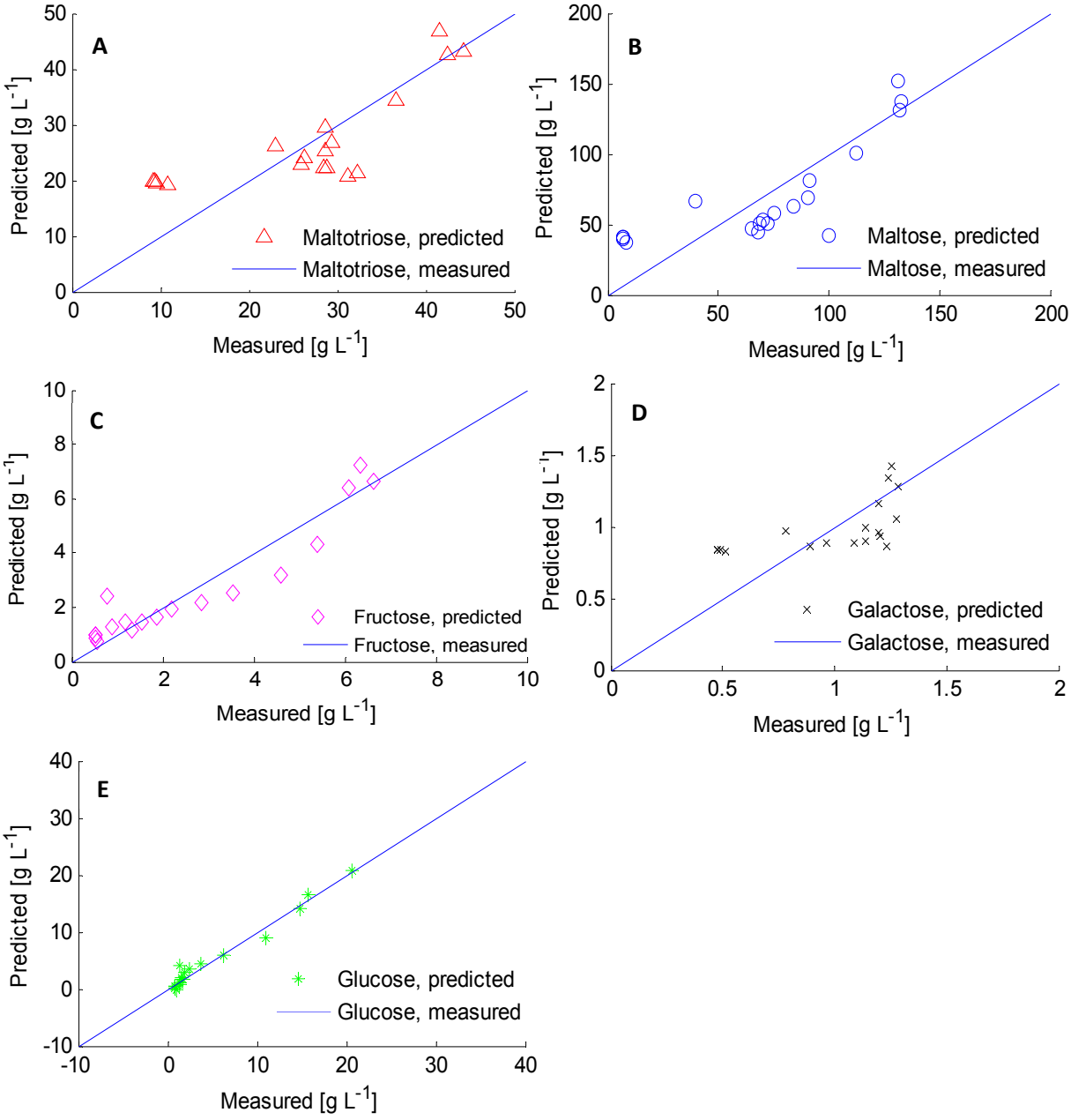

Fig. B 3: Cross-validation of extracellular carbohydrate concentrations measured in the 170/199 m³ scale (E 2, see Fig. 67). A: Maltotriose, B: Maltose, C: Fructose, D: Galactose, E: Glucose.

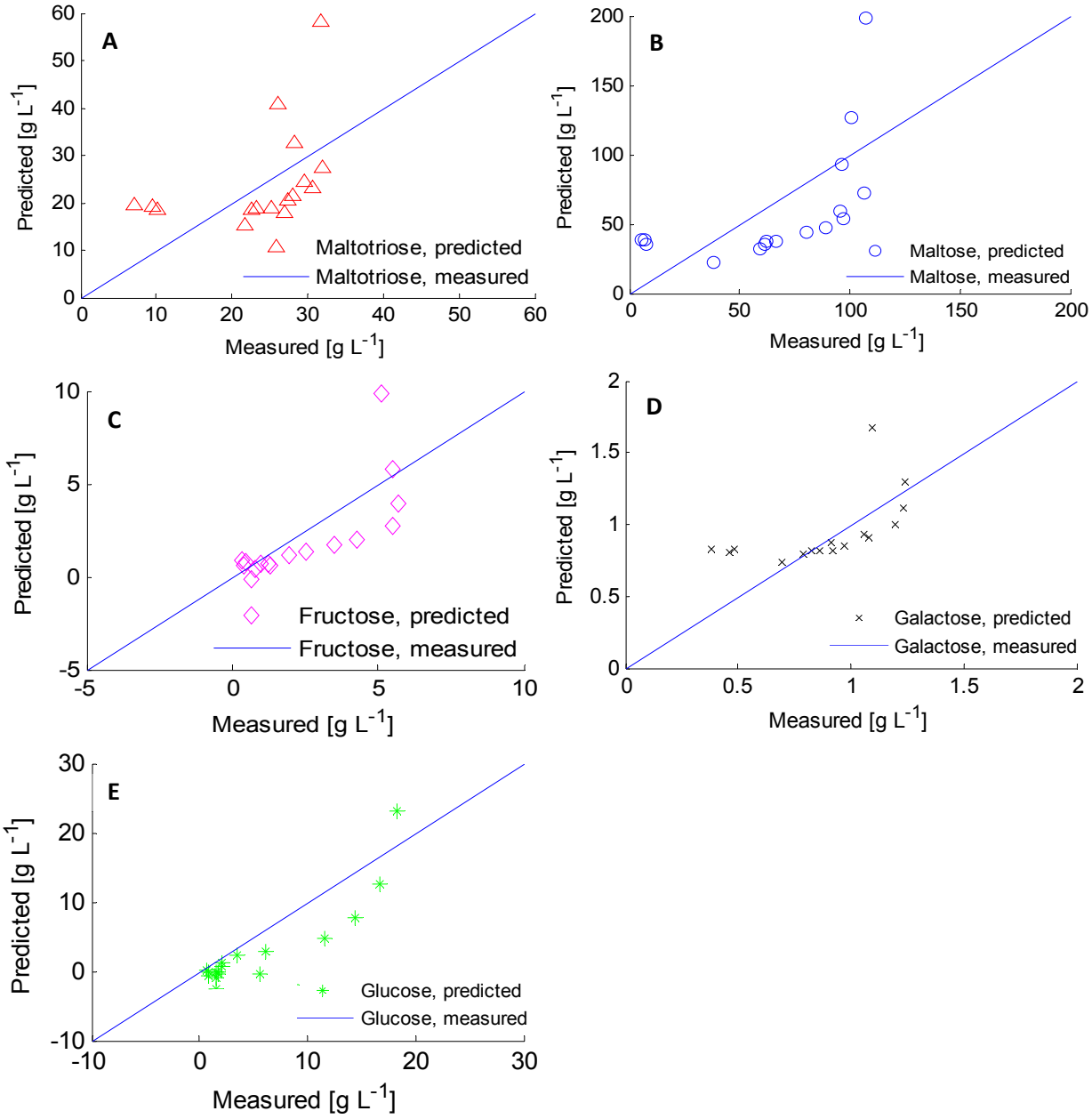

Fig. B 4: Validation of the regression model for the concentration of extracellular carbohydrates measured in the 170/199 m^3 scale
(see Fig. 68) with independent data from the same scale. The predicted values are based on the PLS regression of the *on-line* and *off-line* data of the 2nd experiment, the measured values are based on the carbohydrate concentration data from the 1st experiment. A: Maltotriose, B: Maltose, C: Fructose, D: Galactose, E: Glucose.

iii. Loading Plots of PCA with Contributions < 10 % of PC 2
(Chapter 5.3.1)

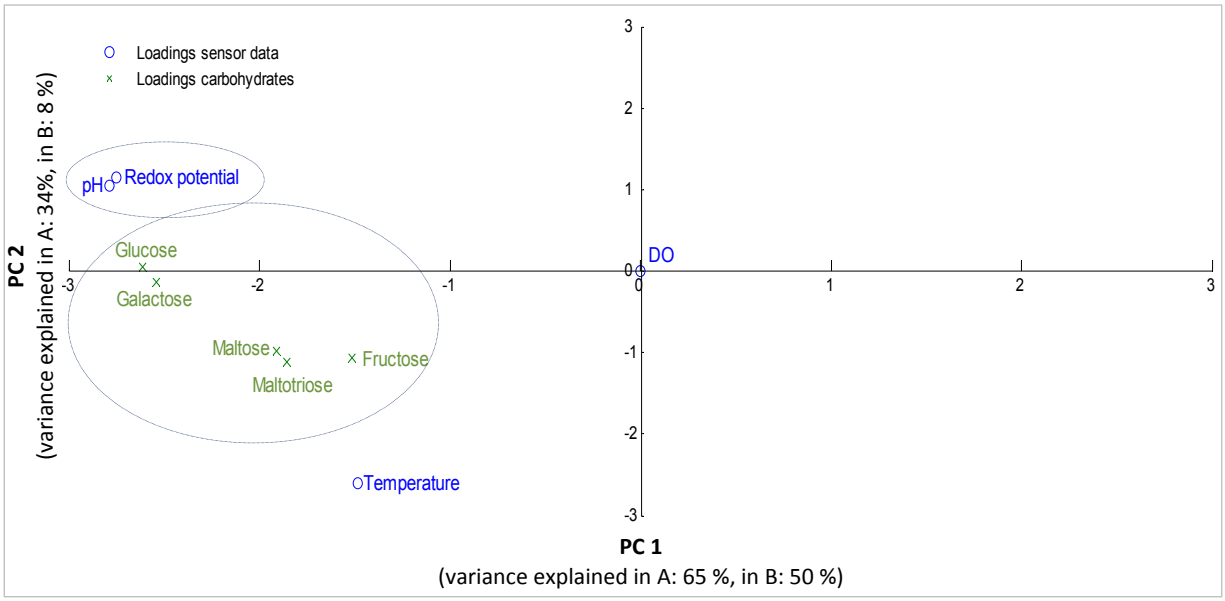

Fig. B 5: Loadings of the *on-line* sensor data vs. the concentration of extracellular carbohydrates measured in the 3 m^3 scale (E 1).
Presented are the loadings of the sensor data (blue circles) and concentrations of extracellular metabolites (green crosses).

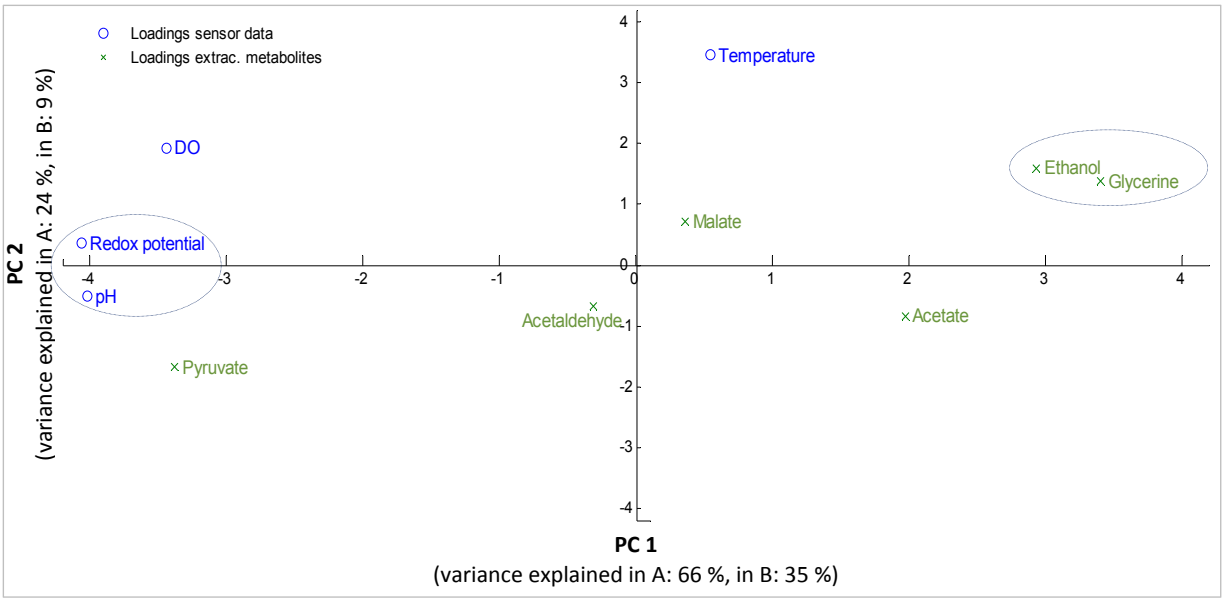

Fig. B 6: Loadings of the *on-line* sensor data vs. the concentrations of extracellular main carbon metabolites measured in the 170/199 m^3 scale (E 2).
Presented are the loadings of the sensor data (blue circles) and the concentrations of extracellular main carbon metabolites (green crosses).

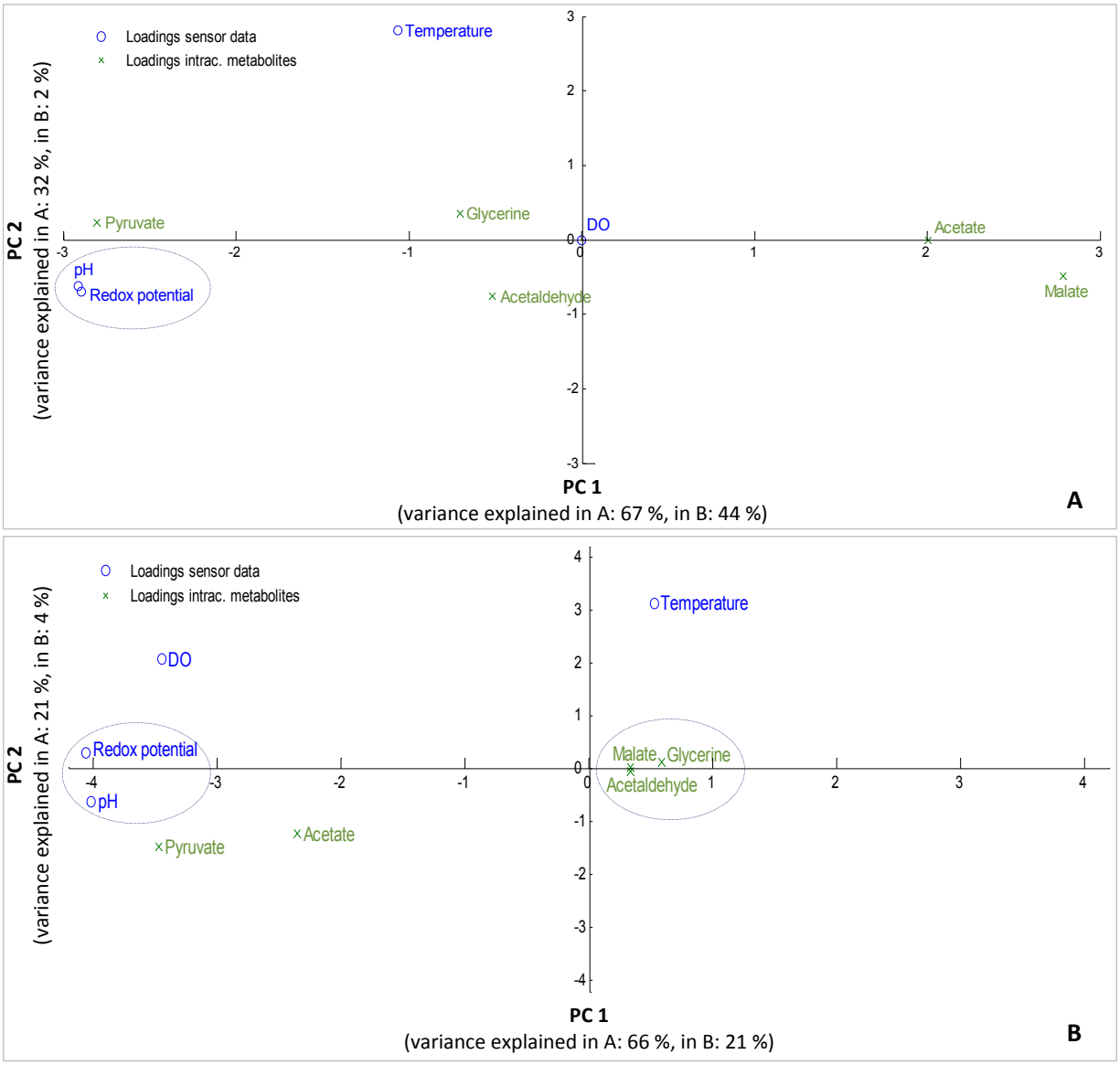

Fig. B 7: Loadings of the *on-line* sensor data vs. the concentrations of intracellular main carbon metabolites. A: 3 m^3 scale (E1); B: 170/199 m^3 scale (E 2). Presented are the loadings of the sensor data (blue circles) and the concentrations of extracellular main carbon metabolites (green crosses).

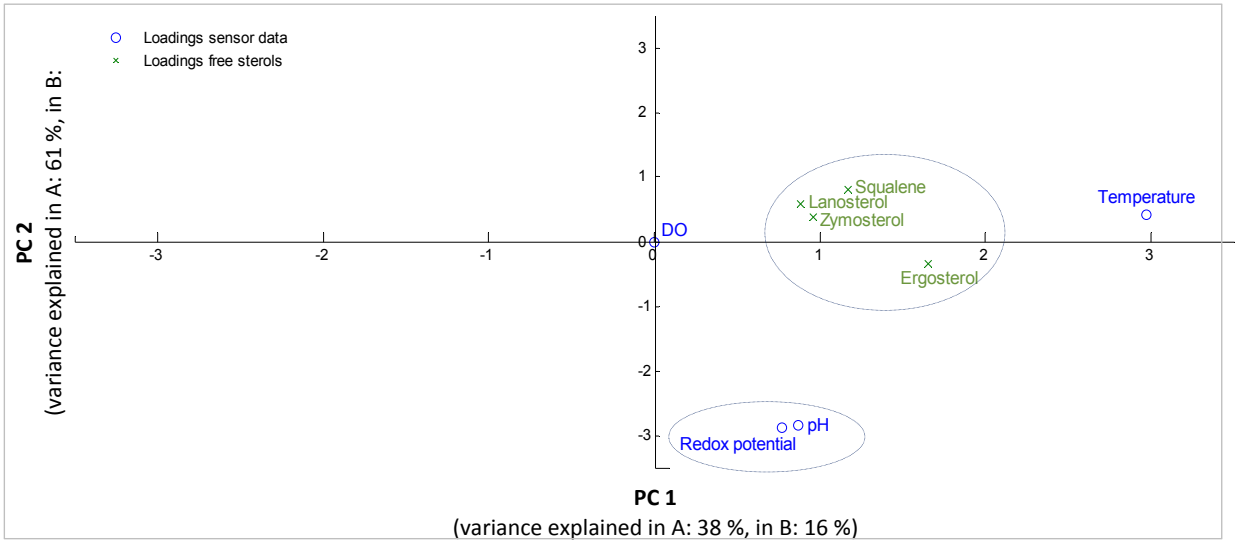

Fig. B 8: Loadings of the *on-line* sensor data vs. the free sterol content measured in the 3 m^3 scale (E1). Presented are the loadings of the sensor data (blue circles) and the concentrations of free sterols (green crosses).

iv. Correlation Coefficients for the PLS Regression Models (Chapter 5.3.2)

Table 31: Coefficients for the correlation of extracellular carbohydrate concentrations with *on-line* sensor data (Fig. 62).

	3 m^3 scale, E1	199 m^3 scale, E1	170 m^3 scale, E2	170 m^3 scale, E1 on E2
Maltotriose	0.52	0.61	0.54	0.35
Maltose	0.51	0.81	0.71	0.65
Glucose	0.76	0.93	0.92	0.88
Galactose	0.72	0.90	0.43	0.73
Fructose	0.38	0.93	0.91	0.80

Table 32: Coefficients for the correlation of the concentrations of extracellular main carbon metabolites with *on-line* sensor data (Fig. 63).

	3 m^3 scale. E1	199 m^3 scale. E1	170 m^3 scale. E2	170 m^3 scale. E1 on E2
Pyruvate	0.55	0.92	0.83	0.74
Acetaldehyde	0.50	0.52	0.03	0.06
Glycerin	0.71	0.92	0.80	0.88
Acetate	0.34	0.65	0.27	0.17
Malate	0.30	0.58	0.04	0.24
Ethanol	0.60	0.82	0.66	0.72

Table 33: Coefficients for the correlation of the concentrations of intracellular main carbon metabolites with *on-line* sensor data (Fig. 64).

	3 m^3 scale, E1	199 m^3 scale, E1	170 m^3 scale, E2	170 m^3 scale, E1 on E2
Pyruvate	0.88	0.88	0.84	0.81
Acetaldehyde	0.10	0.23	0.01	0.06
Glycerin	0.07	0.47	0.02	0.06
Acetate	0.45	0.46	0.41	1.24
Malate	0.89	0.24	0.01	0.08

Table 34: Coefficients for the correlation of total sterol content with *on-line* sensor data (Fig. 65).

	3 m^3 scale, E1	199 m^3 scale, E1	170 m^3 scale, E2	170 m^3 scale, E1 on E2
Squalene	0.42	0.24	0.51	0.51
Zymosterol	0.57	0.95	0.87	0.87
Lanosterol	0.32	0.88	0.62	0.62
Ergosterol	0.48	0.87	0.68	0.68

Table 35: Coefficients for the correlation of free sterol content with *on-line* sensor data (Fig. 66).

	3 m^3 scale, E1	199 m^3 scale, E1	170 m^3 scale, E2	170 m^3 scale, E1 on E2
Squalene	0.22	0.81	0.58	0.27
Zymosterol	0.12	0.44	0.72	0.18
Lanosterol	0.32	0.81	0.59	0.15
Ergosterol	0.12	0.90	0.96	0.89